

AN ABSTRACT OF THE DISSERTATION OF

Nicholas E. Larkey for the degree of Doctor of Philosophy in Chemistry presented on May 22, 2017.

Title: Displacement-based Fluorescent microRNA Biosensors: Design Principles and Analytical Metrics

Abstract approved: _____

Sean M. Burrows

One post-transcriptional mechanism that regulates the progression of cancer and other diseases involves small 22-23 nucleotide sequences called microRNA (miR). Early detection of small changes in concentration of these biomarkers holds potential to diagnose diseases at their earliest stages. Use of current nucleic-acid based biosensors, like molecular beacons, for *in situ* cellular and tissue analysis is hindered by false signals from nuclease degradation and off-analyte binding. For this reason, this work describes a new miR biosensor that was created to improve upon existing miR biosensors and overcome some of their weaknesses.

The reporter+probe biosensor that was developed consists of two partially complementary strands of DNA that form a double-stranded complex. One strand, called the reporter, contains two dyes capable of energy transfer located on opposite ends of the strand. The other strand, called the probe, is partially complementary to the reporter and is fully complementary to the miR of interest. When the miR of interest is presented to the reporter-probe complex, the reporter is displaced and a probe-target complex is formed. The displaced reporter forms a hairpin conformation to bring the dyes together. This causes a quantifiable change in analytical signal dependent on miR concentration. In the first portion of this research, a reporter+probe biosensor was developed for miR let-7a. This biosensor showed improved defense against false positive signal generation from nuclease degradation when compared to a molecular beacon. The biosensor was shown to have low nM LODs for analyte let-7a.

In the second part of this research, reporter+probe biosensors were developed for two miR analytes, miR-26a and miR-27a. It was discovered that there are numerous design parameters that need to be considered when making a reporter+probe biosensor for a given analyte. Among the discovered parameters, limiting the number of ‘non-ideal hairpin’ conformations that the reporter can sample maximizes the signal change upon analyte binding. Low nM LODs were found for miR-26a and miR-27a with their respective reporter+probe biosensors.

In the third portion of this research, a miR-26a reporter from the previous study was used to test whether hexaethylene glycol spacer molecules could be used between the reporter nucleic acid sequence and the fluorescent dyes to allow FRET (Förster Resonance Energy Transfer) enhancement to occur. It was found that the hexaethylene glycol spacers did increase FRET enhancement, and that the 6-FAM|ATTO 633 dye pair was superior to Cy3|Cy5 for FRET enhancement.

In the final stage of this research, directionality of the reporter+probe biosensor was studied to determine if it would increase specificity for the analyte by limiting off-analyte binding. It was found that taking into consideration where the off-analytes will bind to the probe allow for a more selective biosensor to be developed. In this study, the two reporter+probe biosensors were developed for miR-146a. Low pM LODs for miR-146a were obtained.

©Copyright by Nicholas E. Larkey
May 22, 2017
All Rights Reserved

Displacement-based Fluorescent microRNA Biosensors: Design Principles and Analytical Metrics

by
Nicholas E. Larkey

A DISSERTATION

submitted to

Oregon State University

in partial fulfillment of
the requirements for the
degree of

Doctor of Philosophy

Presented May 22, 2017
Commencement June 2017

Doctor of Philosophy dissertation of Nicholas E. Larkey presented on May 22, 2017

APPROVED:

Major Professor, representing Chemistry

Chair of the Department of Chemistry

Dean of the Graduate School

I understand that my dissertation will become part of the permanent collection of Oregon State University libraries. My signature below authorizes release of my dissertation to any reader upon request.

Nicholas E. Larkey, Author

ACKNOWLEDGEMENTS

I would like to principally thank my advisor Dr. Sean M. Burrows. Sean has guided me over the past 5 years and has aided me in my goal to become a better chemist and all-around scientist. I must also thank the other members of my graduate committee: Dr. Vincent Remcho, Dr. Ryan Mehl, Dr. Emily Ho, Dr. Molly Megraw, and Dr. Shelley Su.

A big ‘thank you’ goes out to all the wonderful people I have worked with at OSU in the department of chemistry: Dr. Neal Sleszynski, Dr. Chris Pastorek, Dr. Rick Nafshun, Dr. Kristin Ziebart, Margie Haak, Paula Weiss, and Kristi Edwards.

Dr. Carmen Wong – thank you for teaching me everything I know about mammalian cell culture.

I would like to thank my parents Landon, Kim, Kimberly, and Howard. You have always been there to bring me back down to earth when I get too fixed on the minutiae. I love you.

To my labmates Kyle Almlie, Lulu Zhang, Lixia Zhou, Kuan-Jen Chen, Annie Bluhm, Shan Lansing, Jake Ramsey, Victoria Tran, Cori Brucks, Sophia Le, Natasha Smith, and Chen Ng; I couldn’t have done any of this without you. Thank you.

To the breakfast club - Michaela, David, Sam, and Caitlyn – thank you for making my Sunday mornings a little brighter.

All my other friends in Corvallis, including all my BMES friends, thank you for being there for me. You all helped me in more ways than you know.

Shoshana and Jesse - Thank you for being a lifeline for me in Corvallis.

Lindsey Sequeira - thank you for being you. I love you.

Kayla Naas - I will always remember our “OB-LA-DI” when the going gets tough.

To my undergraduate mentors, Dr. Tina Saxowsky and Dr. Rosemarie (Romey) Haberle, the only reason I ever made it to graduate school was because of you. Thank you.

Another special thanks go to Dr. Justin Lytle and Dr. Neal Yakelis. The passion of these two professors inspired me to pursue Chemistry as a profession.

I would also like to thank the N. L. Tartar Research Fellowship and the Dorothy and Ramon Barnes Graduate Fellowship for supporting my research.

“Whose woods these are I think I know.
His house is in the village, though;
He will not see me stopping here
To watch his woods fill up with snow.

My little horse must think it queer
To stop without a farmhouse near
Between the woods and frozen lake
The darkest evening of the year.

He gives his harness bells a shake
To ask if there is some mistake
The only other sound's the sweep
Of easy wind and downy flake.

The woods are lovely, dark, and deep,
But I have promises to keep,
And miles to go before I sleep,
And miles to go before I sleep.”

-Robert Frost

“When I heard the learn'd astronomer,
When the proofs, the figures, were ranged in columns
before me,
When I was shown the charts and diagrams, to add, divide, and
measure them,
When I sitting heard the astronomer where he lectured with
much applause in the lecture-room,
How soon unaccountable I became tired and sick,
Till rising a gliding out I wander'd off by myself,
In the mystical moist night-air, and from time to time,
Look'd up in perfect silence at the stars”

-Walt Whitman, *Leaves of Grass*

CONTRIBUTION OF AUTHORS

Chapter 2. Sean M. Burrows contributed in part to the preparation and review of this manuscript. C. Kyle Almlie and Victoria Tran performed some experiments for the manuscript. Marianne Egan worked on the graphic design of the biosensor mechanism.

Chapter 3. Sean M. Burrows contributed in part to the preparation and review of this manuscript. Corinne N. Brucks developed the MATLAB code used to originate sensor sequences. Shan S. Lansing, Sophia D. Le, Natasha M. Smith, Victoria Tran, and Lulu Zhang all performed experiments for the manuscript.

Chapter 4. Sean M. Burrows contributed in part to the preparation and review of this manuscript. Lulu Zhang, Shan S. Lansing, and Victoria Tran all performed experiments for the manuscript. Victoria L. Seewaldt collaborated in the design process of the sensor.

Chapter 5. Sean M. Burrows contributed in part to the preparation and review of this manuscript. Jessica L. Phillips, Hyo Sang Jang, and Siva K. Kolluri were involved in the design of the sensors.

TABLE OF CONTENTS

	<u>Page</u>
Chapter 1. Introduction	1
1.1 MicroRNAs	1
1.1.1 MicroRNAs as biomarkers	3
1.1.2 Disease-related miRs of Interest	4
1.2 Conventional Detection Methods	4
1.2.1 In vitro methods	4
1.2.2 In situ methods	6
1.2.3 Signal generation methods	9
1.3 Thermodynamics of nucleic acid biosensors	9
1.4 Benefit of two-photon excitation for imaging	10
1.5 FRET enhancement for signal generation	10
1.6 Development of the Reporter+Probe biosensor	11
1.7 References	12
Chapter 2. Detection of miRNA Using a Double-Strand Displacement Biosensor with a Self-Complementary Reporter	18
2.1 Abstract	19
2.2 Introduction	19
2.3 Experimental	20
2.3.1 Single- and Two-Photon Spectral Characteristics of the Reporter	20
2.3.2 Oligonucleotides and Materials	23
2.3.3 Binding Kinetics and Analytical Signal Dynamics	24
2.3.4 Cell Lysate Protocol	25
2.3.5 Analytical Figures of Merit	25
2.3.6 False Positives from Nuclease Degradation	26
2.4 Results and Discussion	27
2.4.1 Thermodynamic Considerations for the Recognition Mechanism	27
2.4.2 Transduction Mechanism	28
2.4.3 Excitation Spectra of Reporter	32
2.4.4 Binding Kinetics and Analytical Signal Dynamics	33
2.4.5 Sensitivity	38
2.4.6 Reporter Specificity	39
2.4.7 False Positives from Endonuclease Degradation	39
2.5 Conclusion	41
2.6 Acknowledgements	42
2.7 References	42
Chapter 3. Molecular Structure and Thermodynamic Predictions to Create Highly Sensitive microRNA Biosensors	43
3.1 Abstract	44
3.2 Introduction	44
3.3 Experimental	46
3.3.1 Reporter Design Procedure	46

TABLE OF CONTENTS (Continued)

	<u>Page</u>
3.3.2 Thermodynamic, molecular structure, and molarity fraction predictions	48
3.3.3 Fluorimetry apparatus	49
3.4 Results and Discussion	51
3.4.1 Comparison of molecular structures and thermodynamics to signal change for reporter+probe biosensors	51
3.4.2 Analytical figures of merit for reporter+probe biosensors	64
3.5 Conclusions	64
3.6 Acknowledgements	65
3.7 References	66
Chapter 4. Förster resonance energy transfer impart signal-on and -off capabilities in a single microRNA biosensor	68
4.1 Abstract	69
4.2 Introduction	69
4.3 Materials and Methods	71
4.3.1 Biosensor Design	71
4.3.2 Fluorimeter design	72
4.3.3 Calibration curves	73
4.3.4 Analysis of reporter+probe formation	73
4.4 Results and discussion	74
4.4.1 Biosensor response	74
4.4.2 Influence of spacers on the detection limits and sensitivity	78
4.4.3 MicroRNA-induced reporter+probe displacement efficiency	85
4.4.4 Reporter+probe formation analysis of the 6-FAM ATTO 633 reporter with 18 spacers	86
4.5 Conclusions	86
4.6 Acknowledgements	88
4.7 References	88
Chapter 5. MicroRNA biosensor design strategies to mitigate off-analyte response	90
5.1 Abstract	91
5.2 Introduction	91
5.3 Materials and Methods	92
5.3.1 Thermodynamic Calculations	92
5.3.2 Off-analyte discovery	94
5.3.3 Biosensor Design	94
5.3.4 Fluorimeter design	95
5.3.5 Cell Lysate	96
5.3.6 Off-analyte testing	96
5.3.7 Calibration curves	97
5.4 Results and Discussion	97
5.4.1 Biosensor's toehold location considerations	97
5.4.2 Biosensor Selectivity	101

TABLE OF CONTENTS (Continued)

	<u>Page</u>
5.4.3 Biosensor sensitivity and analytical metrics	104
5.5 Conclusion	106
5.6 Acknowledgements	106
5.7 References	106
Chapter 6. Summaries and Conclusions	108
6.1 Summaries and Conclusions	108
6.2 References	111
Bibliography	112
Appendices	119
Appendix I: Supplemental Information for Chapter 2	120
Appendix II: Supplemental Information for Chapter 3	124
Appendix III: Supplemental Information for Chapter 4	140
Appendix IV: Supplemental Information for Chapter 5	154

LIST OF FIGURES

<u>Figure</u>	<u>Page</u>
Figure 1.1 Biological synthesis of miRs from DNA to mature miRs	3
Figure 1.2 Microarray methodology	6
Figure 1.3 Fluorescence In-Situ Hybridization (FISH)	7
Figure 1.4 Diagram of molecular beacon design and potential problems	8
Figure 2.1 Schematic of Recognition Mechanism	20
Figure 2.2 Experimental apparatus	22
Figure 2.3 Fluorescence emission from the reporter	29
Figure 2.4 Comparison of observed fluorescence quenching	31
Figure 2.5 Excitation spectra of 1 μ M reporter with and without 1 μ M probe1	32
Figure 2.6 Background corrected averaged summed Cy5 intensity	34
Figure 2.7 Background corrected averaged summed intensity of reporter	35
Figure 2.8 Comparison of observed percent decrease of reporter Cy5 Emission	37
Figure 3.1 Response of reporter+probe biosensor to miRNA analyte	45
Figure 3.2 Outline of the procedure to design a reporter and probe for a given miRNA analyte	47
Figure 3.3 Predicted miR-27a-reporter hairpin conformations	52
Figure 3.4 Reporter response to probe and reporter+probe response to analytes and off-analytes	55
Figure 3.5 Energy minima structures and partition function probability maps for miR-27a-R2	57
Figure 3.6 Energy minima structures and partition function probability maps for miR-26a-R1	60

LIST OF FIGURES (Continued)

<u>Figure</u>	<u>Page</u>
Figure 3.7 Molarity fraction of each of the reporters with their respective Probes	61
Figure 4.1 Recognition and transduction mechanisms for a miRNA biosensor to visualize the over-/under-expression of miRNA	75
Figure 4.2 Emission spectra from 100 nM of reporters with and without Probe	77
Figure 4.3 Calibration curves from miRNA analyte additions to 100 nM reporter+probe biosensors	83
Figure 5.1 Comparison of the binding initiation of off-analytes to miR-146b-5p for both R1+P1 and R2+P2 reporter+probe biosensors	98
Figure 5.2 Reporter+probe biosensor predicted binding structures for R1+P1 and R2+P2	99
Figure 5.3 Signal change between equimolar R1+P1 and R1-hairpin for both donor and acceptor dyes	101
Figure 5.4 Selectivity tests for R1+P1 and R2+P2 with analyte and off-analytes	102
Figure 5.5 Calibration curves in cell lysate	105

LIST OF TABLES

<u>Table</u>	<u>Page</u>
Table 1.1 Sequences for miRs associated with disease progression	4
Table 2.1 Oligonucleotide Sequences and Predicted Thermodynamic Complexation Values	21
Table 2.2 Analytical Figures of Merit Describing Sensitivity of Reporter-Probe Biosensor for Let-7a	38
Table 3.1 Comparison of thermodynamic values and molecular structure information for reporter hairpins, reporter+probe complexes, and conversion of reporter+probe complexes to probe+analyte complexes	52
Table 4.1 Biosensor figures of merit (FOM) from the Cy5 emission center (670 nm) for the IAbRQ Cy5 reporters with 0 and 18 spacers excited at 740 and 945 nm	79
Table 4.2 Comparison of Cy3 Cy5 biosensor FOM from reporters with 0 and 18 spacers	80
Table 4.3 Comparison of 6-FAM ATTO 633 biosensor FOM from reporters with 0 and 18 spacers	81
Table 5.1. Nucleic acid sequences	95
Table 5.2. Thermodynamic calculations for reporter hairpins, reporter+probe biosensors, and probes binding to analytes/off-analytes	100
Table 5.3 Percent quenching ΔS_Q and percent enhancement ΔS_E	101
Table 5.4 Analytical slope and limits of detection (LODs) for both R1+P1 and R2+P2 reporter+probe biosensors	105
Table 6.1 Possible pitfalls of reporter+probe biosensors and potential solutions	108

Displacement-based Fluorescent microRNA Biosensors: Design Principles and Analytical Metrics

Chapter 1. Introduction

1.1 MicroRNAs

MicroRNAs (miRNAs or miRs) are an emerging class of biomarkers that may aid in understanding, diagnosing, and tracking both normal and disease cell progression. One major role of miRs in biology is to regulate protein expression by interacting with messenger RNA (mRNA) to disrupt translation, leading to a decrease in protein concentration. If the protein manufacture is disrupted long enough to significantly decrease their concentration in the cell, it can lead to altered cellular function. In addition to different miRs being regulated different based on cell- or tissue-type, miRs are found to be dysregulated differently depending on the disease. In different diseases, miRs will be upregulated or downregulated compared to normal cells, which could result in altered phenotype.¹⁻⁵ Differential expression of miR has been associated with the regulation and progression of numerous cancers such as breast⁶⁻⁸ thyroid^{9,10}, colorectal^{11,12}, prostate^{13,14}, lung,^{15,16} and ovarian^{17,18}. Although miRNAs are critical in the regulation of cancers, many other diseases such as cardiovascular diseases¹⁹, neurological diseases²⁰, and immunological diseases²¹ also exhibit miRNA-based regulation. If intracellular miRs can be monitored, then more information about disease progression can be obtained. To develop our own molecular tools to detect and study miRs, we selected several conserved disease-associated miRs as model systems: let7a, miR-26a, miR-27a, miR-29b, and miR-146a.²²⁻³⁸

To understand how microRNAs (miRs) are created we rely on the central dogma of molecular biology. In its simplified form the central dogma states that DNA leads to the formation of RNA that in turn leads to the formation of proteins.³⁹ DNA (deoxyribonucleic acid) in the nucleus of the cell is transcribed by polymerases into RNA (ribonucleic acid). These RNAs can either be translated into proteins (coding RNA) or can perform an array of alternative functions within the cell (non-coding RNA). One particular class of non-coding RNAs that serve a regulatory function are known as microRNAs (miR). MiRs are an important genetic regulator because they bind to mRNA to inhibit translation of proteins.

In the first step of miR creation (Figure 1.1), RNA polymerase II transcribes what is known as the primary miR (pri-miR). The Pri-miR is a hairpin structured nucleic acid that contains both the 5-prime and 3-prime mature miR sequences. In the second step, a protein known as Drosha processes the pri-miR by removing a portion of the sequence to form what is referred to as a precursor miR (pre-miR). Third, the pre-miR is then exported out of the nucleus into the cytoplasm by an exportin protein. Fourth, the enzyme Dicer converts the pre-miR from a hairpin to a double-stranded mature miR. Fifth, the Argonaute protein binds to the double-stranded miR to form RISC (RNA-induced silencing complex, containing Argonaute, Dicer, and transactivation response RNA binding protein or TRBP). In Figure 1.1, this is known as the miR-RISC complex. During this process, one strand (known as the guide strand) is bound to Argonaute; the other strand (the anti-sense strand) is discarded. After miR-RISC complex is formed it is able to regulate mRNA via three primary mechanisms⁴⁰⁻⁴³:

Mechanism 1. When the miR-RISC complex binds to a partially complementary mRNA, the ribosome will be hindered by the partially double-stranded miR-mRNA complex. This will cause the ribosome to dissociate from the mRNA strand, leading to the termination of translation.

Mechanism 2. If the miR is completely complementary to its mRNA target, RISC will initiate degradation of the mRNA through its endonuclease activity.

Mechanism 3. When the miR-RISC complex binds to a partially complementary mRNA, RISC can deadenylate the mRNA, leading to the mRNA being labeled for degradation.

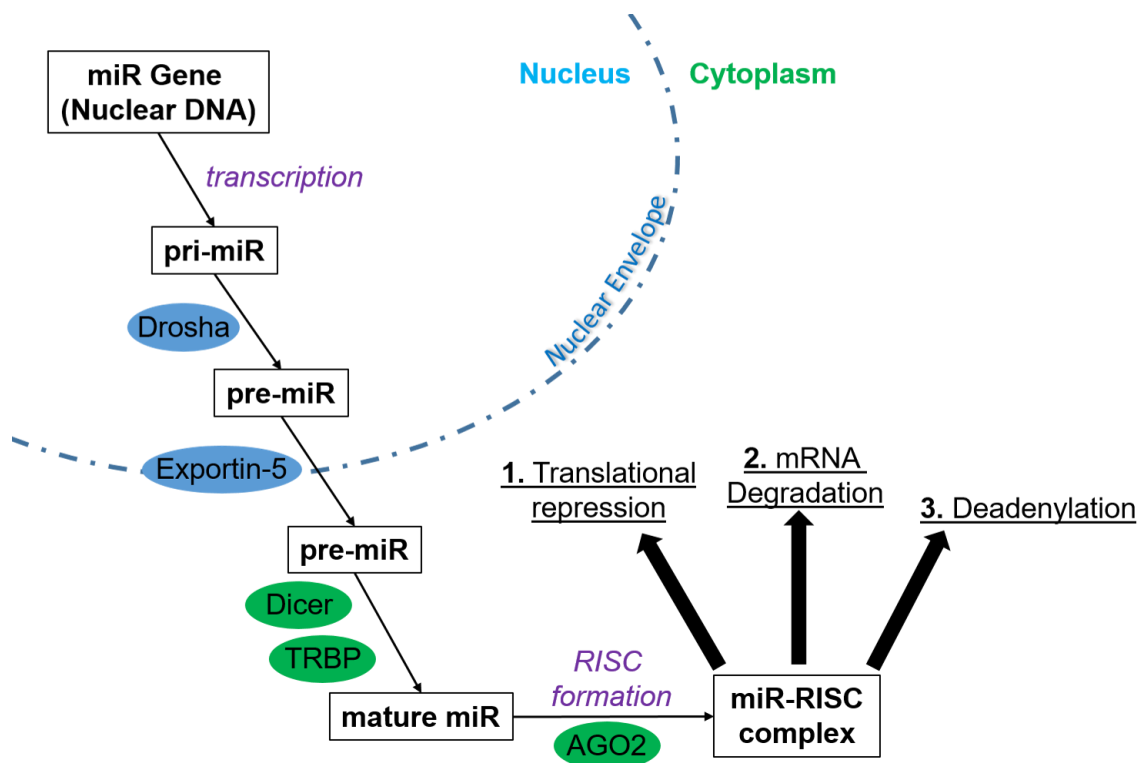


Figure 1.1 Biological synthesis of miRNAs from DNA to mature miRNAs⁴³. Adapted from Li et al. *Chem. Soc. Rev.* **2014**, 43, 506

1.1.1 MicroRNAs as biomarkers

Monitoring changes in microRNA (miR) biomarkers can illuminate important cellular regulation pathways and may help identify early onset of disease. *In situ* miR analysis is needed to fully understand how miR regulate gene expression as miR often target different messenger RNA in a temporal (intracellular location), cell-, and tissue-specific manner.⁴⁴ This is because each cell and tissue type has a specific miR profile that requires the ability to monitor miR expression *in situ*.^{45–47} Thus, *in situ* analysis is critical to validate disease-associated miRNA derived from RNAseq and other chip-based methods. Furthermore, *in situ* analysis can serve to develop clinical diagnostics⁴⁴. A majority of the current biosensor technologies for *in situ* analysis were not designed for the demands of miRNA analysis.^{48–50} To achieve this goal miRNA biosensors are needed that can detect low levels and small changes in miRNA concentration, particularly in the femtomolar to nanomolar range.^{1–5}

1.1.2 Disease-related miRs of interest

A well-known disease for us to design a sensor around is miRs as potential biomarkers in Triple negative breast cancer (TNBC). Many breast cancers respond to chemotherapy targeting through one or more receptors: 1) estrogen receptor (ER), 2) progesterone receptor (PR), or 3) human epidermal growth factor receptor (HER2). Cancers that exhibit decreased expression for these receptors and do not respond to their targeted hormone therapies are known as being triple-negative, hence their namesake TNBC.⁵¹ Changes in different miR expression have been previously associated with the progression of TNBC.⁵² One miR that has been associated with TNBC progression is miR-146a.^{34–37} Table 1.1 lists five different miRs that have been found to be associated with various different diseases and are of interest for potential biomarkers.

Table 1.1 Sequences for miRs associated with disease progression. The ‘5p’ indicates it is the portion of the double-stranded mature miR that is on the 5-prime end, and in this case is guide strand. *mmu* (*mus musculus*) describes mouse-derived miR sequences, and *hsa* (*homo sapiens*) is human-derived.

microRNA	Sequence (5' to 3')	Example disease-associated function
mmu-let-7a-5p	UGAGGUAGUAGGUUGUAUAGUU	Decreased expression levels associated with carcinogenesis of breast cancer. ²⁷
mmu-miR-26a-2-3p	CCUGUUCUUGAUUACUUGUUUC	Down-regulation in breast tissue associated with an increase in breast cancer through EZH2. ³⁸
mmu-miR-27a-5p	GCUGGUUUCAUAUGGUGGUUUA	Shows oncogenic activity in breast cancer cells by regulating ZBTB10, a repressor of specificity proteins (Sp) that contribute to cancer phenotype. ³²
mmu-miR-29b-1-5p	UGAGAACUGAAUCCAUGGGUU	Expression induced by GATA3, increased levels associated with decreased angiogenesis and metastasis of breast cancer. ³³
hsa-miR-146a-5p	UGAGAACUGAAUCCAUGGGUU	Upregulated in TNBC - associated with increased tumorigenesis and altered p53 function. ³⁴

1.2 Conventional Detection Methods

1.2.1 In vitro methods

In vitro methods such as quantitative reverse-transcriptase polymerase chain reaction^{53,54} (qRT-PCR), microarrays^{6,55–57}, and Northern blotting^{54,58–61} are routine for nucleic acids, but these methods only work for cell lysates and not *in situ* cellular analysis – which has already been outlined as superior to *in vitro*. For detection of miR, qRT-PCR or microarray technologies can be

quantitative and can achieve some degree of multiplexing, but they require amplification (some requiring thermocycling) to increase the signal to a detectable level.⁶²

With qRT-PCR, first the miR sequences are reverse-transcribed into cDNA (complementary DNA). Then primers amplify the cDNA strands and fluorescent probe strands (such as TaqMan®) are added to detect the miR as they are amplified. However, detection of low levels of miRs with multiplex PCR is susceptible to amplification of off-analytes, thereby reducing selectivity.³ Another major limitation of PCR and chip based methods is the requirement of extracting whole RNA from cells and tissue. If the miR are only expressed at low levels and in a few out of hundreds of cells, then the miR signature will be lost during dilution from pooling the cells for analysis. Moreover, these two methods cannot image miRs in cells and tissues where the miRs are naturally expressed. This is a significant limitation because miRs often target different messenger-RNA in a temporal, cell, and tissue specific manner.⁴⁴ This is what causes different types of cancers to occur in different places in the body, and why types of cancers are most likely to be classified based on where they originate.

RNA sequencing methods are commonly known as RNA-Seq, and in particular miRNA-Seq for miR analysis.⁶³⁻⁶⁶ Similar to techniques required for qRT-PCR, the miRs need to be reverse transcribed to cDNA. Next adapters are ligated onto the cDNA library, and then the strands are conjugated onto a substrate. Next the strands are amplified and finally sequenced-by-synthesis (SBS, Illumina Inc.)

Microarrays are another way to screen for miRs in cell lysates (Figure 1.2).^{67,68} Nucleic acids are first purified from the lysate, and then miRs are reversed transcribed into cDNA (similar to both qRT-PCR and RNA-Seq). This new cDNA is then tagged with a fluorescent dye. The microarray plate is set up with conjugated DNA sequences of the desired analyte and the cDNA is flowed over the plate. The desired cDNA will then stick to the conjugated probes after washing, and will light up when excited by a light source.

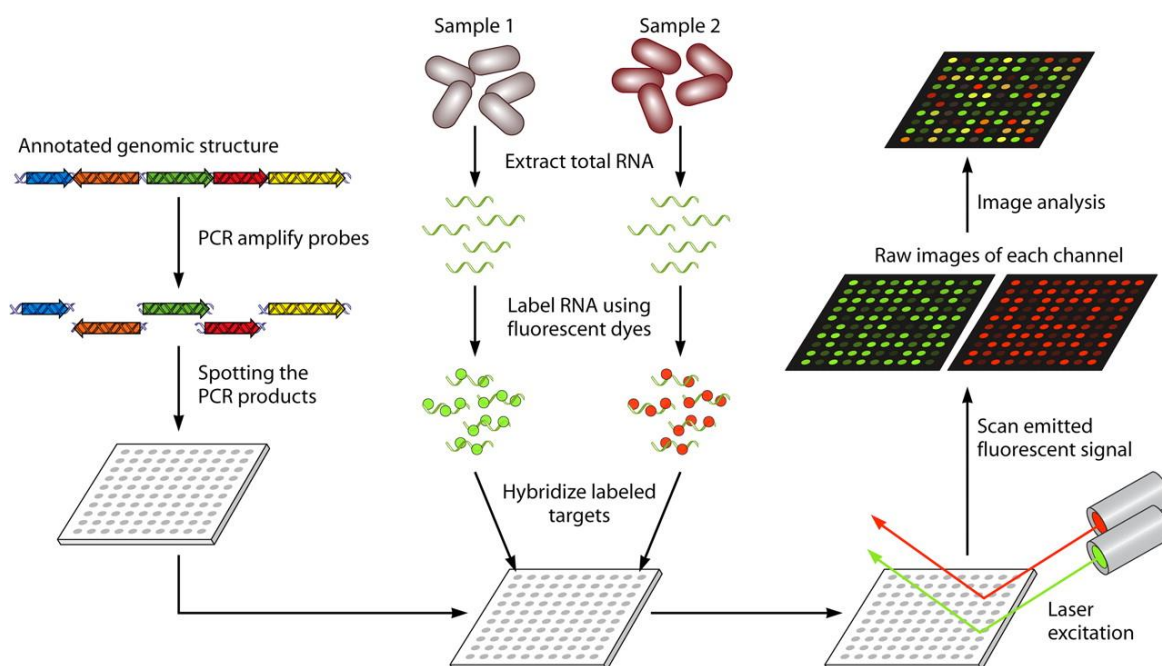


Figure 1.2 Microarray methodology⁶⁸ Melissa B. Miller, and Yi-Wei Tang Clin. Microbiol. Rev. 2009;22:611-633

1.2.2 In situ methods

In general, in situ miRNA detection is qualitative or semi-quantitative.^{5,44,69,70} Recent reports indicate that in situ detection of miRNA profiles in cells and tissues as a means for diagnostics and the study of disease progression are limited by technology capabilities.^{48,49} Progress in intracellular and whole tissue analysis has been hampered largely due to insufficient miRNA biosensors in terms of: 1) sensitivity, 2) selectivity, and 3) robustness.³

Biosensors that are currently used for in situ cellular analysis of RNA – including but not limited to miRs - are: molecular beacons⁷¹⁻⁸¹, dual molecular beacons^{73,82,83}, dual linear probes⁸⁴⁻⁸⁶, intercalator biosensors⁸⁷⁻⁸⁹, double-strand displacement biosensors^{90,91}, SmartFlares™ (previously known as Nanoflares)^{92,93}, and molecular sentinels^{94,95}. In general, these methods provide selectivity and high sensitivity but suffer from slow analysis, false positives, or a lack of high selectivity. Not all of these sensors are able to work for miR detection due to miRs being too small in size, and will only work for mRNA.

The most common *in situ* miR analysis tool is Fluorescence In-Situ Hybridization (FISH). In this method (Figure 1.3) the cells are fixed and permeabilized in order to transfect fluorescently-labeled probe strands.⁹⁶ These probe strands are fully complementary to their analyte. Before analysis, uncomplexed probes need to be rinsed away to remove non-specific binding. This along with potential secondary labeling steps (for signal amplification) are disadvantageous when a

quick time to result and live-cell analysis is desired.^{5,97} Standard fluorescence in situ hybridization (FISH) techniques have several limitations for low abundance miRNA detection: (1) loss of miRNA from copious rinsing steps, (2) often require secondary sensing with horseradish peroxidase or other enzymatic treatment, (3) long time-to-result, and (4) can only be used on fixed cells and tissues.^{5,97} Newer techniques such as MERFISH have significant capability in terms of multiplexing – meaning that an increased number of miRs that can be analyzed during FISH - but it still has the same limitations discussed previously.^{98,99} The enhancements that allow for multiplexing complicate the FISH process by requiring an increased number of FISH probes over normal FISH. This increased number of probes increases the number of photobleaching cycles needed for analysis, which significantly increases time-to-result. Currently this technology has not been used for miR analysis due to the increased probe length needed to characterize an mRNA strand.

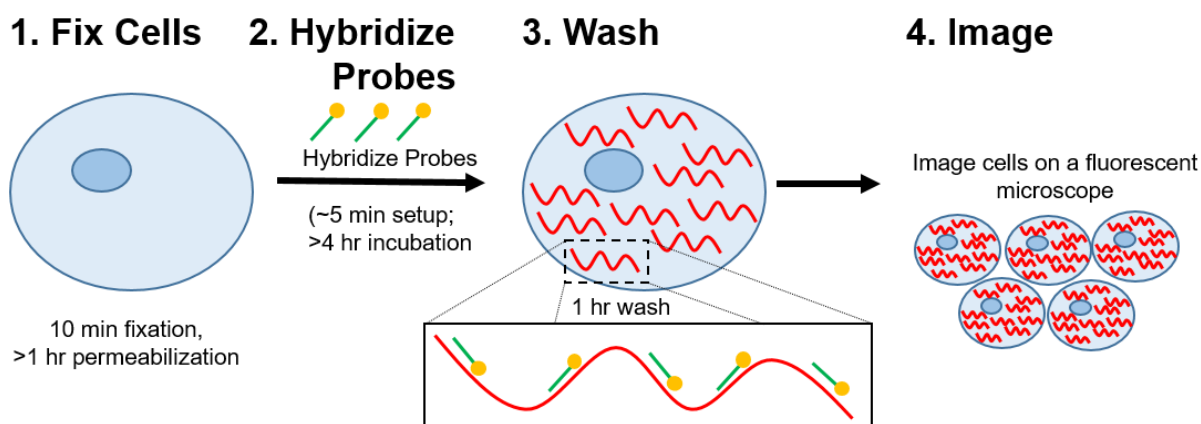


Figure 1.3 Fluorescence In-Situ Hybridization (FISH) protocol. Figure adapted from Stellaris RNA FISH protocol.¹⁰⁰

Molecular beacons and ratiometric bimolecular beacons^{72,74} can be transfected into cells to detect high levels of miR (nM or greater). Molecular beacons are typically nucleic acid strands that can form a stem-loop. One end of the strand has a dye and the other end has quenching molecule. The beacons OFF state has the strand in the stem-loop with dye and quencher next to each other (Figure 1.4a). In the presence of analyte, the molecular beacon will bind to the analyte, open the stem-loop, and moves the dye and quencher away from one another. The movement of the dye and quencher away from each other creates the detectable signal change (this is the sensors ON state). However, detection of low abundance miR is limited by intracellular nucleases that often degrade the biosensors.^{72,74} These nucleases increase false signals (positive and negative) by

cleaving nucleotides near to the dyes, liberating the dyes from the biosensor (Figure 1.4b). As a result, the background signal becomes very high and masks any signal from low levels of miR. With the wrong background intensity, signal from nanomolar or lower concentrations of miRNA is masked. Thus, minimal false signals are required to more accurately determine changes in miRNA expression without losing any analytical signal to the background. Another disadvantage of molecular beacons is their lack of selectivity for different miRs with similar sequences¹⁰¹, which we will comment on further in Chapter 2.

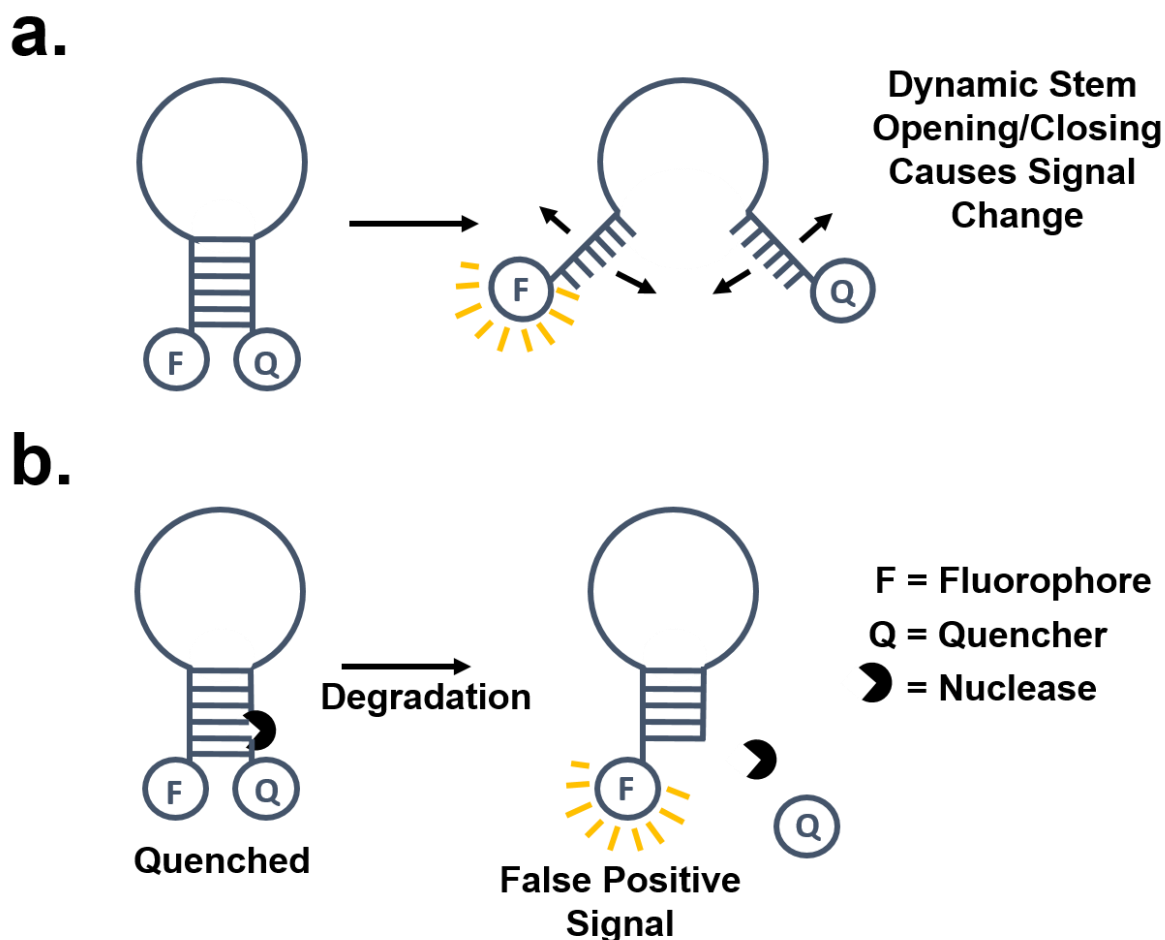


Figure 1.4 Diagram of molecular beacon design and potential problems. (a) shows how the biosensor’s signal is generated by moving a quencher molecule away from a fluorophore upon opening up of the hairpin. (b) shows how false signal generation can occur from nuclease degradation of the sensor.

Smartflares® (previously known as Nanoflares) are another miR sensor that is a ‘spherical nucleic acid’ with partially double-stranded nucleic acids bound to a gold nanoparticle.^{55,92,93,102} Spherical nucleic acids are able to enter and exit cells without transfection agents. The gold

nanoparticle has nucleic acid ‘probe’ strands functionalized to the surface that are complementary to the analyte of interest. Attached to the probe strands are partially complementary ‘flare’ strands that contain a fluorescent dye. The fluorescent dyes on the flare strands are quenched when attached to the probe strands because they are close to the gold nanoparticle. In the presence of miR analyte the flare will release, causing an increase in fluorescent signal. Both molecular beacons and Smartflares® have signal changes that are susceptible to false signal generation.

Dual molecular beacons and dual linear probes reduce enzymatic-related false positives, but both require a three to four nucleotide gap between adjacent oligonucleotide sensing strands.^{73,82–86} This gap, needed to reduce steric hindrance between the two sensing strands upon target binding, creates two potential problems: (1) true single nucleotide polymorphism (SNP) specificity cannot be realized without exhaustive optimization of the dual sensing strands and (2) stable binding to short 19 to 22 nucleotide RNAs will be thermodynamically difficult. Other approaches like dual linear probes suffer from worse nonspecific binding issues than dual molecular beacons.^{73,82,84–86}

Section 1.2.3 Signal generation methods

Other types of nucleic acid sensing applications have transducers other than organic dyes that include but are not limited to: (1) silver nanoclusters (AgNCs)^{103–110}, (2) plasmonic gold nanoparticles¹¹¹, (3) quantum dots¹¹², (4) carbon nanodots (C-dots)¹¹³, and (5) semiconducting polymer dots (Pdots)¹¹⁴. These methods either have toxic components, and/or have issues with manufacturing fluorophores with reproducible spectral properties. Signal generators that overcome these obstacles are currently being developed, and are not commercially available.

1.3 Thermodynamics of nucleic acid biosensors

In general, the recognition mechanisms for nucleic acid based biosensors are controlled by increased thermodynamic stability. Stabilization comes from nucleotide bases forming hydrogen bonds between complementary strands and pi-stacking within each strand. Gibbs energy and other thermodynamic metrics help predict if the biosensor’s recognition mechanism for the analyte will be favorable. Adenine-Thymine/Uracil (A-T/U) pairs only form two hydrogen bonds making them less stable than Guanine-Cytosine (G-C) pairs that form three hydrogen bonds. The fraction of A-

T/U contained in the sequences versus that of G-C will influence the binding stability and competition reactions for miR analyte recognition.¹¹⁵

The thermodynamics of the system is dependent on the type of nucleic acid binding. Different types of ribonucleic acids (DNA vs. RNA) have different strengths of interaction for DNA-DNA, RNA-RNA, and DNA-RNA hybridization. The thermodynamics of base pairing interactions can be calculated at the appropriate temperature for sensor analyte-detection, typically between 25 °C (room temperature) and 37 °C (ideal mammalian cell growth temperature). Often the nearest neighbor approximations enable the thermodynamic stability to be theoretically calculated.^{115–117} There are several freeware sources that will perform these tasks for sequences of interest.^{118–124}

1.4 Benefit of two-photon excitation for imaging

Although the sensors presented here work with single-photon techniques, I characterize the sensors for two-photon applications. The reason for two-photon characterization is because multi-photon microscopy for 3D cell and tissue imaging is gaining popularity. Multi-photon microscopy benefits from reduced levels of photobleaching, photodamage, and light scattering.¹²⁵ As a result, better penetration depth and lower background signal than conventional single-photon confocal methods are possible. These advantages are because multi-photon excitation only occurs at the focal point.¹²⁶

The future goal is to combine in-situ fluorescent molecular sensors and multi-photon imaging for analysis of intracellular miRs. The first step in achieving this goal is to optimize the biosensor design process to produce biosensors that will reliably respond to the desired analyte under multi-photon excitation. Combining miR biosensors with two-photon imaging of cells and tissues can lead to better understanding of disease progression.

1.5 FRET enhancement for signal generation

Förster resonance energy transfer or FRET, is a signal generation mechanism that employs two different dyes that undergo an energy transfer. This phenomenon only occurs if the two dyes have spectral overlap in that the ‘donor’ dye emission region overlaps with the excitation region of the ‘acceptor’ dye. The donor dye can be excited within its own excitation region, and – if the acceptor dye is close enough to the acceptor dye, then energy is transferred from the donor to the

acceptor non-radiatively. In this way the acceptor dye becomes excited and can then emit fluorescent photons within its own emission wavelength. This will only happen if the dyes are close enough together – within the Förster distance of 1 – 10 nm – and if the dyes are oriented in such a way that there can be coupling between their transition moments.

1.6 Development of the Reporter+Probe biosensor

The text herein describes the foundational work of developing the reporter+probe miR biosensor, a partially double-stranded biosensor with a toehold-mediated strand displacement analyte recognition mechanism. To overcome the limitations in the miR biosensor field, I have pioneered a new approach for luminescent biosensors. My innovative work combines the attributes of: 1) locked nucleic acids, 2) speed, 2) selectivity, 3) sensitivity, and 4) low false positives.

Chapter 2, entitled “Detection of miRNA Using a Double-Strand Displacement Biosensor with a Self-Complementary Reporter” contains the first reporter+probe biosensor design (at the time called reporter-probe biosensor). The reporter+probe biosensor in this chapter was designed for analyte *mmu-let-7a*. The signal generation mechanism in this sensor is a quenching mechanism, with both the donor (Cy3) and acceptor (Cy5) dyes decreasing in signal when progressing from reporter+probe to reporter-hairpin in the presence of analyte. This chapter demonstrates that the reporter+probe biosensor shows less susceptibility to false positive signal changes than conventional molecular beacons.

Chapter 3, entitled “Molecular Structure and thermodynamic predictions to create highly sensitive microRNA biosensors” contains design metrics for reliably and reproducibly making reporter+probe biosensors for different analytes, in this case *mmu-miR-26a-2-3p* and *mmu-miR-27a-5p*. The concept of an ‘ideal’ and ‘non-ideal’ hairpin was introduced, these fundamental principles help understand how to design reliable sensors. Other thermodynamic considerations were defined in order to describe how to design a reporter+probe biosensor for any miR analyte. The reporter+probe biosensors operated in a quenching modality much like the sensor in chapter 2.

Chapter 4, entitled “Förster resonance energy transfer to impart signal-on and -off capabilities in a single microRNA biosensor” contains a study on how polyethylene glycol spacer molecules (hexaethylene glycol, 18-spacers) affect the FRET enhancement potential for different donor/acceptor dye pairs (Cy3/Cy5 and 6-FAM/ATTO 633). A previously described sensor design

for mmu-miR-26a-2-3p (Chapter 3) was used for this analysis. Sensors were found to have FRET quenching and FRET enhancement properties depending on the excitation wavelength, and it was found that longer spacer molecules increased FRET enhancement ability, while decreasing the FRET quenching.

Chapter 5, entitled “MicroRNA biosensor design strategies to mitigate off-analyte response” contains a study on how to design reporter+probe biosensors to increase specificity for a given analyte, while decreasing interactions between the sensor and off-analytes with similar sequence to the given analyte.

Chapter 6 contains the conclusions and future directions for the reporter+probe biosensor, and a forward-look at the miR biosensor field.

1.7 References

- (1) Liang, Y.; Ridzon, D.; Wong, L.; Chen, C. *BMC Genomics* **2007**, *8* (1), 166.
- (2) Subkhankulova, T.; Gilchrist, M. J.; Livesey, F. J. *BMC Genomics* **2008**, *9* (1), 268.
- (3) Shum, J.; Paul, N. *Anal. Biochem.* **2009**, *388* (2), 266.
- (4) Ragan, C.; Zuker, M.; Ragan, M. A. *PLoS Comput. Biol.* **2011**, *7* (2).
- (5) Sempere, L. F. *Expert Rev. Mol. Diagn.* **2014**, *14* (7), 853.
- (6) Volinia, S.; Calin, G. A.; Liu, C.-G.; Ambs, S.; Cimmino, A.; Petrocca, F.; Visone, R.; Iorio, M.; Roldo, C.; Ferracin, M.; Prueitt, R. L.; Yanaihara, N.; Lanza, G.; Scarpa, A.; Vecchione, A.; Negrini, M.; Harris, C. C.; Croce, C. M. *Proc. Natl. Acad. Sci. U. S. A.* **2006**, *103* (7), 2257.
- (7) Zhu, S.; Wu, H.; Wu, F.; Nie, D.; Sheng, S.; Mo, Y.-Y. *Cell Res.* **2008**, *18* (3), 350.
- (8) Iorio, M. V.; Ferracin, M.; Liu, C.-G.; Veronese, A.; Spizzo, R.; Sabbioni, S.; Magri, E.; Pedriali, M.; Fabbri, M.; Campiglio, M. *Cancer Res.* **2005**, *65* (16), 7065.
- (9) Mitomo, S.; Maesawa, C.; Ogasawara, S.; Iwaya, T.; Shibazaki, M.; Yashima-Abo, A.; Kotani, K.; Oikawa, H.; Sakurai, E.; Izutsu, N.; Kato, K.; Komatsu, H.; Ikeda, K.; Wakabayashi, G.; Masuda, T. *Cancer Sci.* **2008**, *99* (2), 280.
- (10) Visone, R.; Russo, L.; Pallante, P.; Martino, I. D.; Ferraro, A.; Leone, V.; Borbone, E.; Petrocca, F.; Alder, H.; Croce, C. M.; Fusco, A. *Endocr. Relat. Cancer* **2007**, *14* (3), 791.
- (11) Akao, Y.; Nakagawa, Y.; Naoe, T. *Oncol. Rep.* **2006**, *16* (4), 845.
- (12) Shi, B.; Sepp-Lorenzino, L.; Prisco, M.; Linsley, P.; deAngelis, T.; Baserga, R. *J. Biol. Chem.* **2007**, *282* (45), 32582.
- (13) Sylvestre, Y.; Guire, V. D.; Querido, E.; Mukhopadhyay, U. K.; Bourdeau, V.; Major, F.; Ferbeyre, G.; Chartrand, P. *J. Biol. Chem.* **2007**, *282* (4), 2135.
- (14) Shi, X.-B.; Xue, L.; Yang, J.; Ma, A.-H.; Zhao, J.; Xu, M.; Tepper, C. G.; Evans, C. P.; Kung, H.-J.; White, R. W. deVere. *Proc. Natl. Acad. Sci.* **2007**, *104* (50), 19983.
- (15) Johnson, S. M.; Grosshans, H.; Shingara, J.; Byrom, M.; Jarvis, R.; Cheng, A.; Labourier, E.; Reinert, K. L.; Brown, D.; Slack, F. J. *Cell* **2005**, *120* (5), 635.
- (16) Fabbri, M.; Garzon, R.; Cimmino, A.; Liu, Z.; Zanesi, N.; Callegari, E.; Liu, S.; Alder, H.; Costinean, S.; Fernandez-Cymering, C.; Volinia, S.; Guler, G.; Morrison, C. D.;

- Chan, K. K.; Marcucci, G.; Calin, G. A.; Huebner, K.; Croce, C. M. *Proc. Natl. Acad. Sci.* **2007**, *104* (40), 15805.
- (17) Shell, S.; Park, S.-M.; Radjabi, A. R.; Schickel, R.; Kistner, E. O.; Jewell, D. A.; Feig, C.; Lengyel, E.; Peter, M. E. *Proc. Natl. Acad. Sci.* **2007**, *104* (27), 11400.
- (18) Giannakakis, A.; Sandaltzopoulos, R.; Greshock, J.; Liang, S.; Huang, J.; Hasegawa, K.; Li, C.; O'Brien-Jenkins, A.; Katsaros, D.; Weber, B. L.; Simon, C.; Coukos, G.; Zhang, L. *Cancer Biol. Ther.* **2008**, *7* (2), 255.
- (19) Ikeda, S.; Kong, S. W.; Lu, J.; Bisping, E.; Zhang, H.; Allen, P. D.; Golub, T. R.; Pieske, B.; Pu, W. T. *Physiol. Genomics* **2007**, *31* (3), 367.
- (20) Fiore, R.; Siegel, G.; Schratt, G. *Biochim. Biophys. Acta BBA - Gene Regul. Mech.* **2008**, *1779* (8), 471.
- (21) Taganov, K. D.; Boldin, M. P.; Chang, K.-J.; Baltimore, D. *Proc. Natl. Acad. Sci.* **2006**, *103* (33), 12481.
- (22) Pasquinelli, A. E.; Reinhart, B. J.; Slack, F.; Martindale, M. Q.; Kuroda, M. I.; Maller, B.; Hayward, D. C.; Ball, E. E.; Degnan, B.; Müller, P. *Nature* **2000**, *408* (6808), 86.
- (23) Pasquinelli, A. E.; McCoy, A.; Jiménez, E.; Salo, E.; Ruvkun, G.; Martindale, M. Q.; Baguna, J. *Evol. Dev.* **2003**, *5* (4), 372.
- (24) Roush, S.; Slack, F. J. *Trends Cell Biol.* **2008**, *18* (10), 505.
- (25) Reinhart, B. J.; Slack, F. J.; Basson, M.; Pasquinelli, A. E.; Bettinger, J. C.; Rougvie, A. E.; Horvitz, H. R.; Ruvkun, G. *Nature* **2000**, *403* (6772), 901.
- (26) Esquela-Kerscher, A.; Slack, F. J. *Nat. Rev. Cancer* **2006**, *6* (4), 259.
- (27) Shi, X.-B.; Tepper, C. G.; deVere White, R. W. *Cell Cycle* **2008**, *7* (11), 1529.
- (28) Deng, M.; Tang, H.; Lu, X.; Liu, M.; Lu, X.; Gu, Y.; Liu, J.; He, Z. *PLoS ONE* **2013**, *8* (8), e72662.
- (29) Gao, J.; Li, L.; Wu, M.; Liu, M.; Xie, X.; Guo, J.; Tang, H.; Xie, X. *PLoS ONE* **2013**, *8* (6), e65138.
- (30) Dang, X.; Ma, A.; Yang, L.; Hu, H.; Zhu, B.; Shang, D.; Chen, T.; Luo, Y. *Cancer Genet.* **2012**, *205* (3), 113.
- (31) Li, J.; Wang, Y.; Song, Y.; Fu, Z.; Yu, W. *Mol. Cancer* **2014**, *13* (1), 193.
- (32) Mertens-Talcott, S. U.; Chintharlapalli, S.; Li, X.; Safe, S. *Cancer Res.* **2007**, *67* (22), 11001.
- (33) Melo, S. A.; Kalluri, R. *Nat. Cell Biol.* **2013**, *15* (2), 139.
- (34) Sandhu, R.; Rein, J.; D'Arcy, M.; Herschkowitz, J. I.; Hoadley, K. A.; Troester, M. A. *Carcinogenesis* **2014**, *35* (11), 2567.
- (35) Li, Y.; Xu, Y.; Yu, C.; Zuo, W. *Cancer Biomark.* **2015**, *15* (6), 881.
- (36) M'hamed, I. F.; Privat, M.; Ponelle, F.; Penault-Llorca, F.; Kenani, A.; Bignon, Y.-J. *Cell. Oncol.* **2015**, *38* (6), 433.
- (37) Zavala, V.; Pérez-Moreno, E.; Tapia, T.; Camus, M.; Carvallo, P. *Cancer Biomark.* **2016**, *16* (1), 99.
- (38) Lu, J.; He, M.-L.; Wang, L.; Chen, Y.; Liu, X.; Dong, Q.; Chen, Y.-C.; Peng, Y.; Yao, K.-T.; Kung, H.-F.; Li, X.-P. *Cancer Res.* **2011**, *71* (1), 225.
- (39) Crick, F. *Nature* **1970**, *227* (5258), 561.
- (40) Winter, J.; Jung, S.; Keller, S.; Gregory, R. I.; Diederichs, S. *Nat. Cell Biol.* **2009**, *11* (3), 228.
- (41) Eulalio, A.; Huntzinger, E.; Nishihara, T.; Rehwinkel, J.; Fauser, M.; Izaurralde, E. *RNA* **2009**, *15* (1), 21.

- (42) Wu, L.; Fan, J.; Belasco, J. G. *Proc. Natl. Acad. Sci. U. S. A.* **2006**, *103* (11), 4034.
- (43) Li, J.; Tan, S.; Kooger, R.; Zhang, C.; Zhang, Y. *Chem. Soc. Rev.* **2014**, *43* (2), 506.
- (44) Croce, C. M. *Nat. Rev. Genet.* **2009**, *10* (10), 704.
- (45) Leung, A. K.; Calabrese, J. M.; Sharp, P. A. *Proc. Natl. Acad. Sci.* **2006**, *103* (48), 18125.
- (46) Liu, J.; Valencia-Sanchez, M. A.; Hannon, G. J.; Parker, R. *Nat. Cell Biol.* **2005**, *7* (7), 719.
- (47) Nishi, K.; Takahashi, T.; Suzawa, M.; Miyakawa, T.; Nagasawa, T.; Ming, Y.; Tanokura, M.; Ui-Tei, K. *Nucleic Acids Res.* **2015**, *43* (20), 9856.
- (48) Glinsky, G. V. *J. Clin. Invest.* **2013**, *123* (6), 2350.
- (49) Sternberg, J. B.; Pierce, N. A. *Nano Lett.* **2014**, *14* (8), 4568.
- (50) Graybill, R. M.; Bailey, R. C. *Anal. Chem.* **2016**, *88* (1), 431.
- (51) Foulkes, W. D.; Smith, I. E.; Reis-Filho, J. S. *N. Engl. J. Med.* **2010**, *363* (20), 1938.
- (52) D'Ippolito, E.; Iorio, M. V. *Int. J. Mol. Sci.* **2013**, *14* (11), 22202.
- (53) Chen, C.; Ridzon, D. A.; Broomer, A. J.; Zhou, Z.; Lee, D. H.; Nguyen, J. T.; Barbisin, M.; Xu, N. L.; Mahuvakar, V. R.; Andersen, M. R.; Lao, K. Q.; Livak, K. J.; Guegler, K. *J. Nucleic Acids Res.* **2005**, *33* (20), e179.
- (54) Calin, G. A.; Liu, C.-G.; Sevignani, C.; Ferracin, M.; Felli, N.; Dumitru, C. D.; Shimizu, M.; Cimmino, A.; Zupo, S.; Dono, M.; Dell'Aquila, M. L.; Alder, H.; Rassenti, L.; Kipps, T. J.; Bullrich, F.; Negrini, M.; Croce, C. M. *Proc. Natl. Acad. Sci. U. S. A.* **2004**, *101* (32), 11755.
- (55) Alhasan, A. H.; Kim, D. Y.; Daniel, W. L.; Watson, E.; Meeks, J. J.; Thaxton, C. S.; Mirkin, C. A. *Anal. Chem.* **2012**, *84* (9), 4153.
- (56) Liu, C.-G.; Calin, G. A.; Meloon, B.; Gamliel, N.; Sevignani, C.; Ferracin, M.; Dumitru, C. D.; Shimizu, M.; Zupo, S.; Dono, M.; Alder, H.; Bullrich, F.; Negrini, M.; Croce, C. M. *Proc. Natl. Acad. Sci. U. S. A.* **2004**, *101* (26), 9740.
- (57) Thomson, J. M.; Parker, J.; Perou, C. M.; Hammond, S. M. *Nat. Methods* **2004**, *1* (1), 47.
- (58) Várallyay, É.; Burgyán, J.; Havelda, Z. *Nat. Protoc.* **2008**, *3* (2), 190.
- (59) Valoczi, A.; Hornyik, C.; Varga, N.; Burgyan, J.; Kauppinen, S.; Havelda, Z. *Nucleic Acids Res.* **2004**, *32* (22), e175.
- (60) Calin, G. A.; Sevignani, C.; Dumitru, C. D.; Hyslop, T.; Noch, E.; Yendamuri, S.; Shimizu, M.; Rattan, S.; Bullrich, F.; Negrini, M.; Croce, C. M. *Proc. Natl. Acad. Sci. U. S. A.* **2004**, *101* (9), 2999.
- (61) Viereg, J. R.; Nelson, H. M.; Stoltz, B. M.; Pierce, N. A. *J. Am. Chem. Soc.* **2013**, 130618134902008.
- (62) Schmittgen, T. D. *Nucleic Acids Res.* **2004**, *32* (4), 43e.
- (63) Eminaga, S.; Christodoulou, D. C.; Vigneault, F.; Church, G. M.; Seidman, J. G. *Curr. Protoc. Mol. Biol.* **2013**, *04*, Unit.
- (64) Chang, Y.-Y.; Kuo, W.-H.; Hung, J.-H.; Lee, C.-Y.; Lee, Y.-H.; Chang, Y.-C.; Lin, W.-C.; Shen, C.-Y.; Huang, C.-S.; Hsieh, F.-J.; Lai, L.-C.; Tsai, M.-H.; Chang, K.-J.; Chuang, E. Y. *Mol. Cancer* **2015**, *14*, 36.
- (65) Schee, K.; Lorenz, S.; Worren, M. M.; Günther, C.-C.; Holden, M.; Hovig, E.; Fodstad, Ø.; Meza-Zepeda, L. A.; Flatmark, K. *PLOS ONE* **2013**, *8* (6), e66165.
- (66) Szeto, C. Y.-Y.; Lin, C. H.; Choi, S. C.; Yip, T. T. C.; Ngan, R. K.-C.; Tsao, G. S.-W.; Li Lung, M. *FEBS Open Bio* **2014**, *4*, 128.
- (67) Li, W.; Ruan, K. *Anal. Bioanal. Chem.* **2009**, *394* (4), 1117.
- (68) Miller, M. B.; Tang, Y.-W. *Clin. Microbiol. Rev.* **2009**, *22* (4), 611.

- (69) Hanna, J.; Wimberly, H.; Kumar, S.; Slack, F.; Agarwal, S.; Rimm, D. *BioTechniques* **2012**, *52* (4).
- (70) Zhang, X.; Song, Y.; Shah, A. Y.; Lekova, V.; Raj, A.; Huang, L.; Behlke, M. A.; Tsourkas, A. *Nucleic Acids Res.* **2013**, *41* (15), e152.
- (71) Tyagi, S.; Kramer, F. R. *Nat. Biotechnol.* **1996**, *14* (3), 303.
- (72) Li, J. J.; Geyer, R.; Tan, W. *Nucleic Acids Res.* **2000**, *28* (11), e52.
- (73) Santangelo, P. J.; Nix, B.; Tsourkas, A.; Bao, G. *Nucleic Acids Res.* **2004**, *32* (6), e57.
- (74) Chen, A. K.; Davydenko, O.; Behlke, M. A.; Tsourkas, A. *Nucleic Acids Res.* **2010**, *38* (14), e148.
- (75) Baker, M. B.; Bao, G.; Searles, C. D. *Nucleic Acids Res.* **2012**, *40* (2), e13.
- (76) Ko, H. Y.; Lee, J.; Joo, J. Y.; Lee, Y. S.; Heo, H.; Ko, J. J.; Kim, S. *Sci. Rep.* **2014**, *4*.
- (77) Ko, H. Y.; Lee, J.; Moon, S. U.; Lee, Y. S.; Cho, S.; Kim, S. *Chem Commun* **2015**, *51* (93), 16679.
- (78) Ko, H. Y.; Lee, J.; Lee, Y. S.; Gu, H.-N.; Ali, B. A.; Al-Khedhairi, A. A.; Heo, H.; Cho, S.; Kim, S. *Chem Commun* **2015**, *51* (11), 2159.
- (79) Conlon, P.; Yang, C. J.; Wu, Y.; Chen, Y.; Martinez, K.; Kim, Y.; Stevens, N.; Marti, A. A.; Jockusch, S.; Turro, N. J.; Tan, W. *J. Am. Chem. Soc.* **2008**, *130* (1), 336.
- (80) Tan, X.; Chen, W.; Lu, S.; Zhu, Z.; Chen, T.; Zhu, G.; You, M.; Tan, W. *Anal. Chem.* **2012**, *84* (19), 8272.
- (81) Yao, Q.; Zhang, A.; Ma, H.; Lin, S.; Wang, X.; Sun, J.; Chen, Z. *Mol. Cell. Probes* **2012**, *26* (5), 182.
- (82) Tsourkas, A.; Behlke, M. A.; Xu, Y.; Bao, G. *Anal. Chem.* **2003**, *75* (15), 3697.
- (83) King, F. W.; Liszewski, W.; Ritner, C.; Bernstein, H. S. *Stem Cells Dev.* **2011**, *20* (3), 475.
- (84) Mergny, J. L.; Boutorine, A. S.; Garestier, T.; Belloc, F.; Rougee, M.; Bulychev, N. V.; Koshkin, A. A.; Bourson, J.; Lebedev, A. V.; Valeur, B. *Nucleic Acids Res.* **1994**, *22* (6), 920.
- (85) Tsuji, A.; Koshimoto, H.; Sato, Y.; Hirano, M.; Sei-Iida, Y.; Kondo, S.; Ishibashi, K. *Biophys. J.* **2000**, *78* (6), 3260.
- (86) Tsuji, A.; Sato, Y.; Hirano, M.; Suga, T.; Koshimoto, H.; Taguchi, T.; Ohsuka, S. *Biophys. J.* **2001**, *81* (1), 501.
- (87) Sau, S. P.; Kumar, P.; Sharma, P. K.; Hrdlicka, P. J. *Nucleic Acids Res.* **2012**, *40* (21), e162.
- (88) Sau, S. P.; Hrdlicka, P. J. *J. Org. Chem.* **2012**, *77* (1), 5.
- (89) Bag, S. S.; Kundu, R.; Jana, S. *Tetrahedron Lett.* **2013**, *54* (21), 2627.
- (90) Baker, B. A.; Mahmoudabadi, G.; Milam, V. T. *Colloids Surf. B Biointerfaces* **2013**, *102*, 884.
- (91) Hemphill, J.; Deiters, A. *J. Am. Chem. Soc.* **2013**, 130624125941004.
- (92) Prigodich, A. E.; Randeria, P. S.; Briley, W. E.; Kim, N. J.; Daniel, W. L.; Giljohann, D. A.; Mirkin, C. A. *Anal. Chem.* **2012**, *84* (4), 2062.
- (93) Yang, Y.; Huang, J.; Yang, X.; Quan, K.; Wang, H.; Ying, L.; Xie, N.; Ou, M.; Wang, K. *J. Am. Chem. Soc.* **2015**, *137* (26), 8340.
- (94) Wabuyele, M. B.; Vo-Dinh, T. *Anal. Chem.* **2005**, *77* (23), 7810.
- (95) Cao, Y. C.; Jin, R.; Mirkin, C. A. *Science* **2002**, *297* (5586), 1536.
- (96) Santangelo, P.; Nitin, N.; Bao, G. *Ann. Biomed. Eng.* **2006**, *34* (1), 39.
- (97) de Planell-Saguer, M.; Rodicio, M. C. *Clin. Biochem.* **2013**, *46* (10–11), 869.

- (98) Chen, K. H.; Boettiger, A. N.; Moffitt, J. R.; Wang, S.; Zhuang, X. *Science* **2015**, *348* (6233), aaa6090.
- (99) Moffitt, J. R.; Hao, J.; Bambah-Mukku, D.; Lu, T.; Dulac, C.; Zhuang, X. *Proc. Natl. Acad. Sci.* **2016**, *113* (50), 14456.
- (100) Stellaris RNA FISH | LGC Biosearch Technologies <https://www.biosearchtech.com/support/education/stellaris-rna-fish> (accessed Jun 7, 2017).
- (101) Almlie, C. K.; Larkey, N. E.; Burrows, S. M. *Anal Methods* **2015**, *7* (17), 7296.
- (102) Thaxton, C. S.; Georganopoulou, D. G.; Mirkin, C. A. *Clin. Chim. Acta* **2006**, *363* (1–2), 120.
- (103) Yeh, H.-C.; Sharma, J.; Han, J. J.; Martinez, J. S.; Werner, J. H. *Nano Lett.* **2010**, *10* (8), 3106.
- (104) Yeh, H.-C.; Sharma, J.; Han, J.; Martinez, J.; Werner, J. *IEEE Nanotechnol. Mag.* **2011**, *5* (2), 28.
- (105) Yeh, H.-C.; Sharma, J.; Shih, I.-M.; Vu, D. M.; Martinez, J. S.; Werner, J. H. *J. Am. Chem. Soc.* **2012**, *134* (28), 11550.
- (106) Obliosca, J. M.; Liu, C.; Yeh, H.-C. *Nanoscale* **2013**, *5* (18), 8443.
- (107) Obliosca, J. M.; Babin, M. C.; Liu, C.; Liu, Y.-L.; Chen, Y.-A.; Batson, R. A.; Ganguly, M.; Petty, J. T.; Yeh, H.-C. *ACS Nano* **2014**, *8* (10), 10150.
- (108) Shah, P.; Rørvig-Lund, A.; Chaabane, S. B.; Thulstrup, P. W.; Kjaergaard, H. G.; Fron, E.; Hofkens, J.; Yang, S. W.; Vosch, T. *ACS Nano* **2012**, *6* (10), 8803.
- (109) Shah, P.; Thulstrup, P. W.; Cho, S. K.; Bhang, Y.-J.; Ahn, J. C.; Choi, S. W.; Bjerrum, M. J.; Yang, S. W. *The Analyst* **2014**, *139* (9), 2158.
- (110) Shah, P.; Choi, S. W.; Kim, H.; Cho, S. K.; Bhang, Y.-J.; Ryu, M. Y.; Thulstrup, P. W.; Bjerrum, M. J.; Yang, S. W. *Nucleic Acids Res.* **2016**, *44* (6), e57.
- (111) Hu, Y.; Zhang, L.; Zhang, Y.; Wang, B.; Wang, Y.; Fan, Q.; Huang, W.; Wang, L. *ACS Appl. Mater. Interfaces* **2015**, *7* (4), 2459.
- (112) Qiu, X.; Hildebrandt, N. *ACS Nano* **2015**, *9* (8), 8449.
- (113) Noh, E.-H.; Ko, H. Y.; Lee, C. H.; Jeong, M.-S.; Chang, Y. W.; Kim, S. *J. Mater. Chem. B* **2013**, *1* (35), 4438.
- (114) Wu, C.; Chiu, D. T. *Angew. Chem. Int. Ed.* **2013**, *52* (11), 3086.
- (115) Lesnik, E. A.; Freier, S. M. *Biochemistry (Mosc.)* **1995**, *34* (34), 10807.
- (116) Sugimoto, N.; Nakano, S.; Yoneyama, M.; Honda, K. *Nucleic Acids Res.* **1996**, *24* (22), 4501.
- (117) Dimitrov, R. A.; Zuker, M. *Biophys. J.* **2004**, *87* (1), 215.
- (118) Markham, N. R.; Zuker, M. *Nucleic Acids Res.* **2005**, *33* (suppl 2), W577.
- (119) Markham, N. R.; Zuker, M. In *Bioinformatics*; Keith, J. M., Ed.; Walker, J. M., Series Ed.; Humana Press: Totowa, NJ, 2008; Vol. 453, pp 3–31.
- (120) DINAMelt | mfold.rit.albany.edu <http://mfold.rna.albany.edu/?q=DINAMelt> (accessed Jul 22, 2015).
- (121) Reuter, J. S.; Mathews, D. H. *BMC Bioinformatics* **2010**, *11* (1), 129.
- (122) RNAstructure | rna.urmc.rochester.edu <http://rna.urmc.rochester.edu/RNAstructureWeb/> (accessed Jul 22, 2015).
- (123) Hofacker, I. L. *Nucleic Acids Res.* **2003**, *31* (13), 3429.
- (124) ViennaRNA Web Services | rna.tbi.univie.ac.at <http://rna.tbi.univie.ac.at/> (accessed Jul 22, 2015).

- (125) Oheim, M.; Michael, D. J.; Geisbauer, M.; Madsen, D.; Chow, R. H. *Adv. Drug Deliv. Rev.* **2006**, *58* (7), 788.
- (126) Denk, W.; Strickler, J. H.; Webb, W. W. *Science* **1990**, *248* (4951), 73.

Chapter 2.

Detection of miRNA Using a Double-Strand Displacement Biosensor with a Self-Complementary Fluorescent Reporter

Nicholas E. Larkey, C. Kyle Almlie, Victoria Tran, Marianne Egan, and Sean M. Burrows

Analytical Chemistry

ACS Publications: 1155 Sixteenth Street N.W. Washington, DC 20036

2014, 86 (3), pp 1853–1863. DOI: [10.1021/ac403866g](https://doi.org/10.1021/ac403866g)

2.1 Abstract

Design of rapid, selective, and sensitive DNA and ribonucleic acid (RNA) biosensors capable of minimizing false positives from nuclease degradation is crucial for translational research and clinical diagnostics. We present proof-of-principle studies of an innovative micro-ribonucleic acid (miRNA) reporter-probe biosensor that displaces a self-complementary reporter, while target miRNA binds to the probe. The freed reporter folds into a hairpin structure to induce a decrease in the fluorescent signal. The self-complementarity of the reporter facilitates the reduction of false positives from nuclease degradation. Nanomolar limits of detection and quantitation were capable with this proof-of-principle design. Detection of miRNA occurs within 10 min and does not require any additional hybridization, labeling, or rinsing steps. The potential for medical applications of the reporter-probe biosensor is demonstrated by selective detection of a cancer regulating microRNA, Lethal-7 (Let-7a). Mechanisms for transporting the biosensor across the cell membrane will be the focus of future work.

2.2 Introduction

Our approach to improve RNA sensing technology involves a target RNA displacing a self-complementary reporter from a reporter-probe complex (Figure 2.1). Self-complementarity of the reporter causes it to fold into a hairpin configuration upon displacement from the probe. This forces two dyes at distal ends of the reporter together, accommodating intermolecular energy coupling mechanisms that govern the change in the analytical signal and consequently aid in reducing false positives. The reporter and probe are only partially complementary but stable at room temperature with a melting temperature of 39 °C. The full complementarity of the probe and target form a more thermodynamically stable complex at room temperature with a melting temperature of 54 °C. This condition drives the reaction in Figure 2.1 to the right. The reporter-probe biosensor presented here has great potential to provide improved selectivity and stronger binding to target miRNA over dual sensing strand designs because the unlabeled probe is fully complementary to the target.

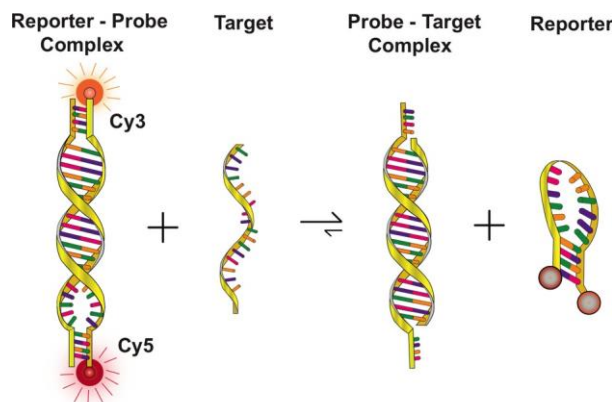


Figure 2.1 Schematic of Recognition Mechanism

In this work, we present proof-of-principle studies of a reporter-probe displacement biosensor capable of selectively detecting a cancer regulating miRNA, Lethal-7 (Let-7a). We used Let-7a because the Let-7 family is highly conserved across many animal species and has been linked to cell-based diseases.¹⁻⁶ The reporter-probe displacement biosensor presented here combines the positive attributes of competitive binding with a change in luminescence from intramolecular binding to provide high selectivity and reduce false positives. The complexation thermodynamics, two-photon characteristics, spectral properties, binding kinetics, binding selectivity, analytical figures of merit, and extent of false positives for the reporter-probe biosensor are discussed. The reporter-probe biosensor is an attractive alternative to current biosensors because nanomolar amounts of miRNA were detected within 10 min of hybridization. In addition, false positives were reduced by more than 20% compared to molecular beacons.

2.3 Experimental

2.3.1 Single- and Two-Photon Spectral Characteristics of the Reporter

The reporter is an oligonucleotide with a cyanine-3 dye (Cy3) on the 3-prime end and a cyanine-5 dye (Cy5) on the 5-prime end. These dyes were selected for their energy coupling prospects. Excitation and emission spectra of the reporter in the hairpin and open configurations were recorded. Working solutions of the reporter, reporter-probe, and reporter-probe plus target were prepared to contain approximately 1 μM of each reagent. Similar solutions were used to investigate the linearity and nonlinearity of photon absorption of the reporter in both the hairpin and open configurations. A more detailed description of the reporter and probe sequence and configuration will be discussed below and presented in Table 2.1.

Table 2.1 Oligonucleotide Sequences and Predicted Thermodynamic Complexation Values

Name	Sequence (5'-3')	Gibbs Energy (kcal/mole)†		
		Target	Nonsense	Reporter
Reporter	Cy5/ <u>CATCGTTGAATAC</u> +TAGGTTGT+ATAGTT <u>CGA</u> <u>T+G</u> /Cy3Sp	-3.2	-6.2	---
Reporter (NO Cy3)	Cy5/ <u>CATCGTTGAATACTAGGTTGTATAGTT</u> <u>CGATG</u>	-3.2	-6.2	---
Probe1	ACTATAACAACCTACTACCTC	-23.0	-2.5	-13.1
Probe2	<u>CATCGTACTATAACAACCTACTACCTCACGATG</u>	-24.7	-2.5	-19.5
Let-7a Target	U*GA*GGmUAmGUAGGUUmGUmAU*AGU*U	---	---	-3.2
Let-7a Variation (Let-7aV)	U*GA*<i>u</i>GUAc_aAGGUUGUAU*AGU*U	---	---	-3.3
miR-9 Nonsense	U*CA*UAmCAmGCUAGAUmAAmCC*AAA*GA	-5.7	---	-6.2
Molecular Beacon	Cy5/ <u>TCATCGAACTATAACA</u> + ACCTACTAC +CTCAC <u>GAT+GA</u> /IAbRQSp	-25.4	-2.9	---
Cy3-linear Reporter	AACTATAACAACCTACTACCTCA /Cy3Sp	---	---	---
Cy5-linear Reporter	Cy5/ TGAGGTAGTAGGTTGTATAGTT	---	---	---

† All thermodynamic values were obtained using software available from The DINAMelt Web Server⁷⁻⁹ managed by The RNA Institute at SUNY-Albany. The 'Two State melting (hybridization)' function was used for double-strand binding calculations. Experimental parameters used for thermodynamic calculations were: 25 °C, 10 mM Na⁺, 2.5 mM Mg²⁺, and 1 μM oligonucleotide. Calculations could not incorporate added stability provided by chemical modifications. Bold sections of the sequences refer to complementary binding sites. Underlined sections depict complementary regions of the stems for the reporter, probe2, and molecular beacon. The bold thermodynamic values correspond to significant complexation reactions. (+) symbol represents location of locked nucleic acid. (*) symbol represents location of a phosphorothioated modification, (m) symbol represents location of a 2'-O-Methyl modification.

Figure 2.2 is a diagram of the custom-built fluorimeter used for characterization of the reporter-probe displacement biosensor. A Titanium-Sapphire (Mai Tai, Spectra Physics, Newport) laser produced 100 femtosecond (fs) long pulses at a repetition rate of 80 MHz. The Mai Tai laser wavelength is tunable from 690 to 1040 nm. The excitation beam reflects off a mirror and passes through a half-wave-plate and Glan-polarizer (Newport) to control the power. A beam sampler (Newport, 10B20-01NC.2) reflects ~4% of the excitation beam to a photodiode (Newport, 918D-SL-OD3R) to monitor and control the power. The transmitted beam continues to a second mirror (Newport, 10Q20UF.35P) to be directed through a 705 nm long-pass dichroic beam splitter

(Semrock, FF705-Di01-25x36). After passing through the dichroic, the laser beam is focused into a cuvette using a 25 mm focal length plano-convex lens (Newport, KPX076 AR.16). Emission from the sample is collected with the same lens used to focus the excitation beam. The emission beam is reflected by the dichroic mirror and passes through a 720 nm short-pass filter (Semrock, FF01-720/ SP-25) to remove any backscattered photons from the source. A 10 \times , 0.25 Numerical Aperture (NA) objective focuses the emission beam into a 2 m long fiber optic (Ocean Optics, QP1000-2-VIS-NIR). The fiber optic connects to a QE65 Pro spectrometer (Ocean Optics). For experiments using the QE65 Pro, the charge coupled device (CCD) was thermoelectrically cooled to -20 °C to reduce dark noise. The spectrometer has a grating with 1200 grooves/mm and a spectral range from 520 to 690 nm. For sensitivity and limit of detection characterization of the biosensor, we used an Acton Spectrometer (SP-2356) containing a grating with 300 grooves/mm blazed at 500 nm (Princeton Instruments). An electron-multiplied CCD (Princeton Instruments, 512B-eXcelon3-EMCCD) was used as the detector. Acquisition parameters depended on the concentration of reporter-probe complex. The slit width, grating center, and CCD temperature were constant at 1000 μ m, 650 nm, and -70 °C. The spectral window ranged from 613.3 to 698.1 nm. Such a grating position minimized spectral interference from residual scatter from the excitation source that was not removed by the dichroic mirror and short pass spectral clean up filter.

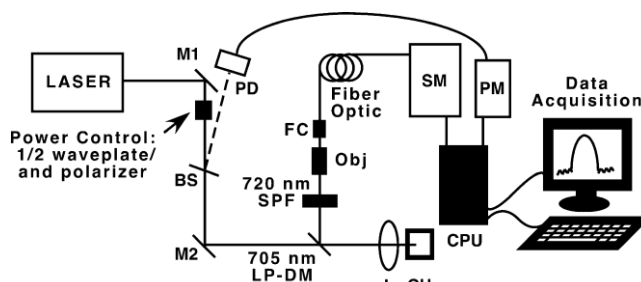


Figure 2.2 Experimental apparatus. Laser = Mai Tai (690 to 1040 nm); M1 = Mirror1, M2 = Mirror2, BS = Beam Sampler, PD = Photo Diode, LP-DM = 705 nm Long-Pass Dichroic Mirror, L = 25 mm Focal Length Lens, CH = Cuvette Holder, SPF = 720 nm Short-Pass Filter, Obj = Objective (10 \times , 0.25 NA), FC = Fiber Coupler, SM = Spectrometer, PM = Power Meter, and CPU = Central Processing Unit.

The wavelength from the Mai Tai was controlled using the Mai Tai GUI program (Spectra Physics, Newport). As mentioned previously, the Mai Tai laser power is controlled with a half-wave-plate and a Glan-polarizer. Rotation of the half-wave-plate with respect to the Glan-polarizer allows precise control of the average power at the sample. The rotation of the half-wave-plate is controlled by software available from Newport (CCVA-PR). A power meter (Newport, 1918-R) measured the average power of the reflected excitation beam at the photodiode. Assuming no

absorption by the beam sampler, the Newport software mentioned above also calculates transmitted power using the Fresnel equation¹⁰ and the measured reflected laser power. Spectral emission data was collected and stored using either SpectraSuite software from Ocean Optics or Lightfield from Princeton Instruments. All experimental data was processed using custom-written Matlab algorithms.

To confirm emission characteristics observed using the pulsed source, we conducted experiments using a continuous wave source. The continuous-wave experiments use a diode pumped solid-state laser (Gem, LaserQuantum) operating at 532 nm. The same type of fiber optic coupler and QE65 Pro spectrometer described previously were also used for continuous-wave experiments.

2.3.2 Oligonucleotides and Materials

Oligonucleotides were purchased from Integrated DNA Technologies and Exiqon and used as received. Only probe1 was purchased from Exiqon. Oligonucleotide sequences and predicted thermodynamic data are shown in Table 1. Open-source software available on the DINAMelt Web Server^{51–53} was used to calculate all the thermodynamic data presented in Table 1. The reporters and probes were made out of DNA and locked nucleic acids (LNA). The miRNA have a 2'-O-methylation and/or a phosphorothiolation modification to improve long-term stability of the oligonucleotide. The 2'-O-methylation of the miRNA adds a methyl group to the 2'-hydroxyl group of the ribose moiety. Phosphorothiolate bond modification substitutes a sulfur atom for a nonbridging oxygen on the phosphate backbone of an oligonucleotide. The reporter was designed to contain three strategically placed LNAs. The probe sequence contained patent protected placement of LNAs (Exiqon, 4100170-00). LNAs help stabilize the oligonucleotide against nuclease degradation by implementation of a carbon bridge between the 4' carbon and the 2' oxygen of the ribose moiety. Use and determination of optimum placement of LNA to reduce false positives can be cost-prohibitive. Furthermore, recent studies have found LNA to have a toxic effect to some cell lines.¹¹ The reporter-probe biosensor presented here uses LNA in low concentration to limit toxicity. LNA-LNA form stronger intermolecular bonds than LNA-DNA and LNA-RNA bonds. Since double strand displacement mechanisms usually use more complementary base pairs than molecular beacons, getting displacement to occur will be difficult if too many LNAs are needed to minimize false positives. We suggest that the reporter-probe biosensor adds an extra level of rejection to false positives and can help reduce cost. Future

reporter-probe designs will explore the need for LNA modifications. If LNA do not contribute to reducing false positives, then the reporter-probe could be free of LNA and reduce a potential source of toxicity of the biosensor.

Tris buffer (pH 10), Tween 20, phosphate buffered saline (PBS, pH 7.0), and 2 M magnesium chloride (MgCl_2) were obtained from Fisher Scientific and used as received. Stock solutions of all oligonucleotides were prepared with 18 M Ω RNase-free water (complements of the Remcho Lab at Oregon State University). Working solutions of oligonucleotides were prepared using a buffer solution containing 10 mM Tris buffer, 2.5 mM MgCl_2 , and 0.005% Tween 20 in PBS. The final pH of the buffer solution was approximately 8. Concentrations of oligonucleotides were verified using a Nanodrop spectrometer (Thermo Scientific, ND-1000 UV-vis Spectrometer).

2.3.3 Binding Kinetics and Analytical Signal Dynamics.

To confirm selectivity of the reporter-probe biosensor, the analytical signals from the reporter were observed before and after in situ addition of probe, target Let-7a, or non-complementary miR-9. The signal change was observed in real time to track how different reagent additions changed the analytical signal and to monitor signal stability. These experiments started with the reporter in the hairpin configuration to establish a starting point for Cy3 and Cy5 emission intensities. The reporter-probe complex was formed by incubation of the reporter with probe for 20 min at room temperature. A 10 min incubation period was used after addition of either target or noncomplementary miRNA to the reporter-probe biosensor. Dilution controls involved sequential addition of buffer to the reporter. These controls were used to determine dilution factors and confirm signal changed according to dilution factor.

Preliminary studies of the change in analytical signal were carried out with working solutions containing approximately 1 μM of reporter. Addition of probe resulted in a solution of 833 nM reporter and 833 nM probe. Addition of target Let-7a, Let-7a variant (Let-7aV), or miR-9 produced solutions containing 750 nM reporter, 750 nM probe, 750 nM target Let-7a, 750 nM Let-7aV, or 750 nM miR-9. Dilution control solutions were prepared by successive addition of buffer to the 1 μM reporter solution to dilute it to 833 and 750 nM. The same dilution protocol was used when a reporter without Cy3 had its signal change analyzed.

Analytical signal intensity was acquired for 1 min time intervals every 5 min over at least 30 min. Each 1 min signal acquisition consisted of 6 replicate measurements of a 10 s exposure

time. The average Let-7aV signal included cuvette placement error by repositioning the cuvette after each 1 min exposure time, and the signal was monitored over a 5 min period. The laser beam was blocked during incubation times and in-between time-point measurements to minimize photo-damage of oligonucleotides and the dyes. All average signal counts are background corrected.

2.3.4 Cell Lysate Protocol

DH10b *E. coli* cells (complements of the Mehl Lab at Oregon State University) were cultured to saturation in 2×YT (yeast extract tryptone) media at 37 °C and gently shaken at 250 rpm. Cells were centrifuged at 5000 rpm for harvesting, and a 50 µL aliquot of cells was stored in a –80 °C freezer. On the day the cell lysate was needed, a sample of cells was taken out of the freezer and thawed at room temperature. The cells were resuspended in 50 mL of dilution buffer and lysed at 18 000 psi with a Microfluidizer (Microfluidics M-110P) at 0 °C. The cell lysate was then centrifuged at 20 000 relative centrifugal force for 20 min. Finally, the supernatant lysate passed through a 0.20 µm filter to remove large cell debris and maintain DNA, RNA, proteins, and other cell lysate materials. The filtered cell lysate was then diluted in half using buffer solution described above. The half-diluted cell lysate solution was then used to look for interferences in biosensor response in the presence of cell debris. Buffer controls were performed in parallel with cell lysate studies for comparison of the reporter's response in each type of environment. Reporter at 1 µM was analyzed before the addition of either diluent or probe to reduce the concentration to 833 nM. After 10 min of hybridization, the solution was analyzed. Then, either another addition of diluent or Let-7a was added. After a 20 min incubation period, the solution was analyzed. This solution contained 750 nM probe-Let-7a and reporter. As described above, the signal from the reporter was collected over a 1 min period. Each signal acquisition consisted of 6 replicate measurements with a 10 s exposure time. After each 1 min exposure time, the cuvette was repositioned three times to incorporate cuvette placement error into the average signal.

2.3.5 Analytical Figures of Merit

Reporter-probe complex solutions were prepared by incubating equimolar amounts of reporter and probe for one hour. All standard solutions were prepared to contain either 1 µM or 100 nM reporter-probe complex. The sensitivity of the 1 µM reporter-probe complex was evaluated using standard solutions containing 0, 5, 25, 125, 250, 500, 750, and 1000 nM of Let-7a. The 100 nM reporter-probe complex standard solutions contained 0, 1, 5, 10, 25, and 50 nM Let-7a. After addition of Let-7a to the reporter-probe complex, the solutions were allowed to

hybridize for at least 1 h prior to analysis. For sensitivity evaluations, the changes in fluorescence of the standard solutions were analyzed using a 300 mm focal length spectrometer (Acton SP-2356 spectrometer, Princeton Instruments, 300 grooves/mm grating) equipped with an electron-multiplied charge coupled device (ProEM 512B-eXcelon3-EMCCD, Princeton Instruments). The fiber optic delivering fluorescence to the spectrometer had a 1000 μm core diameter and was placed directly at the entrance slit of the spectrometer. To optimize light throughput, the spectrometer slits were opened to 1000 μm in order to match the core diameter of the fiber.

Various data acquisition parameters were evaluated for optimal signal-to-noise and detector response sensitivity. Optimum acquisition parameters for the 1 μM reporter-probe complex were: 100 ms exposure time, low noise analog to digital conversion, 100 kHz full frame readout rate, and high analog-to-digital conversion gain. For the 100 nM reporter-probe complex, only the exposure time was increased to 500 ms. To improve signal-to-noise and establish instrumental error, ten exposures were averaged and six replicates were taken. After the six replicates were taken, the cuvette was repositioned three times and the acquisition process was repeated. This procedure allowed cuvette placement error to be determined. The samples were excited with 742 nm at 75 mW average power.

2.3.6 False Positives from Nuclease Degradation

Solutions of reporter-probe complexes, molecular beacons, and double-strand displacement biosensors were tested for false positive signal generation. An endonuclease degradation procedure was adapted from the Promega RT-PCR DNase treatment protocol. The enzyme solution containing endonuclease was added to the samples in excess and then incubated at 37 °C for 30 min. RQ1 DNase stop solution was added to the solutions and incubated at 65 °C for 10 min. Each solution was then diluted to approximately 833 nM of oligonucleotide biosensor of interest. Control solutions without nucleases only contained the nucleic acids of interest at equivalent concentrations to those in the endonuclease test solutions. The control solutions were not heated or treated to endonucleases. Solutions containing the endonuclease were analyzed for an increase or decrease in signal intensity compared to their respective control solutions.

2.4 Results and Discussion

2.4.1 Thermodynamic Considerations for the Recognition Mechanism

Thermodynamic stability of the reporter-probe complex governed whether or not a potential target would displace the reporter. The reporter-probe complex is designed to be resistant to nonspecific binding; however, presence of a complementary target miRNA will disrupt the reporter-probe complex to form a more thermodynamically stable probe-target complex, freeing the reporter in the process. The freed reporter uses intramolecular binding to fold into a hairpin configuration. This intramolecular binding event is used to force the donor and acceptor resonant energy pairs into close proximity to cause a change in the analytical signal. The reporter behaves similarly to a reverse molecular beacon (rMB)^{12,13} but differs in that the reporter presented here works at room temperature and is not complementary to the target miRNA. Figure 2.1, discussed in the introduction, shows the recognition mechanism for the reporter-probe biosensor.

Key Gibbs energy values are reported in Table 2.1 and highlighted in bold. Two probe designs were investigated; probe1 with partial complementarity to the loop region of the reporter and probe2 with partial complementarity to the loop and stem regions of the reporter. Both probe1 and probe2 are designed to be fully complementary to Let-7a. The Gibbs energies of reporter-probe1 and reporter-probe2 complex are -13.1 and -19.5 kcal/mol, respectively. The Gibbs energies for probe1-target and probe2-target complex are -23.0 and -24.7 kcal/mol, respectively. The more negative Gibbs binding energy of the probe-target complex drives the reaction to form probe-target complexes and free reporters. Table 1 also shows that potential nonspecific binding interactions have non-favorable thermodynamic values. These values demonstrate the reporter-probe complex is indeed more stable than any potential nonspecific complexation. All values were obtained using the Two State melting (hybridization) application available from The DINAMelt Web Server available at The RNA Institute at SUNY-Albany.⁷⁻⁹

If the reporter-probe biosensors are to be used at 37 °C, then the binding thermodynamics would need to be re-evaluated. By tuning the nucleic acid sequence of the reporter, the binding thermodynamics can be adjusted to demonstrate competitive binding at other temperatures. There will also be other competing binding mechanisms with nonspecific species that need to be accounted for at the different operating temperatures.

2.4.2 Transduction Mechanism

The reporter has Cy3 and Cy5 fluorophores located at the distal ends of the oligonucleotide strand. Table 2.1 lists the dye and oligonucleotide configuration of the reporter. Figure 2.3 shows the fluorescent transduction mechanism of the reporter-probe1 biosensor. The emission in Figure 2.3 resulted from excitation of the reporter at 742 nm with approximately 100 mW of average power. The hairpin configuration of 1 μ M reporter has a maximum emission from Cy5 at 670 nm with approximately 8000 counts per 10 s (blue line, Figure 2.3a). Complexation of 1 μ M probe1 with 1 μ M reporter causes the Cy5 signal to increase to about 18 000 counts per 10 s (green dash, Figure 2.3a). When 1 μ M reporter, 1 μ M probe1, and 1 μ M Let-7a are added together, the Cy5 signal returns to approximately 7000 counts per 10 s (red dash-dot, Figure 2.3a). Addition of probe1 caused the Cy5 signal to increase by \sim 10 000 counts per 10 s compared to the Cy3 signal increase of \sim 100 counts per 10 s (Figure 2.3). Thus, emission from Cy5 is the dominant contributor to the reporter's analytical signal.

Figure 2.3 demonstrates the current reporter-probe displacement biosensor behaves as a signal-off type biosensor. To confirm the reduction in signal was from the folding of the reporter into a hairpin and not an artifact from the ultrafast laser, we used a continuous-wave laser to look at the signal dynamics. Samples containing reporter, reporter-probe1, and reporter-probe1 plus target were excited with 532 nm laser irradiation from the Gem laser at \sim 3.4 mW. Emission spectra from the continuous-wave source confirmed the reporter-probe1 displacement biosensor decreased the Cy5 and Cy3 emission when the reporter was in the hairpin configuration (Figures A1.1 and A1.2, Appendix I).

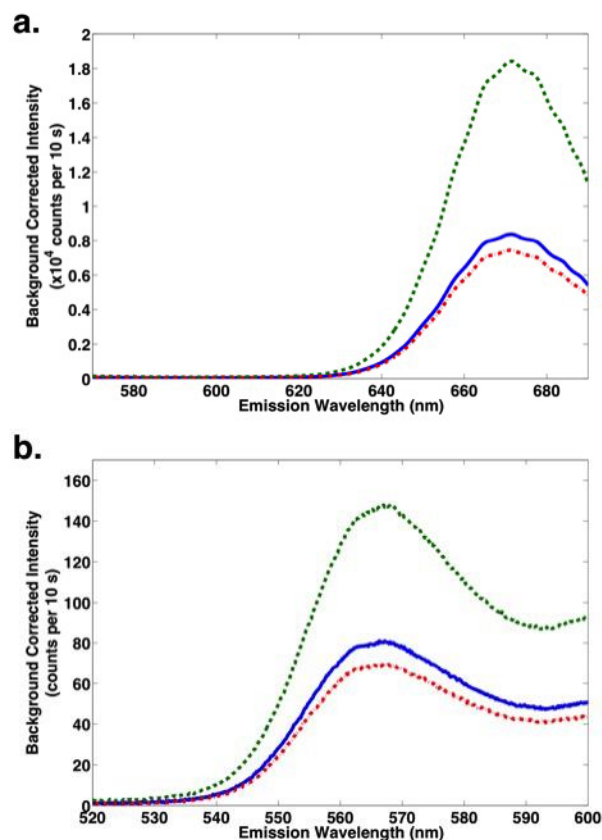


Figure 2.3 Fluorescence emission from the reporter started at about 530 nm and went to approximately 690 nm. (a) Cy5 emission ranged from 620 to 690 nm. (b) Cy3 emission went from 540 to 590 nm. (blue line) = 1 μ M reporter, (green dash) = 1 μ M reporter-probe1 complex, and (red dash-dot) = 1 μ M reporter-probe1 plus 1 μ M target. The reporter was excited with 742 nm at \sim 100 mW.

The signal from the solutions containing only reporter (blue line, Figure 2.3) and the reporter-probe1 plus Let-7a (red dash-dot, Figure 2.3) should be approximately the same because both contain 1 μ M of the reporter in the hairpin configuration. We found that the \sim 10% difference in signal between the two solutions was from cuvette placement. Examination of the relative standard deviation of the reporter's average summed intensity from cuvette placement experiments revealed a 1.7% to 8.8% error (data not shown). The cuvette error comes from the cuvette holder not being able to lock the cuvette in place, like in a commercial instrument. Data was collected using a custom-built fluorescence detection system, and the cuvette holder was made in our machine shop. The system used to collect fluorescence is only used to characterize and validate biosensor efficacy prior to cell and tissue applications. Future studies will use an average background signal that accounts for changes in cuvette placement.

For the remainder of the discussion, the region of the spectrum where Cy5 emits (620–690 nm, Figure 2.3a) will be referred to as the Cy5 emission region. The region of the spectrum where Cy3 emits (540–590 nm, Figure 2.3b) will be referred to as the Cy3 emission region.

As demonstrated in Figure 2.3, addition of probe causes the reporter signal to increase as the hairpin unfolds and moves the Cy3 and Cy5 away from one another. When Let-7a is added, the fluorescence decreases back to the original value. From these observations, we hypothesize the Cy3 and some of the nucleic acids are causing the emission from the Cy5 to decrease when the reporter is in the hairpin configuration. To test this hypothesis, we conducted two studies that compared the percent decrease in the fluorescence of Cy5 when in proximity to either nucleic acids or Cy3. These studies used hairpin and linear reporters. Table 2.1 and Table A1.1, Appendix I, lists the oligonucleotide sequences used in the study. A reporter that lacked Cy3 on the 3-prime end was obtained and used to compare to the reporter with Cy3 on the 3-prime end. Three linear reporters were purchased; one had Cy5 on the 5-prime end, while the complementary strand was labeled with or without Cy3 at the 3-prime end of the oligonucleotide.

Figure 2.4 compares the average decrease in signal of the reporter-probe complex with and without Cy3 on the 3-prime end of the reporter upon probe-Let-7a binding. The reporter with Cy3 and Cy5 causes the signal to decrease by $57.7 \pm 1.9\%$ ($N = 3$) after addition of Let-7a. The reporter without the Cy3 only results in a $32.6 \pm 2.4\%$ ($N = 3$) decrease in signal. Addition of Cy3 provides an additional $25.1 \pm 3.1\%$ contribution to the decrease in signal when the reporter changes configuration after releasing the probe. Comparing the means shows that at the 99% confidence interval the means are statistically different and we conclude that Cy3 adds a statistically significant improvement to the dynamic range of the signal change.

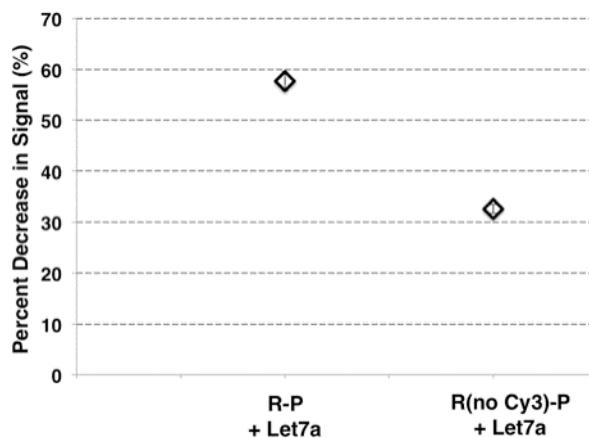


Figure 2.4 Comparison of observed fluorescence quenching of a 5-prime-Cy5-reporter with and without Cy3 at the 3-prime end. Displayed as percent decrease in signal. R-P = reporter-probe1 complex. Error bars for $N = 3$ are the same size as the symbols. Samples were excited with 742 nm at 100 mW.

To further confirm Cy3 and nucleic acid proximity contributes to Cy5 quenching, we conducted studies using a 22 nucleic acid long linear oligonucleotide labeled with Cy5 on the 5 prime end. In these experiments, linear strands of 5-prime Cy5 were exposed to buffer, noncomplementary DNA, complementary DNA with No Cy3, and a complementary DNA labeled with Cy3 on the 3-prime end. Nucleic acids alone decrease the Cy5 signal by $44.8 \pm 2.0\%$ ($N = 4$). The Cy3 contributes an additional $29.2 \pm 2.5\%$ to the decrease in signal (Figure A1.3, Appendix I). Addition of noncomplementary DNA oligonucleotide showed no decrease in signal, confirming only complementary binding of nucleic acids contributes to observed decrease in Cy5 signal. Using non-complementary DNA provides a negative control to confirm nucleic acids must be close to the Cy5 in order to decrease the emission (Figure A1.3, Appendix I). From these experiments, we conclude the Cy5 is interacting with any of the four nucleic acids and the Cy3. Both studies demonstrate the Cy3 provides an additional 30% decrease in signal. It is likely that different combinations of adenine (A), thymine (T) and cytosine (C), and guanine (G) lead to different extents of quenching. Further studies will be needed to resolve the nature of the observed quenching from nucleic acids. We are currently exploring use of a quencher, Iowa Black, to further improve quenching. We hypothesize a quencher like Iowa Black will have more quenching of Cy5 than the Cy3-Cy5 pair. We further hypothesize that more quenching will lead to lower limits of detection and/or better signal resolution between different concentrations. From our preliminary data, we are finding that using the Iowa Black quencher reduces the signal by an additional $\sim 33\%$, improving the total quenching to $\sim 89\%$ when the reporter is in the hairpin configuration.

2.4.3 Excitation Spectra of Reporter

Figure 2.5 shows the excitation spectra of the reporter with and without probe1. The excitation wavelength varied from 742 to 1032 nm (specifically 742, 782, 832, 862, 932, 992, and 1032 nm) with a constant power of 100 mW. The background corrected averaged summed intensity of the Cy3 and Cy5 emission regions were plotted as a function of excitation wavelength (Figure 2.5). The Cy3 and Cy5 dyes were chosen for their potential to demonstrate Förster resonance energy transfer (FRET). However, as demonstrated in Figure 2.5, no excitation wavelength was capable of producing FRET enhancement when the reporter is in the hairpin configuration. Instead, the excitation study revealed that, at each excitation wavelength, the hairpin configuration of the reporter had less emission intensity than the “open” reporter-probe1 configuration. Excitation at 742 nm was found to be the wavelength that had the largest change in analytical signal for both dyes. From this observation, we decided to use 742 nm excitation for the remainder of the studies.

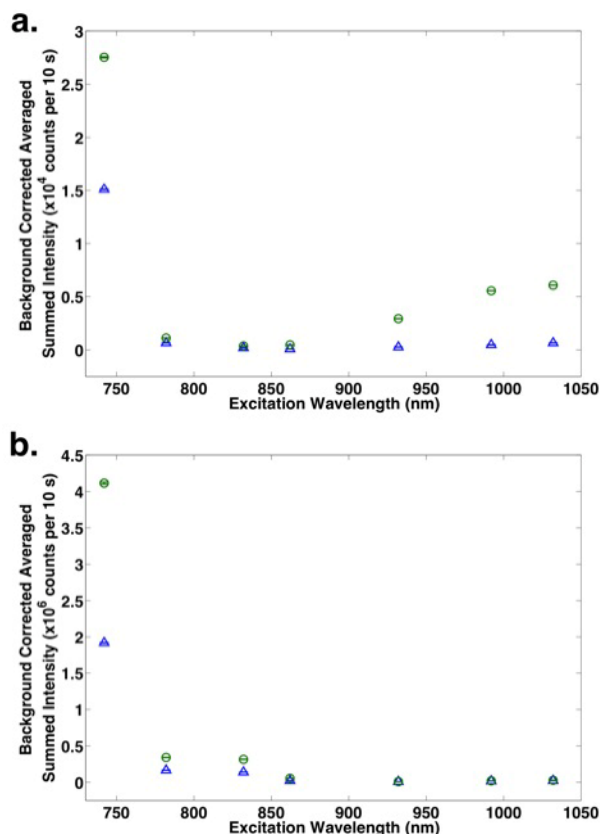


Figure 2.5 Excitation spectra of 1 μM reporter with and without 1 μM probe1. Excitation wavelength varied from 742 to 1032 nm at constant excitation power of approximately 100 mW. (a) Excitation spectra obtained by observing emission in the Cy3 region. (b) Excitation spectra obtained by observing emission in the Cy5 region. Error bars from 5 replicates are the same size or smaller than the symbols (blue triangles = reporter; green circles = reporter-probe1).

Nonlinear absorption characteristics of the reporter and the reporter-probe1 complex were investigated by increasing the excitation power from 25 to 200 mW in 25 mW steps. After processing data in Matlab, log–log plots of emission intensity vs average excitation power were prepared (data not shown). From these experiments, only the Cy3 showed nonlinear absorption over the 25 to 75 mW average power range. The hairpin configuration demonstrated three-photon absorption, but the reporter-probe1 complex demonstrated two-photon absorption. Both the hairpin and reporter-probe1 complex demonstrated a mixture of single- and two-photon absorption with excitation powers over 75 mW. Cy5 emission demonstrated single-photon absorption in both the hairpin and reporter-probe1 complex over the entire excitation power range from 25 to 200 mW. The deviations from expected two-photon observation most likely resulted from interactions between Cy3 and Cy5 and/or between the dyes and the nucleic acids. Future studies are planned to examine the photon absorption and emission characteristics of these dyes in more detail and are beyond the scope of this preliminary report on the biosensor.

2.4.4 Binding Kinetics and Analytical Signal Dynamics

Signal change, binding kinetics, signal stability, and specificity of the biosensor were investigated before and after addition of probe1. These studies were then applied to the reporter-probe1 complex before and after addition of Let-7a, noncomplementary miR-9, or a three-nucleotide variant of the Let-7a (Let-7aV). Table 2.1 lists the sequences and predicted thermodynamics for each type of miRNA. For each sample, fluorescence was observed for 1 min time intervals over a 30 min time period (each time interval was spaced by 5 min). These experiments were repeated four times to demonstrate and establish stability and reproducibility of the signal. The biosensor exhibited a signal stability of about 2–5% over a 30 min time period. The excitation beam was blocked in-between measurement time points to prevent photodamage of the oligonucleotides and dyes.

The length of time needed for hybridization of reporter-probe1 was determined by monitoring changes in Cy5 fluorescence over time after addition of probe1 to the reporter. Figure 2.6 shows an overlay of the background corrected averaged summed intensity ($N = 4$) of Cy5 before and after addition of probe1 to the reporter. The solutions contained 1 μM reporter (blue circles) and 833 nM reporter plus 833 nM probe1 (green circles). The reporter signal is reproducible and stable at about $1.88 \times 10^6 \pm 0.05 \times 10^6$ ($N = 5$) counts per 10 s over a 24 min time period (Figure 2.6). The first datum for the reporter plus probe1 hybridization experiment was

taken within 1 min after adding probe1 to the reporter. The time it takes for the signal to stabilize after addition of probe1 was used as a metric to determine hybridization time. According to Figure 2.6, the reporter-probe1 hybridization process takes about 6 min. After 6 min, the reporter-probe1 complex signal is reproducible and stable at $3.65 \times 10^6 \pm 0.17 \times 10^6$ (N = 4) counts per 10 s. The increase in signal observed in Figure 2.6 after addition of probe1 to reporter provides convincing evidence that the signal change can be related to probe addition. In the Cy3 emission region (data not shown), three of the four replicates took about 20 min for the signal to stabilize. However, one of the four replicates took only 5 min to stabilize. After 45 min (data not shown), the error in the signal from both the Cy3 and Cy5 emission was about 4% (N = 4). From these studies, we decided a 20 min hybridization period should be used to form the reporter-probe1 complex.

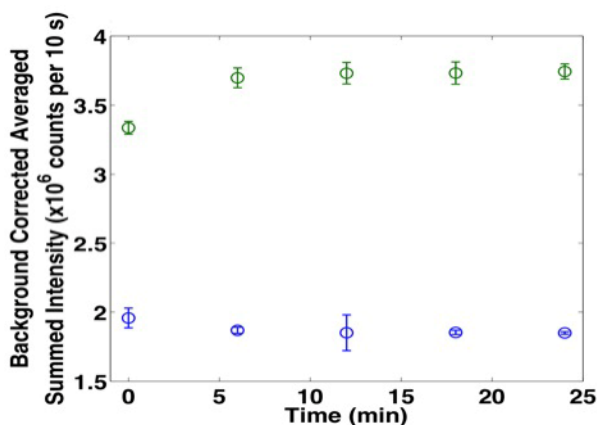


Figure 2.6 Background corrected averaged summed Cy5 intensity (N = 4) time trace of 1 μ M reporter before probe1 addition (blue circles) and 833 nM reporter and probe1 (green circles) after probe addition. Error bars from 4 replicate measurements are the same size or smaller than the symbols. Both solutions were excited with 742 nm at 100 mW average power.

The specificity of the reporter-probe1 complex for Let-7a was investigated. In order to correlate the changes in the signal to a specific reagent being added, each experiment started with the reporter alone and then different reagents were added directly to the cuvette prior to analysis. Each experiment started by monitoring the signal stability of 1 μ M reporter over time. Probe1 was added to the reporter and allowed to incubate for 20 min in the cuvette with the laser beam blocked. The final concentration was 833 nM probe1 and 833 nM reporter. Then, the signal stability was monitored over 36 min. Finally, either target Let-7a or noncomplementary miR-9 was added to the cuvette containing the reporter-probe1 complex. A 10 min incubation period was used for addition of target or non-complementary miRNA, with the laser beam blocked during incubation. The final concentration was 750 nM Let-7a target or noncomplementary miR-9, 750 nM probe1, and 750 nM reporter. The signal stability was monitored for 30 min.

As different oligonucleotides were sequentially added to a solution containing the reporter, a dynamic change in signal is observed (Figure 2.7). Because probe1, target Let-7a, and noncomplementary miR-9 were added to the reporter solution in situ, dilution effects on the signal had to be taken into account (blue circles). Addition of probe1 results in more than doubling of signal for both dyes (compare reporter plus buffer to reporter plus probe1 at minute 73, in Figure 2.7). Addition of the Let-7a to the reporter-probe1 complex resulted in the signal decreasing to approximately the same value as reporter alone, with dilution taken into account (compare minute 120 for reporter plus buffer to reporter plus probe1 plus target, in Figure 2.7).

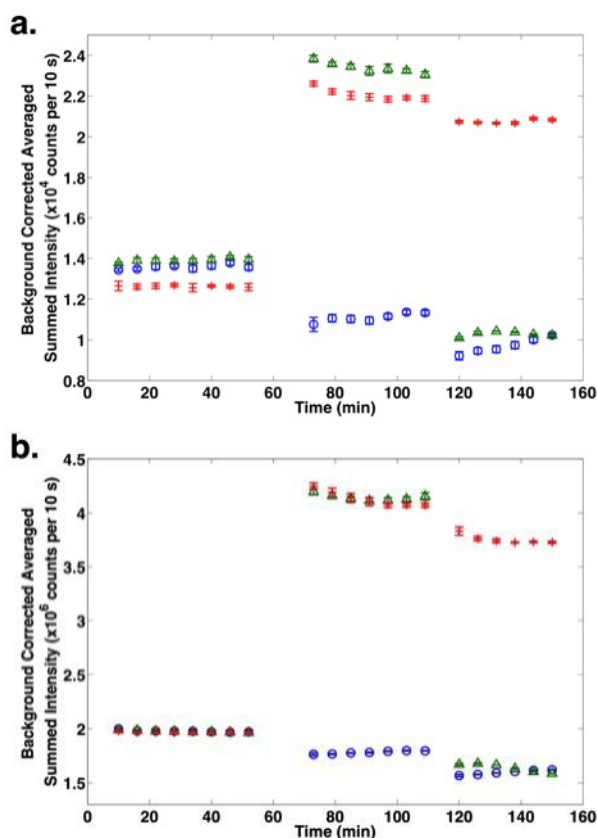


Figure 2.7 Background corrected averaged ($N = 6$) summed intensity of reporter from (a) Cy3 and (b) Cy5. Over time, diluent, probe1, target Let-7a, or noncomplementary miR-9 was added. The change in signal from minute 52 to minute 73 confirms reporter-probe1 complexation. The change in signal from minute 109 to minute 120 confirms specificity of the reporter-probe1 complex for the target of interest. Blue circles, reporter plus buffer dilution controls; green triangles, reporter plus probe1 plus Let-7a; red pluses, reporter plus probe1 plus noncomplementary miR-9. Samples were excited with 742 nm at ~ 100 mW. Error bars from 6 replicates are the same size or smaller than the symbols.

Slight fluctuation in the signal is observed over the 73 to 109 min and the 120 to 150 min time intervals. Variation in signal corresponded to about a 1–2% relative standard deviation over the two time intervals. These fluctuations could be attributed to binding stability and/or photobleaching. Photobleaching was observed for the earlier binding kinetic studies, but the effects

on signal were minor (data not shown). Future studies will use lower excitation powers to reduce photobleaching and other photodamaging effects. The difference between the green triangles and red plus symbols in Figure 2.7a over the first 109 min is most likely a result of cuvette placement error. Notice this difference was negligible in Figure 2.7b. In general, the instrumental error was around 1%. The signal stability of the reporter-probe complex is around 1–4%. We found the dominant source of variability in our measurements is cuvette placement error, with this error varying between 1% and 10%.

A nonspecific binding study demonstrated the ability of the sensor to distinguish Let-7a target (green triangles) from noncomplementary miR-9 (red plus). The small decrease in signal observed in Figure 2.7 upon addition of miR-9 (compare minute 109 to minute 120) was expected from the dilution factor. A 10% decrease in signal was expected from dilution of the reporter-probe complex. Adding miR-9 only decreased the signal by $6\% \pm 2\%$ ($N = 6$) in the Cy3 emission region and by $9\% \pm 2\%$ ($N = 6$) in the Cy5 emission region.

We further evaluated the specificity of the biosensor by presenting it with a miRNA that was nearly identical to the Let-7a except three nucleic acids were changed. Figure 2.8 compares the percent decrease in Cy5 signal upon addition of different types of miRNA to the reporter-probe complex. The values presented in Figure 2.8 take the dilution factor into account when determining the percent decrease in signal. A three nucleotide Let-7a variant (Let-7aV) demonstrated a $-0.6 \pm 3.3\%$ ($N = 3$) change in signal. Addition of the miR-9 showed a $-1.6 \pm 2.0\%$ ($N = 6$) change in signal. The negative sign here indicates the signal increases slightly but is not statistically different from 0% change. Addition of the Let-7a target resulted in a decrease in signal of $\sim 57\%$. These results provide further evidence that the biosensor design has great potential as a selective biosensor.

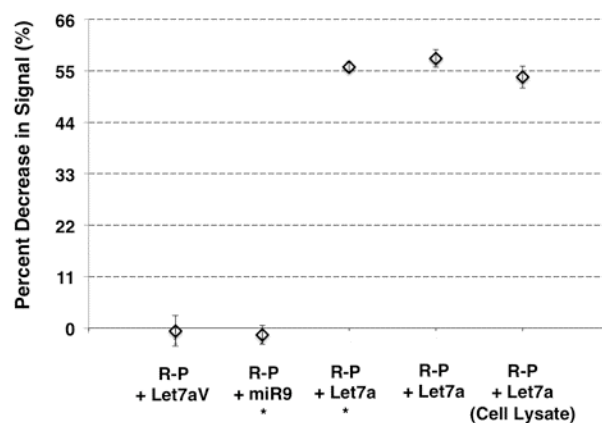


Figure 2.8 Comparison of observed percent decrease of reporter Cy5 emission to evaluate specificity, stability, and effects of cell lysate on reporter-probe biosensor. Displayed as percent decrease in signal. R-P = reporter-probe complex. Unless otherwise stated, all solutions were prepared in buffer. Some error bars are the same size as the symbol. The * indicates N = 6 and the long-term study, otherwise N = 3; each replicate consisted of a 1000 ms exposure time that was averaged over 10 spectra to enhance the signal-to-noise.

The long-term stability of the biosensor can also be seen in Figure 2.8 (indicated by the * under the data point label). The response of biosensor over a four month time period was statistically similar at the 99% confidence interval. At month one, the percent decrease in signal from Let-7a addition was $55.8 \pm 1.1\%$ (N = 6), and it was $57.7 \pm 1.9\%$ (N = 3) at month four. The biosensor is stable for at least four months. For this case, the instrument response error and the cuvette placement error are similar. During the four months of storage, the reporter and probe were stored separately at a concentration of 100 μM in RNase/DNase free 18-M Ω water at $-20\text{ }^{\circ}\text{C}$. When reporter-probe biosensor was to be used, the reporter and probe were first individually diluted to a concentration of 10 μM in the dilution buffer. The reporter and probe were then hybridized together at the desired concentration (1 μM or 100 nM) prior to presenting miRNAs to the reporter-probe complex.

The signal response of the biosensor in cell lysate was studied to determine if proteins, DNA, and other RNA species found in a cell will cause interference in the measurement of Let7a. Raw cell lysate was diluted in half with buffer to lower the concentration of potential interfering species. Determinations of protein and oligonucleotide concentrations were made on the Nanodrop using 280 and 260 nm, respectively. The concentration of DNA and RNA species in cell lysate was ~ 30 times greater than the amount of reporter-probe complex and Let-7a. The amount of protein in the cell lysate was ~ 480 times more concentrated than the reporter-probe complex and Let-7a. Cell lysate solutions were used to prepare the reporter-probe biosensor and to test the recognition and transduction mechanism. A comparison of percent decrease in Cy5 signal from

the biosensor in clean buffer and in cell lysate environments is presented in Figure 2.8. Cell lysate reduced the signal by $53.7 \pm 2.4\%$ ($N = 3$) compared to $57.7 \pm 1.9\%$ ($N = 3$) in the clean buffer. At the 99% confidence interval, these values are not statistically different. This result indicates components in the cell lysate do not have an observable effect on the percent decrease in signal upon addition of Let-7a. Furthermore, the reporter-probe biosensor demonstrates great potential for in vivo applications.

2.4.5 Sensitivity

The limits of detection, limits of quantitation, and sensitivity of the biosensor at 1 μM and 100 nM concentration levels were evaluated and presented in Table 2.2.

Table 2.2 Analytical Figures of Merit Describing Sensitivity of Reporter-Probe Biosensor for Let-7a

	100 nM Reporter-Probe *	1 μM Reporter-Probe
Detection Limit	4 nM (± 1 nM)	9 nM (± 4 nM)
Quantitation Limit	16 nM (± 2 nM)	18 nM (± 4 nM)
Sensitivity (counts/nM)	3.6×10^5 ($\pm 0.23 \times 10^5$)	9.5×10^4 ($\pm 0.1 \times 10^5$)
Linear Dynamic range (nM)	4 to 100	9 to 1,000
Signal to Noise (S/N) at zero analyte addition	1,047	1,601

*Exposure time for 100 nM reporter-probe was 500 ms instead of 100 ms for the 1 μM reporter-probe complex.

Statistical analysis of the calibration studies suggests the 1 μM reporter-probe biosensor has a limit of detection and quantitation of 9 ± 4 nM ($N = 3$) and 18 ± 4 nM ($N = 3$), respectively. Making a crude estimation of the focal volume to be around 1 μL and considering 9 femtomoles of Let-7a, at the detection limit, and 1 picomole from the 1 μM reporter-probe complex, we find ~100 times more fluorescent species than quenched-fluorescent species. To determine if this was a limiting factor on the detection limit, a 100 nM solution of reporter-probe complex will decrease the number of fluorescent to quenched-fluorescent species by a factor of 10 and perhaps the limit of detection will be lowered.

Reducing the reporter-probe concentration to 100 nM yields 4 ± 1 nM ($N = 3$) and 16 ± 1 nM ($N = 3$) for limits of detection and quantitation, respectively. The sensitivity of the 1 μM reporter-probe biosensor to the Let-7a was around 9.5×10^4 counts/nM. Increasing the exposure time to 500 ms for the 100 nM reporter-probe biosensor resulted in a sensitivity of 3.6×10^5

counts/nM. The dynamic range of the concentration was approximately 10^2 orders of magnitude for both concentrations of reporter-probe complex. There was a relatively small $\sim 0.4\%$ error between the zero analyte addition and the y-intercept for both concentrations of reporter-probe biosensor. This error was propagated into the precision of the quantitation limit. The precision of the LOQ for the $1\ \mu\text{M}$ and $100\ \text{nM}$ reporter-probe biosensor was 22% and 12%, respectively. Precision in the limit of quantitation in the signal was less than 1%. Considering excellent precision in the signal limit of quantitation, we suspect pipetting errors were the major source of error in determination of the limits of detection and quantitation.

Decreasing the reporter-probe concentration by a factor of 10 has a marginal impact on the limits of detection and quantitation; however, the precision was improved by a factor of 2. Given the signal-to-noise is on the order of 10^3 for the $100\ \text{nM}$ reporter-probe complex with zero analyte addition, it is possible the reporter-probe concentration can be decreased by at least 2 orders of magnitude to picomolar levels. Assuming a similar concentration dynamic range, it is possible that picomolar limits of detection can be achieved for target miRNA. Use of quenchers and signal-on approaches are currently being investigated to improve the analytical figures of merit.

2.4.6 Reporter Specificity

Noncomplementary Let-7a and miR-9 were added to a solution containing the reporter to test the specificity of the reporter for the probe. Minor nonspecific binding of Let-7a to the reporter was noticed in the Cy3 emission region ($\sim 30\%$) but not in the Cy5 emission region. Addition of miR-9 exhibited about 17% nonspecific binding to reporter in both the Cy3 and Cy5 emission regions. Future experiments will focus on redesigning the reporter to minimize nonspecific binding effects to a negligible amount.

2.4.7 False Positives from Endonuclease Degradation

Enzymatic degradation from nucleases remains a problem plaguing oligonucleotide biosensors. The reporter-probe biosensor was designed specifically to address this problem. Nuclease degradation studies were performed to demonstrate the reduced false positives of the reporter-probe biosensor compared to other biosensors. For these experiments, a reporter-probe biosensor, a molecular beacon, and a traditional double-strand displacement biosensor were subjected to nuclease degradation. Table 2.1 provides the sequences and thermodynamic information for the various types of biosensors. The double-strand displacement biosensor used a

Cy3-Cy5 dye pair for signal transduction. The molecular beacon used a Cy5 reporting dye and an Iowa Black quencher for signal transduction. Equations 2.1, 2.2, and 2.3 were used to determine the percent change in signal due to enzyme degradation:

$$\% \Delta I_{RP} = 100 \times \frac{I_{RP+Enzyme} - I_{Reporter}}{I_{RP} - I_{Reporter}} \quad (Eqn 2.1)$$

$$\% \Delta I_{MB} = 100 \times \frac{I_{MB+Enzyme} - I_{MB}}{I_{MB+Target} - I_{MB}} \quad (Eqn 2.2)$$

$$\% \Delta I_{DSD} = 100 \times \frac{I_{DSD+Enzyme} - I_{DSD}}{I_{Cy5} - I_{DSD}} \quad (Eqn 2.3)$$

$\% \Delta I_{RP}$, $\% \Delta I_{MB}$, and $\% \Delta I_{DSD}$ are the percent changes in signal of the reporter-probe biosensor, the molecular beacon, and the double-strand displacement biosensor, respectively. The numerator corresponds to the change in signal from addition of enzyme; the denominator corresponds to the dynamic range of the biosensors.

Both the molecular beacon and the reporter-probe biosensor have LNA modifications. The molecular beacon showed the most false positive error with a $62\% \pm 2\%$ ($N = 3$) change in signal. The reporter-probe1 complex showed reduced false positives with only a $47\% \pm 1\%$ ($N = 3$) change in signal. This false positive resulted from the stems of the reporter not being thoroughly degraded by the endonuclease. The stems of the reporter in the reporter-probe1 complex were not digested because endonucleases do not effectively react with single-stranded oligonucleotides. As a result, the stems survived endonuclease treatment and were able to rebind and cause a false change in the analytical signal. These results demonstrate that even with LNA both molecular beacons and the reporter-probe1 biosensor are susceptible to false positives. However, the reporter-probe1 demonstrates promise to reduce the extent of false positives. The double-strand displacement biosensor showed a false positive error of $27\% \pm 1\%$ change in signal.

To solve the false positive problem with probe1, a different probe was designed. Probe2 was designed to bind the stems of the reporter and force the endonuclease to degrade those regions as well. The reporter-probe2 complex showed no false positives. In fact, the percent change in signal was $-25\% \pm 5\%$. The negative percent change in signal from reporter-probe2 is attributed to residual quenching of Cy5 from nucleic acids and Cy3 on the reporter-probe2 complex. Therefore, degradation of the reporter-probe2 complex will cause the Cy3 and Cy5 to move apart, disrupting any quenching and increasing the Cy5 signal. Since the reporter-probe complex works as a signal-off sensor, the increase in signal will not contribute to a false positive. Future reporter designs will add carbon-based spacer moieties to increase the distance between dyes and nucleic acids. Future probe designs will only bind one of the stems to improve displacement kinetics and

reduce false negatives. The overall aim will be to redesign the reporter-probe complex to reduce false negatives and false positives to a negligible amount. Adding spacers will have an additional benefit of reducing other forms of nonradiative quenching when the reporter hairpin configuration is formed. Signal-on techniques are more desirable for in situ analysis so we are also currently exploring other resonance energy transfer pairs so the signal will turn on when the reporter folds into the hairpin configuration.

2.5 Conclusion

Early onset of disease can be detected by monitoring changes in miRNA expression levels. This information can be used to initiate timely treatment and/or develop customized treatments for specific diseases. The reporter-probe biosensor has potential to be implemented into existing miRNA therapeutics to serve as a simple indirect indicator of miRNA drug-target binding. The speed, sensitivity, selectivity, and reduced false positive characteristics of the reporter-probe biosensor make it an attractive alternative over current biosensors for miRNA analysis. Low nanomolar limits of detection and a sensitivity of 105 counts/nM were observed for the reporter-probe biosensor. Given the analytical figures of merit, we anticipate that reduction of reporter-probe concentration by 2 to 3 orders of magnitude will improve our detection limits by a corresponding amount.

With the commercial availability of designer oligonucleotides, the reporter-probe biosensor can be reconfigured so it is selective for any RNA or DNA of interest. Using cell membrane transport methods currently employed for molecular beacons, the reporter-probe biosensor has potential for in situ cellular analysis. The ability of the reporter-probe biosensor to reduce false positives gives it a conceivable advantage when used for in situ applications due to the abundance of nucleases within cells. We have established the foundation for a new class of displacement biosensors that use reporter-probe complexes; future studies will focus on optimization of the recognition and transduction mechanisms to increase selectivity and sensitivity.

2.6 Acknowledgements

We thank the labs of Dr. Ryan Mehl and Dr. Vince Remcho for supplying cell lysates and RNase-free water. This work was funded by Oregon State University and the N. L. Tartar Graduate Research Fellowship.

2.7 References

- (1) Pasquinelli, A. E.; Reinhart, B. J.; Slack, F.; Martindale, M. Q.; Kuroda, M. I.; Maller, B.; Hayward, D. C.; Ball, E. E.; Degnan, B.; Müller, P. *Nature* **2000**, *408* (6808), 86.
- (2) Pasquinelli, A. E.; McCoy, A.; Jiménez, E.; Salo, E.; Ruvkun, G.; Martindale, M. Q.; Baguna, J. *Evol. Dev.* **2003**, *5* (4), 372.
- (3) Roush, S.; Slack, F. J. *Trends Cell Biol.* **2008**, *18* (10), 505.
- (4) Reinhart, B. J.; Slack, F. J.; Basson, M.; Pasquinelli, A. E.; Bettinger, J. C.; Rougvie, A. E.; Horvitz, H. R.; Ruvkun, G. *Nature* **2000**, *403* (6772), 901.
- (5) Esquela-Kerscher, A.; Slack, F. J. *Nat. Rev. Cancer* **2006**, *6* (4), 259.
- (6) Shi, X.-B.; Tepper, C. G.; deVere White, R. W. *Cell Cycle* **2008**, *7* (11), 1529.
- (7) Markham, N. R.; Zuker, M. *Nucleic Acids Res.* **2005**, *33* (suppl 2), W577.
- (8) Markham, N. R.; Zuker, M. In *Bioinformatics*; Keith, J. M., Ed.; Walker, J. M., Series Ed.; Humana Press: Totowa, NJ, 2008; Vol. 453, pp 3–31.
- (9) DINAMelt | mfold.rit.albany.edu <http://mfold.rna.albany.edu/?q=DINAMelt> (accessed June 20, 2013).
- (10) Ingle, J. D.; Crouch, S. R. *Spectrochemical Analysis*; Prentice Hall: New Jersey, 1988.
- (11) Lennox, K. A.; Owczarzy, R.; Thomas, D. M.; Walder, J. A.; Behlke, M. A. *Mol. Ther. - Nucleic Acids* **2013**, *2*, e117.
- (12) Peng, Z.; Soper, S. A.; Pingle, M. R.; Barany, F.; Davis, L. M. *Anal. Chem.* **2010**, *82* (23), 9727.
- (13) Wabuyele, M. B.; Farquar, H.; Stryjewski, W.; Hammer, R. P.; Soper, S. A.; Cheng, Y.-W.; Barany, F. *J. Am. Chem. Soc.* **2003**, *125* (23), 6937.

Chapter 3.

Molecular Structure and Thermodynamic Predictions to Create Highly Sensitive microRNA Biosensors

Nicholas E. Larkey, Corinne N. Brucks, Shan S. Lansing, Sophia D. Le, Natasha M. Smith,
Victoria Tran, Lulu Zhang, Sean M. Burrows

Analytica Chimica Acta

Elsevier: Radarweg 29, 1043 NX Amsterdam, The Netherlands

2016, 909, 109-120. DOI:10.1016/j.aca.2015.12.040

3.1 Abstract

Many studies have established microRNAs (miRNAs) as post-transcriptional regulators in a variety of intracellular molecular processes. Abnormal changes in miRNA have been associated with several diseases. However, these changes are sometimes subtle and occur at nanomolar levels or lower. Several biosensing hurdles for in situ cellular/tissue analysis of miRNA limit detection of small amounts of miRNA. Of these limitations the most challenging are selectivity and sensor degradation creating high background signals and false signals. Recently we developed a reporter+probe biosensor for let-7a that showed potential to mitigate false signal from sensor degradation. Here we designed reporter+probe biosensors for miR-26a-2-3p and miR-27a-5p to better understand the effect of thermodynamics and molecular structures of the biosensor constituents on the analytical performance. Signal changes from interactions between Cy3 and Cy5 on the reporters were used to understand structural aspects of the reporter designs. Theoretical thermodynamic values, single stranded conformations, hetero- and homodimerization structures, and equilibrium concentrations of the reporters and probes were used to interpret the experimental observations. Studies of the sensitivity and selectivity revealed 5-9 nM detection limits in the presence and absence of interfering off-analyte miRNAs. These studies will aid in determining how to rationally design reporter+probe biosensors to overcome hurdles associated with highly sensitive miRNA biosensing.

3.2 Introduction

In our previous work, we developed a reporter+probe biosensor that was selective for let-7a [1,2]. Our sensor (the reporter+probe biosensor), has a partially complementary double-stranded design containing a probe sequence and a reporter sequence with dyes on the 3' (3-prime) and 5' (5-prime) ends. The probe strand is completely complementary to the analyte of interest, and the reporter strand is only partially complementary to the probe to permit competitive binding of the miRNA analyte to the probe. The competitive reaction, referred to by some as a toehold-mediated strand displacement/exchange [3], releases the self-complementary reporter from the probe, allowing the reporter to fold onto itself (Figure 3.1). Reporters are designed to form an ideal hairpin structure that brings the 3' and 5' ends (containing the reporting dyes) into the FRET distance. However, some reporter designs can form a non-ideal internal hairpin that raises the baseline signal due to increased dye-to-dye distance. Designing these reporter sequences to work

in an ideal manner takes into account thermodynamics [4–6], kinetics [7,8], and conformation of the reporter strand.

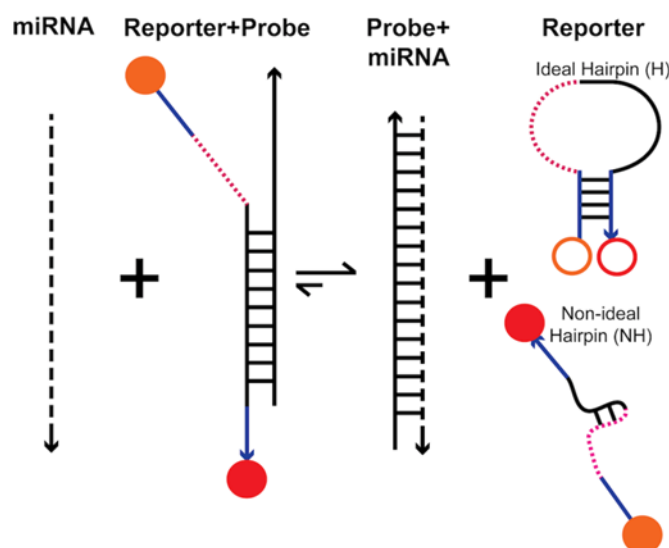


Figure 3.1 Response of reporter+probe biosensor to miRNA analyte. The miRNA (down arrow with dashed line) reacts with reporter+probe complex to form the probe+miRNA complex and free reporter. Reporter (Down arrow with solid and dashed regions) is only partially complementary to probe (Up arrow with solid line) in the region indicated in black. The dotted red region of the reporter is not complementary to probe, and the blue region represents the reporters stems. When in the hairpin conformation, the reporter forms a stem-loop that is either ideal with 5' and 3' ends directly adjacent to each other, or a non-ideal hairpin that separates the dyes at different distances (Colored circles, orange for Cy3 and red for Cy5). Empty colored circles indicate quenched emission, and filled circles indicate unquenched emission.

Let-7a is only one of the thousands of miRNAs that have been discovered and only one among those that have been found to regulate disease progression [9–15]. Here we investigated multiple reporters to be used in reporter+probe biosensors for two different mouse-derived miRNAs associated with cancer progression: miR-26a-2-3p and miR-27a-5p [16–20]. In this work we will build upon our previous research [1,2] to further examine how the predicted thermodynamic and structural parameters of the reporters, probes, and analytes influence the analytical performance of reporter+probe biosensors. Similar to work by others [7,21,22], the relationship between the Cy3 and Cy5 dye emission was used to understand the conformational states of the reporters in solution with and without probe, and was related to the predicted conformations. Specifically, we will discuss the importance of changes in thermodynamic values, molecular structures, and base pairing before and after reporter+probe formation and subsequent probe+analyte formation. To the best of our knowledge, we were the first group to describe a competitive nucleic acid biosensor that uses a self-complementary reporting molecule to reduce

false signals [1,2]. This design has since grown in popularity for use in other technologies like Nanoflares for messenger RNA (commercially known as SmartFlares®) [23] and molecular sentinels [24]. The results of the work presented here will enable the community to rationally design reporter+probe biosensors to achieve a robust, selective, and sensitive biosensor with minimal false signals.

3.3 Experimental

3.3.1 Reporter Design Procedure

The process for designing the biosensor sequences is outlined in Figure 3.2. DNA analogs of each miRNA strand were used as a substitute because RNA is more susceptible to degradation than DNA. A MATLAB program developed in-house was used to design the nucleic acid sequences for the reporter+probe biosensors based on a particular miRNA analyte, in this case they were miR-26a-2-3p and miR-27a-5p. The computer program starts by designing a probe strand that is fully complementary to a given miRNA analyte. Several reporter strands were then made to be partially complementary to the probe. For consistency, each of the reporters in this study contained the same stem sequence, 5'-CGATG—CATCG-3'. The computer program allows control over the length of both the complementary and non-complementary regions on the reporter. The non-complementary regions of the reporters were made of random nucleic acid sequences. The reporters were then filtered to remove those reporters whose non-complementary region bind to the probe. Several additional filtering steps were used to remove potential reporters that may bind to the miRNA analyte and off-analytes. All of the MATLAB filtering steps were based mainly on Watson-Crick binding and brought the number of potential reporters down from thousands to tens of reporters.

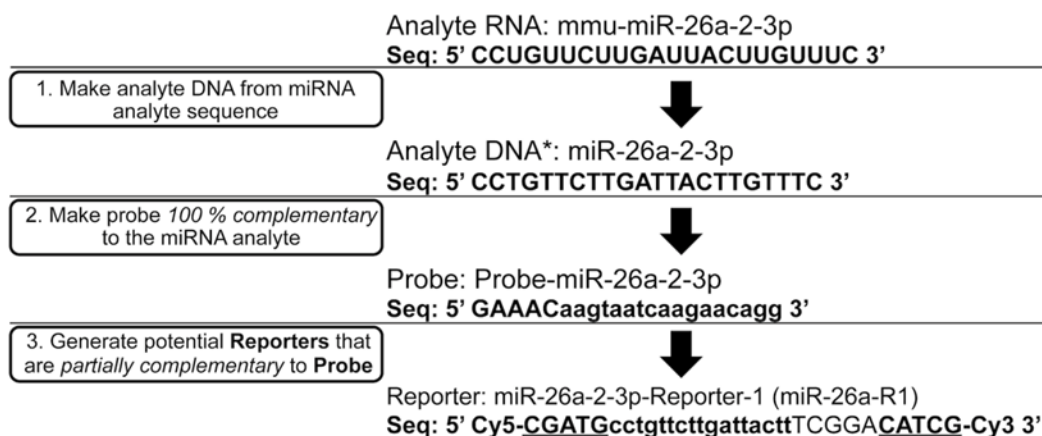


Figure 3.2 Outline of the procedure to design a reporter and probe for a given miRNA analyte. Bold regions indicate complementary binding. The bold, uppercase, and underlined region of the reporter indicates the self-complementary stem. The bold and lowercase regions represent the complementary regions between the reporter and probe. The non-bold uppercase region of the reporter represents the non-complementary section of the reporter. * DNA was used instead of RNA because DNA is less susceptible to degradation and easier to work with.

The remaining reporter candidates were then more rigorously evaluated for suitable thermodynamics using freeware from the RNA Institute at SUNY Albany [25–27]. See Section 3.3.2 below for a more detailed description of how the thermodynamic values, molecular structures, and equilibrium concentrations of the best reporter candidates were predicted. The differences in Gibbs energy (ΔG), enthalpy (ΔH), entropy (ΔS), and melting temperature (T_m) were examined as metrics to predict if a sensor will work, as the differences drive the formation of the reporter+probe complex and subsequently the probe+analyte complex. Reporter+probe biosensors that exhibited a large negative $\Delta\Delta G$ when going from reporter+probe complex to probe analyte complex were sought after (See Section 3.4.1 below for a discussion on the magnitude of the $\Delta\Delta G$ values).

To increase the stability of the reporters and combat enzymatic degradation, three locked nucleic acids (LNAs) [28,29] were strategically placed into each of the reporters. Table A2.1 in Appendix II lists the sequences chosen and where the LNAs were placed. Multiple reporter designs were investigated to determine if the theoretical thermodynamic values would serve as a predictive tool for functional reporters.

Two different reporter sequences with similar thermodynamic metrics were chosen for each miRNA to investigate any alterations in biosensor functionality. Reporters miR-26a-2-R1/R2 were made for use in reporter+probe biosensors for miR-26a-2-3p. Reporters miR-27a-R1/R2 were made for use in reporter+probe biosensors for miR-27a-5p. Each biosensor was subject to

miR-29b-1-5p as a common off-analyte [30]. For the remainder of this study, miR-26a-2-3p, miR-27a-5p, and miR-29b-1-5p will be referred to as miR-26a, miR-27a, and miR-29b, respectively.

The reporters contain two Cyanine (Cy) dyes, a 3' Cy3 and a 5' Cy5. Based on our previous work [14,15], the Cy5 dye was used as the major reporting signal. When Cy3 and Cy5 are in close proximity (primarily in the hairpin conformation), the Cy3 acts as a quencher of Cy5. Previously, we found that the Cy3-Cy5 pair does not effectively stimulate Förster Resonance Energy Transfer (FRET) enhancement with our current reporter design, but still worked in a quenching mechanism. While quenching molecules like Iowa Black Red-Quencher (IAbRQ) further reduce Cy5 emission [14], the limits of detection were not any better than using Cy3 as a quencher. The signal-off approach used here differs from molecular beacons that use signal-on, but we found that for nucleic acid biosensors the figures of merit (FOM) for signal-on and signal-off approaches were similar [14]. We have successfully made signal-on reporter+probe designs that will be the subject of future work.

All the oligonucleotides were obtained from Integrated DNA Technologies (IDT) pre-diluted in their IDTE buffer at pH 7.5 and used as received. The samples were then diluted as needed to the required concentrations in a buffer solution composed of Phosphate-buffered saline containing 10 mM Tris buffer, 2.5 mM MgCl₂, and 0.005% Tween 20 (final pH ~ 8). Concentrations of solutions were confirmed by a Nanodrop spectrophotometer (ND-1000).

3.3.2 Thermodynamic, molecular structure, and molarity fraction predictions

All predictions were performed using UNAFold freeware (a combination of mfold and DINAMelt) from SUNY Albany [25–27]. Calculations for the reporter hairpin thermodynamic values and conformations were performed using the Quikfold application under the UNAFold family. The parameters used were: DNA, 25 °C, 10 mM [Na⁺], 2.5 mM [Mg²⁺], Linear sequence type, 5% suboptimal structures, maximum of 50 foldings, no limit on distance between paired bases. Calculations for reporter+probe, probe analyte, and other dimer hybridizations were performed using the Two State melting (hybridization) tool. The parameters used were: DNA, 25 °C, 10 mM [Na⁺], 2.5 mM [Mg²⁺], and 100 nM strand concentration.

The molarity fraction, secondary structure, and base pair probability of hairpins, homodimers, and heterodimers were calculated from DINAMelt. The 'homodimer' function was used to evaluate homodimers and the 'hybridization of two different strands' function was used to evaluate heterodimers. Different combinations of reporter, probe, and analyte were evaluated for

their heterodimer or homodimer formation. To determine molarity fraction and predict secondary structure, the advanced form of the application was chosen and the energy minimization mode was selected. A temperature range of 18-40 °C was selected to span the experimentally relevant temperature window. The polymer mode was left unselected. The parameters chosen were: DNA, reporter [A₀] and probe [B₀] concentrations set to 0.1 mM (100 nM), [Na⁺] concentration set to 10 mM, [Mg²⁺] concentration set to 2.5 mM. All other settings were set to default. Secondary structures were predicted at 25 °C. Base pair probability was obtained from partition function figures using the partition function mode instead of energy minimization, but all the parameters remained the same.

3.3.3 Fluorimetry apparatus

A custom-built fluorimeter, previously described [1], was used to characterize the biosensors. Briefly, a titanium-sapphire ultrafast tunable laser (Mai Tai, Spectra Physics) was used to achieve two-photon excitation. The dyes were excited at 742 nm with 75 mW average power. The only difference from the instrument outlined in our earlier publication was the spectrometer. Here, a Princeton Instruments Acton SP2300 Spectrometer with a 300 grooves mm⁻¹ grating blazed at 500 nm was used. Unless otherwise stated, the grating was centered at 650 nm (spectral range covered 607.569-692.347 nm, 0.165 nm pixel⁻¹) to look primarily at the Cy5 emission. Emission from Cy5 above 692 nm was not collected because the 705 nm long-pass dichroic mirror does not reflect wavelengths above ~690 nm to the detector. The Cy5 emission range did not contain much of the Cy3 emission peak.

The detector was a Princeton Instruments electron-multiplied CCD camera (ProEM: 512B eXcelon) that used LightField software with the following parameters for acquisition: 500 ms acquisition time, 3 frames, 20 frame averages, 100 kHz analog to digital conversion (ADC) speed, high analog gain, low noise ADC quality, and full frame readout, unless otherwise stated. A locking cuvette holder was installed for the ‘reporter response and calibration curve’ experiments outlined in Experimental Section 3.3.4. All other experiments were conducted prior to installation of the locking cuvette holder. Samples that did not use the locking cuvette holder were susceptible to cuvette placement error due to the cuvette sitting in a different spot in the holder, leading to as much as 10-15% error [1] between replicates. The locking cuvette holder reduced inter-sample error to 1-2%.

The ability of the reporters to respond to probes and the reporter+probe biosensor's ability to respond to analyte were examined first. To show that the reporter+probe biosensors were selective for their intended analyte, two off-analytes were presented to the biosensors in the absence of analyte. No signal change upon addition of off-analytes indicated selectivity for a given biosensor. Solutions were made to contain 100 nM reporter, hybridized reporter+probe biosensor, or reporter+probe biosensor with equimolar analyte or off-analytes. A total of nine frames were obtained from 3 samples each containing 3 frames (3 frames * 3 samples = 9 frames total). The 9 frames were averaged and the standard deviation was reported as the error.

For calibration experiments, the reporter+probe solutions were prepared by hybridization of equimolar concentrations of each reporter and probe in a microcentrifuge tube. The miR-26a-R1 or miR-26a-R2 was hybridized with probe-miR-26a for at least 1 h. Hybridization of miR-27a-R1 and miR-27a-R2 with probe-miR-27a took at least 2 h. A longer reaction time was needed for miR-27a reporters with probe due to slow kinetics (Figs. A2.1 and A2.2). Aliquots of the hybridized solution were then added to another microcentrifuge tube containing analyte in enough buffer to bring the concentrations of the reporter+probe to 100 nM and 0-100 nM miRNA analyte in 20 nM increments. The reporter+probe biosensors were allowed to hybridize with the analytes for at least 1 h. All hybridizations were carried out at room temperature (~22 °C). Three calibration curves were performed for each reporter+probe biosensor (with the exception of miR-27a-R2+probe because that biosensor did not work, see Results and Discussion below).

To test for matrix effects from the off-analytes, a mixture of reporter+probe with increasing concentration of miRNA analyte and a constant concentration of two off-analytes was investigated. For all experiments each solution contained 100 nM reporter+probe, 100 nM off-analytes, and 0-100 nM analyte in 20 nM increments. The reporter+probe biosensors for miR-26a were allowed to react with analyte and off-analytes for at least 1 h before analysis. MiR-27a-R1+probe was allowed to react with analyte and off-analytes for at least 2 h before analysis. The solutions were then analyzed using the fluorimeter described above (Section 3.3.3).

Cy5 intensity values were obtained by summing averaged emission spectra from 620.07 nm to 690.86 nm. To determine the detection limits, the linear fit for each calibration curve was performed to 100 nM of analyte added. The intensity values of all the data points in the calibration curves were normalized to the intensity of the 100 nM reporter+probe solution without analyte. The linear fits were then forced through the y-intercept at one (the 0 nM miRNA and 100 nM

reporter+probe normalized intensity), which served as the “zero” point, correlating to no analyte added. The limit of detection (LOD) was determined as $3 \times SD^{\text{zero}}/m$ and limit of quantitation (LOQ) was $10 SD^{\text{zero}}/m$, where SD^{zero} was the standard deviation of the “zero” point normalized intensity and m was the slope of the calibration curve.

3.4 Results and discussion

3.4.1 Comparison of molecular structures and thermodynamics to signal change for reporter+probe biosensors

The sequences of miR-26a-R1 and miR-26a-R2 (Table A2.1) were different in that R1 had a longer complementary region than R2 by four bases. The first 18 bases in the reporters' sequences (from 50 to 30) were the same. After the 19th base the sequence ‘act+t’ in R1 became ‘GTG+G’ in R2 decreasing the complementarity. The remainder of the non-complementary sequences in R1 and R2 were also quite different: (TC)G(G)A to (TC)C(G)T, respectively (sequence similarity indicated by parentheses).

The reporters for miR-27a (Table S1) were different in the complementary region by three bases, with the miR-27a-R1 having three more base-pairs to the probe than R2. The first nucleic acid after the 50 stem in R1 was complementary to the probe as an Adenine, but the first nucleic acid after the stem in R2 was non-complementary as a Thymine. The two reporters for miR-27a had the order of Guanine and Thymine flipped at the sequence positions 16 and 17 (with R2 being flipped with respect to R1). The remainder of non-complementary sequences of R1 and R2 were also quite different: GGAC+GTTCGG vs. TCGT+CCGATT, respectively.

The four reporter designs outlined in this study were chosen because they met three criteria that we had hypothesized would result in a functional reporter+probe biosensor. First, the most probable and stable conformation of the reporter was an ideal hairpin that would bring the two dyes close enough to permit quenching (Figure 3.1, 3.3, and A2.3). Second, the melting temperature for the first reporter hairpin conformation had to be at least 10 °C above operating temperature (in this study 25 °C), and the Gibbs energy had to be about -2 kcal mol⁻¹ or more negative (Table 3.1 and Table A2.2). Third, the $\Delta G_{\text{hybridization}}$ between the reporter and probe, as well as the $\Delta\Delta G$ between reporter+probe (R+P) and probe+analyte (P+A), had to be sufficiently large and negative to drive the reaction forward (Figs. A2.4 and A2.5 show a threshold around 10 and 5 kcal mol⁻¹ for (R+P) hybridization and conversion of (R+P) to (P+A), respectively) [1,2].

These criteria also require the reporters and reporter+probe complexes minimize off-analyte interactions as described in Section 3.3.1 and validated in Table A2.3. Based on these criteria, the fewest reporter hairpins obtained for miR-26a was one. Finding just one reporter hairpin that met all the design criteria for miR-27a was more difficult and the fewest number of hairpins was three.

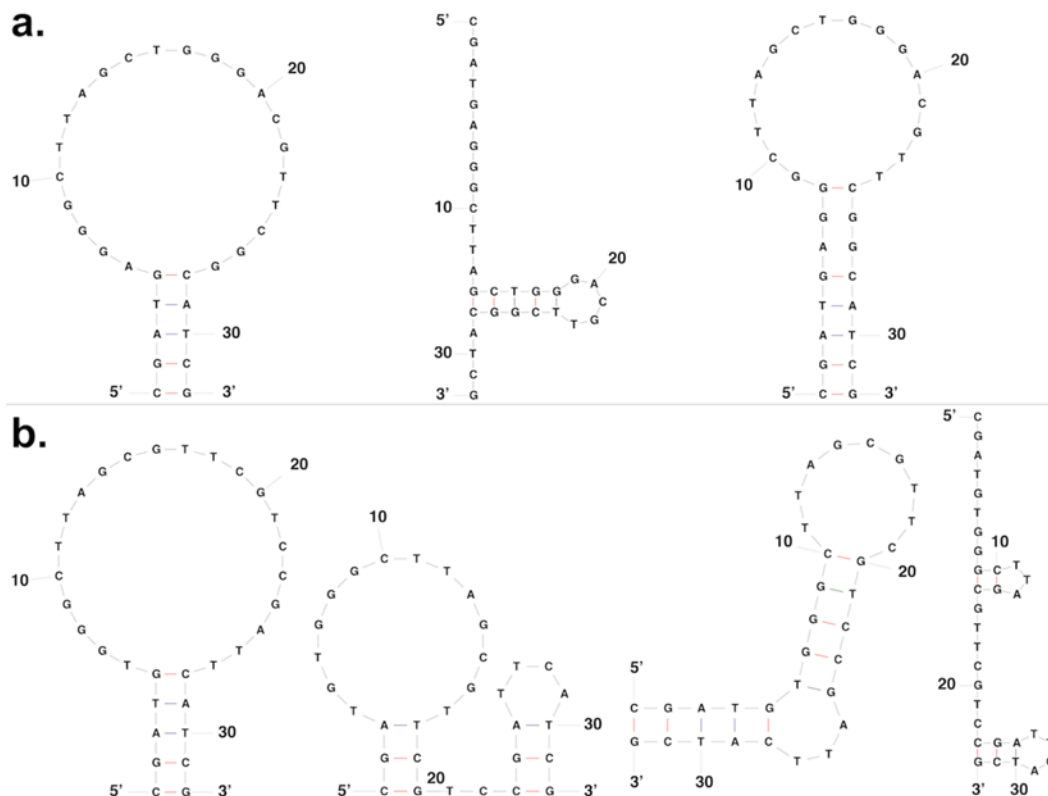


Figure 3.3 Predicted miR-27a-reporter hairpin conformations in order from left to right according to decreasing stability: (a) corresponds to miR-27a-R1 with three hairpin conformations: ideal hairpin, a non-ideal hairpin, and another ideal hairpin. (b) Corresponds to miR-27a-R2 with four hairpin conformations: ideal hairpin, non-ideal hairpin, ideal hairpin, and non-ideal hairpin. Structures were obtained from Quikfold using parameters described in Experimental Section 3.3.2. Figure does not indicate 3-dimensional structure.

Table 3.1 and Table A2.2 outline the thermodynamic values, including ΔG , ΔH , ΔS , T_m ($^{\circ}\text{C}$), as well as the number of total base pairs, GC base pairs, and changes in base-pairs. The number of GC base pairs was included as a separate value due to their greater stability than AT pairs.

Table 3.1 Comparison of thermodynamic values and molecular structure information for reporter hairpins, reporter+probe complexes, and conversion of reporter+probe complexes to probe+analyte complexes.

	miR26a-R1	miR26a-R2	miR27a-R1	miR27a-R2
$\Delta G(R)^*$ kcal mol $^{-1}$	-2.33	-1.85	-1.95	-2.15
$\Delta H(R)^*$ kcal mol $^{-1}$	-55.4	-37.8	-37.9	-40.6
$\Delta S(R)^*$ cal mol $^{-1}$ K $^{-1}$	-178	-120.58	-120.58	-128.96
$T_m(R)^*$ $^{\circ}\text{C}$	38.1	40.3	40.3	41.7

Number of predicted reporter structures	1	2	3	4
H:NH	1:0	2:0	2:1	2:2
Total base pairs in R*	7	5 (7**)	5(6**)	5(10**)
Total base pairs in RP	17	13	12	9
Δ Bases R-(1 st hairpin)* to RP	+10	+8(+5**)	+7(+6**)	+4 (-1**)
R-Homodimer T _m	-4.6	-9	14.8	15.7
R-hairpin to R-homodimer probability	Hairpin > Homodimer	Hairpin ~ Homodimer	Hairpin ~< Homodimer	Hairpin < Homodimer
Total number of base pairs in R-homodimer	5	5	10	24
Δ Bases homodimer to RP	+12	+8	+2	-15
Δ G(RP) kcal mol ⁻¹	-19.8	-16.1	-16.9	-12.9
Δ H(RP) kcal mol ⁻¹	-126.8	-107.5	-98.1	-83.1
Δ S(RP) cal mol ⁻¹ K ⁻¹	-359	-306.4	-272.5	-235.5
T _m (RP) °C	48.9	41.9	46.1	34.3
$\Delta\Delta$ G(RP to PA) kcal mol ⁻¹	-5.5	-9.2	-14.2	-18.2
$\Delta\Delta$ H(RP to PA) kcal mol ⁻¹	-41.5	-60.8	-80.7	-95.7
$\Delta\Delta$ S(RP to PA) cal mol ⁻¹ K ⁻¹	-120.5	-173.1	-223.1	-260.1
Δ T _m (RP to PA) °C	5.2	12.2	17.9	29.7
Δ Base pairs (RP to PA)	5	9	8	11

*=most stable ideal hairpin, ** = second stable ideal hairpin. H = ideal hairpin and NH = non-ideal hairpin.

Fig. A2.3 and Table 3.1 and Table A2.2 reveal that miR-26a-R1 had only one stable ideal hairpin (H) but miR-26a-R2 had two stable H's. The most stable structure of both the miR-26a reporters was an ideal hairpin, in line with our initial design criteria. Recall from Figure 3.1 that

an ideal hairpin conformation for a reporter has the 50 and 30 ends of the stems close enough to cause the dyes to interact with each other and adequately quench the signal.

Fig. 3.3 and Table 3.1 and Table A2.2 shows that the most stable theorized conformations for the miR-27a reporters were ideal hairpins. Fig. 3.3 also shows the miR-27a reporters contained non-ideal hairpins as theorized stable structures. As depicted in Figure 3.1, a non-ideal hairpin conformation (NH) has the two dyes further apart and causes less quenching than that of the ideal hairpin (H). Fig. 3.1 and Table 3.1 and Table A2.2 show that miR-27a-R1 had three conformations: H, NH, and H (in order of decreasing stability). However, miR-27a-R2 had four conformations: H, NH, H, and NH (in order of decreasing stability). The two most stable conformations of miR-27a-R2 were an ideal hairpin followed by a non-ideal hairpin, with Gibbs energies of -2.15 and -1.98 kcal mol⁻¹, respectively. The small difference in favorability between these two conformations, seen in Fig. 3.3b and Table A2.2, suggest the reporter molecules assume both ideal and non-ideal conformations in solution, or even switch back and forth between them as the molecule tests different binding motifs. This argument is strengthened by the fact that the Gibbs energy for the most stable NH of miR-27a-R2 was more stable than the most stable ideal hairpins of miR-26a-R2 and miR-27a-R1 (-1.85 and -1.95 kcal mol⁻¹, respectfully - Table A2.2).

Table 3.1 and Fig. A2.4 shows the thermodynamic values, total base pairs, and changes in base pairs associated with reporter+probe complex formation for each of the four reporters. From a thermodynamic standpoint, miR-27a-R2 probe complex was the least stable. The low thermodynamic stability of miR-27a-R2 probe was likely due to it containing the fewest number of predicted base pairs and changes in base pairs amongst all the reporters. From Table 3.1, miR-27a-R2 had nine base pairs and depending on the ideal hairpin structure, but only gained four or lost one base pair upon complex formation (based on ideal hairpin base pairs).

Table A2.4 shows the thermodynamic values and base pairs associated with forming probe analyte complexes. Table 3.1 and Fig. A2.5 show that among the reporters, miR-26a-R1 had the smallest changes in base pairs and melting temperature upon conversion from reporter+probe to probe+analyte, but the most positive-but still negative- $\Delta\Delta G$, $\Delta\Delta H$, and $\Delta\Delta S$. In contrast, miR-27a-R2 had the largest changes in base pairs and melting temperature as well as the most negative $\Delta\Delta G$, $\Delta\Delta H$, and $\Delta\Delta S$. Recall large magnitudes in $\Delta\Delta G$, $\Delta\Delta H$, $\Delta\Delta S$, ΔT_m , and changes in base pairs were desired to push the reaction forward, provided the reporter+probe formed.

Considering the thermodynamic and base pairing analysis described above, we expected all the reporters to form reporter+probe complexes and function as biosensors. In fact, from a thermodynamic standpoint we expected miR-27a-R2 to work the best. However, Fig. 3.4 shows this was not the case.

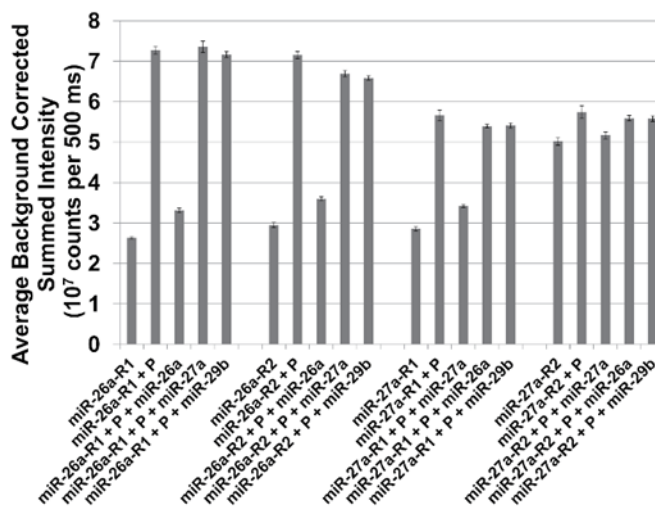


Figure 3.4 Reporter response to probe and reporter+probe response to analytes and off-analytes (n = 9). Each reporter+probe biosensor was sensitive to equimolar analyte, and not sensitive towards off-analytes.

To understand how the difference in sequence, molecular structure, and thermodynamic values for each reporter affected their performance as part of a biosensor, we evaluated the reporter signal change before and after adding probe and then analyte (Fig. 3.4). The experimental baseline signal from each reporter was an average from the hairpin sampling different conformations accompanied by opening and closing of the hairpin as the hairpins are not static. While the dynamic nature of the hairpin causes varying amounts of fluorescent signal, the detection volume contained many reporters in various conformations that change states on time scales faster than the acquisition time. Thus, the signal from a given reporter was stable (~1-3% RSD) over the acquisition times used in this work.

Comparison of the hairpin signal among the different reporters in Fig. 3.4 reveals that a reporter with more than one predicted hairpin did statistically increase the baseline signal (95% confidence interval, n = 9). Ideal hairpins for the reporters demonstrated quenched fluorescence $\sim 3 \times 10^7$ counts per 500 ms, but the extent of quenching depended on the proximity and orientation of the dyes. If a NH forms as much or more than an H (Figure 3.1 and Fig. 3.4), then less quenching will occur resulting in more fluorescence observed from the dyes on the reporter ($\sim 5 \times 10^7$ counts per 500 ms for miR-27a-R2). Both miR-26a-R2 and miR-27a-R1 had more than one H and signals near 3×10^7 counts per 500 ms, but miR-27a-R1 had one NH - as the second stable structure -

compared to no NH's for miR-26a-R2. From these results, the presence of a NH alone - as a second stable structure - did not raise the reporter baseline signal above that of a reporter with two H's.

Signal change from the reporter before and after probe addition was used to determine the expected signal change from the reporter+probe biosensor in the presence of miRNA. Addition of probe to reporter also served as a control to confirm the probe opened the hairpin. Upon probe binding the intensities of miR-26a-R1 and miR-26a-R2 increased by $176 \pm 4\%$ and $142 \pm 4\%$, respectively. Addition of probe to miR-27a-R1 and miR-27a-R2 caused the signal to increase by $98 \pm 5\%$ and $14 \pm 4\%$, respectively. A similar trend in percent signal change was observed upon miRNA addition: $120 \pm 4\%$ (miR-26a-R1), $99 \pm 3\%$ (miR-26a-R2), $65 \pm 4\%$ (miR-27a-R1), and $11 \pm 3\%$ (miR-27a-R2). Of these changes in signal, miR-27a-R2 was the smallest, but statistically significant ($p < 0.05$, $n = 9$). Preliminary data of the discrepancies between the percent changes in signal from reporter hairpin to reporter+probe and reporter+probe to reporter hairpin after miRNA addition suggest the biosensors were about 70% quantitative.

One major difference observed among the reporters was that miR-27a-R2 had a baseline signal that was over ~ 1.7 times greater than the other reporter hairpin signals in Fig. 3.4. Considering the large baseline signal from miR-27a-R2, along with the evidence that the reporter hairpin had a similar intensity to the other reporter probe complexes ($\sim 5 \times 10^7$ counts per 500 ms), suggested that on average the dyes were far apart for miR-27a-R2 alone. However, Fig. A2.6 shows all reporters had low Cy3 relative to Cy5, suggesting a structure with the dyes close to one another. Thus, the miR-27a-R2 must have dyes close enough for quenching, but not close enough to fully quench the Cy3 and Cy5 emission. From the experimental data in Fig. 3.4, Fig. A2.6, and the predicted Gibbs energies of the H and NH, we hypothesize that the high baseline signal from miR-27a-R2 came from an equilibrium between the most stable H and NH conformations of the reporter.

To further support the structure of miR-27a-R2, both the miR-27a-R2 hairpin and reporter probe complex exhibited about a 5 nm red shift in the Cy5 emission with respect to the other reporters (Fig. A2.7). A red shift in the Cy5 emission arises from the molecular environment that the Cy5 exists in and has previously been traced to interactions between DNA and cyanine dyes [31]. The observed red shift confirms the miR-27a-R2 had a different structure than the other reporters. See Fig. A2.6 to A2.9 for more evidence and discussion regarding the structure of miR-27a-R2 compared to other reporters as a hairpin and complexed to probe. Another possible state

miR-27a-R2 may have existed in was a homodimer. We looked into the occurrence of possible homodimers that could be affecting the signal of the reporter (Fig. 3.5 and Table 3.1 and Table A2.5). Amongst all of the reporters in Table A2.5, miR-27a-R2 formed the second most stable homodimer in terms of Gibbs energy ($-5.6 \text{ kcal mol}^{-1}$, miR-27a-R1 was the most stable) and the most stable in terms of enthalpy ($\Delta H = -122.2 \text{ kcal mol}^{-1}$), melting temperature ($15.7 \text{ }^\circ\text{C}$), and number of base pairs (24 total and 14 GC).

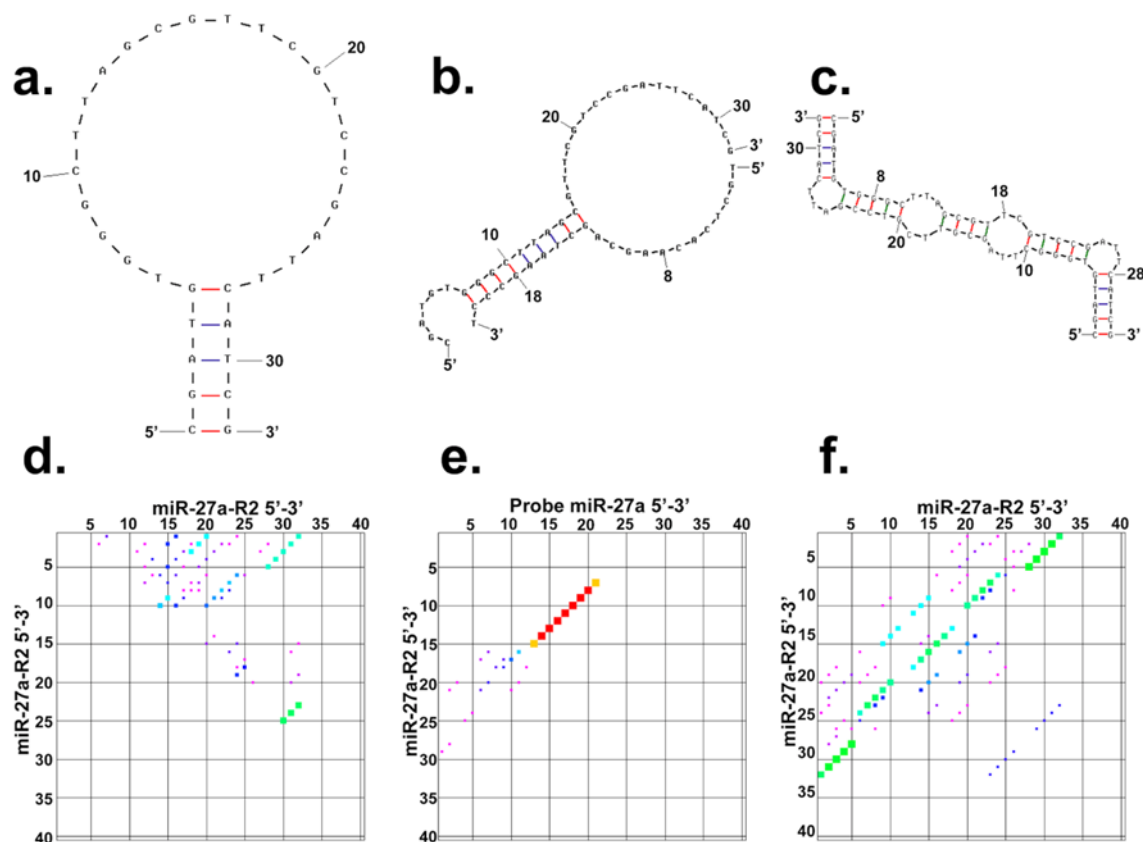


Figure 3.5 Energy minima structures and partition function probability maps for miR-27a-R2. The predicted energy minima structures for (a) miR-27a-R2 folded, (b) miR-27a-R2+Probe complex, and (c) miR-27a-R2 homodimer, respectively, at $25 \text{ }^\circ\text{C}$. Figure does not indicate 3-dimensional structure. (d)-(f) are partition function probability maps that correspond to energy minima structures (a)-(c), respectively. (Size and color of dots in partition function probability map indicate probability). The largest boxes are the most probable base pairs. For the color, the probability increases from violet (least probable) to red (most probable). See Fig. S11 for probability maps color code. Structures and probability maps were obtained using parameters described in Experimental Section 3.3.2. (For interpretation of the references to colour in this figure legend, the reader is referred to the web version of this article.)

While the miR-27a-R2 homodimer was favored by Gibbs energy and enthalpy, it was not favored by entropy ($\Delta S = -391 \text{ cal mol}^{-1} \text{ K}^{-1}$) and the melting temperature was below room temperature ($15.7 \text{ }^\circ\text{C}$). Since the reporter did have locked nucleic acids that likely increased the melting temperature near to room temperature, combined with the 24 base pairs in the homodimer, suggests a homodimer may have formed. However, the high Cy5 signal ($\sim 5 \times 10^7$ counts per 500

ms) observed did not support the predicted reporter homodimer structure (Fig. 3c) as a major product because the Cy3 and Cy5 would be next to each other much like an ideal hairpin, quenching the signal. Instead, the homodimer may be dynamically forming and unforming such that the Cy3 and Cy5 are not close enough to fully quench the signal. All the results for miR-27a-R2 presented support the claim that it exists in many states including a dynamic homodimer along with the two ideal and two non-ideal hairpin conformations.

While reporters may form homodimers, the biosensor can still function provided the probe can react with a reporter to form a reporter+probe complex and change the signal. Comparing the conversion of reporter homodimers to reporter+probe complexes in Fig. A2.10 reveals some key differences between miR-27a-R2 and the other reporters. Mainly the conversion of miR-27a-R2 homodimer to reporter+probe was the most positive in terms of $\Delta\Delta G$ (about -7 kcal mol^{-1}) and the change in melting temperature was the smallest ($\sim 19 \text{ }^\circ\text{C}$). In addition, the process was endothermic and resulted in the loss of 15 base pair interactions (Fig. A2.10).

To better understand the structural states of miR-27a-R2 and how it could affect the biosensor functionality, we compared the energy minima predicted structures and probability maps of miR-27a-R2 to the reporter that worked the best (miR-26a-R1). Figs. 3.5 and 3.6 show the theorized interaction structures (a-c) and probabilities (d-f) between reporter hairpin, reporter+probe, and reporter homodimer for miR-27a-R2 and miR-26a-R1, respectively. In (d-f) of Figs. 3.5 and 3.6, increasing size and color change from cold (blue) to hot (red) followed increasing probability (The color code key for the probability maps can be found in Fig. A2.11).

Comparison of Fig. 3.5d to 3.5f reveals that the homodimer had large green boxes compared to the smaller light green boxes of the hairpin, suggesting that the homodimer was more probable for miR-27a-R2. Now compare the most stable NH of miR-27a-R2 from Fig. 3.3b at positions 23, 24, and 25 to those positions in the probability map of Fig. 3.5d. Note the hairpin in Fig. 3.5d had positions 23, 24, and 25 bound to positions 32, 31, and 30, respectively with large green boxes suggesting a highly probable state (the green boxes indicate over 50% probability). We will use a bullet (\bullet) to represent binding between two base pair positions. The 23 \bullet 32, 24 \bullet 31, and 25 \bullet 30 binding positions were present in both the most and least stable NH. The most stable NH also had positions 18 \bullet 3, 19 \bullet 2, and 20 \bullet 1 binding but with small teal boxes that were about 20% probable. The other NH also had positions 9 \bullet 15 and 10 \bullet 14 bound with 10-20% probability. Finally, the most stable ideal hairpin had small light green boxes indicating 30-50% probability in

the stem. The variety of probable hairpin structures was the main basis to suspect the non-ideal hairpins were in equilibrium with ideal hairpins. In fact the most stable NH was likely as probable if not more probable than the most stable H. This analysis of H and NH probabilities combined with the observed signals in Fig. 3.4 and low melting temperature of the homodimer (Table A2.5) suggest the homodimer will most likely not form in large amounts despite the high predicted probability. Any small amount of homodimer that may form will likely restrict formation of reporter+probe because such a process was endothermic and decreased the number of base pairs formed (Table A2.5 and Fig. A2.10). Considering the small change in signal upon probe binding for miR-27a-R2 in Fig. 3.4 in relation to Fig. 3.5b and 3e show that even with highly (over 90%) probable base pairs in the reporter+probe complex, probability alone was not enough to predict reporter probe complex formation.

The stability of a miR-27a-R1 homodimer was predicted to be $\Delta G = -6.5 \text{ kcal mol}^{-1}$, $\Delta H = -84.8 \text{ kcal mol}^{-1}$, $\Delta S = -262.5 \text{ cal mol}^{-1} \text{ K}^{-1}$, T_m 14.8 °C, 10 base pairs, and 6 GC base pairs (Table A2.5). In terms of probability, the homodimer was predicted to be as or slightly more probable than the hairpin (Fig. A2.12). Moreover, examination of the equilibrium between homodimer and reporter+probe heterodimer for miR-27a-R1 reveals the $\Delta\Delta H$ and $\Delta\Delta S$ were $-13.39 \text{ kcal mol}^{-1}$ and $-10 \text{ cal mol}^{-1} \text{ K}^{-1}$ (Fig. A2.10). While presence of homodimers may have contributed to issues with the kinetics of miR-27a reporters, there were some key differences between the homodimers for miR-27a-R1 and R2. The magnitudes of ΔH and ΔS for miR-27a-R1 were smaller than miR-27a-R2 by about 35 kcal mol^{-1} and $130 \text{ cal mol}^{-1} \text{ K}^{-1}$, respectively (Table A2.5). The big difference was in the base pair interactions with 10 (6 GC) for miR-27a-R1 compared to 24 (14 GC) for miR-27a-R2. While a miR-27a-R1 homodimer may form, the fact there were fewer base pairs in the homodimer, a gain in base pairs on reporter+probe formation, and the reporter+probe formation was exothermic, unlike R2, suggests a reporter+probe complex will still form with miR-27a-R1. The melting temperatures of the miR-27a reporters were similar near 15 °C, but probably closer to room temperature with the locked nucleic acids. The $\sim 3 \times 10^7$ counts per 500 ms for miR-27a-R1 did not support the predicted homodimer structure. Thus melting temperature alone cannot help determine if a homodimer will or will not form.

In Fig. 3.6, the miR-26a-R1 reporter hairpin had large green boxes compared to smaller light green boxes of the homodimer, suggesting hairpin formation was more probable. Hairpin formation for miR-26a-R1 was supported by its observed relatively low signal ($\sim 3 \times 10^7$ counts

per 500 ms) and high melting temperature (38.1 °C). (Similar probability maps for miR-26a-R2 can be found in Fig. A2.13).

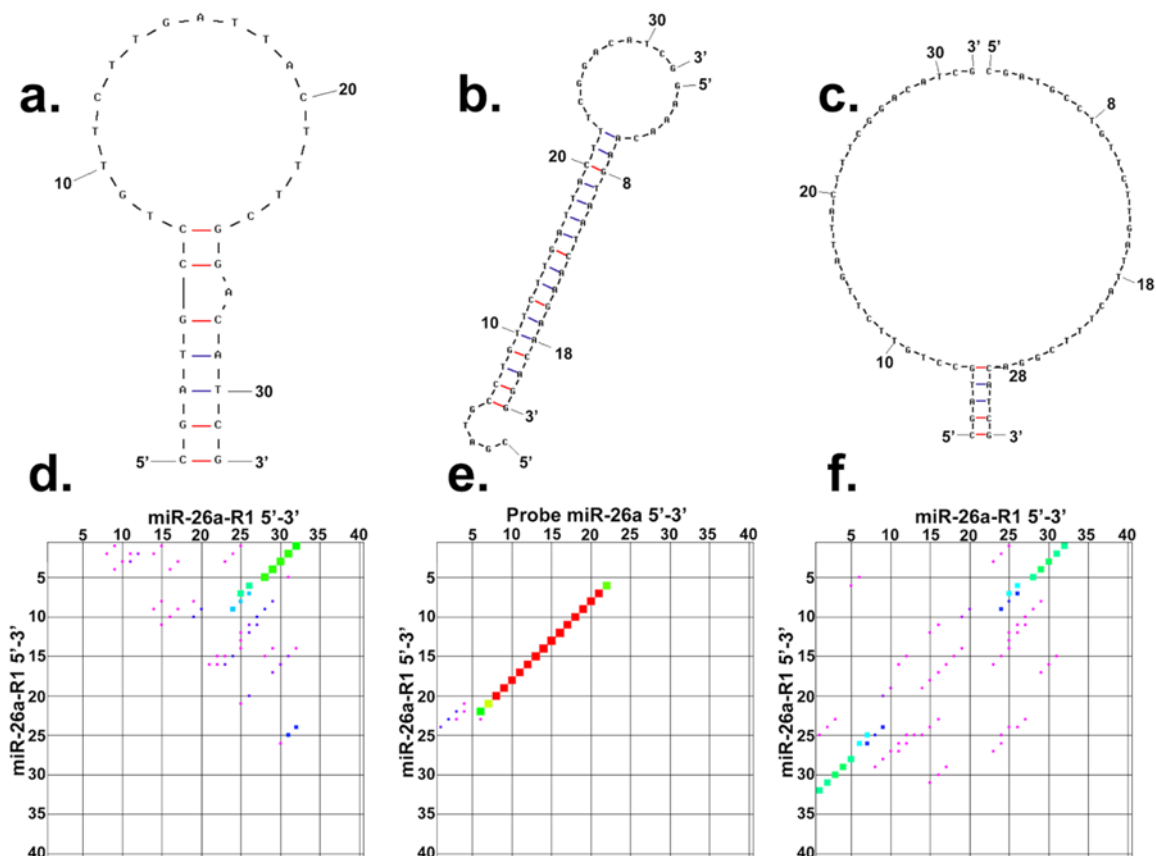


Figure 3.6 Energy minima structures and partition function probability maps for miR-26a-R1. The predicted energy minima structures are for (a) miR-26a-R1 folded, (b) miR-26a-R1+Probe complex, and (c) miR-26a-R1 homodimer, respectively, at 25 °C. Figure does not indicate 3-dimensional structure. (d)-(f) are partition function probability maps that correspond to energy minima structures (a)-(c), respectively. (Size and color of dots in partition function probability map indicate probability). The largest boxes are the most probable base pairs. For the color, the probability increases from violet (least probable) to red (most probable). See Fig. S11 for probability maps color code. Structures and probability maps were obtained using parameters described in Experimental Section 3.3.2. (For interpretation of the references to colour in this figure legend, the reader is referred to the web version of this article.)

Fig. 3.7 shows the predicted molarity fraction of each species from the UNAFold ‘Hybridization of two different strands’ function. Fig. 3.7a and 3.7b shows both miR-26a-R1 and R2 had a majority (above 95%) of the reporter and probe molecules complexed at 25 °C. Fig. 3.7c shows ~85% of the species were miR-27a-R1+probe complexes. These large percent formations were reflected in the observed signal changes of Fig. 3.4. The fact that miR-27a-R1 had ~10% of the reporters in the hairpin structure explains why the signal change of Fig. 3.4 was not greater than ~98% upon probe addition. The molarity fraction in Fig. 3.7d shows that only ~5% of the solution was predicted to contain miR-27a-R2+probe complex, at 25 °C. A majority of the species

were free reporters and probes. The fact that miR-27a-R2 probe was predicted to form in a small amount was in-line with the observed small ~14% signal change in Fig. 3.4.

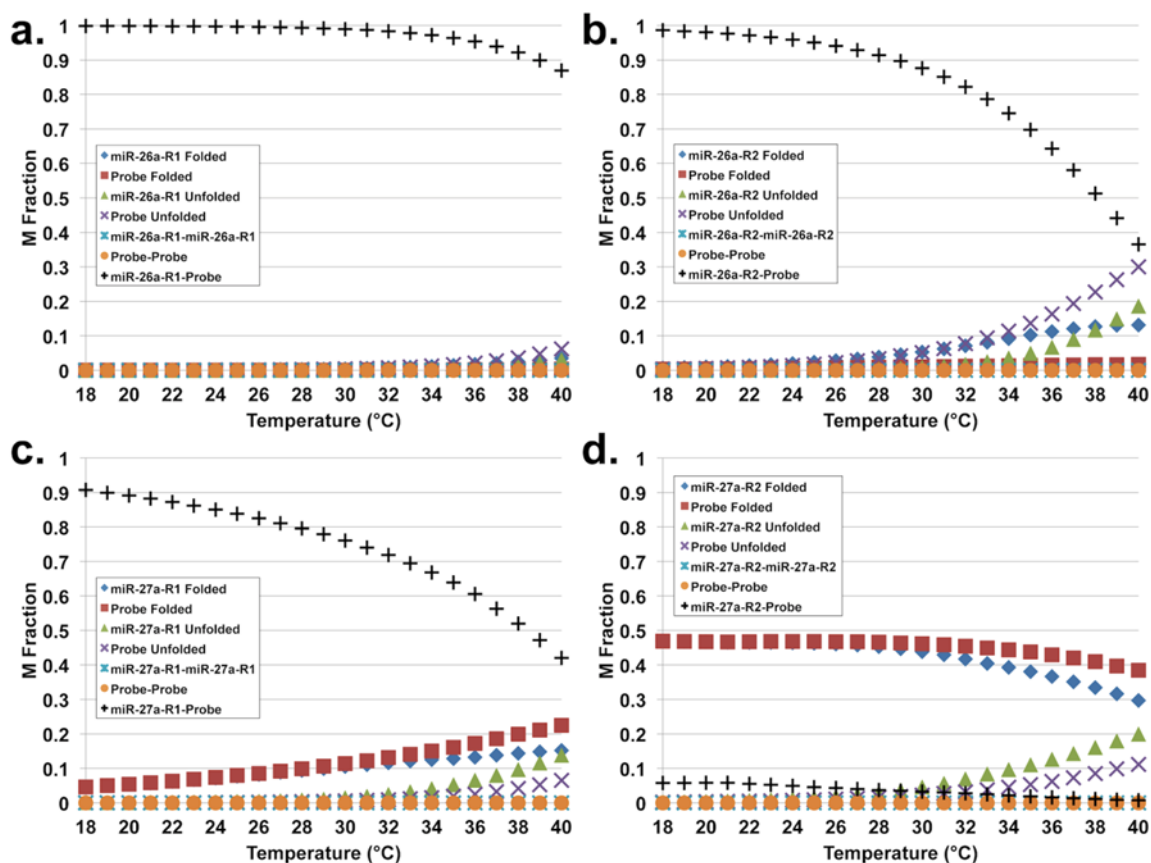


Figure 3.7 Molarity fraction of each of the reporters with their respective probes. The molarity of each structure formed was divided by the total molarity of each individual substance. (a) miR-26a-R1, (b) miR-26a-R2, (c) miR-27a-R1, and (d) miR-27a-R2. The reporter+probe complex was predicted to form in great abundance at room temperature (>90%) in (a) and (b) but not (c) and (d). Molarity fractions were obtained from ‘Hybridization of two different strands’ using parameters described in Experimental Section 3.3.2.

Considering Fig. 3.4 in relation to Fig. 3.7, the molarity fraction calculation from ‘Hybridization of two different strands’ was an excellent tool to predict extent of reporter probe formation. Figs. A2.6, A2.8, and A2.9 further explore the relationships between Figs. 3.4 and 3.7 by examining reporter+probe complex formation upon addition of 1x, 2x, and 100x probe to each of the reporters.

There were a few major problems with the molarity fraction tool. One problem was that it assumes a nucleic acid molecule that can form hairpins cannot form a homodimer complex, no matter how stable or probable. This assumption weakens the capabilities of the molarity fraction tool for the purpose of reporter design because it does not provide insight into the extent of homodimer formation. Another limitation was only one reporter and probe at a time could be

analyzed. Thus molarity fraction analysis was only useful near the end of the design process, when there were only a handful of reporters to investigate further.

Comparison of predicted and experimental data reveals that thermodynamics, molecular structure, and predicted equilibrium concentrations need to be analyzed as a whole rather than independently. For example, while the reporter hairpin and reporter+probe complex for miR-27a-R2 showed the worst-case scenario, it was the best for reporter+probe to probe analyte conversion in terms of thermodynamics. From the analysis here, we found molecular structure, thermodynamic metrics, reporter+probe equilibrium concentrations, changes in base pairs, and homodimer probabilities were key to selecting an optimal reporter. In summary, to design a reporter for reporter+probe biosensors, first generate reporter candidates based on the probe such that off-analyte interactions are minimized. Second, perform thermodynamic analysis to further reduce off-analyte interactions and ultimately reduce the number of reporters. Third, evaluate changes in base pairs upon reporter+probe formation. Fourth, assess the predicted reporter hairpin and homodimer structures. Fifth, evaluate equilibrium molarity fractions of different reporters with their probe. Finally, compare thermodynamics and changes in base pairs upon probe+analyte formation.

Below is a summary of some design principles from Table 3.1 for 100 nM reporter (R), 100 nM probe (P), and 100 nM analyte (A) at an operating temperature of 25 °C:

1. The most probable and thermodynamically stable conformation of the reporter must be an ideal hairpin.
2. Reporter Hairpin
 - a. Molecular Structure Metrics
 - i. Number of predicted structures: as few as possible.
 1. Just one H
 2. $H > NH$
 - ii. Total number of hairpin base pairs depends more on difference in base pairs from R to R+P
 1. Total base pairs: 5 to 7
 2. Change in base pairs (R to RP) ≥ 6
 - b. Thermodynamic Metrics: most stable hairpin thermodynamic metrics (with at least one locked nucleic acid in the stem)
 - i. $\Delta G_{\text{hairpin}}$: -1.85 kcal mol⁻¹ or more negative.
 - ii. $\Delta H_{\text{hairpin}}$: -37.8 kcal mol⁻¹ or more negative.
 - iii. $\Delta S_{\text{hairpin}}$: -120.58 cal mol⁻¹ K⁻¹ or more positive.
 - iv. $T_{\text{m, hairpin}} \geq 40.3$ °C (18 °C above operating temperature, a melting temperature of 38 °C is acceptable provided $\Delta G_{\text{hairpin}} \leq -2.33$ kcal mol⁻¹ and $\Delta H_{\text{hairpin}} \leq -55.4$ kcal mol⁻¹)

3. Reporter+Probe (with at least two locked nucleic acids in the loop)
 - a. Molecular Structure Metrics
 - i. Total number of base pairs depends on number of base pairs in stem of reporter. (See principle 2.a.ii.1)
 1. For a reporter with a 5 base pair stem, the RP complex should have at least 11 base pairs.
 - b. Thermodynamic Metrics
 - i. ΔG_{RP} : -16.1 kcal mol⁻¹ or more negative.
 - ii. ΔH_{RP} : -98.1 kcal mol⁻¹ or more negative.
 - iii. ΔS_{RP} : -272.5 cal mol⁻¹ K⁻¹ or more positive.
 - iv. $T_{m,RP} \geq 41.9$ °C (20 °C above operating temperature)
 - c. Percent reporter+probe formation
 - i. over 95%
4. Conversion of (R+P) to (P+A)
 - a. Molecular Structure Metrics
 - i. Total number of RP base pairs depends more on difference in base pairs from RP to PA
 1. Change in Base Pairs (RP to PA): gain of at least 5 base pairs
 - b. Thermodynamic Metrics
 - i. $\Delta \Delta G$: -5 kcal mol⁻¹ or more negative.
 - ii. $\Delta \Delta H$: -41.5 kcal mol⁻¹ or more negative.
 - iii. $\Delta \Delta S$: -120.5 cal mol⁻¹ K⁻¹ or more positive.
 - iv. $\Delta T_m > 5.2$ °C
5. Homodimer considerations for reporters and probes:
 - a. While one type of homodimer (reporter+reporter or probe+probe) is tolerable, one or more runs the risk of slowing the kinetics of reporter+probe formation. If possible, homodimers of reporters and probes should be avoided. The probability and thermodynamics of the homodimer formation should not be favorable.
 - b. Molecular Structure Metrics
 - i. The probability of a reporter hairpin or probe single strand must be greater than or about the same as the homodimer
 - ii. Change bases from homodimer to RP ≥ 2
 - c. Thermodynamic Metrics:
 - i. $\Delta G_{\text{homodimer}}$: -7.5 kcal mol⁻¹ or more positive.
 - ii. $\Delta H_{\text{homodimer}}$: -93.65 kcal mol⁻¹ or more positive.
 - iii. $\Delta S_{\text{homodimer}}$: -262.5 cal mol⁻¹ K⁻¹ or more negative.
 - iv. $T_m, \text{homodimer} < 15$ °C

The summary of design principles are best for use with fixed cells and tissue. However, these metrics can be extended to other temperatures. For analysis in cells or in vivo at 37 °C, the number of base pairs in the reporter hairpin and reporter+probe will likely need to be increased to achieve similar thermodynamic values as outlined above and in Table 1. If the same ΔG value can be obtained at 37 °C, then the equilibrium constants for the various species will increase by about 16%. At elevated temperatures, the reporters should give functional reporter+probe biosensors

provided the magnitude of changes in base pairs and thermodynamic values are in the same range as those summarized above and in Table 3.1.

3.4.2 Analytical figures of merit for reporter+probe biosensors

The reporter+probe biosensors for miR-26a and miR-27a had LODs that ranged from 5 to 9 nM (Table A2.6). Table A2.6 shows the sensitivity (slopes) and limits of detection and quantitation (LOD and LOQ) derived from the calibration curves for the biosensors in this study. The linear dynamic ranges of the biosensors were fit from 0 to 100 nM analyte added. LOD can be improved by decreasing the reporter+probe concentrations. We have previously demonstrated that decreasing the concentration of the reporter+probe complex to 500 pM gave an LOD of 49.38 ± 1.77 pM [2]. A calibration curve was performed using miR-27a-R2 probe out to 100 nM miR-27a, but the slope was non-linear and small due to the ~11% decrease in signal between reporter+probe and reporter, upon addition of analyte. The percent relative standard deviation (RSD) for the LOD and LOQ ranged from 10 to 67%. This error was a reflection of the sample preparation error rather than the sensor itself.

Comparison of the sensitivity from analysis of the calibration curve slopes and derived LOD/LOQ in Table A2.6 with and without the addition of off-analytes to each reporter showed no significant difference at the 95% confidence interval. The fact that the slopes and detection limits were similar with and without off-analytes indicated the biosensors were selective for their analyte. Comparison of the slopes between the reporters for miR-26a and miR-27a reveal a factor of about 1.26 difference. This change in slope was attributed to the larger maximum signal change for the miR-26a reporters with respect to miR-27a-R1 (over 90% compared to ~65%, respectively).

3.5 Conclusions

This work outlines design procedures and the design principles to make reporters for reporter+probe biosensors. Specifically reporter+probes for miR-26a and miR-27a were made and showed a dynamic range from 5 to 100 nM. Analysis of the calibration data showed that reporters with a maximum signal difference from 65% to 120% gave comparable detection limits and dynamic ranges. The fact that these biosensors demonstrated excellent selectivity in the presence of off-analytes will be of great value for future use in cellular and tissue matrices. Despite the semi-quantitative (~70%) nature of the sensors, the responses to concentration were reproducible (1-2%).

Predicting reporters that will bind probe and get displaced from probe when miRNA analyte is present is not trivial. Furthermore, reporters that will have maximum signal change between the open reporter+probe state and the closed reporter stem-loop hairpin conformation are difficult to identify. Many thermodynamic, molecular structure, and equilibrium concentration considerations need to be taken into account when picking the reporter sequence that will result in a functional biosensor. While only 3 out of the 4 reporters were functional, the poor functionality of miR-27a-R2 allowed discovery of key design principles for these displacement based reporters with self-complementarity.

From this study, we have found additional guidelines (in addition to the original three) to follow when designing reporter+probe biosensors. A good reporter will have an ideal stem-loop hairpin conformation that brings the dyes close together as the most stable structure and limits the number of non-ideal hairpins. Minimizing the stability and probability of potential homodimers of the reporter and probe is an important design criterion to ensure formation of the reporter+probe complex. A solution of reporter and probe should consist of over 95% reporter+probe. When considering the change in thermodynamics amongst reporter hairpins and subsequent formation of the reporter+probe complexes, ΔG , ΔH , ΔS , T_m and base pairs (related to ΔH and ΔS) must be evaluated simultaneously. These guidelines are important when designing sensors that use a displacement mechanism since being confident that a sequence will work as intended before purchasing will save time and decrease cost.

Looking towards the future, we will study the kinetics of analyte binding to reporter+probe biosensors. Other chemical modifications will be incorporated into the reporter to reduce chances of stems and non-complementary regions binding to endogenous RNA, DNA, and to ensure no interaction with off-analytes. Another consideration for the stem sequences is that they should be customized to each reporter to avoid the stem complexing to the probe or analyte. We will use these technologies to design reporter+probe biosensors that can be delivered into cells and tissue for in situ miRNA analysis.

3.6 Acknowledgements

Oregon State University start-up funds, the OSU Research Office through the General Research Fund, and the Dorothy and Ramon Barnes Research Fellowship supported this work.

3.7 References

- [1] N.E. Larkey, C.K. Almlie, V. Tran, M. Egan, S.M. Burrows, Detection of miRNA Using a Double-Strand Displacement Biosensor with a Self-Complementary Fluorescent Reporter, *Anal. Chem.* 86 (2014) 1853–1863. doi:10.1021/ac403866g.
- [2] C.K. Almlie, N.E. Larkey, S.M. Burrows, Fluorescent microRNA biosensors: a comparison of signal generation to quenching, *Anal Methods.* 7 (2015) 7296–7310. doi:10.1039/C5AY00504C.
- [3] N. Srinivas, T.E. Ouldridge, P. Sulc, J.M. Schaeffer, B. Yurke, A.A. Louis, J.P.K. Doye, E. Winfree, On the biophysics and kinetics of toehold-mediated DNA strand displacement, *Nucleic Acids Res.* 41 (2013) 10641–10658. doi:10.1093/nar/gkt801.
- [4] E.A. Lesnik, S.M. Freier, Relative thermodynamic stability of DNA, RNA, and DNA:RNA hybrid duplexes: relationship with base composition and structure, *Biochemistry (Mosc.)*. 34 (1995) 10807–10815.
- [5] N. Sugimoto, S. Nakano, M. Yoneyama, K. Honda, Improved thermodynamic parameters and helix initiation factor to predict stability of DNA duplexes, *Nucleic Acids Res.* 24 (1996) 4501–4505.
- [6] R.A. Dimitrov, M. Zuker, Prediction of Hybridization and Melting for Double-Stranded Nucleic Acids, *Biophys. J.* 87 (2004) 215–226. doi:10.1529/biophysj.103.020743.
- [7] C. Chen, W. Wang, Z. Wang, F. Wei, X.S. Zhao, Influence of secondary structure on kinetics and reaction mechanism of DNA hybridization, *Nucleic Acids Res.* 35 (2007) 2875–2884. doi:10.1093/nar/gkm177.
- [8] G. Bonnet, O. Krichevsky, A. Libchaber, Kinetics of conformational fluctuations in DNA hairpin-loops, *Proc. Natl. Acad. Sci.* 95 (1998) 8602–8606.
- [9] C.M. Croce, Causes and consequences of microRNA dysregulation in cancer, *Nat. Rev. Genet.* 10 (2009) 704–714. doi:10.1038/nrg2634.
- [10] A.E. Pasquinelli, B.J. Reinhart, F. Slack, M.Q. Martindale, M.I. Kuroda, B. Maller, D.C. Hayward, E.E. Ball, B. Degnan, P. Müller, Conservation of the sequence and temporal expression of let-7 heterochronic regulatory RNA, *Nature.* 408 (2000) 86–89.
- [11] A.E. Pasquinelli, A. McCoy, E. Jiménez, E. Salo, G. Ruvkun, M.Q. Martindale, J. Baguna, Expression of the 22 nucleotide let-7 heterochronic RNA throughout the Metazoa: a role in life history evolution?, *Evol. Dev.* 5 (2003) 372–378.
- [12] S. Roush, F.J. Slack, The let-7 family of microRNAs, *Trends Cell Biol.* 18 (2008) 505–516. doi:10.1016/j.tcb.2008.07.007.
- [13] B.J. Reinhart, F.J. Slack, M. Basson, A.E. Pasquinelli, J.C. Bettinger, A.E. Rougvie, H.R. Horvitz, G. Ruvkun, The 21-nucleotide let-7 RNA regulates developmental timing in *Caenorhabditis elegans*, *Nature.* 403 (2000) 901–906. doi:10.1038/35002607.
- [14] A. Esquela-Kerscher, F.J. Slack, Oncomirs — microRNAs with a role in cancer, *Nat. Rev. Cancer.* 6 (2006) 259–269. doi:10.1038/nrc1840.
- [15] X.-B. Shi, C.G. Tepper, R.W. deVere White, Cancerous miRNAs and their regulation, *Cell Cycle.* 7 (2008) 1529–1538.
- [16] M. Deng, H. Tang, X. Lu, M. Liu, X. Lu, Y. Gu, J. Liu, Z. He, miR-26a Suppresses Tumor Growth and Metastasis by Targeting FGF9 in Gastric Cancer, *PLoS ONE.* 8 (2013) e72662. doi:10.1371/journal.pone.0072662.
- [17] J. Gao, L. Li, M. Wu, M. Liu, X. Xie, J. Guo, H. Tang, X. Xie, MiR-26a Inhibits Proliferation and Migration of Breast Cancer through Repression of MCL-1, *PLoS ONE.* 8 (2013) e65138. doi:10.1371/journal.pone.0065138.

- [18] X. Dang, A. Ma, L. Yang, H. Hu, B. Zhu, D. Shang, T. Chen, Y. Luo, MicroRNA-26a regulates tumorigenic properties of EZH2 in human lung carcinoma cells, *Cancer Genet.* 205 (2012) 113–123. doi:10.1016/j.cancergen.2012.01.002.
- [19] J. Li, Y. Wang, Y. Song, Z. Fu, W. Yu, miR-27a regulates cisplatin resistance and metastasis by targeting RKIP in human lung adenocarcinoma cells, *Mol. Cancer.* 13 (2014) 193. doi:10.1186/1476-4598-13-193.
- [20] S.U. Mertens-Talcott, S. Chintharlapalli, X. Li, S. Safe, The Oncogenic microRNA-27a Targets Genes That Regulate Specificity Protein Transcription Factors and the G2-M Checkpoint in MDA-MB-231 Breast Cancer Cells, *Cancer Res.* 67 (2007) 11001–11011. doi:10.1158/0008-5472.CAN-07-2416.
- [21] R. Wahlroos, J. Toivonen, M. Tirri, P. Hänninen, Two-Photon Excited Fluorescence Energy Transfer: A Study Based on Oligonucleotide Rulers, *J. Fluoresc.* 16 (2006) 379–386. doi:10.1007/s10895-006-0084-x.
- [22] M. Massey, W.R. Algar, U.J. Krull, Fluorescence resonance energy transfer (FRET) for DNA biosensors: FRET pairs and Förster distances for various dye–DNA conjugates, *Anal. Chim. Acta.* 568 (2006) 181–189. doi:10.1016/j.aca.2005.12.050.
- [23] Y. Yang, J. Huang, X. Yang, K. Quan, H. Wang, L. Ying, N. Xie, M. Ou, K. Wang, FRET Nanoflares for Intracellular mRNA Detection: Avoiding False Positive Signals and Minimizing Effects of System Fluctuations, *J. Am. Chem. Soc.* 137 (2015) 8340–8343. doi:10.1021/jacs.5b04007.
- [24] H.-N. Wang, A.M. Fales, T. Vo-Dinh, Plasmonics-based SERS nanobiosensor for homogeneous nucleic acid detection, *Nanomedicine Nanotechnol. Biol. Med.* 11 (2015) 811–814. doi:10.1016/j.nano.2014.12.012.
- [25] N.R. Markham, M. Zuker, DINAMelt web server for nucleic acid melting prediction, *Nucleic Acids Res.* 33 (2005) W577–W581. doi:10.1093/nar/gki591.
- [26] N.R. Markham, M. Zuker, UNAFold, in: J.M. Keith (Ed.), *Bioinformatics*, Humana Press, Totowa, NJ, 2008: pp. 3–31.
http://www.springerprotocols.com/Abstract/doi/10.1007/978-1-60327-429-6_1 (accessed July 22, 2015).
- [27] DINAMelt | mfold.rna.albany.edu, (n.d.). <http://mfold.rna.albany.edu/?q=DINAMelt> (accessed July 22, 2015).
- [28] L. Wang, C.J. Yang, C.D. Medley, S.A. Benner, W. Tan, Locked Nucleic Acid Molecular Beacons, *J. Am. Chem. Soc.* 127 (2005) 15664–15665. doi:10.1021/ja052498g.
- [29] K. Martinez, M.-C. Estevez, Y. Wu, J.A. Phillips, C.D. Medley, W. Tan, Locked Nucleic Acid Based Beacons for Surface Interaction Studies and Biosensor Development, *Anal. Chem.* 81 (2009) 3448–3454. doi:10.1021/ac8027239.
- [30] S.A. Melo, R. Kalluri, miR-29b moulds the tumour microenvironment to repress metastasis, *Nat. Cell Biol.* 15 (2013) 139–140. doi:10.1038/ncb2684.
- [31] A. Fegan, P.S. Shirude, S. Balasubramanian, Rigid cyanine dye nucleic acid labels, *Chem. Commun.* (2008) 2004. doi:10.1039/b801629a.

Chapter 4.

Förster resonance energy transfer to impart signal-on and -off capabilities in a single microRNA biosensor

Nicholas E. Larkey, Lulu Zhang, Shan S. Lansing, Victoria Tran, Victoria L. Seewaldt, Sean M. Burrows

Analyst

Royal Society of Chemistry (RSC) USA: 1050 Connecticut Ave NW, Suite 500 Washington DC 20036

2016, *141*, 6239-6250. DOI: 10.1039/C6AN01555G

4.1 Abstract

Many studies have found that over- or under-expression of biomolecules called microRNAs (miRNA) regulates several diseases. Biosensors are in need to visually identify the relative expression level of miRNA to determine the direction these miRNA change in cells and tissues. Our established reporter+probe miRNA biosensor design requires that miRNA outcompete and displace the reporter from the probe. Once displaced, the reporter folds into a hairpin structure to force together a pair of Förster Resonance Energy Transfer (FRET) dyes. The donor and acceptor signal changes can be used to indicate the over-/under-expression of miRNA. The bright signal from the donor will indicate miRNA under-expression; the bright acceptor signal will indicate miRNA over-expression. Since close proximity of the dyes to each other and nucleic acids often quench fluorescence, polyethylene glycol spacers were added in-between the dyes and nucleic acids. We compared reporter designs with and without spacers to investigate the effects on the following analytical metrics: (1) extent of signal change, (2) limits of detection and quantitation, and (3) sensitivity. Systematic errors and amount of reporter+probe biosensor formed were evaluated for one of the biosensors. Cy3|Cy5 and 6-carboxyfluorescein (6-FAM)|ATTO 633 dye pairs on reporters containing spacers showed an increase in the acceptor signal change by ~190 and ~484%, respectively, compared to no spacers. Transduction mechanisms that enhance and quench the signal both showed LODs that ranged from 3–17 nanomolar (nM) with 100 nM of the biosensor.

4.2 Introduction

When a biosensor uses a FRET mechanism, it means that the analytical signal can either be quenched (signal-off) or enhanced (signal-on) depending on whether the donor or acceptor dye is observed.¹ As a signal-off sensor, the donor signal starts high when the dyes are apart and decreases when the dyes come together. Sensors with a signal-on mechanism start with the acceptor signal low and the signal increases when the dyes come together. For in situ miRNA analysis the benefits of a signal-off or -on biosensor depends on the miRNA expression in the disease state compared to the pre-disease state. Signal-off is beneficial as a 'NOT' logic gate sensor to visualize miRNA under-expression compared to a pre-disease state. However, if the miRNA expression becomes over-expressed compared to the pre-disease state, then a signal-on mechanism is preferable. Here we exploited the donor and acceptor signal changes to create a single biosensor

to indicate either the over-/under-expression of miRNA. To the best of our knowledge, current sensors do not capitalize on the donor and acceptor signal changes concurrently to extract information on miRNA over-/under-expression.

With our original reporter+probe biosensor for the miRNA let-7a, Cy3 and Cy5 were used as a FRET dye pair on the reporter and the sensor was benchmarked against a molecular beacon.^{2,3} The let7a reporter+probe biosensor showed low picomolar (pM) to low nM detection limits without amplification. We will show the reporter+probe biosensor described here has low nM detection limits when 100 nM of the biosensor was used. Other sensors for miRNA that use quantum dots^{4,5} and AgNCs⁶⁻⁹ have demonstrated high picomolar (pM) to low nM detection limits without amplification. Compared to other types of miRNA biosensors, the reporter+probe performs just as well if not better in terms of detection limits.

However, the original reporter+probe biosensors exhibited quenching at all excitation wavelengths with no observable FRET enhancement.² From our previous results with reporters lacking spacers between the Cy3 and Cy5 we found that Cy3 quenched the signal from Cy5 by $57.7 \pm 1.9\%$.² We hypothesize that the original reporter did not display FRET enhancement with Cy3 and Cy5 dyes because the stem-loop structure did not permit the dyes to assume a conformation that facilitated a FRET-induced increase in acceptor emission. Instead, quenching of the donor and acceptor by each other and the nucleic acids provided alternative non-radiative pathways to the ground state.¹⁰⁻¹²

To remedy poor FRET-induced enhancement, spacers between the dyes and the terminal nucleic acids on the reporter were added to move the dyes away from both the nucleic acids and from each other. With the dyes farther from the nucleobases there will be fewer chances for non-radiative deactivation due to nucleobase-dye interactions. Less non-radiative deactivation means more chances for radiative de-activation and thus greater observed FRET-induced acceptor enhancement. Another possible contribution the added spacers make to improve the acceptors FRET-induced enhancement is if the spacers put the dye pairs in a more favorable FRET distance and FRET orientation from each other. Previous studies have included long spacers (also known as linkers) between the oligonucleotide and the dyes/quenchers in molecular beacons¹³, but to our knowledge the use of spacers in a displacement sensor to improve both signal-on and signal-off analytical figures of merit has not been extensively studied.

Here the reporter+probe biosensors were designed to sense the miRNA, miR-26a-2-3p. This miRNA has been found to be associated with the progression of various cancers.¹⁴⁻¹⁶ Incorporated into the biosensor's reporter were hexaethylene glycol (18-carbon) spacers to change the dye-to-nucleotide distance. We compared signal change and analytical metrics from reporters with spacers to those with no spacers. Systematic errors and amount of reporter+probe biosensor formed were evaluated for one of the biosensors. The following dye pairs were used: Cy3|Cy5 and 6-FAM|ATTO 633. The 6-FAM was an amine reactive fluorescein derivative. For a fully signal-off control, one reporter was labeled with Iowa Black Red Quencher (IAbRQ) and Cy5. The IAbRQ and Cy5 pair will be abbreviated as IAbRQ|Cy5. We hypothesized that the increased length provided by the hexaethylene glycol spacers would increase the signal to background ratio of the acceptor's signal change, and as a result the reporters would be better for signal-on applications. Although these sensors were designed for use in two-photon applications, they are also applicable to excitation with single-photon sources.

4.3 Materials and Methods

4.3.1 Biosensor Design

The reporter+probe biosensor used in this work was for a variant of miR-26a-2-3p found in mice, mmu-miR-26a-2-3p (miR-26a). Recall the reporter is partially complementary to a probe sequence that is itself specific for the microRNA (miRNA). The reporter sequence was designed using a Matlab program developed in-house.¹⁰ Previous work evaluated the selectivity of a biosensor with this reporter sequence and discusses fundamental design principles for reporter+probe biosensors. At the 95% confidence interval, the biosensor was selective against two off-analytes: miR-27a-5p and miR-29b-1-5p.¹⁰

In this work, the same reporter and probe DNA sequences were used for all samples. Each reporter differed in the type of dye pair used as well as the presence or absence of hexaethylene glycol '18' spacers between the terminal nucleobases and each dye. The types of dyes were: cyanine (Cy3 and Cy5), fluorescein (as 6-carboxyfluorescein, 6-FAM), and ATTO 633. Recall one of the reporters was labeled with IAbRQ and a Cy5 dye. The type of spacer and dye pair (or dye/quencher pair) combination on the reporter will be used to identify the type of reporter. A reporter with a 5-prime 0-spacer and 3-prime 0-spacer will be referred to as having '0 spacers' and similarly a 5-prime 18-spacer, 3-prime 18-spacer will be referred to as having '18 spacers'. The

dye pairs will be referred to by the 3-prime dye followed by the 5-prime dye, separated by a vertical line '|', e.g. Cy3|Cy5 or 6-FAM|ATTO 633. All of the reporters contain three locked nucleic acids (LNAsTM) to improve stability and inhibit nuclease degradation.^{13,17} Sequence and dye information for the tested reporters and other DNA sequences are listed in Appendix III in Table A3.1.

All DNA was ordered from Integrated DNA Technologies (Coralville, IA) and used as received. The samples were delivered suspended in IDTE® buffer (contains Tris and EDTA buffers, pH 7.5). We diluted the DNA from stock concentrations in our own buffer containing phosphate-buffered saline with 10 mM Tris buffer, 2.5 mM MgCl₂, and 0.005% Tween 20 (final pH ~ 8). A Nanodrop Spectrophotometer (ND-1000) was used to verify the concentrations of the DNA solutions.

4.3.2 Fluorimeter design

A custom-built fluorimeter was used and has been described previously.² Briefly, a Ti:Sapphire (Spectra-Physics, Mai Tai HP) ultrafast tunable laser was used to excite the samples. The fluorescence generated from the excited samples was analyzed with a Princeton Instruments Acton Spectrometer (SP2300). The spectrometer had a grating blazed at 500 nm with 300 grooves per mm. A 512 × 512 Princeton Instruments electron multiplied charge coupled device (EMCCD) camera was used to collect the fluorescence spectra. Lightfield software was used with the following parameters: 500 ms integration time, 3 frames, 20 frame averages. The analog conditions were listed as low noise, 100 kHz, and high analog gain. The read out was full frame and the slit width was 1000 μm.

All solutions were excited at 740 nm to simultaneously excite both the donor and acceptor dyes. To selectively excite only the donor, solutions that contained reporters with Cy3|Cy5 were excited at 945 nm, and solutions containing reporters with 6-FAM|ATTO 633 were excited at 935 nm. 945 and 935 nm wavelengths were selected because they showed the best excitation of the respective donor as measured by acceptors signal to background ratio (data not shown). All solutions were excited with 75 mW of power using power control optics previously described.²

For solutions containing reporters with both Cy3 and Cy5 dyes, the grating was centered at either 565 nm (for Cy3, spectral range: 522.3612–607.5636 nm) or 670 nm (for Cy5, spectral range: 627.6193–712.2952 nm). For solutions containing reporters with 6-FAM and ATTO 633, the grating was centered at either 520 nm (for 6-FAM, spectral range: 477.2542–562.6750 nm) or 660 nm (for ATTO 633, spectral range: 617.5942–702.3213 nm). For solutions containing

reporters with Cy5 and IAbRQ, only the 627.6193 to 712.2952 nm spectral range for Cy5 was investigated due to no emission from the quencher molecule.

4.3.3 Calibration curves

Reporters were hybridized with equimolar probe in a microcentrifuge tube for at least one hour. Next, aliquots of reporter+probe were added to microcentrifuge tubes containing increasing amounts of miR-26a. Each tube was then diluted with buffer to a final reporter+probe concentration of 100 nM and miR-26a concentration that ranged from 0–300 nM. A calibration curve was fit using the linear region from 0–100 nM miR-26a. A control solution of 100 nM reporter was made to compare to the 100–300 nM miR-26a analyte solutions.

Calibration curves were run a total of three times for each reporter type. Emission intensities were summed for each of the emitting dyes over pixels 206–306 in each of their respective wavelength regions. For Cy3: 556.6577–573.3330 nm, for Cy5: 661.7091–678.2813 nm, for 6-FAM: 511.6364–528.3545 nm, and for ATTO 633: 651.7041–668.2863 nm. In the text we will refer to the dyes specifically (or their center wavelength) to indicate that we are making observations over a certain wavelength region just described.

Calculations were also performed to determine approximate amount of reporter+probe remaining after either 100 or 300 nM miR-26a added. To perform these calculations, the biosensor with 18 spacers on the 6-FAM|ATTO 633 reporter was chosen. First the intensity per nM from the 6-FAM and ATTO 633 emission regions were estimated for the reporter-hairpin and reporter+probe complex. Then the amount of reporter+probe and reporter-hairpin in solution after miRNA addition was estimated from the intensity of the reporter+probe + 100 nM miR-26a and the reporter+probe + 300 nM miR-26a solutions.

4.3.4 Analysis of reporter+probe formation

Two titration experiments were performed with the reporters that contained 6-FAM|ATTO 633-18 spacers in order to study whether 100 nM reporter and 100 nM probe formed 100 nM reporter+probe. In both experiments the samples were excited at 740 and 935 nm. In one experiment, the signal was analyzed when the reporter concentration was kept constant (100 nM) and the probe concentration was increased from (0–300 nM). The acceptor's signal was expected to stabilize after all the reporters were complexed with probe because there was a constant amount of reporter. The line of fit for the linear dynamic range and static signal were extrapolated to

determine at what concentration the dynamic slope changed. This concentration was taken as the actual amount of reporter+probe formed.

In the second experiment, the signal was analyzed when the probe concentration was kept constant (100 nM) and the reporter concentration was increased (0–300 nM). Once all the probes were complexed to the reporters the signal was expected to continue to increase, but at a different slope because excess reporter-hairpin was added. The concentration where the slopes changed was taken as the amount of reporter+probe formed. A control experiment helped identify where the signal changed over to excess reporter-hairpin by establishing a slope for increasing reporter-hairpin. The control experiment involved adding increasing amounts of reporter in the absence of probe. Comparison of changes in slope and comparison to ‘no probe’ control slope was examined to determine at what concentration the slopes changed.

4.4 Results and discussion

4.4.1 Biosensor response

The biosensor’s mechanisms for miRNA recognition and signal transduction are shown in Figure 4.1. The recognition mechanism is based on competitive binding between the miRNA and the reporter for the probe. The transduction mechanism is based on FRET occurring between donor and acceptor dyes. In the top panel, just the donor was excited to observe acceptor signal as signal-on or donor signal as signal-off. Either 935 or 945 nm light from the laser selectively excited the 6-FAM or Cy3 donor, respectively. The bottom panel shows that 740 nm simultaneously excited both dyes and the sensor functioned only in a signal-off manner. Although the figure shows the 6-FAM|ATTO 633 pair, the recognition and transduction mechanisms were the same for reporters with a Cy3|Cy5 pair. In the case of IAbRQ|Cy5 just the Cy5 was stimulated and observed as a signal-off sensor. The purpose of a reporter that used a quencher-dye pair was to compare the percent change in signal and types of detection limits (next section) from a purely quenching sensor to a sensor not designed for pure quenching (Cy3|Cy5).

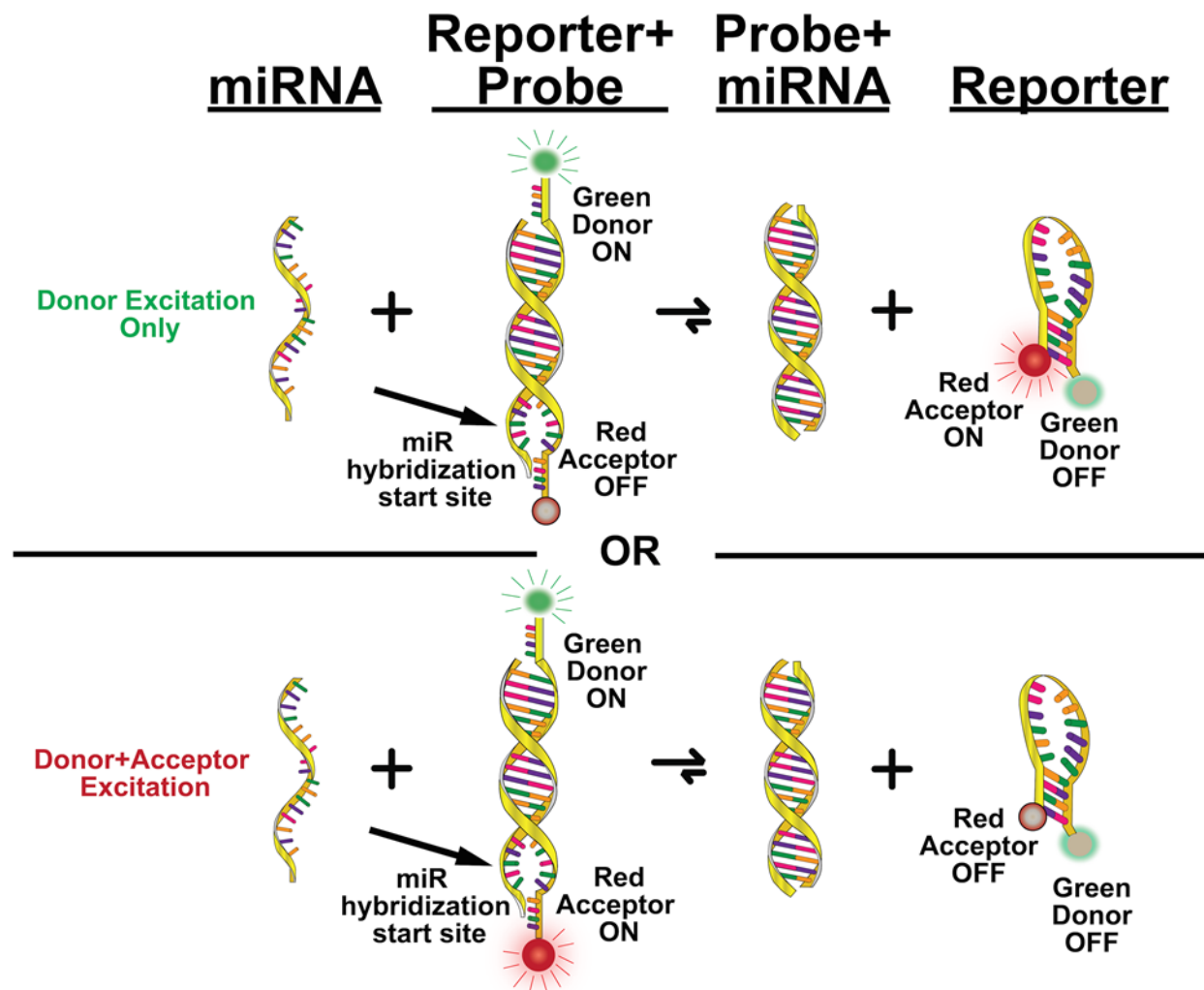


Figure 4.1 Recognition and transduction mechanisms for a miRNA biosensor to visualize the over-/under-expression of miRNA. This figure shows the reporter+probe biosensor's dual signal-on/off functionality. Top shows the excitation of just the donor dye molecule. In this scenario, when in the reporter+probe conformation, a majority of the emission is from the donor dye. When in the presence of miRNA, the reporter forms a stem-loop, allowing the donor and acceptor dye to come into close proximity and for signal change to occur. By observation of donor signal decreasing and acceptor signal increasing, the sensor acts both as a signal-off and -on type biosensor, respectively. Bottom represents excitation of both the donor and acceptor. In the presence of miRNA both signals get quenched and the sensor only works as signal-off.

To investigate how the hexaethylene glycol spacers influenced the signal change, the percent change in signal from the reporter-hairpin conformation to the reporter+probe complex (or vice versa) was evaluated. The magnitude of percent change in signal was used to compare reporters with and without spacers. Percent change in signal was evaluated for the Cy3|Cy5 pair, 6-FAM|ATTO 633 pair, and IAbRQ|Cy5 pair. The following equation was used to calculate the percent change in signal for quenching (% ΔS_Q):

$$\% \Delta S_Q = 100 \times \frac{S_{R+P} - S_R}{S_R} \quad \text{Equation 4.1}$$

The following equation was used for percent change in signal for enhancement (% ΔS_E):

$$\% \Delta S_E = 100 \times \frac{S_R - S_{R+P}}{S_{RP}} \quad \text{Equation 4.2}$$

where SR+P is the signal from the reporter+probe and SR is the signal of the reporter-hairpin. Recall that the dyes are next to each other in the reporter-hairpin conformation and far apart from each other in the reporter+probe complex. The percent signal change for quenching (% ΔS_Q) was the negative percent enhancement from R to R+P, explaining the values over 100%. Averaged summed intensities for the reporters can be found in Table A3.2. Tables A3.3-A3.5 compare the signal change from each type of reporter at different excitation and emission wavelengths.

Overall the data shown in Tables A3.3-A3.5 revealed that the best quenching occurred with reporters that did not contain hexaethylene glycol spacers. In contrast, the FRET-induced acceptor signal enhancement was improved for reporters with spacers. The 6-FAM|ATTO 633 reporter with 18 spacers leveraged better contrast between both the signal-off and -on states for each dye in the FRET pair than the corresponding Cy3|Cy5 reporter ($p < 0.05$). Of all the reporters, the IAbRQ|Cy5 0 spacers exhibited the largest percent quenching when excited at 740 nm ($5\,800.14 \pm 68.71\%$ quenching of Cy5, Table A3.3).

When Cy3 was used instead of IAbRQ (Table A3.4), the percent quenching of Cy5 decreased by a factor of ~ 33 for a reporter with 0 spacers. The next largest percent quenching was $1\,479.93 \pm 151.06\%$ from the 6-FAM dye on the 6-FAM|ATTO 633 reporters with 0 spacers when excited at 935 nm (Table A3.5). The Cy3|Cy5 reporters with 0 spacers came in with the third largest percent quenching of $1\,098.22 \pm 84.59\%$ for Cy3 when excited at 945 nm.

The difference in emission signal between the IAbRQ|Cy5 reporter-hairpin and reporter+probe for reporters with and without spacers are shown in Figure A3.1 (excited at 740 and 945 nm). Figure 4.2 shows the emission spectra from 100 nM Cy3|Cy5 and 6-FAM|ATTO 633 reporters with 0 and 18 spacers. The Cy3|Cy5 and 6-FAM|ATTO 633 reporters were excited at 945 and 935 nm, respectively. The change in signal came from addition of probe to the reporter. Similar emission spectra from 100 nM Cy3|Cy5 and 6-FAM|ATTO 633 reporters excited at 740 nm with and without probe are shown in Figure A3.2.

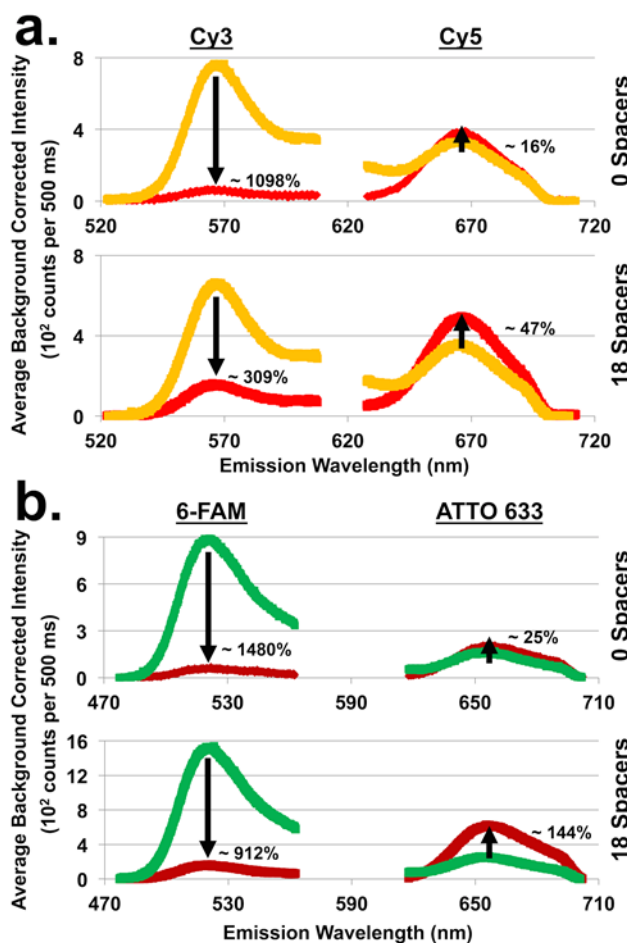


Figure 4.2 Emission spectra from 100 nM of reporters with and without probe. (a) Cy3|Cy5 reporters with 0 and 18 spacers (top and bottom, respectively) and (b) 6-FAM|ATTO 633 reporters with 0 and 18 spacers (top and bottom, respectively). (a) Shows the emission of Cy3 and Cy5 regions when excited at 945 nm (emission was not collected between 607.5636 and 627.6193 nm). The red and yellow lines correspond to reporter-hairpin and reporter+probe, respectively. (b) Shows the emission of 6-FAM and ATTO 633 regions when excited at 935 nm (emission was not collected between 562.6750 and 617.5942 nm). The burgundy and green lines correspond to reporter-hairpin and reporter+probe, respectively. Arrows show direction of signal change from the reporter+probe to the reporter-hairpin. Percent quenching/enhancement are estimated from data summarized in Tables 4.2 and 4.3 using Eqn 4.1 and 4.2.

The dual quenching and signal enhancement functionality can be seen from the emission spectra in Figure 4.2. For Cy3|Cy5 in Figure 4.2a, the dual quenching/enhancement functionality was observed upon excitation at 945 nm. Quenching came from the Cy3 signal where the reporter+probe had ~4 times greater signal than the reporter-hairpin. The signal enhancement functionality came from the Cy5 with the reporter-hairpin signal ~1.5 times larger than the reporter+probe.

For the 6-FAM|ATTO 633 reporter with 18 spacers in Figure 4.2b, the signal-off modality was demonstrated by a decrease in 6-FAM emission. The signal-on modality was observed by an increase in ATTO 633 emission. The 6-FAM signal decreased by a factor of ~10 upon comparison

of reporter+probe to reporter. The ATTO 633 signal increased by a factor of ~ 2.4 when the reporter+probe was compared to the reporter.

Provided the dyes were between 1 nm and 10 nm apart, FRET enhancement was expected to occur. FRET enhancement also requires the donor's emission spectra to overlap with the acceptor's excitation spectra and for their dipole moments to overlap. Typically, fluorescence gets quenched for various reasons when the dyes are within 1 nm of each other and/or nucleic acids. From the results presented here and in Appendix III it is clear that adding spacers both decreased quenching ability and increased enhancement ability for the Cy3|Cy5 and the 6-FAM|ATTO 633 reporters. These observations must stem from an increased distance between the dyes and the nucleic acids on the reporter, as well as between donor and acceptor dyes. Both these possibilities result in less quenching and facilitate more radiative pathways and thus more emission from both dyes. Although the use of spacers reduced the extent of quenching and improved the extent of enhancement, this information does not indicate whether or not the detection limits or sensitivity were influenced.

4.4.2 Influence of spacers on the detection limits and sensitivity

Table 4.1 contains the figures of merit (FOM) for the IAbRQ|Cy5 reporter+probe biosensors when excited at either 740 or 945 nm. Although the extent of quenching may have decreased after spacers were added to the reporters, there was no statistical influence ($p < 0.05$) on the sensitivity or limits of detection (LOD) and quantification (LOQ). Reporter+probe biosensors with 0 spacers and 18 spacers both gave ~ 4 nM LODs from the Cy5 region when excited at 740 nm. Reporter+probes excited at 945 nm gave close to 20 nM LODs for both spacer lengths. Since Cy5 is not excited well at 945 nm high LODs were expected.

Table 4.1 Biosensor figures of merit (FOM) from the Cy5 emission center (670 nm) for the IAbRQ|Cy5 reporters with 0 and 18 spacers excited at 740 and 945 nm. Data obtained from normalized calibration curves over the 0-100 nM miR-26a range in 20 nM steps. N = 3 for each FOM

670 nm center λ				
740 nm Excitation			945 nm Excitation	
Reporter Type	Average Slope \pm RSD (Normalized counts nM ⁻¹)	LOD (nM Analyte) \pm SD LOQ (nM Analyte) \pm SD RSD	Average Slope \pm RSD (Normalized counts nM ⁻¹)	LOD (nM Analyte) \pm SD LOQ (nM Analyte) \pm SD RSD
IAbRQ Cy5 Pair 0 Spacers	-7.22E-3 \pm 1.45 %	4.58 \pm 0.82 15.26 \pm 2.72 17.85 %	-7.25E-3 \pm 0.99 %	23.53 \pm 8.13 78.42 \pm 27.11 34.57 %
IAbRQ Cy5 Pair 18 Spacers	-7.41E-3 \pm 1.06 %	3.09 \pm 0.60 10.30 \pm 1.99 19.28 %	-7.46E-3 \pm 4.24 %	19.38 \pm 7.73 64.59 \pm 25.76 39.88 %

The Cy3|Cy5 reporter+probes' FOM from the emission of each dye when excited at either 740 or 945 nm are given in Table 4.2. Addition of spacers to the reporters did not statistically influence ($p < 0.05$) the LODs, except for the enhancement of Cy5 when excited at 945 nm. The Cy5 signal-on from reporters with 18 spacers had LODs that were more than 4 times lower ($p < 0.05$) than reporters with 0 spacers.

Table 4.2 Comparison of Cy3|Cy5 biosensor FOM from reporters with 0 and 18 spacers. The analytical signal was from Cy3 (565 nm) and Cy5 (670 nm) emission centers. The reporters were excited at 740 and 945 nm. Data obtained from normalized calibration curves over the 0–100 nM miR-26a range in 20 nM steps. N = 3 for each FOM.

	740 nm Excitation				945 nm Excitation			
	565 nm center λ		670 nm center λ		565 nm center λ		670 nm center λ	
Reporter Type	Average Slope \pm RSD (Normalized counts nM ⁻¹)	LOD (nM Analyte) \pm SD LOQ (nM Analyte) \pm SD RSD	Average Slope \pm RSD (Normalized counts nM ⁻¹)	LOD (nM Analyte) \pm SD LOQ (nM Analyte) \pm SD RSD	Average Slope \pm RSD (Normalized counts nM ⁻¹)	LOD (nM Analyte) \pm SD LOQ (nM Analyte) \pm SD RSD	Average Slope \pm RSD (Normalized counts nM ⁻¹)	LOD (nM Analyte) \pm SD LOQ (nM Analyte) \pm SD RSD
Cy3 Cy5 Pair 0 Spacers	-7.54E-3 \pm 2.72 %	7.45 \pm 3.29 24.83 \pm 10.96 44.12 %	-5.11E-3 \pm 2.62 %	3.71 \pm 1.50 12.35 \pm 5.01 40.56 %	-7.55E-3 \pm 2.57 %	5.49 \pm 2.47 18.30 \pm 8.23 45.00 %	2.72E1 \pm 19.11 %	79.56 \pm 10.06 265.18 \pm 33.53 12.65 %
Cy3 Cy5 Pair 18 Spacers	-4.89E-3 \pm 8.80 %	5.69 \pm 1.95 18.98 \pm 6.50 34.27 %	-3.71E-3 \pm 3.44 %	3.44 \pm 1.85 11.47 \pm 6.18 53.85 %	-6.08E-3 \pm 3.78 %	5.28 \pm 1.35 17.61 \pm 4.51 25.64 %	9.70E1 \pm 11.12 %	14.82 \pm 7.12 49.40 \pm 23.73 48.03 %

The FOM for 6-FAM|ATTO 633 reporter+probe biosensors excited at either 740 or 935 nm are presented in Table 4.3. Addition of spacers to the reporters did not statistically influence ($p < 0.05$) the LODs at any excitation wavelength, except for one. The signal-off LOD was near 4 nM for ATTO 633 when excited at 740 nm on the reporter with 0 spacers. Addition of 18 spacers to the reporter caused the signal-off LOD to increase by a factor of almost five. Although the ATTO 633 reporter with 0 spacers had the lowest LOD, it also had the largest RSD that was over 100%.

Table 4.3 Comparison of 6-FAM|ATTO 633 biosensor FOM from reporters with 0 and 18 spacers. The analytical signal was from the 6-FAM (520 nm) and ATTO (660 nm) emission centers. The reporters were excited at 740 and 935 nm. Data obtained from normalized calibration curves over the 0-100 nM miR-26a range in 20 nM steps. N = 3 for each FOM.

	740 nm Excitation				935 nm Excitation			
	520 nm center λ		660 nm center λ		520 nm center λ		660 nm center λ	
Reporter Type	Average Slope \pm RSD (Normalized counts nM^{-1})	LOD (nM Analyte) \pm SD LOQ (nM Analyte) \pm SD RSD	Average Slope \pm RSD (Normalized counts nM^{-1})	LOD (nM Analyte) \pm SD LOQ (nM Analyte) \pm SD RSD	Average Slope \pm RSD (Normalized counts nM^{-1})	LOD (nM Analyte) \pm SD LOQ (nM Analyte) \pm SD RSD	Average Slope \pm RSD (Normalized counts nM^{-1})	LOD (nM Analyte) \pm SD LOQ (nM Analyte) \pm SD RSD
6-FAM ATTO 633 Pair 0 Spacers	-6.24E-3 \pm 2.54 %	20.15 \pm 10.87 67.16 \pm 36.23 53.95 %	-4.50E-3 \pm 6.69 %	3.79 \pm 4.29 12.63 \pm 14.31 113.29 %	-6.26E-3 \pm 3.16 %	13.14 \pm 8.46 43.80 \pm 28.20 64.39 %	2.78E1 \pm 8.93 %	74.43 \pm 51.14 248.10 \pm 170.48 68.71 %
6-FAM ATTO 633 Pair 18 Spacers	-5.80E-3 \pm 3.46 %	30.32 \pm 7.25 101.05 \pm 24.17 23.92 %	-1.44E-3 \pm 8.67 %	22.05 \pm 3.91 73.50 \pm 13.04 17.74 %	-5.96E-3 \pm 1.62 %	13.56 \pm 4.78 45.19 \pm 15.93 35.25 %	2.52E2 \pm 3.06 %	17.03 \pm 8.50 56.78 \pm 28.34 49.92 %

For all the biosensors evaluated, a majority of the error in the LODs came from sample preparation error. The instrumental error – recorded as relative standard deviation (RSD) – in the data points for the calibration curves ranged from 0.25 to 14%. However, 96% of the error was below an RSD of 5%. A majority of the instrumental error ranged from 0.25 to 0.75% RSD. The fact that the instrumental error was low suggested the error in LODs was from sample preparation rather than the performance of the biosensor.

There were many nuanced statistical similarities and differences between the spectral conditions evaluated to compare how spacer additions to reporters influenced analytical figures of merit. A detailed description of the approaches for statistical comparisons and results are in Appendix III (A3.3).

In general, neither the use of spacers, excitation wavelength, nor direction of signal change influenced LODs for the Cy3|Cy5 reporters. Statistical differences ($p < 0.05$) in the Cy3 and Cy5 sensitivities (nM^{-1}) were revealed between reporters with and without spacers. For Cy5 signal-on, the sensitivity increased by more than a factor of three due to adding spacers to reporter. In the

case of signal-off under 740 and 945 nm excitation, addition of the spacers showed a decrease in sensitivity for both Cy3 and Cy5.

Overall, when excited at 945 nm the Cy3|Cy5 biosensor with 18 spacers minimized the loss in sensitivity and maintained low nanomolar LODs for signal-off. The most important result from adding spacers was the improvement in LOD for the signal-on when excited at 945 nm. Since this reporter was able to leverage suitable sensitivity and LOD for both signal-on and signal-off it will have the best chance to achieve good contrast to visualize the over- or under-expression of miRNA.

Much like the Cy3|Cy5 reporters, the 6-FAM|ATTO 633 reporter's LODs were not influenced by addition of spacers, excitation wavelength, or direction of signal change. For ATTO 633 signal-on when excited at 935 nm, addition of spacers showed a statistical ($p < 0.05$) increase in the sensitivity by almost a factor of 10. Signal-off sensitivity was only seen to decrease from addition of spacers to reporters for 6-FAM and ATTO 633 when excited at 740 nm. Spacer addition to the 6-FAM when excited at 935 nm did not show a statistical change ($p < 0.05$) in the signal-off sensitivity.

Compared to the other spectroscopic conditions and 6-FAM|ATTO 633 reporters with 0 spacers, the sensitivity and tens of nanomolar LODs for signal-off were maintained when the 6-FAM|ATTO 633 biosensor with 18 spacers was excited at 935 nm. The 6-FAM|ATTO 633-18 spacer reporters excited at 935 nm was able to leverage suitable sensitivities and LODs for both signal-on and signal-off. Thus, a biosensor with the 6-FAM|ATTO 633-18 spacers will have the best chance to achieve good contrast to visualize the over- and under-expression of miRNA.

In some cases, the signal-off LODs for the 6-FAM|ATTO 633 reporters were slightly higher than the Cy3|Cy5 reporters. In other cases, there was no statistical difference between the types of dyes used for the FRET pair. Both 6-FAM|ATTO 633 and Cy3|Cy5 reporters with 18 spacers emerged as the sensors with the best overall signal-on and signal-off sensitivities and LODs. For this reason, these sensors were compared to determine if there was an optimal FRET pair to use on the reporters.

At the 95% confidence level there was no statistical difference in the signal-off LODs, but there was at the 99% confidence level. The signal-off sensitivities were not statistically different at either the 95 or 99% confidence level. Considering the 95% confidence level, there was no difference between the type of dyes used for the FRET pair based on LOD and sensitivity.

Signal-on LODs between the 6-FAM|ATTO 633 and Cy3|Cy5 reporters with 18 spacers were not statistically different ($p < 0.05$). However, the sensitivity for the 6-FAM|ATTO 633 reporters was over two times larger ($p < 0.05$) than the Cy3|Cy5 reporters. These attributes of the 6-FAM|ATTO 633 pair combined with the signal-off FOM, largest percent change in signal, and over 140 nm of spectral resolution between the dyes, make the 6-FAM|ATTO 633 pair attractive for best use as a biosensor to image over-/under-expression of intracellular miRNA.

Figure 4.3 compares the signal on/off calibration curves for the Cy3|Cy5 (3a and b) and 6-FAM|ATTO 633 (4.3c and 4.d) reporters with 18 spacers when the donor dyes were selectively excited. Many of the attributes discussed above for the reporters with 18 spacers are shown in Figure 4.3. Similar calibration curves when excited at 740 nm are in Figure A3.3.

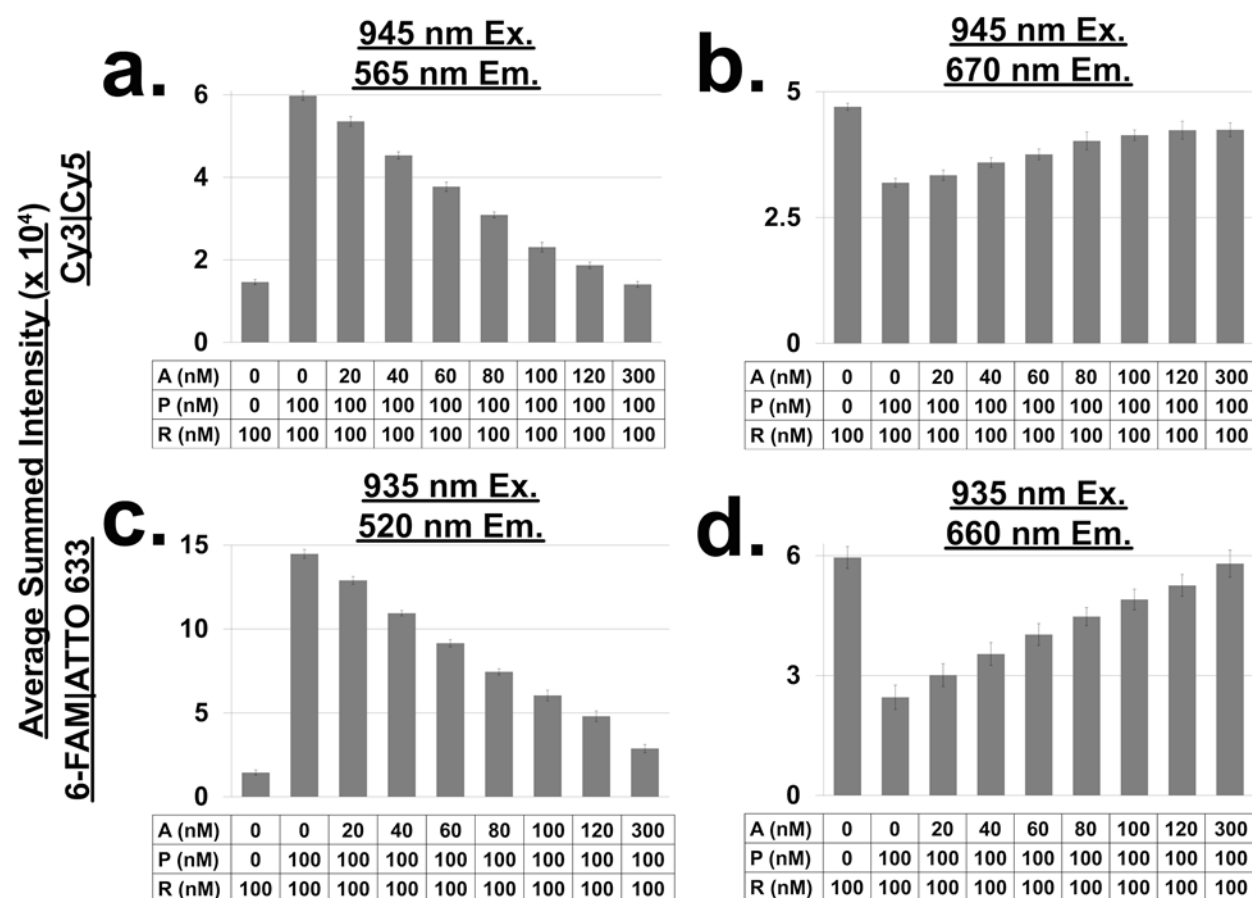


Figure 4.3 Calibration curves from miRNA analyte additions to 100 nM reporter+probe biosensors with Cy3|Cy5-18 spacers excited at 945 nm (a–b) and 6-FAM|ATTO 633-18 spacers excited at 935 nm (c–d). $N = 9$ from three calibration experiments with three frames each collected and averaged. The figure shows how both reporters behave as signal-on and -off that depended on emission wavelength. (a) Emission collected with the grating centered at 565 nm for the Cy3 dye. (b) Emission collected with the grating centered at 670 nm for the Cy5 dye. (c) Emission collected with the grating centered at 520 nm for the 6-FAM dye. (d) Emission collected with the grating centered at 660 nm for the ATTO 633 dye.

Future work will show the ability to image miRNA in cells with these biosensors. For cell work, ratiometric analysis is preferred over intensimetric analysis to differentiate between reporter+probe and reporter-hairpin states of the sensor. The reason for ratiometric analysis rather than intensimetric is to address cell-to-cell variability in biosensor concentration. Another reason for the ratiometric analysis is to combine the donor and acceptor signals to learn about miRNA over- or under-expression. Here, the influence of donor-to-acceptor (D/A) ratiometric analysis on the sensitivity, precision, LODs, and LOQs were evaluated (see Table A3.6). Below is a summary of the key results from Table A3.6.

For each FRET pair on each reporter excited at 740, 935, or 945 nm, the LODs from the D/A ratio did not show statistical differences ($p < 0.05$) based on number of spacers. In general, regardless of the wavelength to excite the dyes, the Cy3|Cy5 reporters showed lower LODs than the 6-FAM|ATTO 633 analogs ($p < 0.05$) by a factor of almost two.

The excitation wavelength did not influence how precise the LOD measurements were at a given spacer length except for the Cy3|Cy5-0 spacers that was more precise when excited at 945 nm than when excited at 740 nm. There was no difference in precision based on spacer lengths for either the Cy3|Cy5 or the 6-FAM|ATTO 633 reporters except for the Cy3|Cy5-0 spacers excited at 945 nm. In the case of 945 nm excitation, the Cy3|Cy5-0 spacers were more precise than the Cy3|Cy5-18 spacers. At 935/945 nm excitation, only the Cy3|Cy5-0 spacers had precisions that were statistically smaller than each of the other reporters. Since a majority of the precision was equal among the reporters, we suspect that the instances of improved precision were just instances of good sample preparation.

Regardless of the wavelength to excite the reporters the following trend in sensitivity was observed: Cy3|Cy5-0 spacers were more sensitive than 18 spacers and 6-FAM|ATTO 633-18 spacers were more sensitive than the 0 spacers. The reporters demonstrated the greatest sensitivity when excited at either 935 or 945 nm, depending on the donor dye excited. Excitation at 935 and 945 nm was statistically more sensitive than the corresponding 740 nm excitation for each type of reporter. However, the precision was not statistically influenced by the excitation wavelength.

There was no obvious best choice for a reporter because the FOM from the D/A ratio were so nuanced. In general, the Cy3|Cy5 reporters excited at 945 nm showed the lowest LODs. However, the sensitivity, contrast, and spectral resolution between donor and acceptor pairs for the Cy3|Cy5 reporters excited at 945 nm were not as good as those for the 6-FAM|ATTO 633

reporters excited at 935 nm. Despite the advantages and disadvantage to each sensor type, the ratiometric results for sensor selection were similar to those from an intensimetric evaluation. That is to say, the reporters with 6-FAM|ATTO 633-18 spacers demonstrated optimal FOM for future cell work. Future work in cells will implement internal standards on the reporter itself to create a more robust ratiometric analysis.

4.4.3 MicroRNA-induced reporter+probe displacement efficiency

Although the reporter+probe biosensor is based on strand displacement, the hairpin reformation adds a level of complexity to the kinetics and reaction completion. The reporter+probe biosensor has to balance the toehold length and sequence – that itself depends on miRNA the sequence – with the ability of the reporter strand to re-form a hairpin conformation upon displacement. The reporter+probe's analytical metrics depend on several factors. First, the amount of reporter+probe biosensor formed from single stranded reporter and probe. Second, the extent of probe+analyte formed and subsequent reporter displacement from the probe. Third, reporter-hairpin reformation when the reporter is displaced from the probe. The reporter+probe biosensor's design has to take into account the thermodynamics of reporter+probe binding, probe+analyte binding, and reporter-hairpin reformation in order to maximize reporter displacement from the probe in the presence of miRNA. Compared to other strand-displacement mechanisms, the reporter+probe's relationship between the three interactions complicates the sensor design and limits the potential thermodynamic 'window' needed to drive the reaction from reporter+probe and probe+analyte complexes.¹⁰ Many other strand-displacement based sensors require amplification and/or are not suitable for in situ analysis.¹⁸⁻²¹

The calibration curves revealed that equimolar levels of miRNA added and biosensor was unable to return the analytical signal to what was considered the reporter-hairpin's baseline signal level. The baseline reporter-hairpin signal was established from a control solution that had 100 nM reporter-hairpin without probe. As Figure 4.3 shows the signal did not return to the same level as the 100 nM reporter-hairpin control even after 300 nM miR-26a was added to 100 nM reporter+probe. Further analysis was performed to establish how much reporter-hairpin formed and reporter+probe remained in solution after miRNA addition.

The molar amount of reporter-hairpin and reporter+probe after addition of 100 and 300 nM miR-26a was estimated from the 6-FAM and ATTO 633 intensities on the reporter with 18 spacers. First, we calculated the counts per nM of each dye from reporter-hairpin and reporter+probe

solutions based on known intensity and concentration values. The calculated counts per nM allowed us to set up two equations with two unknowns to determine the amount of reporter-hairpin formed and reporter+probe remaining in solution. One equation was set equal to the signal intensity after 100 nM of miR-26a was added. The other equation was set equal to the signal intensity after 300 nM of miR-26a was added. The results from the three trials can be found in Table A3.7.

After 100 nM miR-26a was added, ~66–70 nM reporter-hairpin was formed and ~33–36 nM reporter+probe remained complexed. For 300 nM miR-26a, ~90–94 nM reporter-hairpin was formed and only ~9–11 nM reporter+probe remained. Taken together, these results represent a systematic error related to the reporter+probe complex not fully binding all the miRNA in solution. However, because the systematic error was reproducible, the error is consistent and can be addressed. Since the error can be accounted for, the analytical usefulness of the biosensor is retained.

4.4.4 Reporter+probe formation analysis of the 6-FAM|ATTO 633 reporter with 18 spacers

The extent of reporter+probe formation was validated by two titration experiments (Figure A3.4). The reporter with 6-FAM|ATTO 633-18 spacers was chosen for these studies because it showed overall the optimal performance out of all the biosensors. One titration involved increasing the probe concentration to a constant amount of reporter. The other titration involved increasing reporter concentration to a constant amount of probe. Emission from ATTO 633 served as the analytical signal for these titrations. The results from these titrations validated that the amount of reporter+probe formed was ~100 nM with an excess of about 10 nM reporter. A detailed analysis of the extent of reporter+probe formation can be found in Appendix III in regards to Figure A3.4

4.5 Conclusions

We have demonstrated that reporter+probe biosensors for miR-26a function in both a signal-on and signal-off modality. The direction of signal change depended on the excitation and/or emission wavelength. An increase in spacer length was shown to increase the acceptor dye's FRET enhancement and simultaneously decrease the quenching ability of both dyes. Although the quenching efficiency decreased from spacer addition, there was minimal influence on the LODs and sensitivities. Both the signal-off and -on modality of these biosensors demonstrated low (3–17 nM) limits of detection for miR-26a.

The improved signal-on ability from spacer addition was due to an increased distance between the nucleic acids and each dye as well as the distance between the two dyes. The increased distance between these potential couples mitigated competitive non-radiative deactivation pathways and allowed different orientations between the dye molecules to give more effective FRET enhancement interaction. The reason the donor dyes were quenched to a lesser extent upon spacer addition was also related to the increased distance between dyes and potential quenchers.

For a purely signal-off type sensor, the IAbRQ|Cy5 pair had the lowest LODs and largest sensitivities when excited at 740 nm (Table 4.1: ~ 4 nM and about -7×10^{-3} nM⁻¹). If a sensor for both signal-on and -off is desired, then the reporter+probe biosensors with 6-FAM|ATTO 633-18 spacers excited at 935 nm emerged as the optimal sensor. This sensor had the following attributes for signal-on and -off modalities: (1) over 140 nm spectral resolution between FRET pairs, (2) low nanomolar LODs, (3) excellent contrast potential, and (4) suitable sensitivities.

The findings from these studies contribute to ongoing efforts to design an optimal biosensor for intracellular miRNA analysis. These biosensors will maintain high sensitivity, selectivity, and negligible false signals. The biosensors for these studies were designed so the reporter+probe was stable at 100 nM. To achieve pM detection limits like those shown with other sensors,⁴ reporter+probe biosensor designs need to be stable at low nM concentrations. In addition, the change in thermodynamics from reporter+probe to miRNA+probe needs to be favorable. We have done this for a miR-29b-1-5p biosensor and shown pM limits of detection; the results will be the subject of another work that describes the design process for these sensors.

We are still investigating how to fine-tune the thermodynamics and other properties to achieve femtomolar LODs with two-photon excitation. We expect fM to pM LODs with single-photon sources because the single-photon absorption cross-sections will be much larger than two-photon action cross sections. With the larger absorption cross section will come brighter signal and perhaps lower LODs. Thus there is potential for these sensors to avoid need for amplification on the single-photon level. We are planning to conduct this analysis with future sensors designed for intracellular applications.

Currently we are investigating reporter+probe biosensors that were designed to operate at a temperature of 37 °C for intracellular analysis. In a biological mixture there can be several other naturally occurring miRNAs that have similar sequences to the miRNA of interest. The difference in sequence between analyte miRNA and off-analyte miRNAs can be as small as a single

nucleotide. False-positives from off-analytes with small sequence mismatches to analyte are a challenge for miRNA analysis in cellular mixtures. Work by Seeman¹⁹ highlighted how the thermodynamics and Watson–Crick binding nature of branch migration alone helps improve strand displacement sensor’s specificity. Strategically altering the biosensor’s structure and introducing various chemical modifications (e.g. organic residues, non-canonical nucleotides^{22,23}, and LNAs^{TM13,17}) to the reporter and probe can improve hybridization yield as well as reduce off-analyte binding. Such modifications are currently under investigation in our lab and will be the subject of future works. Future design principles will focus on maximizing: (1) probe+analyte hybridization yield, (2) reporter-hairpin folding extent, and (3) the ‘discrimination factor’²⁴ against analytes with similar sequences.

A sensor with a wavelength dependent transduction mechanism will permit either miRNA over- or under-expression to be visualized. Visualization of over-/under-expression is critical to both fundamental and clinical miRNA analysis because these biomolecules become either under- or over-expressed depending on the cell type, tissue type, and stage of development. For example, in a tumor microenvironment sensors are needed to differentiate cells with increased or decreased levels of miRNAs. This has potential to enable a better understanding of how tumors form and become metastatic.

In future cell work we expect the D/A ratio will enable visualization of relative changes in miRNA expression compared to control cells. The D/A ratio method revealed that at least 10 to 20 nM miR-26a was measurable (935 or 945 nm excitation). If this method is coupled with Fluorescence Lifetime Imaging Microscopy (FLIM) further differentiation of reporter-hairpins and reporter+probe biosensors will aid in miRNA quantitation through lifetime analysis.

4.6 Acknowledgements

I would like to thank both the Dorothy and Ramon Barnes Graduate Research Fellowship and the N. L. Tartar Graduate Research Fellowship for sponsoring this research.

4.7 References

- 1 P. Zhang, T. Beck and W. Tan, *Angew. Chem. Int. Ed.*, 2001, **40**, 402–405.
- 2 N. E. Larkey, C. K. Almlie, V. Tran, M. Egan and S. M. Burrows, *Anal. Chem.*, 2014, **86**, 1853–1863.
- 3 C. K. Almlie, N. E. Larkey and S. M. Burrows, *Anal Methods*, 2015, **7**, 7296–7310.
- 4 X. Qiu and N. Hildebrandt, *ACS Nano*, 2015, **9**, 8449–8457.

- 5 J. Lee, S. Moon, Y. Lee, B. Ali, A. Al-Khedhairy, D. Ali, J. Ahmed, A. Al Salem and S. Kim, *Sensors*, 2015, **15**, 12872–12883.
- 6 S. W. Yang and T. Vosch, *Anal. Chem.*, 2011, **83**, 6935–6939.
- 7 P. Shah, A. Rørvig-Lund, S. B. Chaabane, P. W. Thulstrup, H. G. Kjaergaard, E. Fron, J. Hofkens, S. W. Yang and T. Vosch, *ACS Nano*, 2012, **6**, 8803–8814.
- 8 X. Xia, Y. Hao, S. Hu and J. Wang, *Biosens. Bioelectron.*, 2014, **51**, 36–39.
- 9 P. Shah, S. W. Choi, H. Kim, S. K. Cho, Y.-J. Bhang, M. Y. Ryu, P. W. Thulstrup, M. J. Bjerrum and S. W. Yang, *Nucleic Acids Res.*, 2016, **44**, e57–e57.
- 10 N. E. Larkey, C. N. Brucks, S. S. Lansing, S. D. Le, N. M. Smith, V. Tran, L. Zhang and S. M. Burrows, *Anal. Chim. Acta*, 2016, **909**, 109–120.
- 11 M. A. Behlke, L. Huang, L. Bogh, S. Rose and E. J. Devor, *Integr. DNA Technol.*
- 12 S. Ranjit and M. Levitus, *Photochem. Photobiol.*, 2012, **88**, 782–791.
- 13 L. Wang, C. J. Yang, C. D. Medley, S. A. Benner and W. Tan, *J. Am. Chem. Soc.*, 2005, **127**, 15664–15665.
- 14 M. Deng, H. Tang, X. Lu, M. Liu, X. Lu, Y. Gu, J. Liu and Z. He, *PLoS ONE*, 2013, **8**, e72662.
- 15 J. Gao, L. Li, M. Wu, M. Liu, X. Xie, J. Guo, H. Tang and X. Xie, *PLoS ONE*, 2013, **8**, e65138.
- 16 X. Dang, A. Ma, L. Yang, H. Hu, B. Zhu, D. Shang, T. Chen and Y. Luo, *Cancer Genet.*, 2012, **205**, 113–123.
- 17 K. Martinez, M.-C. Estevez, Y. Wu, J. A. Phillips, C. D. Medley and W. Tan, *Anal. Chem.*, 2009, **81**, 3448–3454.
- 18 Y. He and D. R. Liu, *J. Am. Chem. Soc.*, 2011, **133**, 9972–9975.
- 19 H. K. K. Subramanian, B. Chakraborty, R. Sha and N. C. Seeman, *Nano Lett.*, 2011, **11**, 910–913.
- 20 D. Y. Zhang and G. Seelig, *Nat. Chem.*, 2011, **3**, 103–113.
- 21 Y. Wu, D. Y. Zhang, P. Yin and F. Vollmer, *Small*, 2014, **10**, 2067–2076.
- 22 M. J. Moser, *Nucleic Acids Res.*, 2003, **31**, 5048–5053.
- 23 C. B. Sherrill, D. J. Marshall, M. J. Moser, C. A. Larsen, L. Daudé-Snow and J. R. Prudent, *J. Am. Chem. Soc.*, 2004, **126**, 4550–4556.
- 24 D. Y. Zhang, S. X. Chen and P. Yin, *Nat. Chem.*, 2012, **4**, 208–214.

Chapter 5.

MicroRNA biosensor design strategies to mitigate off-analyte response

Nicholas E. Larkey, Jessica L. Phillips, Hyo Sang Jang, Siva K. Kolluri, Sean M. Burrows

Manuscript in preparation for publication

5.1 Abstract

MicroRNAs (miRs) are important regulators of gene expression and are implicated in various diseases. When attempting to detect a single miR intracellularly, there can be several other naturally occurring miRs that have similar sequences to the miR of interest. Often biosensors cannot differentiate small differences in sequence from the analyte and cause false-positive signals. Many sensors have what is called a ‘toehold’ region for the analyte nucleotide to initiate binding to the sensor. This toehold region is an exposed region on one of the strands of a double-stranded nucleic acid strand that allows a third nucleic acid strand to bind and competitively displace one of the strands. Our double-stranded reporter+probe biosensor binds miR through toehold-mediated strand-displacement onto the probe, meaning that the miR initiates binding at the toehold and displaces the reporter strand from the probe. The analyte binding displaces a reporter strand to induce a signal change. Although the reporter protects part of the probe from off-analytes, the toehold region is not protected. If the probe’s toehold sequence matches both the analyte and off-analyte, then false signals occur. To mitigate this problem, the sensor’s molecular configuration was designed so the location of the unprotected toehold region contains bases that are complementary only to the analyte, but not the off-analyte. The mismatched base pairs between the probe’s toehold and the off-analyte weaken the binding interaction between them, as a result the stability of the displacement initiation region is decreased. Thus, the weaker binding will discourage the displacement of the reporter from the probe. Here we reveal the effect of altering the location of the toehold region on the sensor to improve the selectivity for the analyte of interest. In this sensor design, the toehold sequence on the probe is most important as it is what binds the miR first. We will discuss the differences in selectivity and sensitivity for a miR-146a-5p biosensor in the presence of different naturally occurring mismatch sequences. We found that the toehold location did alter the rate of false signal from off-analyte miR, and we found LODs as low as 56 pM when using 5 nM sensor concentration.

5.2 Introduction

In previous iterations of the reporter+probe biosensor, we have shown how thermodynamics are important when designing displacement-based miR biosensors, and how different dyes and different spacer lengths can alter and improve the signal generated by the sensors.¹⁻³ Previous works on toehold thermodynamics have laid the foundation for this field⁴ and novel techniques to regulate strand displacement with blocking strands have been made.

An overarching problem in the nucleic acid biosensor field is the limits of thermodynamic differentiation between strands that have similar sequences to the analyte-of-interest. The variation in sequence between analyte miR and off-analyte miRs can be as little as a single nucleotide difference. Some researchers have developed techniques to differentiate analyte and off-analyte binding by changing the sensor's signal generation depending on the bound nucleotide.⁵⁻⁷ However, this sensor is not selective for a single miR, and would lose the ability to quantify analyte in the presence of a large concentration of off-analytes. Zhang et al. have designed nucleic acid strands called protector+complement probes that can specifically differentiate between nucleic acid strands, but works by using linear sequences that displace a quenching mechanism. However, such quencher based signaling methods are known to be susceptible to nuclease degradation.^{4,8}

The previous reporter+probe biosensors that we have designed¹⁻³, were able to resist off-analytes that were very different than the analyte sequences (at least 3 nucleotide mismatches). This allowed the thermodynamic stability for the binding between the probe and off-analytes to be unfavorable. We have yet to study how the directionality of the biosensor's toehold can be tuned in order to decrease binding by off-analytes with similar sequences.

In this study the reporter+probe biosensors are designed for miR-146a-5p, a miR shown to be either upregulated or downregulated with respect to various cancers and has the potential to be a biomarker for these diseases.⁹⁻¹² MiR-146a-5p has been found to be upregulated in basal-like tumors, related to increased tumorigenesis.¹⁰ MiR-146a-5p has also been found to be downregulated in breast cancer in young women.¹² Here we will test different reporter+probe biosensors for their sensitivity and selectivity miR-146a-5p in a complex matrix. The off analytes that we test against here are miR-146a-3p and miR-146b-5p, two miRs with similar sequences to the analyte.

5.3 Materials and Methods

5.3.1 Thermodynamic Calculations

Several equilibria, thermodynamic, and structural metrics were assessed to determine the biosensors ability to properly function with selectively for the analyte. *In silico* predictions of DNA strand was performed with UNAFold software from the DINAMelt Web Server hosted by SUNY Albany. Different applications under the UNAFold umbrella were used for different functions. 'Homodimer Simulations' was used to predict homodimer formation, 'Hybridization of two

different strands of DNA or RNA' was used to calculate molarity fractions and probability dot plots for the interaction of two strands at the same or different concentrations, 'Quikfold' was used to determine the energy and structure of single-stranded nucleotides, and 'Two State melting (hybridization)' was used to determine the energy and structure of the binding between two different strands.

For the molarity fraction plots and binding probability dot plots, the 'Hybridization of two different strands of DNA or RNA' application was used under the UNAFold software umbrella. We fed the 5' to 3' sequences of the two strands into the 'Sequence 1' and 'Sequence 2' text boxes, and chose 10°C - 60°C (with 0.5°C increments) for the temperature range. DNA was chosen as the nucleic acid, initial concentrations of A_0 (Sequence 1) and B_0 (Sequence 2) were both chosen to be 0.005 μM (5 nM). The $[\text{Na}^+]$ was set to 10 mM, and $[\text{Mg}^{2+}]$ was set to 2.5 mM. The probability dot plots were viewed for the 'A-B' homodimer (Sequence 1 + Sequence 2) at 37°C. All of the experiments in this work have the reporter+probe biosensor at 5 nM concentrations, a 20-fold decrease in concentration from our previous works at 100 nM.¹⁻³ All thermodynamic calculations herein consider consider the 5 nM sensor concentration. Additionally, previous reporter+probe biosensors were made to operate at room temperature (25°C).¹⁻³ We designed the sensors described here to be stable at 37°C.

For thermodynamic analyses that contain the reporters, the poly-T tracts are omitted from the analysis due to the hexaethylene glycol spacer that separates them from the main sequence. Visual representations of the theoretical binding between sequences were predicted using the 'Two-state melting (hybridization)' application in UNAFold. The two sequences were fed into the boxes the 'DNA' was selected. The temperature was set to 37°C, $[\text{Na}^+]$ was set to 10 mM, $[\text{Mg}^{2+}]$ was set to 2.5 mM. The strand concentrations were set to 0.005 μM (5 nM).

To determine the thermodynamics of intramolecular folding for single strands, the 'Quikfold' application was used. The settings used were 'DNA', '37°C' temperature, $[\text{Na}^+]$ was set to 10 mM, $[\text{Mg}^{2+}]$ was set to 2.5 mM, 'linear' sequence type, '5%' suboptimal structures, maximum of '50' foldings, 'no limit' to the maximum distance between paired bases. For formation of homodimers, the 'Homodimer Simulations' application was used. The temperature range was set to 10 - 60°C (with 0.5°C increments). DNA was chosen as the nucleic acid, initial concentration of A_0 (sequence of interest) was 0.005 μM (5 nM). The $[\text{Na}^+]$ was set to 10 mM, and $[\text{Mg}^{2+}]$ was set to 2.5 mM. Polymer mode was left unselected.

5.3.2 Off-analyte discovery

Off-analytes were found with miRBase, a miR database operated by the University of Manchester.¹³⁻¹⁵ We used the ‘search by sequence’ functionality and entered the miR sequence of hsa-miR-146a-5p (5’ UGAGAACUGAAUCCAUGGGUU 3’). We chose to search ‘mature miRNA’ sequences, using the ‘BLASTN’ search method. The E-value cutoff was set to ‘2000’, the maximum number of hits was set to ‘100’, and only ‘human’ miR results were shown. The results of this search can be found in Appendix IV, Figure A4.1.

The miRbase analysis found two naturally occurring off- analytes. One was miR-146a-3p and is from the 3’ end of the same miR stem loop (pre-miR) that miR-146a-5p is derived from, so it has partial complementarity to miR-146a-5p (Figure 4A.1) with a ΔG of -9.1 kcal/mol and a T_m of 21.8 °C.

A diagram of the predicted binding of the miR-146a pre-miR can be found in Appendix IV, Figure A4.2. A calculated folding structure for the miR-146a pre-miR can be found in Appendix IV, Figure A4.3. This folding structure was found using the ‘Quikfold’ application of UNAFold referenced in section 5.3.1. For this pre-miR sequence, the ‘RNA (3.0)’ energy rule was chosen. The sequence type was ‘linear’, structures were ‘5%’ suboptimal, window size was set to ‘default’ with a maximum of ‘50’ foldings. There was ‘no limit’ for the maximum distance between paired bases.

5.3.3 Biosensor Design

Reporter+probe biosensors were designed to be sensitive and selective towards microRNA hsa-miR-146a. In order to increase the reporters FRET enhancement, internal poly-ethylene glycol spacers (hexaethylene glycol) were placed between the nucleic acids and the dyes on both the 5’ and 3’ ends.³ For the analyte and off-analyte miRs, we converted the miR sequences into DNA analogues for testing because DNA is less susceptible to nuclease degradation.

DNA was used as received from Integrated DNA Technologies (Coralville, IA). The samples either arrived as a dry powder and subsequently diluted in DI water, or were delivered suspended in IDTE® buffer (contains Tris and EDTA buffers, pH 7.5). For working solutions, DNA was diluted from stock concentrations in a buffer containing phosphate-buffered saline (PBS) with 10 mM Tris buffer, 2.5 mM MgCl₂, and 0.005% Tween 20 (final pH ~ 8). Concentrations of working solutions of DNA was determined using a Nanodrop Spectrophotometer (ND-1000).

For the remainder of this chapter, Reporter 1 and Reporter 2 will be known as R1 and R2, respectively. Additionally, Probe 1 and Probe 2 will be referred to as P1 and P2, respectively. The analyte and off-analyte sequences will be shortened as well with miR-146a-5p, miR-146a-3p, and miR-146b-5p becoming analyte (A), off-analyte1 (OA1), and off-analyte2 (OA2), respectively.

The probes had Four additional nucleic acids to increase stability of the reporter+probe complexes at 37°C ('GTAT' on the 5' end of P1, and 'ATAC' on the 3' end of P2, Table 5.1). The biotin group at the end of the poly-T tract on the 3' end of R1 was added for potential future conjugation of this sensor with avidin. This biotin group was not added to R2 but the poly-T tract was maintained to ensure the most similarity between the sequences.

Table 5.1. Nucleic acid sequences. Underlined sequences indicate regions where the reporters and probes (R1+P1 and R2+P2) are complementary. Bold regions on the reporters and probes indicate the complementary region between the two that occurs in the reporter stem region. The two nucleotides that are in lower-case italics in miR-146b-5p are the two nucleotides that differ from miR-146a-5p.

Name	Sequence (5' -> 3')
R1	/5ATTO633N//iSp18/GCGTATATCACA <u>CTGAATTCCATGGGTTATACGC</u> /iSp18//iFluorT/TTTTTTTTTT/3Bio/
P1	<u>GTATAACCCATGGAATTCAGTTCTCA</u>
R2	TTTTTTTTTT/iFluorT//iSp18/GC <u>GTATTGAGAACTGAATTCCATAAACGATACGC</u> /iSp18//3ATTO633N/
P2	AACCC <u>ATGGAATTCAGTTCTCAATAC</u>
miR-146a-5p (analyte, A)	TGAGAACTGAATTCCATGGGTT
miR-146a-3p (off-analyte1, OA1)	CCTCTGAAATTCAGTTCTTCAG
miR-146b-5p (off-analyte2, OA2)	TGAGAACTGAATTCCAT <i>aGGc</i> T

5.3.4 Fluorimeter design

To excite our samples and collect fluorescence spectra, a custom-built fluorimeter was used as has been described previously¹ and in Chapter 2. The fluorimeter is composed of a Ti:Sapphire ultrafast tunable laser (Mai Tai HP, Spectra-Physics) as an excitation source, and the detector was a 512 x 512 pixel electron-multiplied charge-coupled-device (EMCCD) camera (Princeton Instruments) attached to an Acton Spectrometer (SP2300, Princeton Instruments) equipped with a grating blazed at 500 nm with 300 grooves per mm.

Samples were excited with 250 mW of 935 nm laser light. This wavelength was experimentally determined to give the highest FRET enhancement (using Equation A4.1) for the Fluorescein|ATTO 633 dye pair in R1 (Appendix IV, Figure A4.2) and is consistent with previous biosensors with similar dyes.³ Lightfield software was used with the following parameters: 2500

ms integration time, 30 frames. The analog conditions were listed as 40X Electron Multiplied (EM) Gain, 5 MHz Speed, and High Analog Gain with 16 bit depth. The read out was full frame and the slit width was 1 000 μm .

For solutions containing reporters with 6-FAM and ATTO 633, the grating was centered at either 520 nm (for Fluorescein, spectral range: 477.2542–562.6750 nm) or 660 nm (for ATTO 633, spectral range: 617.5942–702.3213 nm).

5.3.5 Cell Lysate

MCF-7 cell lysate was prepared with a freeze-thaw method previously used by our group.¹⁶ The MCF-7 cells were grown in RPMI media with 10% FBS and 1% GlutaMAX. The cells were spun-down and resuspended in a solution of 2% sodium dodecyl sulfate (SDS) and 0.5% Tween-20 in Tris-EDTA (TE) buffer. The cells in the surfactant solution were then heated at 55°C for at least 90 minutes. Following the heat step the cells were placed in a -20 freezer until needed (at least one freeze/thaw cycle). When the cell lysate was used in solutions, the cell lysate was thawed and diluted in the previously described buffer (Section 5.3.3) down to 1×10^6 lysed cells per mL.

5.3.6 Off-analyte testing

To form the respective reporter+probe complexes, reporters (R1 and R2) were pre-hybridized with equimolar amounts of their respective probes (P1 and P2) in a microcentrifuge tube at 37°C for 4 hours. Next, aliquots of one of these newly formed reporter+probe complexes or a reporter control were added to microcentrifuge tubes containing enough analyte or off-analyte to be either 1X (5 nM) or 10X (50 nM). Each tube was then diluted with buffer (described in section 5.3.3, to a final reporter+probe concentration of 5 nM (with either 5 nM or 50 nM analyte/off-analyte). From these experiments, R+P and R-hairpin solution intensities were used to determine FRET quenching (Equation 5.1) and FRET enhancement (Equation 5.2) values for each of the reporter+probe biosensors.

The following equation calculated the percent change in signal for quenching ($\% \Delta S_Q$):

$$\% \Delta S_Q = 100 \times \frac{S_{R+P} - S_R}{S_{R+P}} \quad \text{Equation 5.1}$$

The following equation calculated the percent change in signal for enhancement ($\% \Delta S_E$):

$$\% \Delta S_E = 100 \times \frac{S_R - S_{R+P}}{S_{R+P}} \quad \text{Equation 5.2}$$

Emission intensities were summed for each of the emitting dyes over pixels 206–306 in each of their respective wavelength regions. For Fluorescein: 511.6364–528.3545 nm, and for

ATTO 633: 651.7041–668.2863 nm. In the text, we will refer to the dye names specifically or their center wavelength.

5.3.7 Calibration curves

To form the respective reporter+probe complexes, reporters (R1 and R2) were hybridized with equimolar amounts of their respective probes (P1 and P2) in a microcentrifuge tube at 37°C for 4 hours. Next, aliquots of reporter+probe were added to microcentrifuge tubes containing increasing amounts of analyte. Each tube was then diluted with buffer to a final reporter+probe concentration of 5 nM and analyte concentration that ranged from 0–15 nM. A calibration curve was fit using the linear region from 0–5 nM analyte. A control solution of 5 nM reporter was made to compare to the 5–15 nM analyte solutions. Each reporter type and each calibration curve (with control solutions) were conducted at least three separate times ($N = 3$). Excitation and collection parameters are identical with those in section 5.3.6.

5.4 Results and Discussion

5.4.1 Biosensor's toehold location considerations

Two reporter+probe biosensors (R1+P1 and R2+P2) were designed to be sensitive and selective for the miR-146a-5p analyte. We changed the sensor's toehold location on the probe to determine if that would help mitigate off-analyte response. The off-analytes were miR-146a-3p and miR-146b-5p. For the remainder of the text we will refer to miR-146a-5p as the “analyte or A” and miR-146a-3p and miR-146b-5p as “off-analyte1 (OA1)” and “off-analyte2 (OA2)”, respectively

For comparative sensor design, care was taken to ensure that R1 and R2 as well as R1+P1 and R2+P2 were as similar as possible, both in the number of bound nucleotides for the reporter+probe, and in thermodynamic stability. Biosensors R1+P1 and R2+P2 differ only in where the probe strand is exposed for the analyte to initiate binding. For R1+P1, the 5' end of the analyte binds to the 3' end of the probe (P1) first. For R2+P2, the opposite occurs, with the 3' end of the analyte binding to the 5' end of P2 (Figure 5.1 and 5.2).

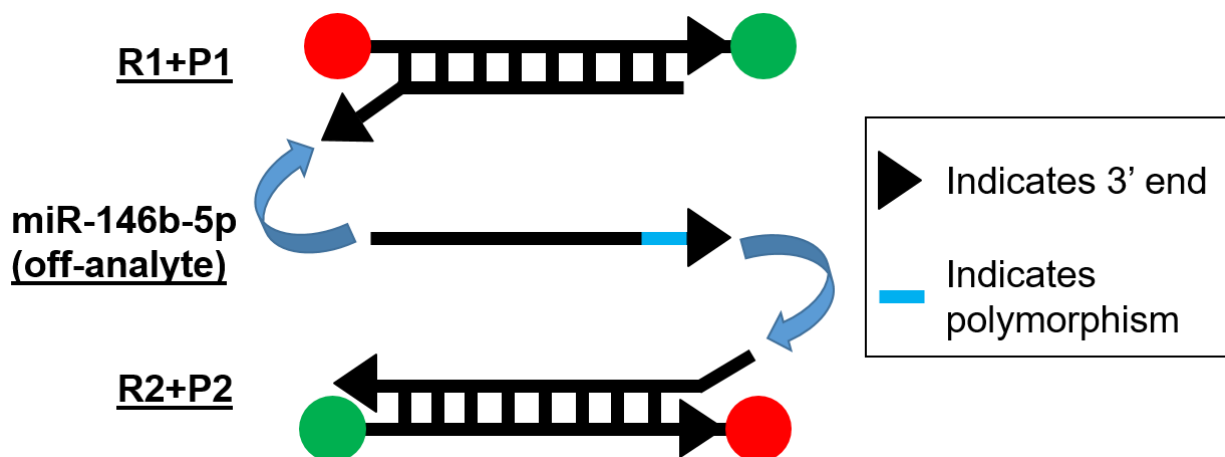


Figure 5.1 Comparison of the binding initiation of off-analytes to miR-146b-5p for both R1+P1 and R2+P2 reporter+probe biosensors. The two-nucleotide polymorphism in off-analyte2 is located near the 3' end of the molecule. The black arrow is on the 3' of each nucleotide strand.

Off-analyte1 (miR-146a-3p) is very dissimilar to analyte, and little binding between probes and off-analyte1 is predicted. The two reporter+probe designs were primarily created to test differences in selectivity against off-analyte2 (miR-146b-5p) because it has two polymorphisms in the 3' end of the strand. As seen in Table 1 when comparing analyte to off-analyte2, the polymorphisms occur in nucleotides 18 (G to A) and 21 (T to C). We hypothesized that having the probe exposed to the off-analyte2's polymorphic region would cause a disruption of the binding between off-analyte2 and the probe. In this way, the reporter is less likely to be displaced. To test the hypothesis, I will evaluate signal change in the presence off-analytes and expect to observe no change in signal.

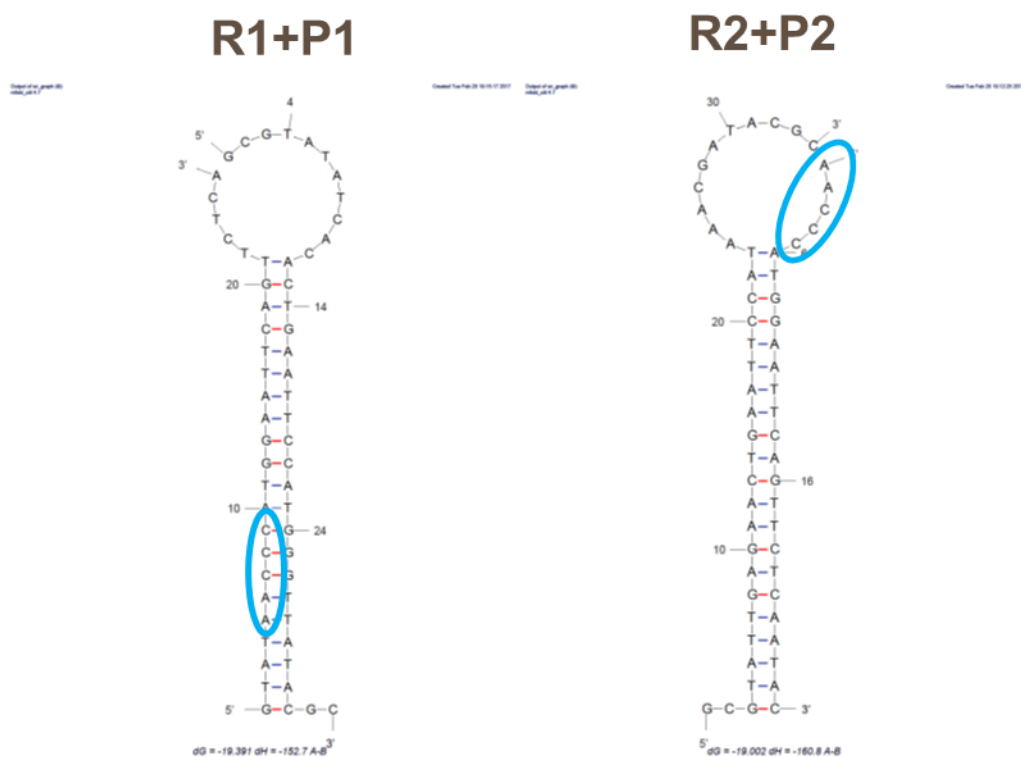


Figure 5.2 Reporter+probe biosensor predicted binding structures for R1+P1 and R2+P2. Outlined in the blue oval is the location of the probe region that will bind to the polymorphic region of off-analyte miR-146b-5p. Structures were calculated from ‘two state melting (hybridization)’ application in UNAFold, with parameters presented in materials and methods section 5.3.1.

The thermodynamic stabilities relevant to the reporter+probe biosensors are included in Table 5.2. Briefly, note that R1-hairpin and R2-hairpin have very similar Gibb’s energy values, with a small 0.05 kcal/mol difference (see Appendix IV, Figure A4.5 for the predicted binding structures of both reporter-hairpins). The stability of R1+P1 and R2+P2 are similar, with R1+P1 and R2+P2 having a difference in Gibb’s energy of 0.4 kcal/mol. The differences in thermodynamic stability for either R1-hairpin/R2-hairpin or R1+P1/R2+P2 are limited to less than or equal to 0.5 kcal/mol, so they are very comparable.

When comparing the stability of the two different probes with the analyte and off-analytes, we would expect both probes to respond exactly the same with regards to their binding partners. This is because the only difference between the two probes is the additional four nucleotides added to either the 5’ (in the case of P1) or 3’ (in the case of P2) ends to bind with the reporter stem. This four-nucleotide region should have no interaction with the three analyzed analyte and off-analytes whatsoever.

Table 5.2. Thermodynamic calculations for reporter hairpins, reporter+probe biosensors, and probes binding to analytes/off-analytes. Calculations were performed using UNAFold applications described in materials and methods section 5.3.1

Name	ΔG (kcal/mol)	ΔH (kcal/mol)	ΔS (cal/mol*K)	T_m (°C)
R1-hairpin	-2.00	-52.80	-163.79	49.2
R2-hairpin	-2.05	-54.60	-169.43	49.1
R1+P1	-19.4	-152.7	-429.8	51.4
R2+P2	-19.0	-160.8	-457.2	49.8
P1+A	-22.1	-176.0	-496.1	54.7
P2+A	-21.5	-169.1	-475.9	54.2
P1+OA1	-3.4	-41.8	-123.9	-19.2
P2+OA1	-3.4	-41.8	-123.9	-19.2
P1+OA2	-15.6	-128.4	-363.6	44.4
P2+OA2	-15.6	-128.4	-363.6	44.4

As shown in Table 5.2, the thermodynamic difference between P1+off-analyte2/P2+off-analyte2 (both have calculated Gibb's energy of -15.6 kcal/mol) and P1+off-analyte1/P2+off-analyte1 (both have calculated Gibb's energy of -3.4 kcal/mol). However, there is a slight difference in the binding energy between P1+analyte and P2+analyte. The sequence difference in the two probe strands allows P1+analyte to be a little more energetically stable than P2+analyte by 0.06 kcal/mol. This may arise due to a slightly different nearest neighbor effect that is calculated in UNAFold. Most importantly, this difference of 0.06 kcal/mol is still relatively small so P1+analyte and P2+analyte are still easily compared. More extensive thermodynamic calculations can be found in Appendix IV in Figures A4.6-A4.10 and Tables A4.1, A4.2, and A4.3.

From equimolar R-hairpin and R+P experiments outlined in section 5.3.6, we determined how much ATTO 633 was quenched by Fluorescein when in the hairpin conformation. Similarly, we determined how much FRET Enhancement the acceptor ATTO 633 undergoes due to the donor Fluorescein. The fluorescent spectra and quenching/enhancement for R1/R1+P1 can be seen in Figure 5.3.

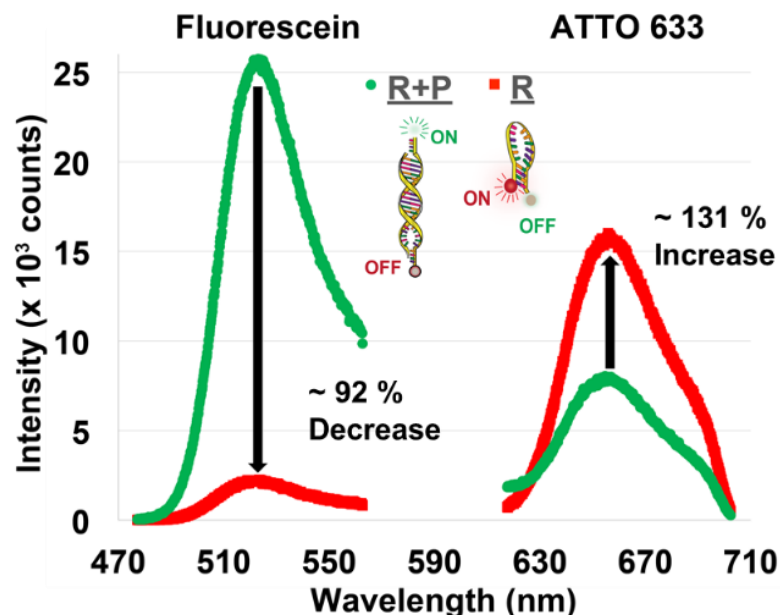


Figure 5.3 Signal change between equimolar R1+P1 and R1-hairpin for both donor and acceptor dyes.

R1/R1+P1 has better quenching ability than R2/R2+P2 by ~7 percentage points (Table 5.3). Conversely, R2/R2+P2 has better enhancement ability than R1/R1+P1 by ~81 percentage points (Table 5.3). Equations 1 and 2, analyze quenching and enhancement, respectively. These equations are outlined in section 5.3.6.

Table 5.3 Percent quenching ΔS_Q and percent enhancement ΔS_E (N = 3)

	$\Delta S_Q \pm \text{STDEV}$	$\Delta S_E \pm \text{STDEV}$
R1/R1+P1	92.42 ± 0.13	130.96 ± 3.07
R2/R2+P2	85.33 ± 0.41	212.14 ± 5.78

5.4.2 Biosensor Selectivity

For selectivity experiments, equimolar amounts of analyte or off-analytes were added to the reporter+probe complexes. Additionally, a 10X concentration of off-analyte2 (miR-146b-5p) was added to determine how that affected binding. In Figure 5.4, analyte caused the most signal change for each R+P complex (R1+P1 and R2+P2, signal change: decrease in signal from R+P to R-hairpin for Fluorescein and increase in signal from R+P to R-hairpin for ATTO 633). This indicates that the sensor is more sensitive to analyte than the two off-analytes.

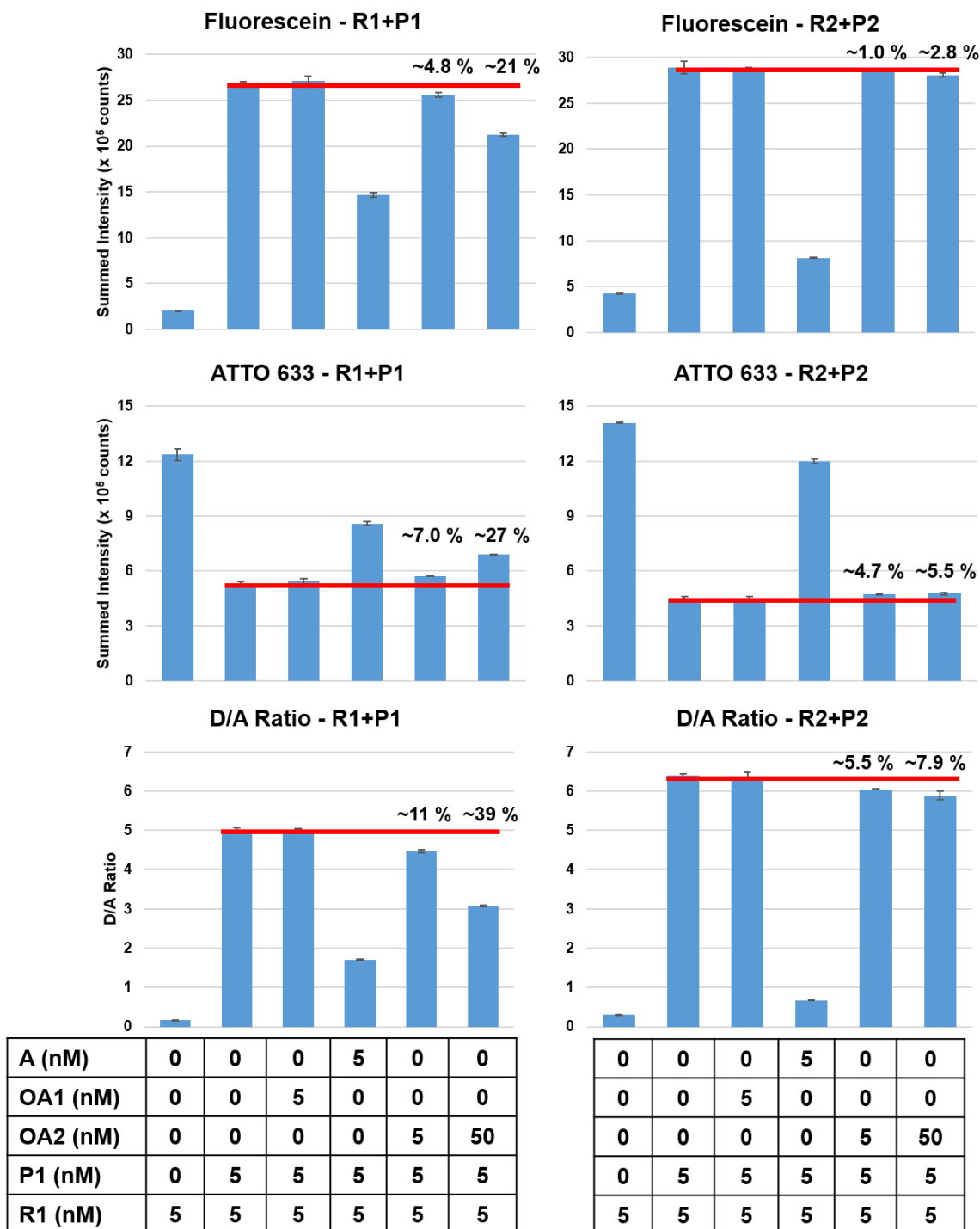


Figure 5.4 Selectivity tests for R1+P1 and R2+P2 with analyte and off-analytes. Either 1X or 10X OA2 was added to determine concentration effect on signal change (N=3).

For off-analyte1 (miR-146a-3p), the Fluorescein signal from R1+P1 had no significant difference between R1+P1 and R1+P1+off-analyte1 ($p < 0.05$, $N = 3$). This result means off-analyte1 did not cause R1+P1 to have a false signal. For off-analyte2, the 1X and 10X additions

to R1+P1 caused a statistically significant decrease in signal of ~ 4.8 and ~ 21 %, respectively ($p > 0.05$, $N = 3$).

For R2+P2, there was no statistically significant difference in signal for R2+P2 and R2+P2+off-analyte1 ($p < 0.05$, $N = 3$). For the 1X and 10X additions of off-analyte2 (R2+P2+off-analyte2), the respective ~ 1.0 and ~ 2.8 % decrease in signal were not statistically significant ($p < 0.05$, $N = 3$).

For ATTO 633, again there was no significant difference between the signal for R1+P1 and R1+P1+ off-analyte1. For the 1X and 10X additions of off-analyte2 (R1+P1+off-analyte2), an increase of signal of ~7.0 and ~27 % were seen when compared to R1+P1, both of which were significantly different ($p < 0.05$, $N = 3$). For R2+P2, there was also no significant difference in signal for R2+P2 and R2+P2+ off-analyte1 ($p > 0.05$, $N = 3$). For the 1X and 10X additions of off-analyte2 (R2+P2+off-analyte2), a decrease of signal of ~4.8 and ~5.5 % were seen when compared to R2+P2, both of which were significantly different ($p < 0.05$, $N = 3$).

For Fluorescein, R2+P2 had less signal change than R1+P1 in response to both the 1X and 10X additions of off-analyte2, and was not significantly different than the signal without off-analyte2. For ATTO 633, even though both R1+P1 and R2+P2 had significantly different responses to off-analyte2 when compared to without, R2+P2 had less signal change than R1+P1 in response to both the 1X and 10X additions of off-analyte2. This demonstrates that R2+P2 is superior to R1+P1 against off-analyte 2, which most likely arises from the movement of the threshold.

When analyzing the D/A ratio, again there was no significant difference between the D/A ratio for R1+P1 and R1+P1+ off-analyte1. For the 1X and 10X additions of off-analyte2 (R1+P1+ off-analyte2), a decrease in the ratio of ~11 and ~39 %, respectively, were seen when compared to R1+P1, both were significantly different ($p < 0.05$, $N = 3$).

For R2+P2, there was no statistical difference in the D/A ratio for R2+P2 and R2+P2+ off-analyte1 ($p > 0.05$, $N = 3$). For the 1X and 10X additions of off-analyte2 (R2+P2+ off-analyte2), a decrease in signal of ~5.5 and ~7.9 %, respectively, was seen when compared to R2+P2, both were statistically different ($p < 0.05$, $N = 3$). Again, for the D/A ratio, even though both R1+P1 and R2+P2 had significantly different responses to off-analyte2 when compared to without, R2+P2 had less change in the D/A ratio than R1+P1 in response to both the 1X and 10X additions of off-

analyte2. These results further demonstrates how changing the location of the sensor's toehold discourages binding by off-analytes.

Additional experiments were performed with 10X off-analyte1 with R1+P1 and R2+P2 (Appendix IV, Figure A4.11). Neither the Fluorescein signal nor the D/A Ratio showed any statistical difference between the R+P+10X off-analyte1 signal and the R+P signal for either of the R+P biosensors. However, when looking at ATTO 633 alone, a statistical decrease in signal by $\sim 2.4\%$ ($p < 0.05$, $N = 3$) was observed between R1+P1 and R1+P1+10X off-analyte1. However, since this significant difference is not seen in either the Fluorescein signal nor the D/A ratio, the effect must be minimal.

Both reporters alone (without probe) were tested against 10X analyte/off-analytes to determine any non-specific binding effects (Appendix IV, Figure A4.11). For both Fluorescein and ATTO 633, neither 10X analyte, off-analyte1, nor off-analyte2 had any effect on the signal of either R1 or R2 ($p > 0.05$, $N = 3$). When considering the D/A ratio, there was no statistical difference between either of the reporters and the 10X analytes/off-analytes apart from R2 + 10X off-analyte1. However, for R2 + 10X off-analyte1 the D/A ratio increased by $\sim 5.2\%$ compared to R2 (statistically different with $p > 0.05$, $N = 3$). When looking at the thermodynamic calculations for R2+off-analyte1, it has a Gibb's energy of -9.1 kcal/mol and a melting temperature of 21.8°C . Both of these values are much higher than those for R1+off-analyte1, which has a Gibb's energy of -5.9 and a melting temperature of 4.8°C . Even so, the change in signal is around 5% with a 10X concentration of off-analyte1, and the changes in signal could not be seen in either the Fluorescein or ATTO 633 intensities, so the effect must be minimal.

5.4.3 Biosensor sensitivity and analytical metrics

Calibration curves were run with both biosensors held at 5 nM in MCF-7 cell lysate. The cell lysate was unfiltered and was at a concentration of 1×10^6 cells per mL. The concentration of analyte was stepped in 1 nM increments from 0-6 nM, and then an additional solution of 15 nM was added to assess the endpoint of the signal change (Figure 5.5). A line was fit between 0 and 5 nM analyte added to create a calibration curve.

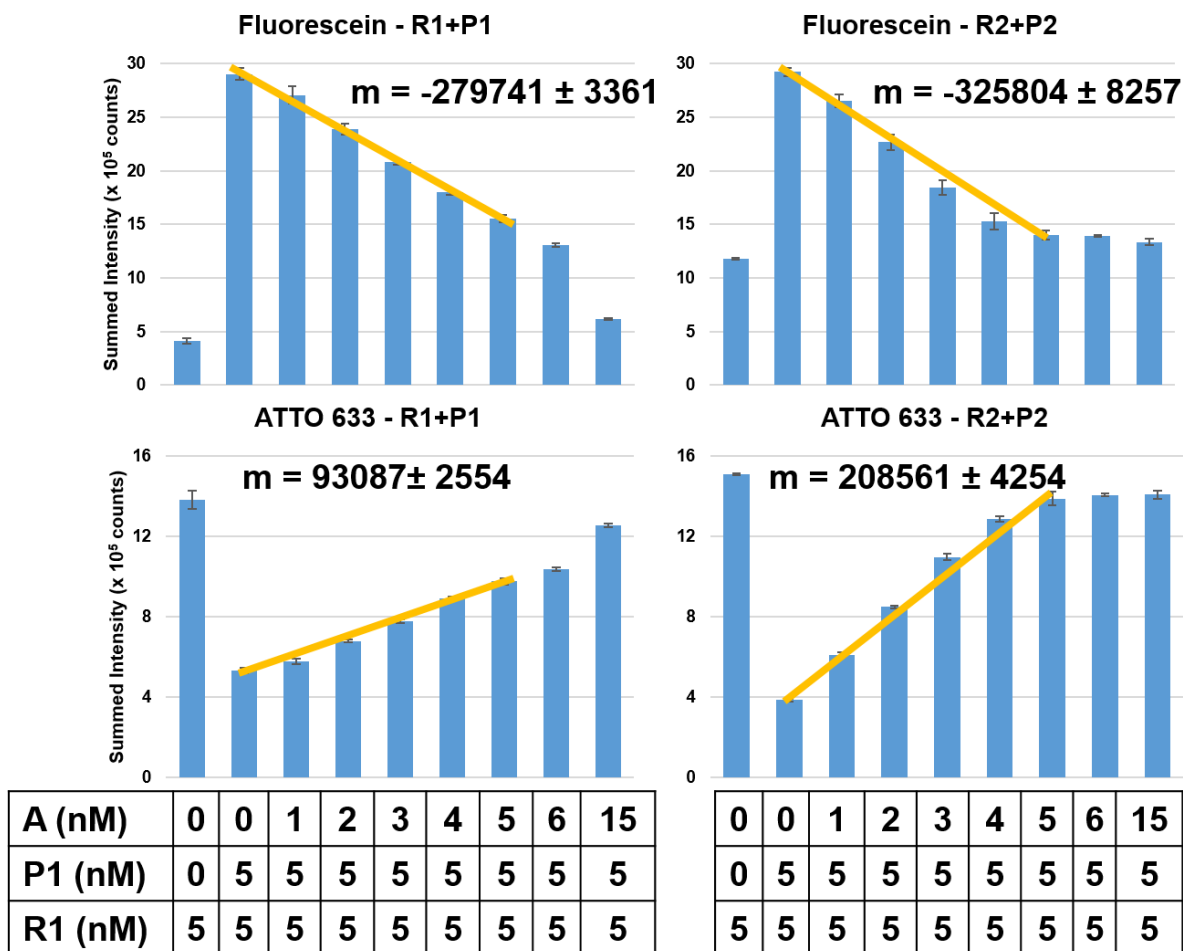


Figure 5.5 Calibration curves in cell lysate (N=3).

The limits of detection were all found to be in the pM range, with the ATTO 633 signal giving better LOD's than the Fluorescein signal. The Fluorescein signal for R1+P1 gave a LOD of 209 pM, while the ATTO 633 signal gave a 142 pM LOD. The R2+P2 LOD's were lower than those for R1+P1, with 123 pM for the Fluorescein signal and 56 pM for the ATTO 633 signal. These LOD's are useful since they are middle of the road for intracellular miRs (pM to nM intracellular concentration).

Table 5.4 Analytical slope and limits of detection (LODs) for both R1+P1 and R2+P2 reporter+probe biosensors.

	Average Slope \pm STDEV (counts/nM)	LOD \pm STDEV (pM)
R1+P1 (Donor Signal)	-279741 \pm 3361	209 \pm 31
R1+P1 (Acceptor Signal)	93087 \pm 2554	142 \pm 27
R2+P2 (Donor Signal)	-325804 \pm 8257	123 \pm 11
R2+P2 (Acceptor Signal)	208561 \pm 4254	56 \pm 7

5.5 Conclusion

We designed two reporter+probe biosensors for hsa-miR-146a-5p with opposite toehold locations. We reported on each toehold location's susceptibility to off-analyte binding. We found that changing the toehold's location on the sensor minimized off-analyte binding as we observed decreased amounts of off-analyte binding with R2+P2 over R1+P1. The new design strategy starts with looking for off-analytes in miRbase to determine sensor's toehold location that limits off-analyte response. This added consideration will increase the selectivity for all future biosensors. Off-analyte consideration is important because off-analyte binding leads to false positive signal generation. False signals lead to false conclusions about a given miR concentration in a sample. Selectivity can be further improved with strategically placed locked nucleic acids (LNAs) that further separate the thermodynamic stability of probe+analyte and probe+off-analytes.

The LODs of both sensors were in the mid-pM range, with the second sensor being slightly better by a factor of ~1.7-2.5. A dynamic range of pM to nM is especially useful for the Intracellular miR concentration range of pico- to nano-molar range. These pM LOD's were determined for sensors in MCF-7 cell lysate, and shows that the sensor can achieve low LOD's inside a complex matrix.

Future work will focus on transfecting these sensors into cells for intracellular imaging, along with biosensor conjugation to avidin to aid with tuning intracellular localization. Additional work will also continue decreasing the LODs even further to get to single pM. These sensors will allow researchers to use a sensitive method for detecting miRs of interest while maintaining selectivity against off-analytes.

5.6 Acknowledgements

The authors would like to thank Oregon State University and the N.L. Tartar Research Fellowship for supporting this research.

5.7 References

- (1) Larkey, N. E.; Almlie, C. K.; Tran, V.; Egan, M.; Burrows, S. M. *Anal. Chem.* **2014**, *86* (3), 1853.
- (2) Larkey, N. E.; Brucks, C. N.; Lansing, S. S.; Le, S. D.; Smith, N. M.; Tran, V.; Zhang, L.; Burrows, S. M. *Anal. Chim. Acta* **2016**, *909*, 109.
- (3) Larkey, N. E.; Zhang, L.; Lansing, S. S.; Tran, V.; Seewaldt, V. L.; Burrows, S. M. *Analyst* **2016**, *141* (22), 6239.

- (4) Zhang, D. Y.; Seelig, G. *Nat. Chem.* **2011**, 3 (2), 103.
- (5) Yeh, H.-C.; Sharma, J.; Shih, I.-M.; Vu, D. M.; Martinez, J. S.; Werner, J. H. *J. Am. Chem. Soc.* **2012**, 134 (28), 11550.
- (6) Yeh, H.-C.; Puleo, C. M.; Ho, Y.-P.; Bailey, V. J.; Lim, T. C.; Liu, K.; Wang, T.-H. *Biophys. J.* **2008**, 95 (2), 729.
- (7) Yeh, H.-C.; Ho, Y.-P.; Wang, T.-H. *Nanomedicine Nanotechnol. Biol. Med.* **2005**, 1 (2), 115.
- (8) Zhang, D. Y.; Chen, S. X.; Yin, P. *Nat. Chem.* **2012**, 4 (3), 208.
- (9) Zavala, V.; Pérez-Moreno, E.; Tapia, T.; Camus, M.; Carvallo, P. *Cancer Biomark.* **2016**, 16 (1), 99.
- (10) Sandhu, R.; Rein, J.; D'Arcy, M.; Herschkowitz, J. I.; Hoadley, K. A.; Troester, M. A. *Carcinogenesis* **2014**, 35 (11), 2567.
- (11) M'hamed, I. F.; Privat, M.; Ponelle, F.; Penault-Llorca, F.; Kenani, A.; Bignon, Y.-J. *Cell. Oncol.* **2015**, 38 (6), 433.
- (12) Li, Y.; Xu, Y.; Yu, C.; Zuo, W. *Cancer Biomark.* **2015**, 15 (6), 881.
- (13) Griffiths-Jones, S. *Nucleic Acids Res.* **2006**, 34 (90001), D140.
- (14) Griffiths-Jones, S.; Saini, H. K.; van Dongen, S.; Enright, A. J. *Nucleic Acids Res.* **2007**, 36 (Database), D154.
- (15) Kozomara, A.; Griffiths-Jones, S. *Nucleic Acids Res.* **2011**, 39 (Database), D152.
- (16) Zhang, Z.; Fan, T. W.; Hsing, I.-M. *Nanoscale* **2017**, 9 (8), 2748.

Chapter 6.

Summaries and Conclusions

6.1. Summaries and Conclusions

The reporter+probe biosensors described herein were designed to overcome the shortcomings associated with previous *in situ* miR biosensors. This work has contributed new designs and key advancements that will benefit the strand-displacement biosensor field. The first iteration of the reporter+probe biosensor (Chapter 2)¹ was designed for miR let-7a and reduced false signals when compared to molecular beacons. The works that followed the first iteration enhanced the biosensor by optimizing:

1. *Design principles for reporter+probe biosensor production (Chapter 3)*²
2. *Sensitivity for various miR analytes (Chapter 3 and 5)*²
3. *Different dye pair and spacer combinations for FRET enhancement (Chapter 4)*³
4. *Design alterations to increase selectivity (Chapter 5)*

There are still many potential issues (Table 6.1) that we need to focus on to improve the reporter+probe biosensor for intracellular analysis. Some of the issues include transfection, enzyme degradation, sensitivity, selectivity, miR lifetime, and detecting multiple miRs at once (multiplexing). If we can overcome these issues, we expect that this biosensor will elucidate the biological roles of miRs intracellularly and possibly inside of tissues.

Table 6.1 Possible pitfalls of reporter+probe biosensors and potential solutions

Possible pitfalls/roadblocks	Summary	Potential Solution(s)
Transfection	Sensors do not fully enter cells or tissues	<ul style="list-style-type: none"> • Streptolysin O⁴ • Electroporation⁴ • New commercial transfection agents^a • Cell-penetrating peptides (CPPs)⁴ • Internal standard dyes on sensors^{5,6}
Enzyme degradation	Sensors degrade inside of cells or tissues leading to false signals	<ul style="list-style-type: none"> • Additional LNAs^{7,8} • Polyethylene glycol (PEG) spacers^a • Morpholinos⁹ • Peptide nucleic acids (PNAs)¹⁰
Sensitivity	miRs concentration is too low to be detected	<ul style="list-style-type: none"> • LNAs^{7,8} • Multiple donor or acceptor dyes¹¹ • Quantum dots¹² • Polymer dots¹³
Selectivity	Sensor binds to off-target sequences	<ul style="list-style-type: none"> • LNAs^{7,8} • Polyethylene glycol (PEG) spacers^a

		<ul style="list-style-type: none"> • Non-canonical bases¹⁴
miR Lifetime	Intracellular miRs may have too short of lifetimes to be detected	<ul style="list-style-type: none"> • Cell-cycle arrest¹⁵
Multiplexing	Detect more than one type of sequence at a time	<ul style="list-style-type: none"> • Multiple biosensors with different dyes³ • Sensors that detect multiple miRs¹⁶ • Quantum dots¹² • Dye-specific offsets¹⁷

^aUnpublished data

Transfection of these sensors into cells has been challenging and needs to be a focus of future work. We have found that various commercial transfection agents quench the signal of our sensors (unpublished data), leading to difficulty in fluorescent signal acquisition. Future research will include studies to find optimal transfection methods and agents. Previous researchers have shown success with electroporation techniques or streptolysin O.⁴ In the interim, experiments are currently being designed to test these sensors with miRs isolated from cells.

Although the reporter+probe biosensor's reduced false signals from enzyme degradation, the actual sensor can still get degraded.¹ More work is needed to study the susceptibility to nuclease degradation of these sensors, as the design of the biosensor has been slightly altered over time and new nuclease degradation studies are needed. Current work is being performed (unpublished data) to determine how adding LNAs^{7,8} and increasing the length of PEG spacers in non-complementary regions can decrease nuclease degradation of the sensor. Additional modifications such as Morpholinos and Peptide Nucleic Acids (PNAs) could potentially help decrease the amount of degradation even further.^{10,11} In addition to aversion to nuclease degradation, PNAs show reduced susceptibility to protease digestion.¹⁸

Through the reporter+probe biosensor's course of the development, the limits of detection (LOD) have decreased from 4 nanomolar to 56 picomolar in concentration, close to a two orders-of-magnitude decrease. The concentration of intracellular miRs has been found to be in the picomolar to nanomolar range, and picomolar LODs demonstrated by the reporter+probe biosensor measure in middle of this range. If a cell is estimated to have a volume of 1 picoliter¹⁹ (pL), a single miR would equate to a concentration of 1-2 pM. Advancements in both the signal transduction mechanism and the sensitivity at low concentrations is needed to decrease the LOD down to this level. For the transduction mechanism, different dyes than the ones described in this work could be incorporated into the reporter. We found that Fluorescein (FAM) and ATTO 633 showed the most FRET signal enhancement.³ However, there may be better dye pairs with larger signal enhancement that could be used for these sensors. Additionally, FRET enhancement could

be increased by adding more donor dye molecules to the sensor in order to increase the amount of incident energy that can be transferred to the acceptor dye.¹¹ For example, Buckhout-White et al. showed enhancement factors near 40 when there were 2 donors to one acceptor.¹¹ Additionally, fluorescent molecules with higher quantum efficiencies could be tried, such as quantum dots.¹²

Selectivity of these sensors can be pushed further by adding DNA modifications such as Locked Nucleic Acids (LNAs) into sensors to increase the thermodynamic specificity for a given analyte. Non-canonical bases¹⁴ and/or poly-ethylene glycol (PEG) spacers can be incorporated in order to create regions of the sensor where unwanted sequences cannot bind. Non-canonical bases will only bind to their corresponding non-canonical pair, which will be advantageous in the stem region of the reporter. PEG spacers could increase the length of reporter or probe strands without adding bases that could be susceptible sites for off-target binding.

Another issue is that the lifetime of intracellular miRs – in some cases - can be less than 4 hours (half-life) depending on the miR and the stage of the cell cycle.¹⁵ In the absence of the enzyme Dicer1, the average half-life of a selection of miRs was found to be around 5 days in mouse embryonic fibroblasts, and as long as 9 days with respect to miR-125b.²⁰ Another study had shown that the *in-vivo* half-life miR-208 in non-dividing cells be up to 12 days.²¹ Since changes in miR concentration can be cell-cycle dependent, arresting the cells in different stages in the cell cycle can stabilize the change in concentration of miRs. This stabilization can increase the half-life of these miRs.

In terms of multiplexing, using multiple dye-pairs can aid in using multiple sensors at the same time to detect different miRs. To decrease cross-talk between dyes, molecules with smaller emission profiles such as quantum dots could be used.¹² Other methods to decrease cross-talk between dyes include using dye-specific offsets with continually variable filters in order to detect more dyes in solution.¹⁷ DNA-nano-assemblies that respond to more than one analyte at a time could allow for complex multiplexing.¹⁶ These nano-assemblies are designed to work as logic gates, so that signal change is only achieved when a particular combination of miRs are present.

MiRs are quickly becoming accepted as important intracellular regulatory biomarkers, and miR biosensors have the potential to increase our understanding of how miRs regulate intracellular activity. Learning more about how cells regulate their own pathways will help us to better understand how diseases progress, and hopefully lead to earlier screening options for patients. Earlier detection of disease will allow quicker administration of treatment to patients, which can

lead to better outcome. The work that I have done designing miR biosensors will aid future researchers in considering thermodynamics and fluorescent signal generation when designing their own sensors to detect miR.

6.2 References

- (1) Larkey, N. E.; Almlie, C. K.; Tran, V.; Egan, M.; Burrows, S. M. *Anal. Chem.* **2014**, *86* (3), 1853.
- (2) Larkey, N. E.; Brucks, C. N.; Lansing, S. S.; Le, S. D.; Smith, N. M.; Tran, V.; Zhang, L.; Burrows, S. M. *Anal. Chim. Acta* **2016**, *909*, 109.
- (3) Larkey, N. E.; Zhang, L.; Lansing, S. S.; Tran, V.; Seewaldt, V. L.; Burrows, S. M. *The Analyst* **2016**, *141* (22), 6239.
- (4) Chen, A. K.; Behlke, M. A.; Tsourkas, A. *Nucleic Acids Res.* **2008**, *36* (12), e69.
- (5) Chen, A. K.; Davydenko, O.; Behlke, M. A.; Tsourkas, A. *Nucleic Acids Res.* **2010**, *38* (14), e148.
- (6) Zhang, X.; Song, Y.; Shah, A. Y.; Lekova, V.; Raj, A.; Huang, L.; Behlke, M. A.; Tsourkas, A. *Nucleic Acids Res.* **2013**, *41* (15), e152.
- (7) Wang, L.; Yang, C. J.; Medley, C. D.; Benner, S. A.; Tan, W. *J. Am. Chem. Soc.* **2005**, *127* (45), 15664.
- (8) Martinez, K.; Estevez, M.-C.; Wu, Y.; Phillips, J. A.; Medley, C. D.; Tan, W. *Anal. Chem.* **2009**, *81* (9), 3448.
- (9) Hudziak, R. M.; Barofsky, E.; Barofsky, D. F.; Weller, D. L.; Huang, S. B.; Weller, D. D. *Antisense Nucleic Acid Drug Dev.* **1996**, *6* (4), 267.
- (10) Borgatti, M.; Romanelli, A.; Saviano, M.; Pedone, C.; Lampronti, I.; Breda, L.; Nastruzzi, C.; Bianchi, N.; Mischianti, C.; Gambari, R. *Oncol. Res.* **2003**, *13* (5), 279.
- (11) Buckhout-White, S.; Spillmann, C. M.; Algar, W. R.; Khachatryan, A.; Melinger, J. S.; Goldman, E. R.; Ancona, M. G.; Medintz, I. L. *Nat. Commun.* **2014**, *5*.
- (12) Gliddon, H. D.; Howes, P. D.; Kaforou, M.; Levin, M.; Stevens, M. M. *Nanoscale* **2016**, *8* (19), 10087.
- (13) Wu, C.; Chiu, D. T. *Angew. Chem. Int. Ed.* **2013**, *52* (11), 3086.
- (14) Johnson, S. C.; Sherrill, C. B.; Marshall, D. J.; Moser, M. J.; Prudent, J. R. *Nucleic Acids Res.* **2004**, *32* (6), 1937.
- (15) Rügger, S.; Großhans, H. *Trends Biochem. Sci.* **2012**, *37* (10), 436.
- (16) Zhang, L.; Bluhm, A. M.; Chen, K.-J.; Larkey, N. E.; Burrows, S. M. *Nanoscale* **2017**.
- (17) Almlie, C. K.; Hsiao, A.; Burrows, S. M. *Anal. Chem.* **2016**, *88* (2), 1462.
- (18) Gan, W.; Xiaoxin, S. X. *Cell Res.* **2004**, *14* (2), 111.
- (19) Fujioka, A.; Terai, K.; Itoh, R. E.; Aoki, K.; Nakamura, T.; Kuroda, S.; Nishida, E.; Matsuda, M. *J. Biol. Chem.* **2006**, *281* (13), 8917.
- (20) Gantier, M. P.; McCoy, C. E.; Rusinova, I.; Saulep, D.; Wang, D.; Xu, D.; Irving, A. T.; Behlke, M. A.; Hertzog, P. J.; Mackay, F.; Williams, B. R. G. *Nucleic Acids Res.* **2011**, *39* (13), 5692.
- (21) Rooij, E. van; Sutherland, L. B.; Qi, X.; Richardson, J. A.; Hill, J.; Olson, E. N. *Science* **2007**, *316* (5824), 575.

Bibliography

(Listed in order cited)

- (1) Liang, Y.; Ridzon, D.; Wong, L.; Chen, C. *BMC Genomics* **2007**, *8* (1), 166.
- (2) Subkhankulova, T.; Gilchrist, M. J.; Livesey, F. J. *BMC Genomics* **2008**, *9* (1), 268.
- (3) Shum, J.; Paul, N. *Anal. Biochem.* **2009**, *388* (2), 266.
- (4) Ragan, C.; Zuker, M.; Ragan, M. A. *PLoS Comput. Biol.* **2011**, *7* (2).
- (5) Sempere, L. F. *Expert Rev. Mol. Diagn.* **2014**, *14* (7), 853.
- (6) Volinia, S.; Calin, G. A.; Liu, C.-G.; Ambros, S.; Cimmino, A.; Petrocca, F.; Visone, R.; Iorio, M.; Roldo, C.; Ferracin, M.; Prueitt, R. L.; Yanaihara, N.; Lanza, G.; Scarpa, A.; Vecchione, A.; Negrini, M.; Harris, C. C.; Croce, C. M. *Proc. Natl. Acad. Sci. U. S. A.* **2006**, *103* (7), 2257.
- (7) Zhu, S.; Wu, H.; Wu, F.; Nie, D.; Sheng, S.; Mo, Y.-Y. *Cell Res.* **2008**, *18* (3), 350.
- (8) Iorio, M. V.; Ferracin, M.; Liu, C.-G.; Veronese, A.; Spizzo, R.; Sabbioni, S.; Magri, E.; Pedriali, M.; Fabbri, M.; Campiglio, M. *Cancer Res.* **2005**, *65* (16), 7065.
- (9) Mitomo, S.; Maesawa, C.; Ogasawara, S.; Iwaya, T.; Shibazaki, M.; Yashima-Abo, A.; Kotani, K.; Oikawa, H.; Sakurai, E.; Izutsu, N.; Kato, K.; Komatsu, H.; Ikeda, K.; Wakabayashi, G.; Masuda, T. *Cancer Sci.* **2008**, *99* (2), 280.
- (10) Visone, R.; Russo, L.; Pallante, P.; Martino, I. D.; Ferraro, A.; Leone, V.; Borbone, E.; Petrocca, F.; Alder, H.; Croce, C. M.; Fusco, A. *Endocr. Relat. Cancer* **2007**, *14* (3), 791.
- (11) Akao, Y.; Nakagawa, Y.; Naoe, T. *Oncol. Rep.* **2006**, *16* (4), 845.
- (12) Shi, B.; Sepp-Lorenzino, L.; Prisco, M.; Linsley, P.; deAngelis, T.; Baserga, R. *J. Biol. Chem.* **2007**, *282* (45), 32582.
- (13) Sylvestre, Y.; Guire, V. D.; Querido, E.; Mukhopadhyay, U. K.; Bourdeau, V.; Major, F.; Ferbeyre, G.; Chartrand, P. *J. Biol. Chem.* **2007**, *282* (4), 2135.
- (14) Shi, X.-B.; Xue, L.; Yang, J.; Ma, A.-H.; Zhao, J.; Xu, M.; Tepper, C. G.; Evans, C. P.; Kung, H.-J.; White, R. W. deVere. *Proc. Natl. Acad. Sci.* **2007**, *104* (50), 19983.
- (15) Johnson, S. M.; Grosshans, H.; Shingara, J.; Byrom, M.; Jarvis, R.; Cheng, A.; Labourier, E.; Reinert, K. L.; Brown, D.; Slack, F. J. *Cell* **2005**, *120* (5), 635.
- (16) Fabbri, M.; Garzon, R.; Cimmino, A.; Liu, Z.; Zanesi, N.; Callegari, E.; Liu, S.; Alder, H.; Costinean, S.; Fernandez-Cymering, C.; Volinia, S.; Guler, G.; Morrison, C. D.; Chan, K. K.; Marcucci, G.; Calin, G. A.; Huebner, K.; Croce, C. M. *Proc. Natl. Acad. Sci.* **2007**, *104* (40), 15805.
- (17) Shell, S.; Park, S.-M.; Radjabi, A. R.; Schickel, R.; Kistner, E. O.; Jewell, D. A.; Feig, C.; Lengyel, E.; Peter, M. E. *Proc. Natl. Acad. Sci.* **2007**, *104* (27), 11400.
- (18) Giannakakis, A.; Sandaltzopoulos, R.; Greshock, J.; Liang, S.; Huang, J.; Hasegawa, K.; Li, C.; O'Brien-Jenkins, A.; Katsaros, D.; Weber, B. L.; Simon, C.; Coukos, G.; Zhang, L. *Cancer Biol. Ther.* **2008**, *7* (2), 255.
- (19) Ikeda, S.; Kong, S. W.; Lu, J.; Bisping, E.; Zhang, H.; Allen, P. D.; Golub, T. R.; Pieske, B.; Pu, W. T. *Physiol. Genomics* **2007**, *31* (3), 367.
- (20) Fiore, R.; Siegel, G.; Schratt, G. *Biochim. Biophys. Acta BBA - Gene Regul. Mech.* **2008**, *1779* (8), 471.
- (21) Taganov, K. D.; Boldin, M. P.; Chang, K.-J.; Baltimore, D. *Proc. Natl. Acad. Sci.* **2006**, *103* (33), 12481.
- (22) Pasquinelli, A. E.; Reinhart, B. J.; Slack, F.; Martindale, M. Q.; Kuroda, M. I.; Maller, B.; Hayward, D. C.; Ball, E. E.; Degan, B.; Müller, P. *Nature* **2000**, *408* (6808), 86.

- (23) Pasquinelli, A. E.; McCoy, A.; Jiménez, E.; Salo, E.; Ruvkun, G.; Martindale, M. Q.; Baguna, J. *Evol. Dev.* **2003**, *5* (4), 372.
- (24) Roush, S.; Slack, F. J. *Trends Cell Biol.* **2008**, *18* (10), 505.
- (25) Reinhart, B. J.; Slack, F. J.; Basson, M.; Pasquinelli, A. E.; Bettinger, J. C.; Rougvie, A. E.; Horvitz, H. R.; Ruvkun, G. *Nature* **2000**, *403* (6772), 901.
- (26) Esquela-Kerscher, A.; Slack, F. J. *Nat. Rev. Cancer* **2006**, *6* (4), 259.
- (27) Shi, X.-B.; Tepper, C. G.; deVere White, R. W. *Cell Cycle* **2008**, *7* (11), 1529.
- (28) Deng, M.; Tang, H.; Lu, X.; Liu, M.; Lu, X.; Gu, Y.; Liu, J.; He, Z. *PLoS ONE* **2013**, *8* (8), e72662.
- (29) Gao, J.; Li, L.; Wu, M.; Liu, M.; Xie, X.; Guo, J.; Tang, H.; Xie, X. *PLoS ONE* **2013**, *8* (6), e65138.
- (30) Dang, X.; Ma, A.; Yang, L.; Hu, H.; Zhu, B.; Shang, D.; Chen, T.; Luo, Y. *Cancer Genet.* **2012**, *205* (3), 113.
- (31) Li, J.; Wang, Y.; Song, Y.; Fu, Z.; Yu, W. *Mol. Cancer* **2014**, *13* (1), 193.
- (32) Mertens-Talcott, S. U.; Chintharlapalli, S.; Li, X.; Safe, S. *Cancer Res.* **2007**, *67* (22), 11001.
- (33) Melo, S. A.; Kalluri, R. *Nat. Cell Biol.* **2013**, *15* (2), 139.
- (34) Sandhu, R.; Rein, J.; D'Arcy, M.; Herschkowitz, J. I.; Hoadley, K. A.; Troester, M. A. *Carcinogenesis* **2014**, *35* (11), 2567.
- (35) Li, Y.; Xu, Y.; Yu, C.; Zuo, W. *Cancer Biomark.* **2015**, *15* (6), 881.
- (36) M'hamed, I. F.; Privat, M.; Ponelle, F.; Penault-Llorca, F.; Kenani, A.; Bignon, Y.-J. *Cell. Oncol.* **2015**, *38* (6), 433.
- (37) Zavala, V.; Pérez-Moreno, E.; Tapia, T.; Camus, M.; Carvallo, P. *Cancer Biomark.* **2016**, *16* (1), 99.
- (38) Lu, J.; He, M.-L.; Wang, L.; Chen, Y.; Liu, X.; Dong, Q.; Chen, Y.-C.; Peng, Y.; Yao, K.-T.; Kung, H.-F.; Li, X.-P. *Cancer Res.* **2011**, *71* (1), 225.
- (39) Crick, F. *Nature* **1970**, *227* (5258), 561.
- (40) Winter, J.; Jung, S.; Keller, S.; Gregory, R. I.; Diederichs, S. *Nat. Cell Biol.* **2009**, *11* (3), 228.
- (41) Eulalio, A.; Huntzinger, E.; Nishihara, T.; Rehwinkel, J.; Fauser, M.; Izaurralde, E. *RNA* **2009**, *15* (1), 21.
- (42) Wu, L.; Fan, J.; Belasco, J. G. *Proc. Natl. Acad. Sci. U. S. A.* **2006**, *103* (11), 4034.
- (43) Li, J.; Tan, S.; Kooger, R.; Zhang, C.; Zhang, Y. *Chem. Soc. Rev.* **2014**, *43* (2), 506.
- (44) Croce, C. M. *Nat. Rev. Genet.* **2009**, *10* (10), 704.
- (45) Leung, A. K.; Calabrese, J. M.; Sharp, P. A. *Proc. Natl. Acad. Sci.* **2006**, *103* (48), 18125.
- (46) Liu, J.; Valencia-Sanchez, M. A.; Hannon, G. J.; Parker, R. *Nat. Cell Biol.* **2005**, *7* (7), 719.
- (47) Nishi, K.; Takahashi, T.; Suzawa, M.; Miyakawa, T.; Nagasawa, T.; Ming, Y.; Tanokura, M.; Ui-Tei, K. *Nucleic Acids Res.* **2015**, *43* (20), 9856.
- (48) Glinsky, G. V. *J. Clin. Invest.* **2013**, *123* (6), 2350.
- (49) Sternberg, J. B.; Pierce, N. A. *Nano Lett.* **2014**, *14* (8), 4568.
- (50) Graybill, R. M.; Bailey, R. C. *Anal. Chem.* **2016**, *88* (1), 431.
- (51) Foulkes, W. D.; Smith, I. E.; Reis-Filho, J. S. *N. Engl. J. Med.* **2010**, *363* (20), 1938.
- (52) D'Ippolito, E.; Iorio, M. V. *Int. J. Mol. Sci.* **2013**, *14* (11), 22202.
- (53) Chen, C.; Ridzon, D. A.; Broomer, A. J.; Zhou, Z.; Lee, D. H.; Nguyen, J. T.; Barbisin, M.; Xu, N. L.; Mahuvakar, V. R.; Andersen, M. R.; Lao, K. Q.; Livak, K. J.; Guegler, K. J. *Nucleic Acids Res.* **2005**, *33* (20), e179.

- (54) Calin, G. A.; Liu, C.-G.; Sevignani, C.; Ferracin, M.; Felli, N.; Dumitru, C. D.; Shimizu, M.; Cimmino, A.; Zupo, S.; Dono, M.; Dell'Aquila, M. L.; Alder, H.; Rassenti, L.; Kipps, T. J.; Bullrich, F.; Negrini, M.; Croce, C. M. *Proc. Natl. Acad. Sci. U. S. A.* **2004**, *101* (32), 11755.
- (55) Alhasan, A. H.; Kim, D. Y.; Daniel, W. L.; Watson, E.; Meeks, J. J.; Thaxton, C. S.; Mirkin, C. A. *Anal. Chem.* **2012**, *84* (9), 4153.
- (56) Liu, C.-G.; Calin, G. A.; Meloon, B.; Gamliel, N.; Sevignani, C.; Ferracin, M.; Dumitru, C. D.; Shimizu, M.; Zupo, S.; Dono, M.; Alder, H.; Bullrich, F.; Negrini, M.; Croce, C. M. *Proc. Natl. Acad. Sci. U. S. A.* **2004**, *101* (26), 9740.
- (57) Thomson, J. M.; Parker, J.; Perou, C. M.; Hammond, S. M. *Nat. Methods* **2004**, *1* (1), 47.
- (58) Várallyay, É.; Burgyán, J.; Havelda, Z. *Nat. Protoc.* **2008**, *3* (2), 190.
- (59) Valoczi, A.; Hornyik, C.; Varga, N.; Burgyan, J.; Kauppinen, S.; Havelda, Z. *Nucleic Acids Res.* **2004**, *32* (22), e175.
- (60) Calin, G. A.; Sevignani, C.; Dumitru, C. D.; Hyslop, T.; Noch, E.; Yendamuri, S.; Shimizu, M.; Rattan, S.; Bullrich, F.; Negrini, M.; Croce, C. M. *Proc. Natl. Acad. Sci. U. S. A.* **2004**, *101* (9), 2999.
- (61) Viereggs, J. R.; Nelson, H. M.; Stoltz, B. M.; Pierce, N. A. *J. Am. Chem. Soc.* **2013**, 130618134902008.
- (62) Schmittgen, T. D. *Nucleic Acids Res.* **2004**, *32* (4), 43e.
- (63) Eminaga, S.; Christodoulou, D. C.; Vigneault, F.; Church, G. M.; Seidman, J. G. *Curr. Protoc. Mol. Biol.* **2013**, *04*, Unit.
- (64) Chang, Y.-Y.; Kuo, W.-H.; Hung, J.-H.; Lee, C.-Y.; Lee, Y.-H.; Chang, Y.-C.; Lin, W.-C.; Shen, C.-Y.; Huang, C.-S.; Hsieh, F.-J.; Lai, L.-C.; Tsai, M.-H.; Chang, K.-J.; Chuang, E. Y. *Mol. Cancer* **2015**, *14*, 36.
- (65) Schee, K.; Lorenz, S.; Worren, M. M.; Günther, C.-C.; Holden, M.; Hovig, E.; Fodstad, Ø.; Meza-Zepeda, L. A.; Flatmark, K. *PLOS ONE* **2013**, *8* (6), e66165.
- (66) Szeto, C. Y.-Y.; Lin, C. H.; Choi, S. C.; Yip, T. T. C.; Ngan, R. K.-C.; Tsao, G. S.-W.; Li Lung, M. *FEBS Open Bio* **2014**, *4*, 128.
- (67) Li, W.; Ruan, K. *Anal. Bioanal. Chem.* **2009**, *394* (4), 1117.
- (68) Miller, M. B.; Tang, Y.-W. *Clin. Microbiol. Rev.* **2009**, *22* (4), 611.
- (69) Hanna, J.; Wimberly, H.; Kumar, S.; Slack, F.; Agarwal, S.; Rimm, D. *BioTechniques* **2012**, *52* (4).
- (70) Zhang, X.; Song, Y.; Shah, A. Y.; Lekova, V.; Raj, A.; Huang, L.; Behlke, M. A.; Tsourkas, A. *Nucleic Acids Res.* **2013**, *41* (15), e152.
- (71) Tyagi, S.; Kramer, F. R. *Nat. Biotechnol.* **1996**, *14* (3), 303.
- (72) Li, J. J.; Geyer, R.; Tan, W. *Nucleic Acids Res.* **2000**, *28* (11), e52.
- (73) Santangelo, P. J.; Nix, B.; Tsourkas, A.; Bao, G. *Nucleic Acids Res.* **2004**, *32* (6), e57.
- (74) Chen, A. K.; Davydenko, O.; Behlke, M. A.; Tsourkas, A. *Nucleic Acids Res.* **2010**, *38* (14), e148.
- (75) Baker, M. B.; Bao, G.; Searles, C. D. *Nucleic Acids Res.* **2012**, *40* (2), e13.
- (76) Ko, H. Y.; Lee, J.; Joo, J. Y.; Lee, Y. S.; Heo, H.; Ko, J. J.; Kim, S. *Sci. Rep.* **2014**, *4*.
- (77) Ko, H. Y.; Lee, J.; Moon, S. U.; Lee, Y. S.; Cho, S.; Kim, S. *Chem Commun* **2015**, *51* (93), 16679.
- (78) Ko, H. Y.; Lee, J.; Lee, Y. S.; Gu, H.-N.; Ali, B. A.; Al-Khedhairi, A. A.; Heo, H.; Cho, S.; Kim, S. *Chem Commun* **2015**, *51* (11), 2159.

- (79) Conlon, P.; Yang, C. J.; Wu, Y.; Chen, Y.; Martinez, K.; Kim, Y.; Stevens, N.; Marti, A. A.; Jockusch, S.; Turro, N. J.; Tan, W. *J. Am. Chem. Soc.* **2008**, *130* (1), 336.
- (80) Tan, X.; Chen, W.; Lu, S.; Zhu, Z.; Chen, T.; Zhu, G.; You, M.; Tan, W. *Anal. Chem.* **2012**, *84* (19), 8272.
- (81) Yao, Q.; Zhang, A.; Ma, H.; Lin, S.; Wang, X.; Sun, J.; Chen, Z. *Mol. Cell. Probes* **2012**, *26* (5), 182.
- (82) Tsourkas, A.; Behlke, M. A.; Xu, Y.; Bao, G. *Anal. Chem.* **2003**, *75* (15), 3697.
- (83) King, F. W.; Liszewski, W.; Ritner, C.; Bernstein, H. S. *Stem Cells Dev.* **2011**, *20* (3), 475.
- (84) Mergny, J. L.; Bourtoune, A. S.; Garestier, T.; Belloc, F.; Rougee, M.; Bulychev, N. V.; Koshkin, A. A.; Bourson, J.; Lebedev, A. V.; Valeur, B. *Nucleic Acids Res.* **1994**, *22* (6), 920.
- (85) Tsuji, A.; Koshimoto, H.; Sato, Y.; Hirano, M.; Sei-Iida, Y.; Kondo, S.; Ishibashi, K. *Biophys. J.* **2000**, *78* (6), 3260.
- (86) Tsuji, A.; Sato, Y.; Hirano, M.; Suga, T.; Koshimoto, H.; Taguchi, T.; Ohsuka, S. *Biophys. J.* **2001**, *81* (1), 501.
- (87) Sau, S. P.; Kumar, P.; Sharma, P. K.; Hrdlicka, P. J. *Nucleic Acids Res.* **2012**, *40* (21), e162.
- (88) Sau, S. P.; Hrdlicka, P. J. *J. Org. Chem.* **2012**, *77* (1), 5.
- (89) Bag, S. S.; Kundu, R.; Jana, S. *Tetrahedron Lett.* **2013**, *54* (21), 2627.
- (90) Baker, B. A.; Mahmoudabadi, G.; Milam, V. T. *Colloids Surf. B Biointerfaces* **2013**, *102*, 884.
- (91) Hemphill, J.; Deiters, A. *J. Am. Chem. Soc.* **2013**, 130624125941004.
- (92) Prigodich, A. E.; Randeria, P. S.; Briley, W. E.; Kim, N. J.; Daniel, W. L.; Giljohann, D. A.; Mirkin, C. A. *Anal. Chem.* **2012**, *84* (4), 2062.
- (93) Yang, Y.; Huang, J.; Yang, X.; Quan, K.; Wang, H.; Ying, L.; Xie, N.; Ou, M.; Wang, K. *J. Am. Chem. Soc.* **2015**, *137* (26), 8340.
- (94) Wabuyele, M. B.; Vo-Dinh, T. *Anal. Chem.* **2005**, *77* (23), 7810.
- (95) Cao, Y. C.; Jin, R.; Mirkin, C. A. *Science* **2002**, *297* (5586), 1536.
- (96) Santangelo, P.; Nitin, N.; Bao, G. *Ann. Biomed. Eng.* **2006**, *34* (1), 39.
- (97) de Planell-Saguer, M.; Rodicio, M. C. *Clin. Biochem.* **2013**, *46* (10–11), 869.
- (98) Chen, K. H.; Boettiger, A. N.; Moffitt, J. R.; Wang, S.; Zhuang, X. *Science* **2015**, *348* (6233), aaa6090.
- (99) Moffitt, J. R.; Hao, J.; Bambah-Mukku, D.; Lu, T.; Dulac, C.; Zhuang, X. *Proc. Natl. Acad. Sci.* **2016**, *113* (50), 14456.
- (100) Stellaris RNA FISH | LGC Biosearch Technologies
<https://www.biosearchtech.com/support/education/stellaris-rna-fish> (accessed Jun 7, 2017).
- (101) Almlie, C. K.; Larkey, N. E.; Burrows, S. M. *Anal. Methods* **2015**, *7* (17), 7296.
- (102) Thaxton, C. S.; Georganopoulou, D. G.; Mirkin, C. A. *Clin. Chim. Acta* **2006**, *363* (1–2), 120.
- (103) Yeh, H.-C.; Sharma, J.; Han, J. J.; Martinez, J. S.; Werner, J. H. *Nano Lett.* **2010**, *10* (8), 3106.
- (104) Yeh, H.-C.; Sharma, J.; Han, J.; Martinez, J.; Werner, J. *IEEE Nanotechnol. Mag.* **2011**, *5* (2), 28.
- (105) Yeh, H.-C.; Sharma, J.; Shih, I.-M.; Vu, D. M.; Martinez, J. S.; Werner, J. H. *J. Am. Chem. Soc.* **2012**, *134* (28), 11550.

- (106) Obliosca, J. M.; Liu, C.; Yeh, H.-C. *Nanoscale* **2013**, 5 (18), 8443.
- (107) Obliosca, J. M.; Babin, M. C.; Liu, C.; Liu, Y.-L.; Chen, Y.-A.; Batson, R. A.; Ganguly, M.; Petty, J. T.; Yeh, H.-C. *ACS Nano* **2014**, 8 (10), 10150.
- (108) Shah, P.; Rørvig-Lund, A.; Chaabane, S. B.; Thulstrup, P. W.; Kjaergaard, H. G.; Fron, E.; Hofkens, J.; Yang, S. W.; Vosch, T. *ACS Nano* **2012**, 6 (10), 8803.
- (109) Shah, P.; Thulstrup, P. W.; Cho, S. K.; Bhang, Y.-J.; Ahn, J. C.; Choi, S. W.; Bjerrum, M. J.; Yang, S. W. *The Analyst* **2014**, 139 (9), 2158.
- (110) Shah, P.; Choi, S. W.; Kim, H.; Cho, S. K.; Bhang, Y.-J.; Ryu, M. Y.; Thulstrup, P. W.; Bjerrum, M. J.; Yang, S. W. *Nucleic Acids Res.* **2016**, 44 (6), e57.
- (111) Hu, Y.; Zhang, L.; Zhang, Y.; Wang, B.; Wang, Y.; Fan, Q.; Huang, W.; Wang, L. *ACS Appl. Mater. Interfaces* **2015**, 7 (4), 2459.
- (112) Qiu, X.; Hildebrandt, N. *ACS Nano* **2015**, 9 (8), 8449.
- (113) Noh, E.-H.; Ko, H. Y.; Lee, C. H.; Jeong, M.-S.; Chang, Y. W.; Kim, S. *J. Mater. Chem. B* **2013**, 1 (35), 4438.
- (114) Wu, C.; Chiu, D. T. *Angew. Chem. Int. Ed.* **2013**, 52 (11), 3086.
- (115) Lesnik, E. A.; Freier, S. M. *Biochemistry (Mosc.)* **1995**, 34 (34), 10807.
- (116) Sugimoto, N.; Nakano, S.; Yoneyama, M.; Honda, K. *Nucleic Acids Res.* **1996**, 24 (22), 4501.
- (117) Dimitrov, R. A.; Zuker, M. *Biophys. J.* **2004**, 87 (1), 215.
- (118) Markham, N. R.; Zuker, M. *Nucleic Acids Res.* **2005**, 33 (suppl 2), W577.
- (119) Markham, N. R.; Zuker, M. In *Bioinformatics*; Keith, J. M., Ed.; Walker, J. M., Series Ed.; Humana Press: Totowa, NJ, 2008; Vol. 453, pp 3–31.
- (120) DINAMelt | mfold.rit.albany.edu <http://mfold.rna.albany.edu/?q=DINAMelt> (accessed Jul 22, 2015).
- (121) Reuter, J. S.; Mathews, D. H. *BMC Bioinformatics* **2010**, 11 (1), 129.
- (122) RNAstructure | rna.urmc.rochester.edu <http://rna.urmc.rochester.edu/RNAstructureWeb/> (accessed Jul 22, 2015).
- (123) Hofacker, I. L. *Nucleic Acids Res.* **2003**, 31 (13), 3429.
- (124) ViennaRNA Web Services | rna.tbi.univie.ac.at <http://rna.tbi.univie.ac.at/> (accessed Jul 22, 2015).
- (125) Oheim, M.; Michael, D. J.; Geisbauer, M.; Madsen, D.; Chow, R. H. *Adv. Drug Deliv. Rev.* **2006**, 58 (7), 788.
- (126) Denk, W.; Strickler, J. H.; Webb, W. W. *Science* **1990**, 248 (4951), 73.
- (127) Ingle, J. D.; Crouch, S. R. *Spectrochemical Analysis*; Prentice Hall: New Jersey, 1988.
- (128) Lennox, K. A.; Owczarzy, R.; Thomas, D. M.; Walder, J. A.; Behlke, M. A. *Mol. Ther. - Nucleic Acids* **2013**, 2, e117.
- (129) Peng, Z.; Soper, S. A.; Pingle, M. R.; Barany, F.; Davis, L. M. *Anal. Chem.* **2010**, 82 (23), 9727.
- (130) Wabuyele, M. B.; Farquar, H.; Stryjewski, W.; Hammer, R. P.; Soper, S. A.; Cheng, Y.-W.; Barany, F. *J. Am. Chem. Soc.* **2003**, 125 (23), 6937.
- (131) Larkey, N. E.; Almlie, C. K.; Tran, V.; Egan, M.; Burrows, S. M. *Anal. Chem.* **2014**, 86 (3), 1853.
- (132) Srinivas, N.; Ouldrige, T. E.; Sulc, P.; Schaeffer, J. M.; Yurke, B.; Louis, A. A.; Doye, J. P. K.; Winfree, E. *Nucleic Acids Res.* **2013**, 41 (22), 10641.
- (133) Chen, C.; Wang, W.; Wang, Z.; Wei, F.; Zhao, X. S. *Nucleic Acids Res.* **2007**, 35 (9), 2875.
- (134) Bonnet, G.; Krichevsky, O.; Libchaber, A. *Proc. Natl. Acad. Sci.* **1998**, 95 (15), 8602.

- (135) Wahlroos, R.; Toivonen, J.; Tirri, M.; Hänninen, P. *J. Fluoresc.* **2006**, *16* (3), 379.
- (136) Massey, M.; Algar, W. R.; Krull, U. J. *Anal. Chim. Acta* **2006**, *568* (1–2), 181.
- (137) Wang, H.-N.; Fales, A. M.; Vo-Dinh, T. *Nanomedicine Nanotechnol. Biol. Med.* **2015**, *11* (4), 811.
- (138) Wang, L.; Yang, C. J.; Medley, C. D.; Benner, S. A.; Tan, W. *J. Am. Chem. Soc.* **2005**, *127* (45), 15664.
- (139) Martinez, K.; Estevez, M.-C.; Wu, Y.; Phillips, J. A.; Medley, C. D.; Tan, W. *Anal. Chem.* **2009**, *81* (9), 3448.
- (140) Fegan, A.; Shirude, P. S.; Balasubramanian, S. *Chem. Commun.* **2008**, No. 17, 2004.
- (141) Zhang, P.; Beck, T.; Tan, W. *Angew. Chem. Int. Ed.* **2001**, *40* (2), 402.
- (142) Lee, J.; Moon, S.; Lee, Y.; Ali, B.; Al-Khedhairy, A.; Ali, D.; Ahmed, J.; Al Salem, A.; Kim, S. *Sensors* **2015**, *15* (6), 12872.
- (143) Yang, S. W.; Vosch, T. *Anal. Chem.* **2011**, *83* (18), 6935.
- (144) Xia, X.; Hao, Y.; Hu, S.; Wang, J. *Biosens. Bioelectron.* **2014**, *51*, 36.
- (145) Larkey, N. E.; Brucks, C. N.; Lansing, S. S.; Le, S. D.; Smith, N. M.; Tran, V.; Zhang, L.; Burrows, S. M. *Anal. Chim. Acta* **2016**, *909*, 109.
- (146) Behlke, M. A.; Huang, L.; Bogh, L.; Rose, S.; Devor, E. J. *Integr. DNA Technol.* **2005**.
- (147) Ranjit, S.; Levitus, M. *Photochem. Photobiol.* **2012**, *88* (4), 782.
- (148) He, Y.; Liu, D. R. *J. Am. Chem. Soc.* **2011**, *133* (26), 9972.
- (149) Subramanian, H. K. K.; Chakraborty, B.; Sha, R.; Seeman, N. C. *Nano Lett.* **2011**, *11* (2), 910.
- (150) Zhang, D. Y.; Seelig, G. *Nat. Chem.* **2011**, *3* (2), 103.
- (151) Wu, Y.; Zhang, D. Y.; Yin, P.; Vollmer, F. *Small* **2014**, *10* (10), 2067.
- (152) Moser, M. J. *Nucleic Acids Res.* **2003**, *31* (17), 5048.
- (153) Sherrill, C. B.; Marshall, D. J.; Moser, M. J.; Larsen, C. A.; Daudé-Snow, L.; Prudent, J. R. *J. Am. Chem. Soc.* **2004**, *126* (14), 4550.
- (154) Zhang, D. Y.; Chen, S. X.; Yin, P. *Nat. Chem.* **2012**, *4* (3), 208.
- (155) Larkey, N. E.; Zhang, L.; Lansing, S. S.; Tran, V.; Seewaldt, V. L.; Burrows, S. M. *The Analyst* **2016**, *141* (22), 6239.
- (156) Yeh, H.-C.; Puleo, C. M.; Ho, Y.-P.; Bailey, V. J.; Lim, T. C.; Liu, K.; Wang, T.-H. *Biophys. J.* **2008**, *95* (2), 729.
- (157) Yeh, H.-C.; Ho, Y.-P.; Wang, T.-H. *Nanomedicine Nanotechnol. Biol. Med.* **2005**, *1* (2), 115.
- (158) Griffiths-Jones, S. *Nucleic Acids Res.* **2006**, *34* (90001), D140.
- (159) Griffiths-Jones, S.; Saini, H. K.; van Dongen, S.; Enright, A. J. *Nucleic Acids Res.* **2007**, *36* (Database), D154.
- (160) Kozomara, A.; Griffiths-Jones, S. *Nucleic Acids Res.* **2011**, *39* (Database), D152.
- (161) Zhang, Z.; Fan, T. W.; Hsing, I.-M. *Nanoscale* **2017**, *9* (8), 2748.
- (162) Chen, A. K.; Behlke, M. A.; Tsourkas, A. *Nucleic Acids Res.* **2008**, *36* (12), e69.
- (163) Hudziak, R. M.; Barofsky, E.; Barofsky, D. F.; Weller, D. L.; Huang, S. B.; Weller, D. D. *Antisense Nucleic Acid Drug Dev.* **1996**, *6* (4), 267.
- (164) Borgatti, M.; Romanelli, A.; Saviano, M.; Pedone, C.; Lampronti, I.; Breda, L.; Nastruzzi, C.; Bianchi, N.; Mischiati, C.; Gambari, R. *Oncol. Res.* **2003**, *13* (5), 279.
- (165) Buckhout-White, S.; Spillmann, C. M.; Algar, W. R.; Khachatryan, A.; Melinger, J. S.; Goldman, E. R.; Ancona, M. G.; Medintz, I. L. *Nat. Commun.* **2014**, *5*.

- (166) Gliddon, H. D.; Howes, P. D.; Kaforou, M.; Levin, M.; Stevens, M. M. *Nanoscale* **2016**, *8* (19), 10087.
- (167) Johnson, S. C.; Sherrill, C. B.; Marshall, D. J.; Moser, M. J.; Prudent, J. R. *Nucleic Acids Res.* **2004**, *32* (6), 1937.
- (168) Rügger, S.; Großhans, H. *Trends Biochem. Sci.* **2012**, *37* (10), 436.
- (169) Zhang, L.; Bluhm, A. M.; Chen, K.-J.; Larkey, N. E.; Burrows, S. M. *Nanoscale* **2017**.
- (170) Almlie, C. K.; Hsiao, A.; Burrows, S. M. *Anal. Chem.* **2016**, *88* (2), 1462.
- (171) Gan, W.; Xiaoxin, S. X. *Cell Res.* **2004**, *14* (2), 111.
- (172) Fujioka, A.; Terai, K.; Itoh, R. E.; Aoki, K.; Nakamura, T.; Kuroda, S.; Nishida, E.; Matsuda, M. *J. Biol. Chem.* **2006**, *281* (13), 8917.
- (173) Gantier, M. P.; McCoy, C. E.; Rusinova, I.; Saulep, D.; Wang, D.; Xu, D.; Irving, A. T.; Behlke, M. A.; Hertzog, P. J.; Mackay, F.; Williams, B. R. G. *Nucleic Acids Res.* **2011**, *39* (13), 5692.
- (174) Rooij, E. van; Sutherland, L. B.; Qi, X.; Richardson, J. A.; Hill, J.; Olson, E. N. *Science* **2007**, *316* (5824), 575.

APPENDICES

Appendix I.

Supplemental Information for Chapter 2

A1.1 Single-photon Studies of Reporter-Probe Biosensor

Cy3 and Cy5 were used because of their potential to resonantly couple in such a way that Cy3 can be selectively excited, transfer its energy via Förster Resonance Energy Transfer (FRET) to Cy5, and enhance the Cy5 emission. However, single-photon studies confirmed Cy5 fluorescence is in fact quenched (see Figure A1.1 and A1.2). We have established that nucleic acids contribute to ~ 30 % of the observed quenching (Figure 2.4 and A1.3). The native confirmation of the reporter in the absence of probe1 must be such that the Cy3 and nucleic acids interact with the Cy5 to quench the fluorescence.

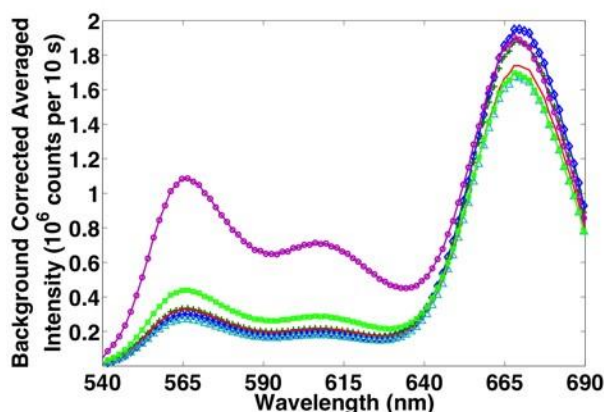


Figure A1.1 The emission spectrum of the reporter confirms the Cy5 fluorescence is quenched when not bound to probe1. Green solid line with plus sign markers = reporter (1 μ M); red solid line with 'x' markers = reporter (833 nM, dilution control 1); teal dashed line with triangle markers = reporter (750 nM, dilution control 2); Blue solid line with diamond markers = reporter (1 μ M); purple solid line with circle markers = reporter plus probe1 (both at 833 nM); lime green solid line with square markers = reporter plus probe1 plus target (all three at 750 nM). Excitation at 532 nm with approximately 3.4 mW of power.

Figure A1.2 plots the summed intensity as a function of probe1 and Let-7a addition. This figure helps demonstrate the Cy5 emission is quenched and returns to the expected value after addition of Let-7a. However, the Cy3 emission does not return all the to the expected value. This could be due to the reporter folding into a slightly different configuration resulting in a different extent of Cy3 quenching. This effect was not observed with two-photon excitation. The Cy5 emission is not as great on the single-photon level because Cy5 is not efficiently excited at 532 nm. Thus for this sensor two-photon excitation yields more reproducible analytical signal and better dynamic range. Notice the first three data points for the Cy3 emission increase as the first three data points of Cy5 emission decrease. This observation suggests there must be some coupling between Cy3 and Cy5. Current studies involve optimizing the reporter to reduce or eliminate these anomalous observations and attempt to produce a FRET Cy5 enhancement.

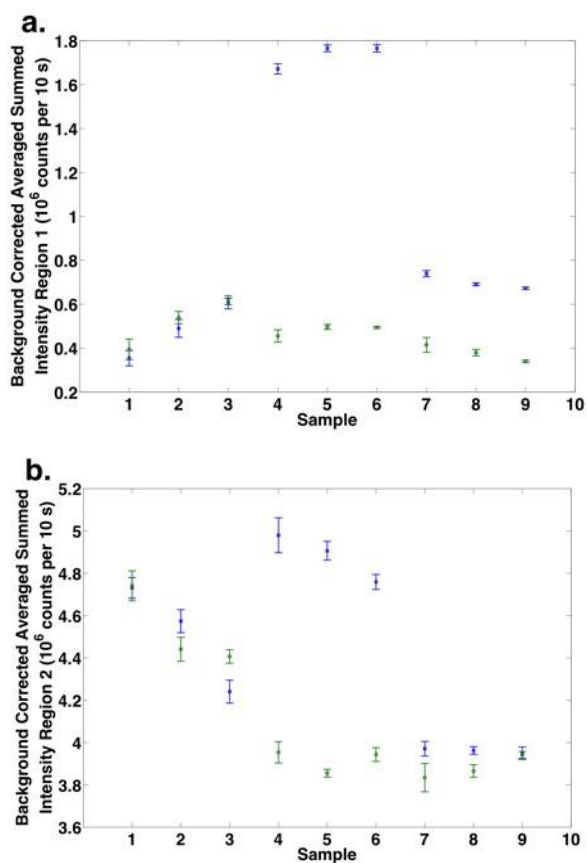


Figure A1.2. Response of reporter as probe1 and Let-7a are added. (a) Summed intensity of the Cy3 emission region (region 1) and (b) summed intensity of the Cy5 emission region (region 2). Replicate samples: 1-3 contained just reporter at 1 μ M; 4-6 contained reporter-probe1 at 833 nM; and 7-9 contained probe1-Let7a and reporter all at 750 nM.

A1.2 Impact of Nucleic acids and Cy3 on Quenching of Cy5

A non-complementary oligonucleotide, complementary oligonucleotide without Cy3, and a complementary oligonucleotide with Cy3 were presented to the 5-prime Cy5 to evaluate and confirm quenching of Cy5 fluorescence. The sequences of the oligonucleotides used in this study are presented in Table A1.1.

Table A1.1 Sequence and predicted thermodynamic values of oligonucleotides used to study impact of nucleic acids and Cy3 on the quenching of Cy5.

Name	Sequence (5'-3')	Gibbs Energy (kcal/mole)†
Complementary Linear Strand	AACTATAACAACCTACTACCTCA	-24.9
Non-complementary linear strand	TGAGGTAGTAGGTTGTATAGTT	-0.9
Cy3-linear Reporter	AACTATAACAACCTACTACCTCA /Cy3Sp	-24.9
Cy5-linear Reporter	Cy5/ TGAGGTAGTAGGTTGTATAGTT	---

† Gibbs energy values for binding to 5-prime Cy5 linear reporter. All thermodynamic values were obtained using software available from The DINAMelt Web Server⁷⁻⁹ managed by The RNA Institute at SUNY-Albany. The 'Two State melting (hybridization)' function was used for double-strand binding calculations. Experimental parameters used for thermodynamic calculations were: 25 °C, 10 mM Na⁺, 2.5 mM Mg²⁺, and 1 μM oligonucleotide. Bold sections of the sequences refer to complementary binding sites.

Figure A1.3 shows that addition of buffer and non-complementary DNA does not change the Cy5 signal by a considerable amount. The non-complementary DNA decreased the Cy5 signal by 2.6 ± 1.9 % (N=4). However, the decrease observed from the non-complementary DNA is not statistically different from the buffer addition. Thus we conclude the non-complementary DNA had no effect on the quenching of Cy5. Complementary DNA did show a significant 44.8 ± 2.0 % decrease in the Cy5. When a 3-prime Cy3 linear strand was added to the 5-prime Cy5 reporter the Cy5 signal decreased by 74.0 ± 1.4 %. This study helps confirm the Cy5 fluorescence is quenched in the presence of nucleic acids and Cy3. Another conclusion drawn from this study is that Cy3 makes a significant contribution to the overall signal change and will enhance the signal to background ratio.

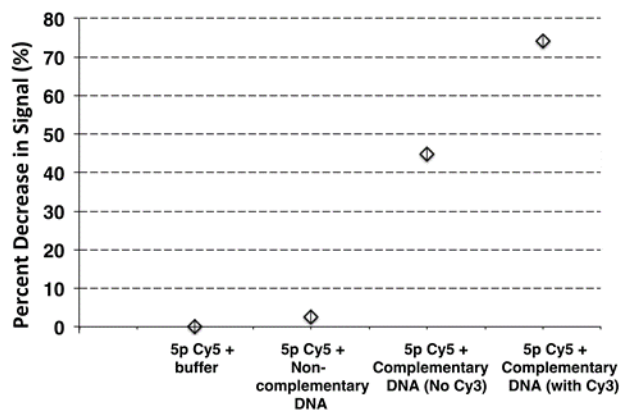


Figure A1.3 Quenching of Cy5 by nucleic acids and Cy3. Buffer and non-complementary DNA does not make a significant contribution to the quenching of Cy5. Use of Cy3 adds an additional 30 % to the decrease in signal.

Appendix II.

Supplemental Information for Chapter 3

Table A2.1 Nucleic Acid Sequences of reporters, probes, and miRNA as DNA. Bold regions indicate complementary binding. ‘R’ stands for reporter. The + symbol indicates the location of a locked nucleic acid. Bold and underlined regions of reporters indicate the location of the self-complementary stem sequence. Bold and lowercase regions designate complementarity between reporter and respective probe sequences. Non-bold and uppercase regions indicate non-complementary regions of the reporters. 5Cy5 indicates a 5’ Cy5 dye; 3Cy3Sp indicates a 3’ Cy3 dye. miR-29b-1-5p DNA was included as another potential off-analyte [30].

Strand Name	Sequence 5'-3'
miR-26a-2-R1	/5Cy5/ <u>CGATG</u> cctgttct+ tgattact +tTCGGA <u>CATC+G</u> /3Cy3Sp/
miR-26a-2-R2	/5Cy5/ <u>CGATG</u> cctgttct+ tgatt GTG+GTCCGT <u>CATC+G</u> /3Cy3Sp/
miR-27a-R1	/5Cy5/ <u>CGATG</u> agggctta+ gctg GGAC+GTTCGG <u>CATC+G</u> /3Cy3Sp/
miR-27a-R2	/5Cy5/ <u>CGATG</u> Tgggctta+ gc GTTTCGT+CCGATT <u>CATC+G</u> /3Cy3Sp/
Probe-miR-26a	GAAACAAGTAATCAAGAACAGG
Probe-miR-27a	TGCTCACAAGCAGCTAAGCCCT
miR-26a-2-3p DNA	CCTGTTCTTGATTACTTGTTTC
miR-27a-5p DNA	AGGGCTTAGCTGCTTGTGAGCA
miR-29b-1-5p DNA	GCTGGTTTCATATGGTGGTTTA

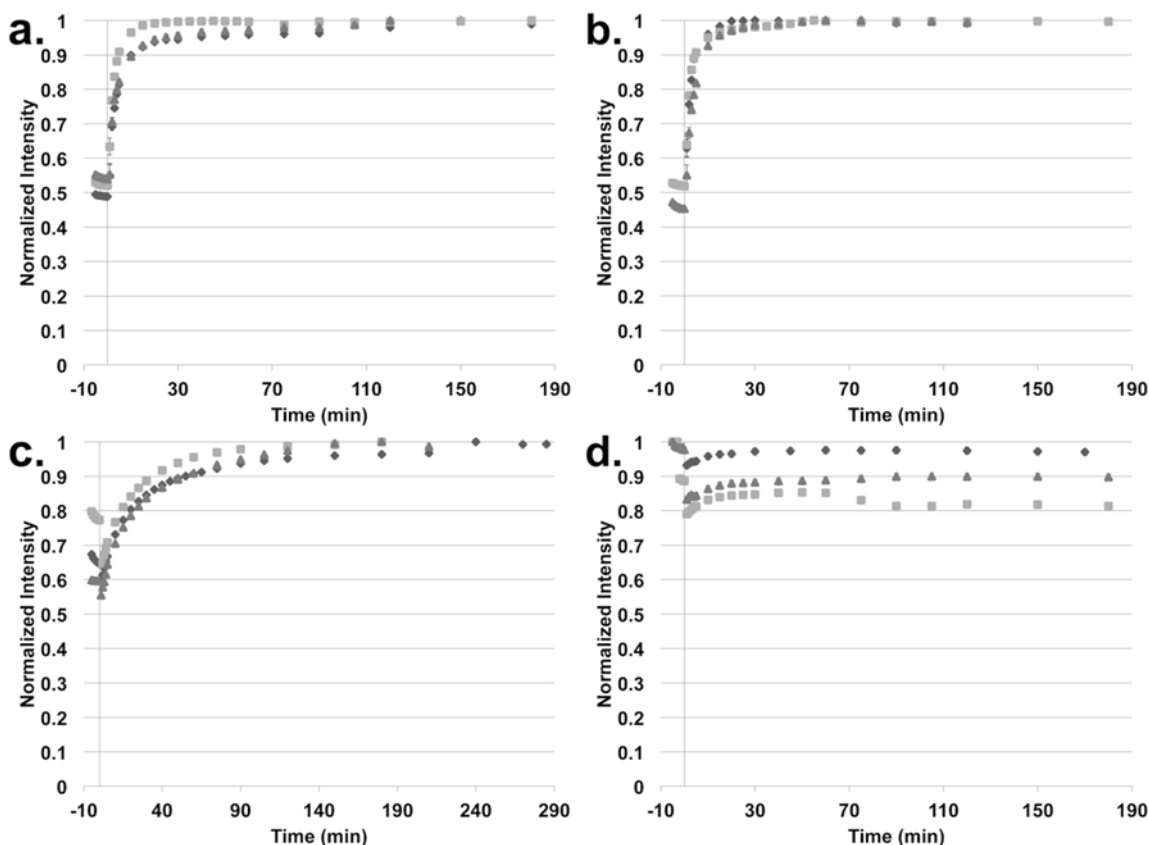


Figure A2.1 Kinetic experiments of probe binding to reporters: (a) miR-26a-R1, (b) miR-26a-R2, (c) miR-27a-R1, and (d) miR-27a-R2. Both miR-26a reporters reached maximum signal within 30 minutes. MiR-27a-R1 reached maximum signal after approximately 2 hours. MiR-27a-R2 did not appear to increase in signal upon probe binding. The variability between replicates comes from the cuvette being placed differently in the holder but no cuvette placement averages being taken to account for this error. All experiments were run in triplicate as indicated by the squares, triangles, and diamonds.

Kinetic studies were performed to determine the optimal hybridization time between the reporter and equimolar probe. For each experiment, the evolution of fluorescence over time was observed. When the reporter was in the hairpin structure, the signal was very low or in an ‘off’ state. Upon addition of an equivalent number of probe to reporter molecules, the signal increased from the off state as the hairpins opened, moving the dyes away from each other. Completion of hybridization was determined as the time for the signal to reach a maximum and steady state.

Fluorescence signal from the reporter was monitored for 30-second intervals before and after probe addition. In between the sampling intervals, the laser beam was blocked to avoid photobleaching and no data was collected. We will refer to these studies as ‘discontinuous kinetic studies’ as the laser light was blocked in between collection time points. Intensity values for each time point were obtained by summing averaged emission spectra of the Cy5 region from 620.07 nm to 690.86 nm. No replicate cuvette placements were taken because the cuvette stayed in the

same place for the duration of the experiment. This was to ensure differences in cuvette placement did not influence the signal changes associated with the reporter+probe binding event.

Baseline fluorescence intensity from 150 μL of 100 nM reporter solution was established by discontinuously sampling the fluorescence over the course of approximately 6 minutes. Time zero was taken as the last time point prior to addition of probe. Immediately after time zero, 30 μL of 500 nM probe solution was added to bring the total volume to 180 μL and the concentration to \sim 83.3 nM reporter and probe. After probe was added, the intensity was measured discontinuously over 2 - 5 hours.

Figure A2.1 shows how long it took the signal to reach maximum intensity after adding equimolar probe to each reporter. Both miR-26a reporters reached 90 % maximum intensity after 5 to 10 minutes (Figures A2.1a and A2.1b). Maximum intensity of the signal was reached after \sim 30 minutes. The reaction was considered complete after the signal reached a maximum steady state. The sequence similarity of the first 13 nucleotides of the complementary loop region for both reporters likely contributed to the similarity in kinetics.

As seen in Figure A2.1c, miR-27a-R1 took about 40 minutes to reach 90 % maximum intensity, and about two hours to reach maximum signal intensity upon equimolar probe addition (\sim 83.3 nM). The kinetics for miR-27a-R2 (Figure A2.1d) showed the reporter+probe signal does not bring the overall signal higher than the reporter signal prior to probe addition. This was expected considering only a 14 % increase in signal from Figure 3, and the fact the reporter was diluted by 16.7 % upon addition of probe. Dilution control experiments for all reporters investigated showed no additional change in signal (apart from dilution) over two hours (Figure A2.2).

Examination of the kinetic data for each reporter+probe formation revealed some differences that were not seen in the thermodynamic analysis. The reporter+probe $\Delta G_{\text{hybridization}}$ values of miR-26a-R2 and miR-27a-R1 were both around $-16 \text{ kcal mol}^{-1}$, yet the hybridization of miR-27a-R1 to its probe was slower than that of both the miR-26a reporters to their respective probes. The reason reporter+probe formation for miR-27a-R1 was slower may be due to dimerization of two miR-27a-R1 reporters.

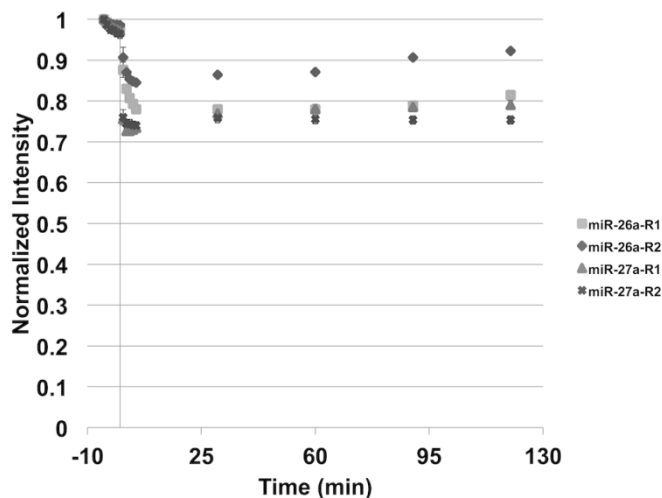


Figure A2.2 Dilution control for reporter+probe discontinuous hybridization studies. 150 μL reporters ran for 6 minutes before dilution with 30 μL buffer. After dilution fluorescence was monitored for at least two hours. Data was normalized to highest value of experiment (set to 1), which all occurred before dilution. Slight increase in normalized intensity likely due to reporter establishing a new equilibrium of conformational states.

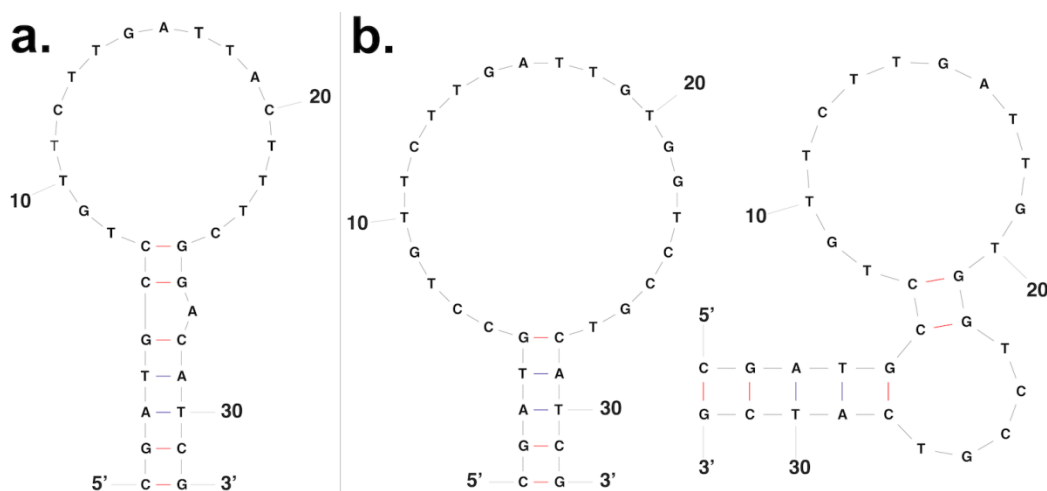


Figure A2.3 Predicted miR-26a-reporter hairpin conformations in order from left to right according to decreasing stability: (a) corresponds to miR-26a-R1 with one ideal hairpin conformation. (b) Corresponds to miR-26a-R2 with two ideal hairpin conformations. Structures were obtained from Quikfold using parameters described in experimental section 2.2. Figure does not indicate 3-dimensional structure.

Table A2.2 Ideal and non-ideal hairpin thermodynamic values, number of base pair interactions, and GC content. Values were obtained from Quikfold using parameters described in experimental section 2.2.

	Hairpin	ΔG (kcal mol ⁻¹)	ΔH (kcal mol ⁻¹)	ΔS (cal mol ⁻¹ K ⁻¹)	T _m (°C)	Base Pairs	GC
miR-26a-R1	H	-2.33	-55.4	-178.00	38.1	7	5
miR-26a-R2	H	-1.85	-37.8	-120.58	40.3	5	3
	H	-0.94	-47.8	-157.17	31.0	7	5
miR-27a-R1	H	-1.95	-37.9	-120.58	41.2	5	3

	NH	-1.50	-25.0	-78.82	44.0	5	3
	H	-1.03	-46.2	-151.50	31.8	6	3
miR-27a-R2	H	-2.15	-40.6	-128.96	41.7	5	3
	NH	-1.98	-53.8	-173.81	36.4	6	4
	H	-1.67	-48.6	-157.40	35.6	10	6
	NH	-1.44	-45.1	-146.44	34.8	5	4

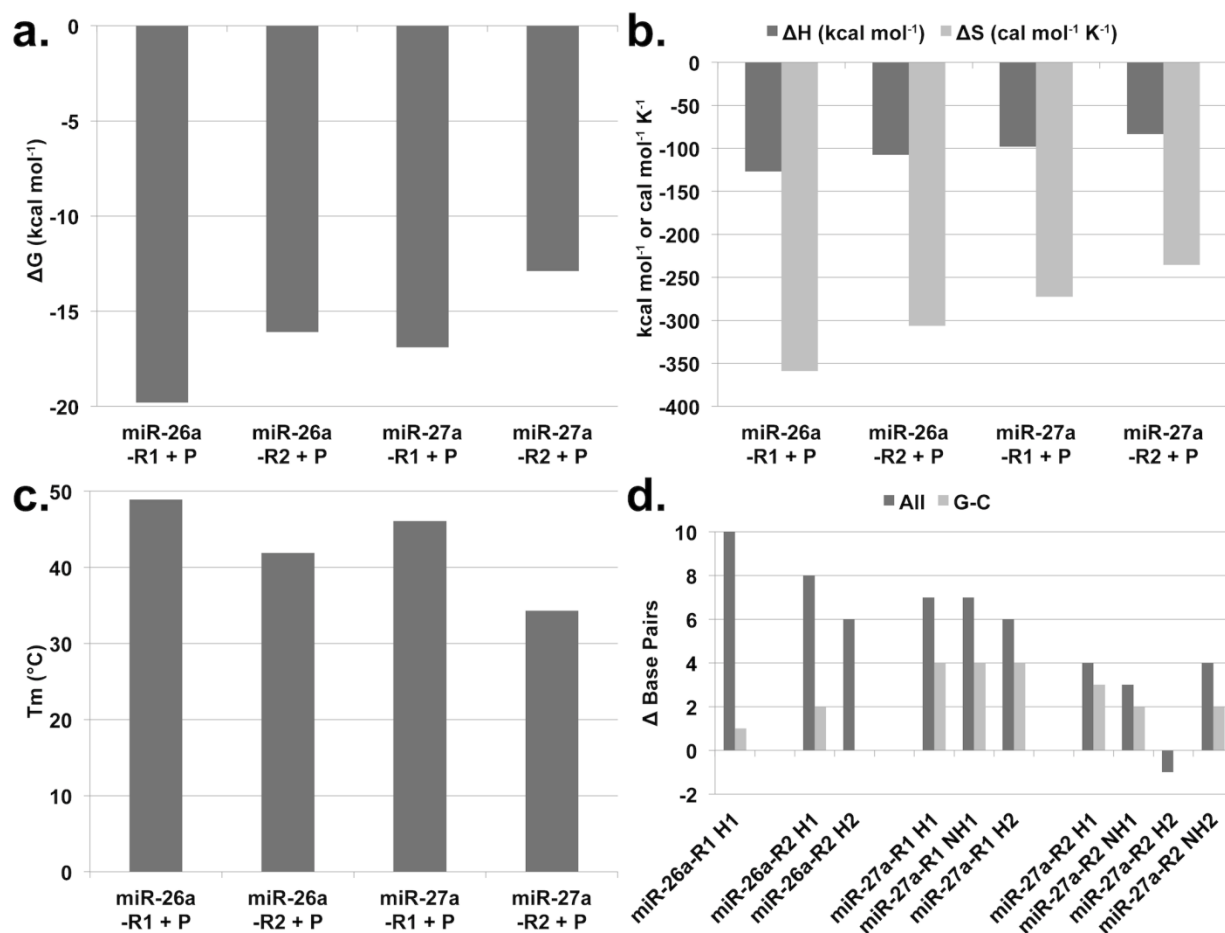


Figure A2.4 Reporter hairpin to reporter+probe complex changes in thermodynamic values, number of base-pairs, and GC content. H refers to hairpin and NH refers to non-ideal hairpin. For each reporter the hairpin conformations are ordered from most to least stable in terms of ΔG . Values that cannot be seen are equal to zero. (a) The difference in Gibb's energy between the reporter hairpins and reporter+probe complex. (b) The difference in enthalpy or entropy. (c) The difference in melting temperature. (d) The change in number of total base-pair interactions or just G-C base pairs.

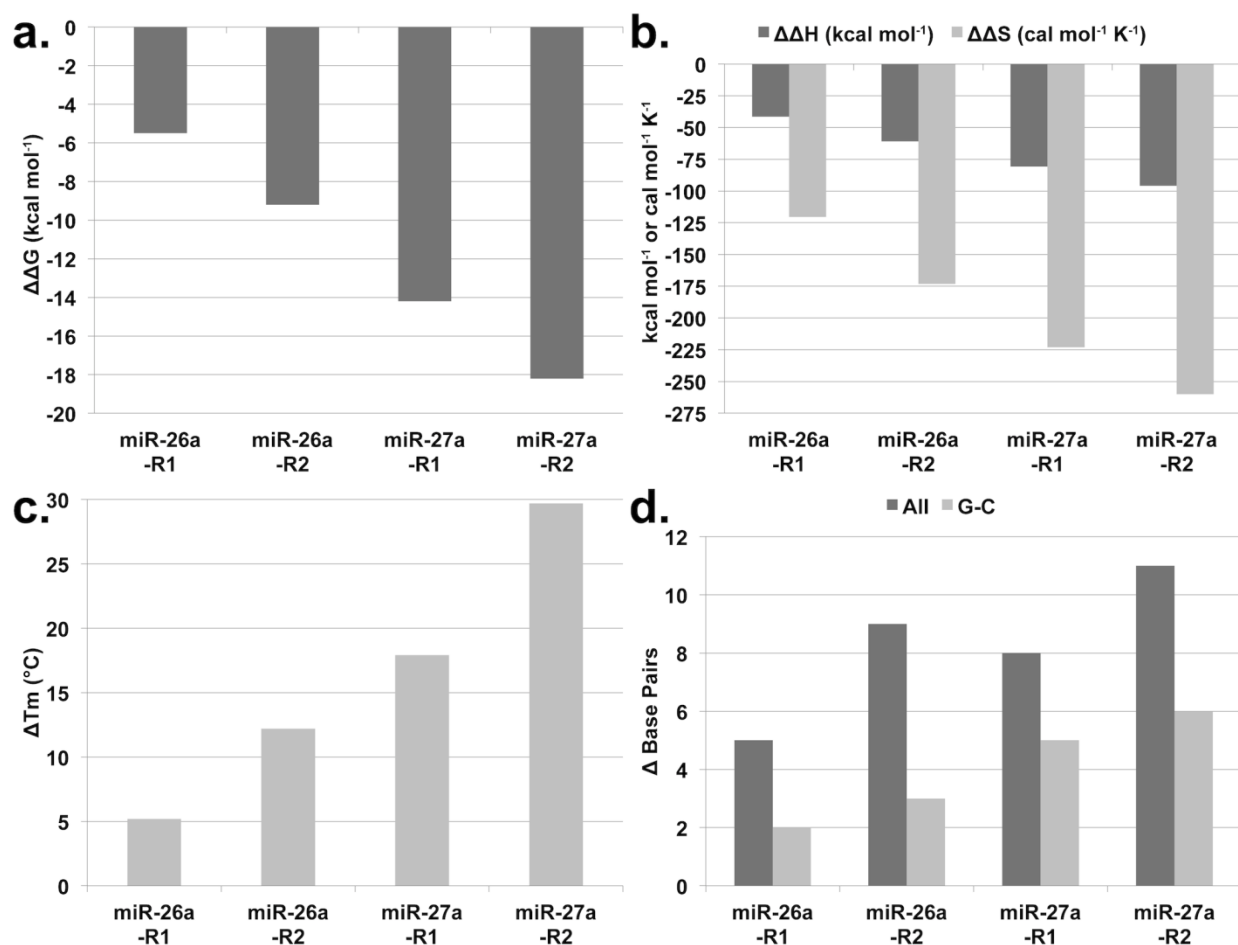


Figure A2.5 Reporter+probe complex to probe+analyte complex changes in thermodynamic values, number of base pairs, and GC content. These values drive the recognition mechanism of the reporter+probe biosensor. (a) The difference in Gibb's energy between the reporter+probe complex and probe+analyte complex. (b) The difference in enthalpy or entropy. (c) The difference in melting temperature at 100 nM concentration. (d) The change in number of total base-pair interactions or just G-C base pairs.

Table A2.3 Potential off-analyte interaction thermodynamic values, number of base pair interactions, and GC content. The number of GC base pairs was included as a separate value due to their greater stability than AT pairs.

	ΔG (kcal mol ⁻¹)	ΔH (kcal mol ⁻¹)	ΔS (cal mol ⁻¹ K ⁻¹)	T_m (°C) at 100 nM	Base Pairs	GC
miR-26a-R1 and miR-26a	-1.9	-19.1	-57.8	-66.9	2	2
miR-26a-R1 and miR-27a	-4.8	-36.8	-107.3	-14.1	3	3
miR-26a-R1 and miR-29b	-2.8	-30.4	-92.4	-34.2	3	1
miR-26a-R2 and miR-26a	-2.1	-24.6	-75.5	-50.2	2	1
miR-26a-R2 and miR-27a	-4.8	-36.8	-107.3	-14.1	3	3
miR-26a-R2 and miR-29b	-2.8	-33.3	-102.4	-30.4	7	3
miR-27a-R1 and miR-26a	-2.7	-20.0	-58.1	-57.9	3	2
miR-27a-R1 and miR-27a	-6.2	-52.8	-156.4	3.0	6	4
miR-27a-R1 and miR-29b	-3.6	-32.2	-95.9	-26.8	5	2
miR-27a-R2 and miR-26a	-2.1	-24.6	-75.5	-50.2	2	1
miR-27a-R2 and miR-27a	-5.6	-50.8	-151.6	-0.6	6	4

miR-27a-R2 and miR-29b	-3.0	-26.9	-80.2	-39.2	3	2
Probe-miR-26a and miR-27a	-5.5	-41.1	-119.5	-6.7	5	2
Probe-miR-26a and miR-29b	-5.6	-47.9	-141.9	-2.1	5	2
Probe-miR-27a and miR-26a	-5.0	-33.2	-94.6	-16.5	5	2
Probe-miR-27a and miR-29b	-6.4	-43.0	-122.7	-0.1	6	3

Table A2.4 Probe+analyte complex thermodynamic values, number of base pair interactions, and GC content. Values were obtained from Two State melting (hybridization) using parameters described in experimental section 2.2. *Two distal A•T pair are not predicted to bind.

	ΔG (kcal mol ⁻¹)	ΔH (kcal mol ⁻¹)	ΔS (cal mol ⁻¹ K ⁻¹)	T _m (°C) at 100 nM	Base Pairs	GC
Probe-miR-26a + miR-26a	-25.3	-168.3	-479.5	54.1	22	8
Probe-miR-27a + miR-27a	-31.1	-178.8	-495.6	64.0	20*	12

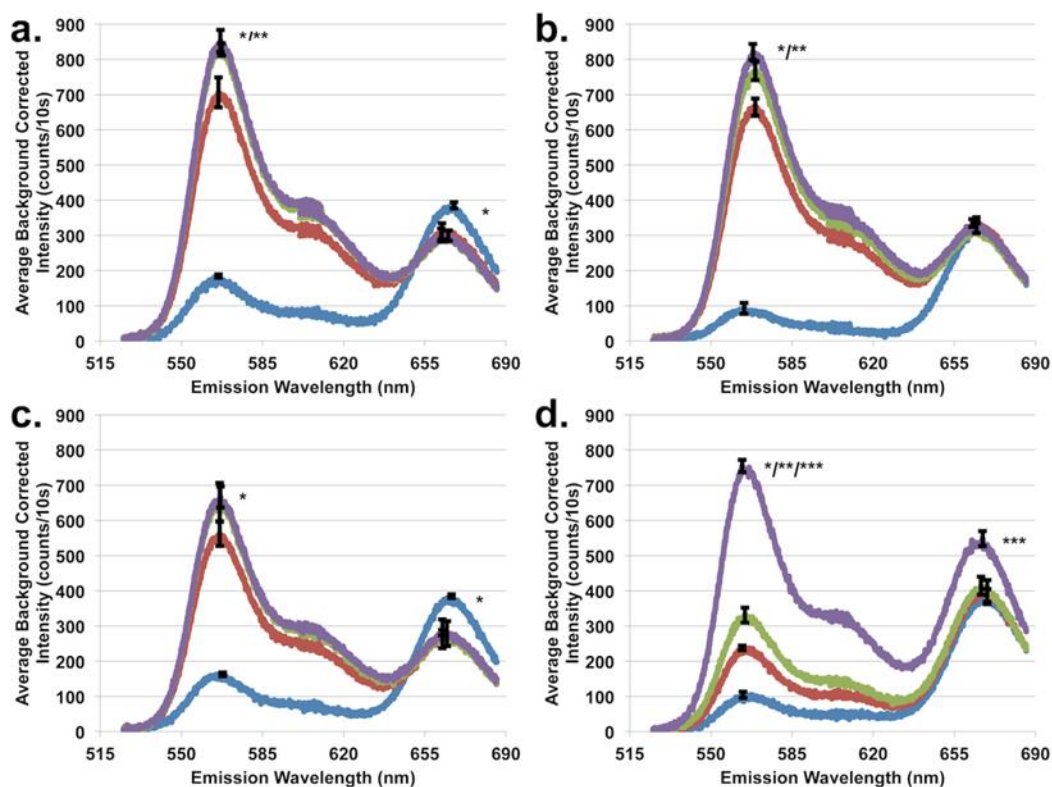


Figure A2.6 Average Cy3 and Cy5 emission spectra of reporters and reporter+probes excited at 940 nm (n = 3). (a) miR-26a-R1, (b) miR-26a-R2, (c) miR-27a-R1, and (d) miR-27a-R2. Blue = reporter, red = reporter + 1x probe, green = reporter + 2x probe, and purple = reporter + 100x probe. Cy5 peak appears near 660 nm, and Cy3 peak was near 560 nm. Spectra were acquired by stitching two grating positions together. Error bars indicate \pm one standard deviation of average signal at maximum intensity for both the Cy3 and Cy5 regions. For both the Cy3 and Cy5 regions, * indicates a statistical difference between 0x and 1x probe, ** indicates a statistical difference between 1x and 2x probe, and *** indicates a statistical difference between 2x and 100x probe (for all statistics $p < 0.05$). Combinations of statistical difference indicated by '/' and lack of asterisk(s) indicates no statistical difference.

Here emission spectra were collected using two-grating positions via the ‘Step and Glue’ function in Lightfield to rotate the grating during collection. The two grating positions allowed observation from 525.030 - 686.023 nm (~ 0.167 nm pixel⁻¹ with some overlapping regions). This was done in an attempt to relate energy transfer between Cy3 and Cy5 to the conformational state of the reporters. Emission spectra were then evaluated to obtain the Cy5/Cy3 ratios by summing the Cy3 from 564.1607 - 570.4966 nm, and the Cy5 region from 665.2051 - 672.9782 nm. Due to the custom nature of the fluorimeter, cuvette placement replicates were performed to account for the variability in measurements caused by cuvette placement in the holder. The three cuvette placements were obtained and averaged. Each cuvette placement had an acquisition time of 500 ms with 20 scans.

The relationship between the Cy3 and Cy5 dye emission was used to understand the structural states of the reporters in solution with and without probe. Emission from Cy3 and Cy5 was analyzed from excitation at 742 nm and 940 nm. While 742 nm excited both the dyes, stimulation at 940 nm was chosen because two-photon coupling between Cy3 and Cy5 was expected, which could give more information about the interactions between the two dyes and ultimately the structural motifs of the reporter hairpins. Upon comparison of the Cy3 and Cy5 emission by excitation at both wavelengths (Figures A2.6 and A2.9), miR-27a-R2 revealed itself to behave unlike any of the other reporters. Figure A2.9 showed that stimulation of miR-27a-R2 hairpin with 742 nm gave about twice the Cy5 intensity relative to the other reporters (similar to Figure 3.4).

To understand the conformation of the miR-27a-R2 reporter with respect to the other reporters, the relationship between Cy3 and Cy5 emission when excited at 940 nm was investigated (Figure A2.6). The emission profile from all four reporter hairpins showed a low Cy3 intensity relative to the Cy5 intensity when stimulated with 940 nm laser radiation. This was due to Cy3 being quenched by Cy5 and/or the nucleotides [1]. Disruption of the Cy3 quenching was expected upon addition of probe to the reporter. For all the reporters besides miR-27a-R2, addition of 1x probe resulted in an immediate change in signal where the Cy3 peak grew larger than the Cy5 peak. This flip in emission intensities was not seen for miR-27a-R2 until addition of 100x probe.

When comparing the Cy5/Cy3 intensity ratios in the absence of probe, the ratio ranged from 2.5 for miR-26a-R1 and miR-27a-R1 to 4.5 for miR-26a-R2 and miR-27a-R2 (Figure A2.8). For miR-26a-R1, miR-26a-R2, and miR-27a-R1 the ratio dropped to around ~ 0.4 - 0.6 for 1x, 2x,

and 100x probe addition (Figure A2.8). In contrast, miR-27a-R2 + 1x probe was ~ 1.94 , 2x probe was ~ 1.47 , and 100x probe was ~ 0.88 . The larger Cy5/Cy3 ratio for miR-27a-R2+100x-probe compared to the other reporters ($p < 0.05$, $n = 3$) again supported the idea that the conformational states of the dyes for miR-27a-R2 were different from those for the other reporters. Furthermore, this evidence suggests there were still unbound reporters in the mixture occupying some non-ideal hairpin state until 100x probe was added. In addition, this evidence supports the hypothesis that there was a mixture of hairpin conformations for miR-27a-R2 as well as a homodimer.

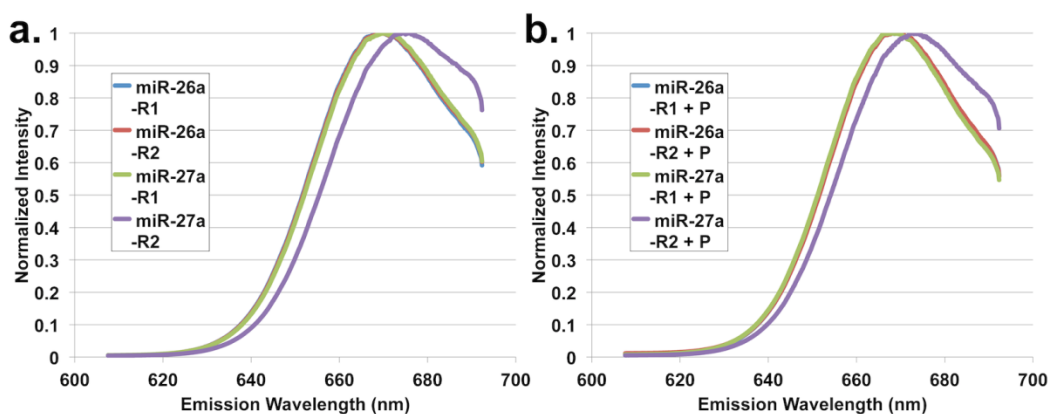


Figure A2.7 Normalized Cy5 emission spectra of (a) reporters and (b) reporter+probe complexes excited at 742 nm and acquired for 500 ms. The emission spectra were taken with the grating center wavelength at 650 nm and each spectrum was normalized to '1' using its maximum intensity value. Maximum Cy5 intensities for each reporter were ($\times 10^5$ counts/500 ms): 1.065 for miR-26a-R1; 1.26 for miR-26a-R2; 1.02 for miR-27a-R1; and 2.21 for miR-27a-R2. For the reporter+probe complexes ($\times 10^5$ counts/500 ms): 2.63 for miR-26a-R1+P; 2.70 for miR-26a-R2+P; 2.23 for miR-27a-R1+P; and 2.17 for miR-27a-R2+P. The miR-27a-R2 and miR-27a-R2+P both showed a red-shifted emission by about 5 nm compared to all other reporters.

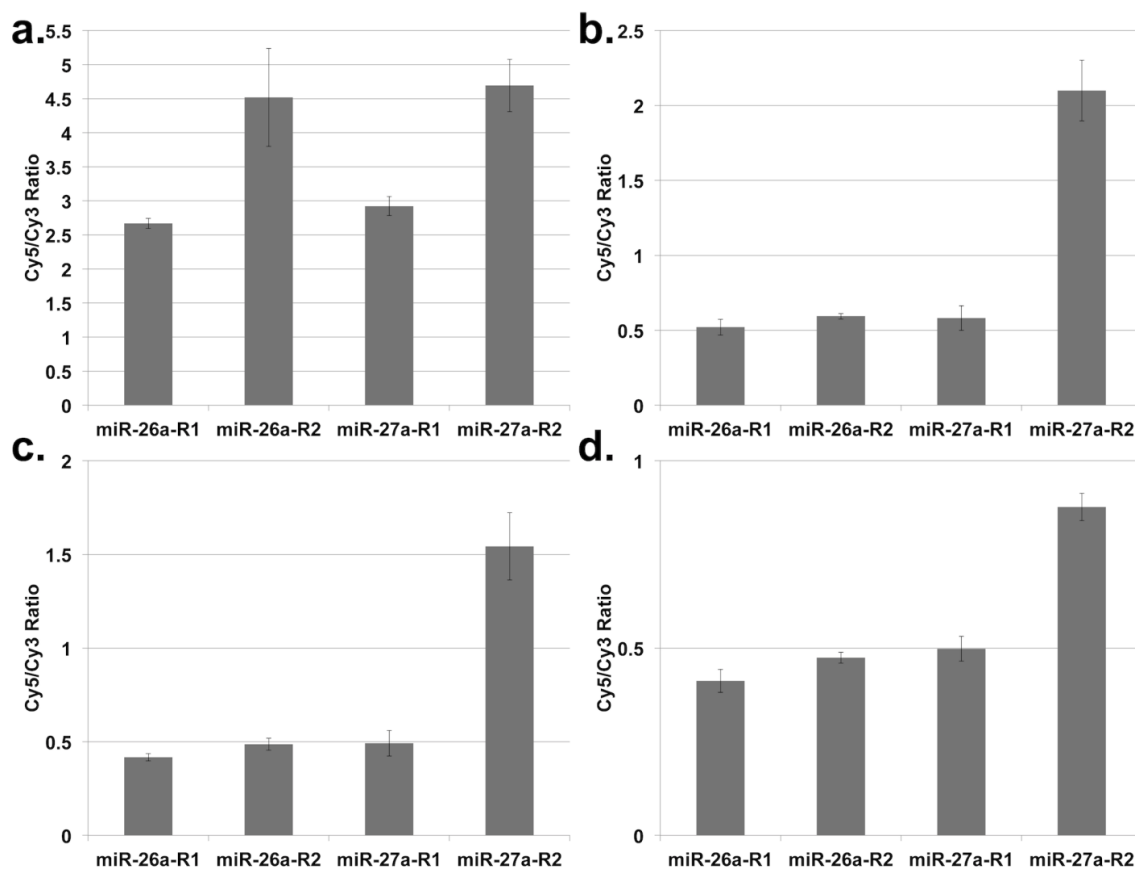


Figure A2.8 Cy5/Cy3 ratio for reporters with increasing amounts of associated probe excited at 940 nm. Cy3 region was 564.1607-570.4966 nm. Cy5 region was 665.2051-672.9782 nm. (a) Reporters with no probe added. (b) Reporters with 1x equivalent probe added. (c) Reporters with 2x equivalent probe added. (d) Reporters with 100x equivalent probe added.

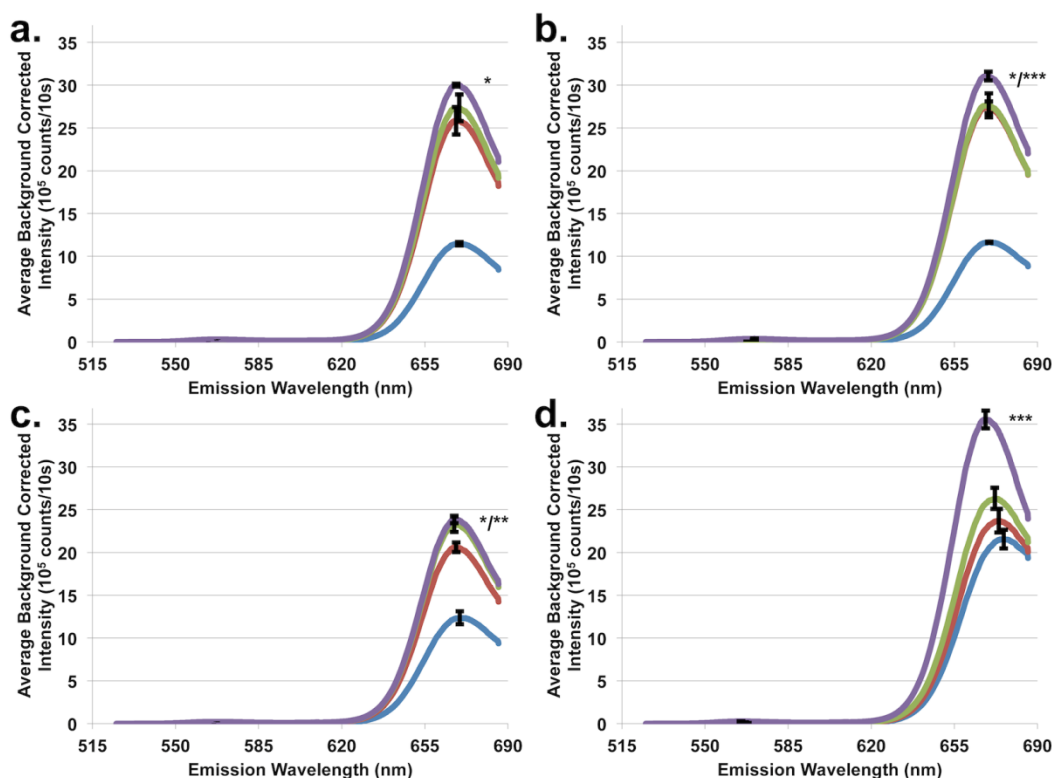


Figure A2.9 Average Cy3 and Cy5 emission spectra of reporters and reporter+probes excited at 742 nm ($n = 3$). (a) miR-26a-R1, (b) miR-26a-R2, (c) miR-27a-R1, and (d) miR-27a-R2. Blue = reporter, red = reporter + 1x probe, green = reporter + 2x probe, and purple = reporter + 100x probe. The predominant Cy5 peak was near 660 nm with Cy3 as a small peak near 560 nm. Spectra were acquired by stitching two grating positions together. Error bars indicate \pm one standard deviation of average signal at maximum intensity for both the Cy3 and Cy5 regions. For the Cy5 region, * indicates a statistical difference between 0x and 1x probe, ** indicates a statistical difference between 1x and 2x probe, and *** indicates a statistical difference between 2x and 100x probe (for all statistics $p < 0.05$). Combinations of statistical difference indicated by '/' and lack of asterisk(s) indicates no statistical difference.

In section 3.1 the experimental and predicted data from Figures 3.4 and 3.7, respectively, suggested different amounts of reporter+probe complexes were formed, with miR-27a-R2 forming the fewest number of complexes. To further explore reporter+probe complex formation 1x, 2x, and 100x probe was added to each of the reporters. For miR-26a-R1, Figure A2.9a shows there was no statistical increase (95 % confidence interval, $n = 3$) in signal after addition of 1x probe. This result was expected based on the ~ 100 % predicted complex formation from Figure 3.7a. Addition of 1x and 100x probe to miR-26a-R2 did show statistical increases in the signal of Figure A2.9b as anticipated from Figure 3.7b that predicted a ~ 5 % uncomplexed reporter. A similar trend was seen for miR-27a-R1 (Figure A2.9c) as that of miR-26a-R2, again in line with predictions made in Figure 3.7c. The Cy5 intensity from miR-27a-R2 only showed a statistical increase (95 % confidence interval, $n = 3$) in signal from the reporter hairpin when 100x probe was added (Figure A2.9d). This change in signal for miR-27a-R2 with 100x probe was about 1.3 times

as great compared to the other reporters with 100x probe. Adding 100x probe caused the Cy5 peak for miR-27a-R2 to blue shift back to the other reporter+probe complexes peak emission wavelengths. This observation provided more evidence that the miR-27a-R2 eventually forms a reporter+probe complex with a similar structure or dye environment as the other reporter+probe complexes.

Table A2.5 Homodimer thermodynamic values, number of base pair interactions, and GC content for miRNA analyte, probe, and reporter. Values were obtained from Two State melting (hybridization) using parameters described in experimental section 2.2.

Homodimer	ΔG (kcal mol ⁻¹)	ΔH (kcal mol ⁻¹)	ΔS (cal mol ⁻¹ K ⁻¹)	T _m (°C) at 100 nM	Base Pairs	GC
miR-26a-R1	-5.0	-40.8	-119.9	-4.6	5	3
miR-26a-R2	-4.6	-38.5	-113.7	-9.0	5	3
miR-27a-R1	-6.5	-84.8	-262.5	14.8	10	6
miR-27a-R2	-5.6	-122.2	-391.0	15.7	24	14
miR-26a	-1.3	-20.1	-63.1	-61.8	2	1
miR-27a	-7.5	-93.6	-288.8	18.6	14	8
Probe-miR-26a	-1.4	-16.1	-49.3	-75.3	2	1
Probe-miR-27a	-5.2	-33.3	-94.2	-9.4	6	4

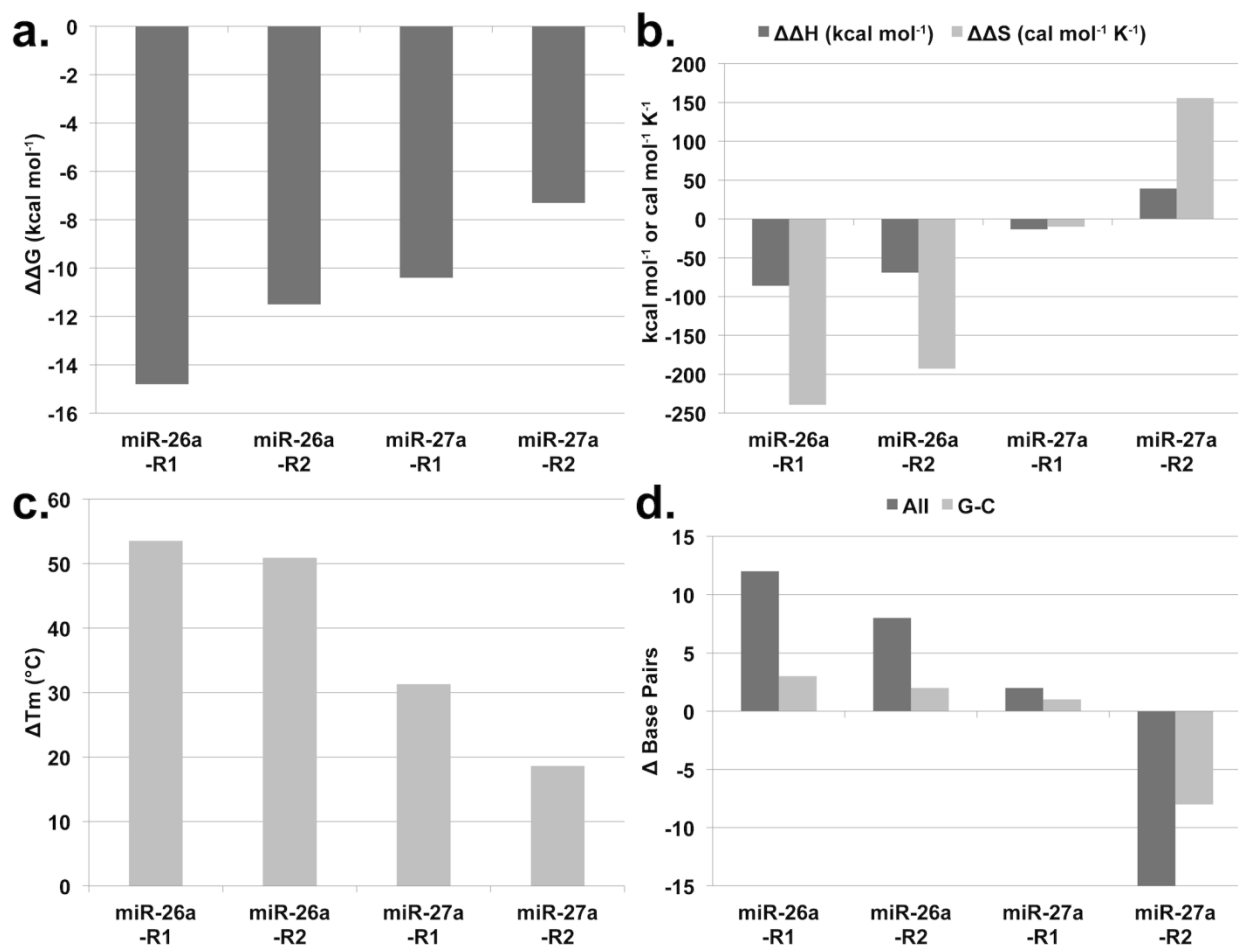


Figure A2.10 Reporter homodimer to reporter+probe complex changes in thermodynamic values, number of base pairs, and GC content. (a) The difference in Gibbs energy between the reporter homodimer and reporter+probe complex. (b) The difference in enthalpy or entropy. (c) The difference in melting temperature at 100 nM concentration. (d) The change in number of total base-pair interactions or just G-C base pairs.

Range	Color
$0.000 \leq P \leq 0.010$	#FF00FF
$0.010 < P < 0.012$	#CC00FF
$0.012 \leq P < 0.017$	#9900FF
$0.017 \leq P < 0.023$	#6600FF
$0.023 \leq P < 0.033$	#3300FF
$0.033 \leq P < 0.046$	#0000FF
$0.046 \leq P < 0.065$	#0033FF
$0.065 \leq P < 0.091$	#0066FF
$0.091 \leq P < 0.128$	#0099FF
$0.128 \leq P < 0.180$	#00CCFF
$0.180 \leq P < 0.253$	#00FFFF
$0.253 \leq P < 0.356$	#00FFCC
$0.356 \leq P < 0.5$	#00FF99
$0.500 \leq P < 0.644$	#00FF66
$0.644 \leq P < 0.747$	#00FF33
$0.747 \leq P < 0.820$	#00FF00
$0.820 \leq P < 0.872$	#33FF00
$0.872 \leq P < 0.909$	#66FF00
$0.909 \leq P < 0.935$	#99FF00
$0.935 \leq P < 0.954$	#CCFF00
$0.954 \leq P < 0.967$	#FFFF00
$0.967 \leq P < 0.977$	#FFCC00
$0.977 \leq P < 0.983$	#FF9900
$0.983 \leq P < 0.988$	#FF6600
$0.988 \leq P < 0.990$	#FF3300
$0.990 \leq P \leq 1.000$	#FF0000

Figure A2.11 Scale bar for partition functions. P signifies probability of the base-pair occurring. Scale increases in probability from violet (least probable) to red (most probable). Scale bar was obtained from the UNAFold website [27].

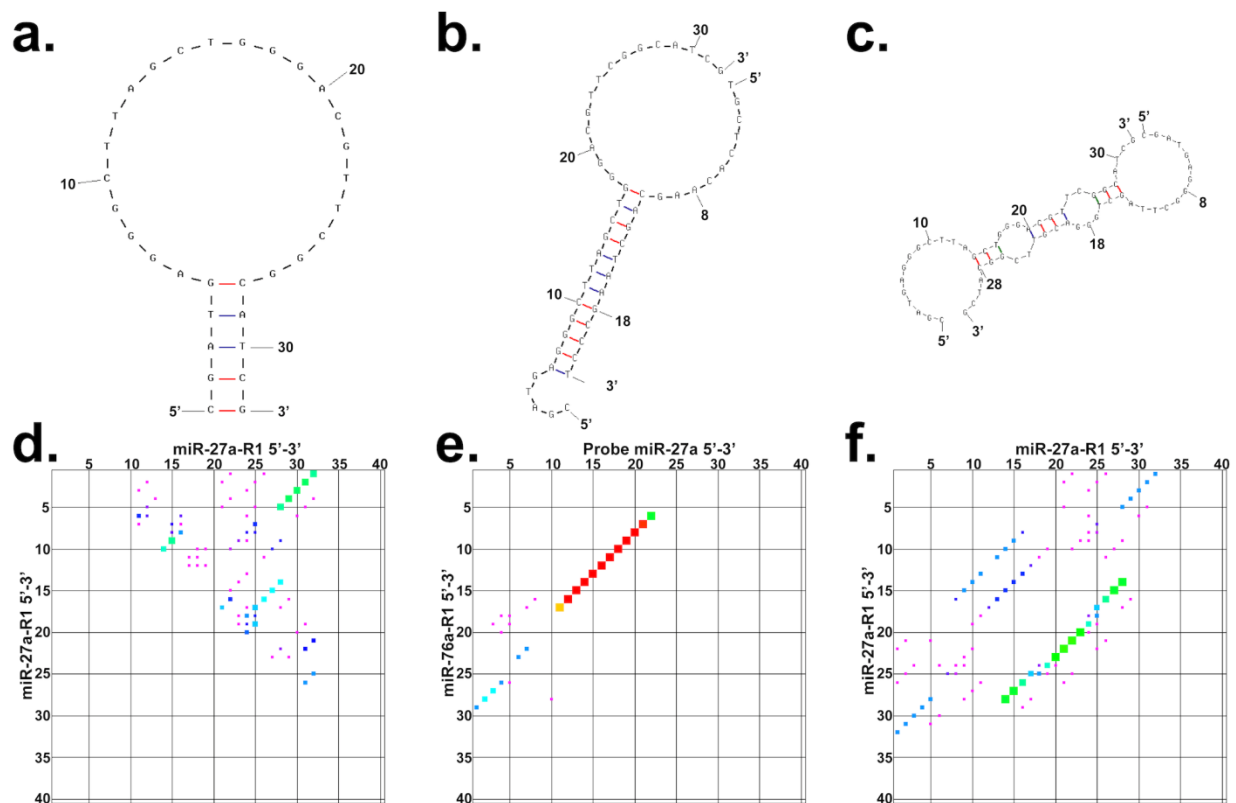


Figure A2.12 Partition functions for miR-27a-R1. The predicted energy minima structures for (a) miR-27a-R1 folded, (b) miR-27a-R1+Probe complex, and (c) miR-27a-R1 homodimer, respectively, at 25 °C. The largest and most probable dots on the partition function probability maps d-f correspond to energy minima structures a-c, respectively.

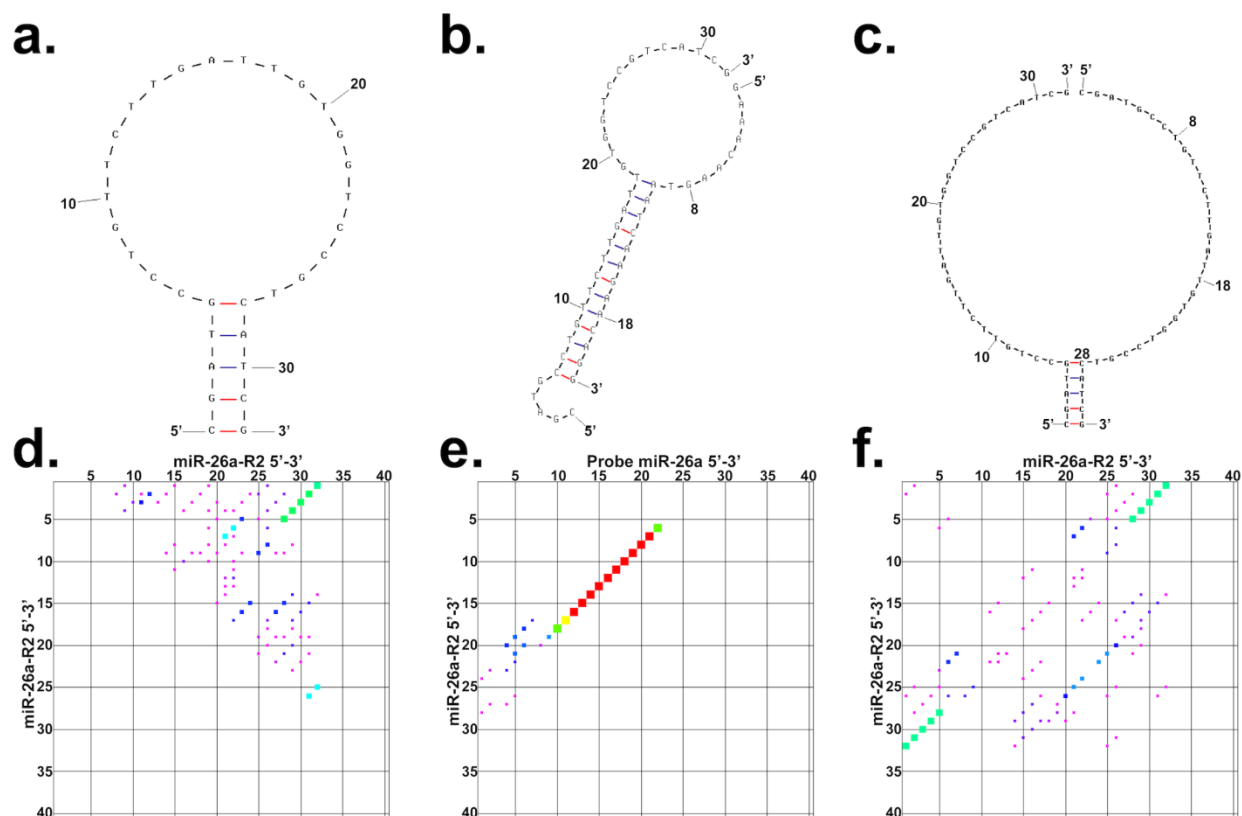


Figure A2.13 Partition functions for miR-26a-R2. The predicted energy minima structures for (a) miR-26a-R2 folded, (b) miR-26a-R2+Probe complex, and (c) miR-26a-R2 homodimer, respectively, at 25 °C. The largest and most probable dots on the partition function probability maps d-f correspond to energy minima structures a-c, respectively.

	Average Slope \pm % RSD (Normalized counts nM^{-1})	LOD \pm STDEV (nM Analyte)	LOQ \pm STDEV (nM Analyte)	% RSD
miR-26a-R1	$-5.49\text{E-}3 \pm 2.49$ %	9.09 ± 4.36	30.31 ± 14.55	48.0 %
miR-26a-R1 + off-analytes	$-5.00\text{E-}3 \pm 6.06$ %	7.00 ± 0.71	23.32 ± 2.36	10.1 %
miR-26a-R2	$-5.01\text{E-}3 \pm 3.27$ %	5.60 ± 0.78	18.66 ± 2.60	13.9 %
miR-26a-R2 + off-analytes	$-5.08\text{E-}3 \pm 2.78$ %	7.28 ± 1.18	24.26 ± 3.95	16.3 %
miR-27a-R1	$-4.12\text{E-}3 \pm 3.55$ %	5.31 ± 2.25	17.71 ± 7.51	42.4 %
miR-27a-R1 + off-analytes	$-4.03\text{E-}3 \pm 1.49$ %	8.98 ± 5.97	29.94 ± 19.90	66.5 %

Table A2.6 Analytical FOM resulting from calibration curves of reporter+probe biosensors for miR-26a and miR-27a. LOD = limit of detection and LOQ = limit of quantitation with or without off-analytes, as well as the linear slope from 0-100 nM analyte addition ($n = 3$). Percent relative standard deviation (% RSD) arises from sample preparation variability.

Appendix III. Supplemental Information for Chapter 4

A3.1 Sequence Information

Table A3.1 List of DNA sequences and modifications. The + symbols indicate locations of Locked Nucleic Acids (LNAs™). The location for a hexaethylene glycol spacer is indicated by iSp18. ‘5ATTO633N’ is a ATTO 633 dye on the 5-prime end, ‘5Cy5’ is a Cy5 dye on the 5-prime end, ‘3FAM’ is a 6-FAM (6-carboxyfluorescein) dye on the 3-prime end, ‘3Cy3’ is a Cy3 dye on the 3-prime end, and ‘3IAbRQSp’ is an Iowa Black Red Quencher on the 3-prime end. Since DNA is more stable it was used instead of actual microRNA. ‘0’ or ‘18’ refers to the type of spacers on the 5-prime and 3-prime ends of the DNA sequences.

Name	Sequences 5' to 3'
IAbRQ Cy5 Pair 0 Spacers	/5Cy5/CGATGCCTGTTCT+TGATTACT+TTCGGACATC+G/3IAbRQSp/
IAbRQ Cy5 Pair 18 Spacers	/5Cy5//iSp18/CGATGCCTGTTCT+TGATTACT+TTCGGACATC+G/iSp18//3IAbRQSp/
Cy3 Cy5 Pair 0 Spacers	/5Cy5/CGATGCCTGTTCT+TGATTACT+TTCGGACATC+G/3Cy3Sp/
Cy3 Cy5 Pair 18 Spacers	/5Cy5//iSp18/CGATGCCTGTTCT+TGATTACT+TTCGGACATC+G/iSp18//3Cy3Sp/
6-FAM ATTO 633 Pair 0 Spacers	/5ATTO633N/CGATGCCTGTTCT+TGATTACT+TTCGGACATC+G/3FAM/
6-FAM ATTO 633 Pair 18 Spacers	/5ATTO633N//iSp18/CGATGCCTGTTCT+TGATTACT+TTCGGACATC+G/iSp18//3FAM/
Probe mmu- miR26a-2-3p	GAAACAAGTAATCAAGAACAGG
mmu-miR26a- 2-3p (as DNA)	CCTGTTCTTGATTACTTGTTC

A3.2 Signal to Background Analysis

Table A3.2 Averaged summed intensities for reporters and reporter+probes. Average was from three trials with three frames each (N = 9).

	Excite 740		Excite 935/945 nm	
	520/565 nm Emission Reporter \pm STDEV (RSD %) Reporter+Probe \pm STDEV (RSD %)	660/670 nm Emission Reporter \pm STDEV (RSD %) Reporter+Probe \pm STDEV (RSD %)	520/565 nm Emission Reporter \pm STDEV (RSD %) Reporter+Probe \pm STDEV (RSD %)	660/670 nm Emission Reporter \pm STDEV (RSD %) Reporter+Probe \pm STDEV (RSD %)
miR-26a-R IAbRQ Cy5 Pair 0 Spacers	N/A	597988.79 \pm 8699.04 (1.45 %) 35277788.44 \pm 289225.84 (0.82 %)	N/A	338.85 \pm 255.45 (75.39 %) 10830.22 \pm 522.32 (4.82 %)
miR-26a-R IAbRQ Cy5 Pair 18 Spacers	N/A	2223216.33 \pm 24899.85 (1.12 %) 35400552.56 \pm 341280.62 (0.96 %)	N/A	794.07 \pm 359.09 (45.22 %) 11207.44 \pm 366.93 (3.27 %)
miR-26a-R Cy3 Cy5 Pair 0 Spacers	16372.74 \pm 1792.66 (10.95 %) 116421.63 \pm 4764.45 (4.09 %)	13469963.18 \pm 111434.72 (0.83 %) 36917823.41 \pm 294813.20 (0.80 %)	5816.67 \pm 381.15 (6.55 %) 69513.33 \pm 1256.26 (1.81 %)	35480.48 \pm 773.32 (2.18 %) 30513.00 \pm 470.84 (1.54 %)
miR-26a-R Cy3 Cy5 Pair 18 Spacers	39933.65 \pm 2110.714 (5.29 %) 102277.44 \pm 4476.76 (4.38 %)	21408227.80 \pm 1230160.78 (5.75 %) 37568744.16 \pm 1048953.21 (2.79 %)	14635.63 \pm 623.94 (4.26 %) 59778.93 \pm 1099.95 (1.84 %)	46985.67 \pm 695.71 (1.48 %) 31926.04 \pm 850.49 (2.66 %)
miR-26a-R 6-FAM ATTO 633 Pair 0 Spacers	1398.93 \pm 391.42 (27.98 %) 14554.89 \pm 907.26 (6.23 %)	2793295.33 \pm 120614.49 (4.32 %) 8311403.17 \pm 281857.10 (3.39 %)	5313.30 \pm 468.76 (8.82 %) 83554.57 \pm 2948.90 (3.53 %)	19262.07 \pm 988.59 (5.13 %) 15439.30 \pm 613.60 (3.97 %)
miR-26a-R 6-FAM ATTO 633 Pair 18 Spacers	3029.96 \pm 483.43 (15.96 %) 24072.41 \pm 1290.44 (5.36 %)	6399413.57 \pm 325245.31 (5.08 %) 8581432.90 \pm 310469.40 (3.62 %)	14452.78 \pm 1557.929 (10.78 %) 144773.14 \pm 2615.30 (1.81 %)	59554.48 \pm 2728.60 (4.58 %) 24554.81 \pm 3038.29 (12.37 %)

Table A3.3 Percent change in signal for quenching, ΔS_Q , (Equation 4.1) from the IAbRQ|Cy5 reporters. Standard deviation and percent relative standard deviation (RSD %) are shown with average percent change in signal (N = 3). Excitation was at 740 and 945 nm. Only the 670 peak emission wavelength range was used for the Cy5 dye.

Reporter Type	740 nm Excitation	945 nm Excitation
	670 nm Emission % $\Delta S_Q \pm$ SD (RSD %)	670 nm Emission % $\Delta S_Q \pm$ SD (RSD %)
IAbRQ Cy5 Pair 0 Spacers	5800.14 \pm 68.71 (1.18 %)	3313.04 \pm 1041.62 (31.44 %)
IAbRQ Cy5 Pair 18 Spacers	1492.60 \pm 34.44 (2.31 %)	1326.94 \pm 176.22 (13.28 %)

The percent change in signal for quenching of a Cy5 dye on reporters with IAbRQ|Cy5 as a quencher-dye pair is presented in Table A3.3. Representative emission spectra of the IAbRQ|Cy5 reporters are in the Figure A3.1. The purpose of a reporter that used a quencher-dye pair was to compare the percent change in signal and types of detection limits (next section) from a purely quenching sensor to a sensor not designed for pure quenching (Cy3|Cy5). Since the Cy3 on the Cy3|Cy5 reporter was excited at 945 nm for FRET enhancement of Cy5, the IAbRQ|Cy5 reporter was also excited at 945 nm to compare how Cy5 behaved in a purely quenching mode.

At 740 nm excitation, addition of 18 spacers caused a significant decrease ($p < 0.05$) in quenching of Cy5 (670 nm emission) by a factor of ~ 4 compared to the 0 spacers. At 945 nm excitation, there was no significant ($p < 0.05$) difference in the percent change in signal for quenching between reporters with 0 and 18 spacers. The statistical similarity in the percent change in signal at 945 nm excitation was due to the poor excitation of Cy5 and subsequent weak emission, as well as poor signal to noise ratio (S/N). Figure A3.1 shows the difference in S/N for the IAbRQ|Cy5 reporters with 0 and 18 spacers excited at 740 and 945 nm.

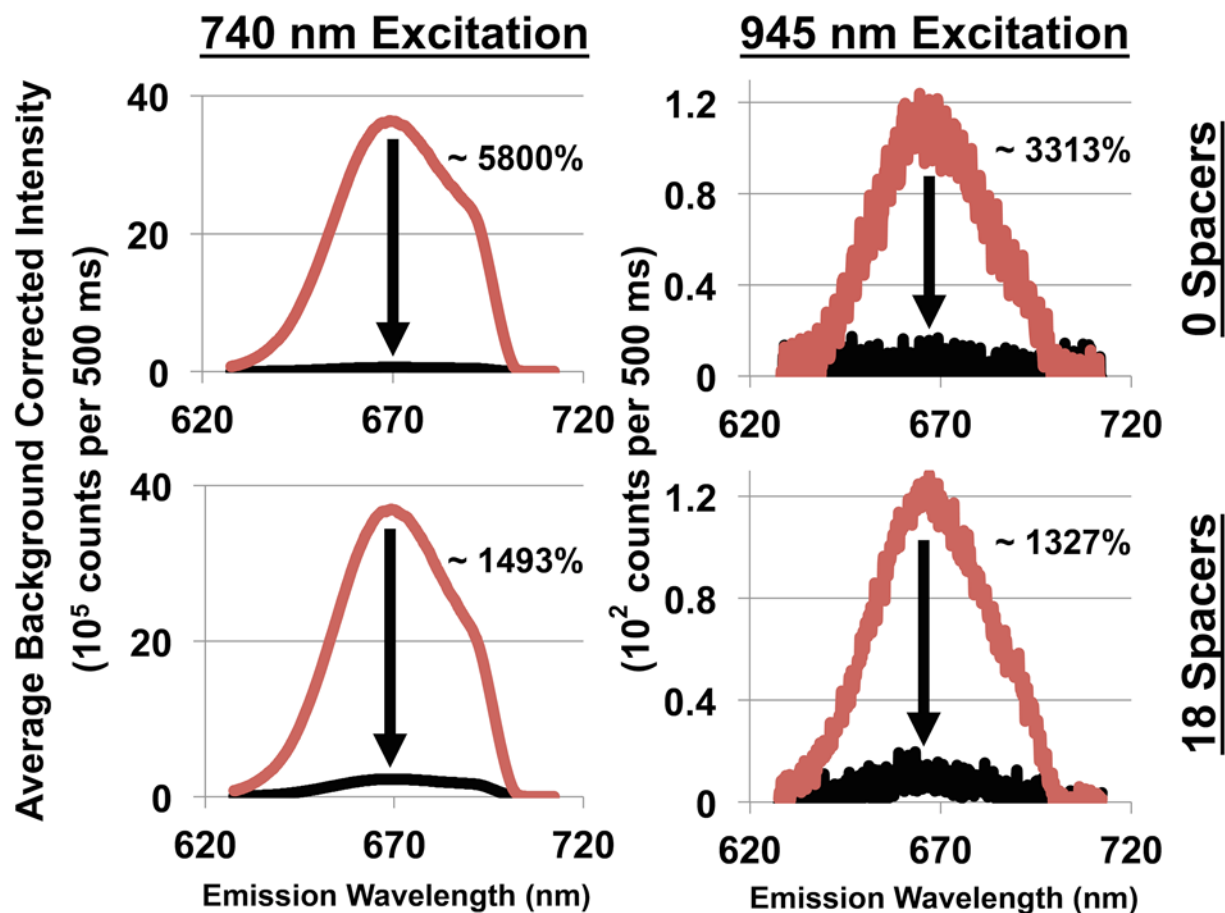


Figure A3.1 Emission Spectra of 100 nM IABRQ|Cy5 reporters with and without probe excited at 740 (left) and 945 nm (Right). Top: 0 and Bottom: 18 spacers. Emission collected with the grating centered at 670 nm for the Cy5 dye. Black emission corresponds to reporter-hairpin, and red for reporter+probe. Arrows show direction of signal change from the reporter+probe to the reporter-hairpin. Percent signal quenching is estimated from data summarized in Table 4.1 using Eqn 4.1.

Table A3.4 Percent change in signal for quenching, ΔS_Q , (Equation 4.1) and percent change in signal for enhancement, ΔS_E , (Equation 4.2) from the Cy3|Cy5 reporters. Standard deviation and percent relative standard deviation (RSD %) are shown with average percent change in signal (N = 3). Emission centers at 565 and 670 nm were used for Cy3 and Cy5, respectively. Both dyes were excited at 740 or 945 nm.

Reporter Type	740 nm Excitation		945 nm Excitation		
	565 nm Emission % $\Delta S_Q \pm SD$ (RSD %)	670 nm Emission % $\Delta S_Q \pm SD$ (RSD %)	565 nm Emission % $\Delta S_Q \pm SD$ (RSD %)	670 nm Emission % $\Delta S_Q \pm SD$ (RSD %)	670 nm Emission % $\Delta S_E \pm SD$ (RSD %)
Cy3 Cy5 Pair 0 Spacers	616.28 \pm 73.97 (12.00 %)	174.10 \pm 4.22 (2.42 %)	1098.22 \pm 84.59 (7.70 %)	-13.97 \pm 2.28 (16.32 %)	16.29 \pm 3.07 (18.85 %)
Cy3 Cy5 Pair 18 Spacers	156.47 \pm 19.51 (12.47 %)	76.28 \pm 17.90 (23.47 %)	308.89 \pm 17.42 (5.64 %)	-32.03 \pm 2.80 (8.74 %)	47.28 \pm 5.93 (12.54 %)

Next we investigated the effect of spacers on the quenching and enhancement ability of reporters with the Cy3|Cy5 dye pair used in previous studies.^{32,34} The values in Table A3.4 indicate that addition of 18 spacers influenced the Cy3|Cy5 dye pair's percent change in signal at 740 and 945 nm excitation. When excited at 740 nm, both Cy3 (565 nm emission) and Cy5 (670 nm emission) showed a reduction in quenching ($p < 0.05$) by a factor of ~ 4 and ~ 2 , respectively, after 18 spacers were added. At 945 nm excitation, the extent that Cy3 was quenched decreased ($p < 0.05$) by a factor of ~ 3.6 upon addition of 18 spacers. However, the Cy5 showed a statistically significant ($p < 0.05$) signal enhancement by a factor of ~ 3 when 18 spacers were added.

Table A3.5 Percent change in signal for quenching, ΔS_Q , (Equation 4.1) and percent change in signal for enhancement, ΔS_E , (Equation 4.2) from the 6-FAM|ATTO 633 reporters. Standard deviation and percent relative standard deviation (RSD %) are shown with average percent change in signal ($N = 3$). Emission centers at 520 and 660 nm were used for 6-FAM and ATTO 633, respectively. Both dyes were excited at either 740 or 935 nm.

Reporter Type	740 nm excitation		935 nm excitation		
	520 nm Emission % $\Delta S_Q \pm SD$ (RSD %)	660 nm Emission % $\Delta S_Q \pm SD$ (RSD %)	520 nm Emission % $\Delta S_Q \pm SD$ (RSD %)	660 nm Emission % $\Delta S_Q \pm SD$ (RSD %)	660 nm Emission % $\Delta S_E \pm SD$ (RSD %)
6-FAM ATTO 633 Pair 0 Spacers	947.42 \pm 76.14 (8.04 %)	197.66 \pm 3.29 (1.66 %)	1479.93 \pm 151.06 (10.21 %)	-19.79 \pm 2.17 (10.97 %)	24.73 \pm 3.38 (13.67 %)
6-FAM ATTO 633 Pair 18 Spacers	702.29 \pm 96.28 (13.71 %)	34.19 \pm 2.39 (6.99 %)	912.09 \pm 129.68 (14.22 %)	-58.89 \pm 3.52 (5.98 %)	144.38 \pm 20.33 (14.08 %)

From unpublished work screening various potential FRET pairs for two-photon imaging, we found the 6-FAM|ATTO 633 pair exhibited FRET enhancement when the 6-FAM was excited at 935 nm. Here reporters with 18 spacers excited at 935 nm showed a statistically significant ($p < 0.05$) increase in the percent enhancement of ATTO 633 (660 nm emission) by a factor of ~ 6 compared to reporters without spacers. When the 6-FAM was excited at 935 nm it showed a statistical ($p < 0.05$) decrease in the quenching of 6-FAM (520 nm emission) by a factor of ~ 1.6 when 18 spacers were added. Excitation of both the 6-FAM and ATTO 633 at 740 nm demonstrated reductions ($p < 0.05$) in the percent change in signal for quenching of the 6-FAM|ATTO 633 reporters with 18 spacers compared to those reporters without spacers.

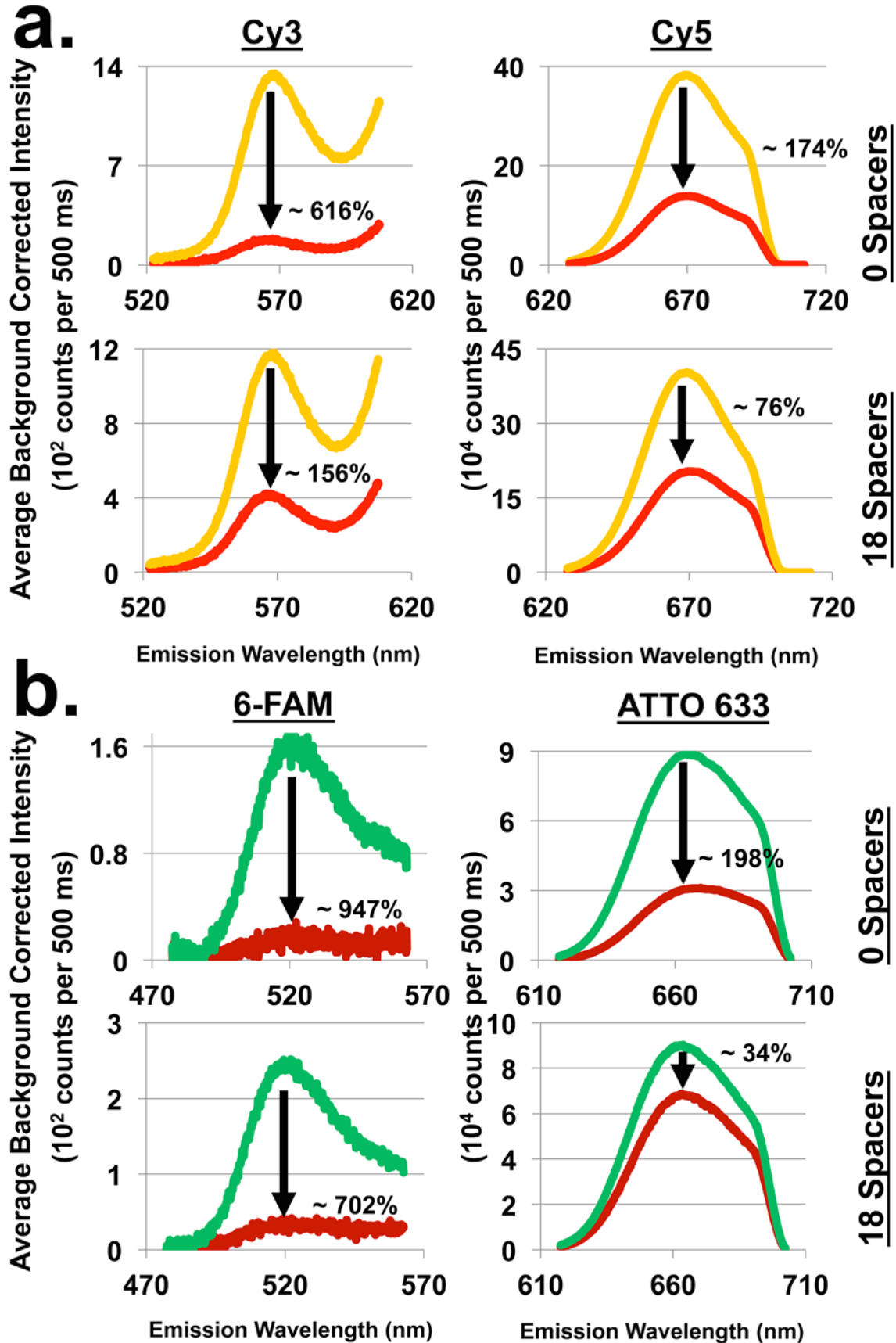


Figure A3.2 Donor and acceptor emission spectra from 100 nM reporters with and without probe when excited at 740 nm. (a.) Cy3|Cy5 reporters with 0 or 18 spacers (top and bottom). The red and yellow lines correspond to reporter-hairpin and reporter+probe, respectively. (b.) 6-FAM|ATTO 633 reporters with 0 and 18 spacers (top and bottom). The maroon and green lines correspond to reporter-hairpin and reporter+probe, respectively. Arrows show direction of signal change from the reporter+probe to the reporter-hairpin. Percent signal quenching is estimated from data summarized in Tables 4.2 and 4.3 using Eqn 4.1.

A3.3 Detection Limits

There was no statistical difference in the 5 nM LODs for signal-off when excited at 945 nm and there was no statistical difference in 3 to 7 nM LODs for signal-off when excited at 740 nm. To test for a difference in the signal-off LODs based on excitation wavelength, the LODs at 945 nm were averaged and compared to the average LODs from 740 nm excitation. From this comparison there was no statistical difference ($p < 0.05$) observed from signal-off LOD based on excitation wavelength.

To see if there was a statistical difference between the signal-on (18 spacers only) and signal-off reporters (0 and 18 spacers), a similar approach as described above was used. In this case there was no statistical difference ($p < 0.05$) between signal-on and -off LODs. Even comparison of just the Cy5 signal-off to signal-on from the reporters with 18 spacers did not show a statistical difference in LOD. In general, neither the use of spacers, excitation wavelength, nor direction of signal change influenced LODs for the Cy3|Cy5 reporters.

The same approach to compare the influence of spacers on LOD was applied to compare the sensitivity (nM^{-1}) of the Cy3 and Cy5 dyes. This analysis revealed statistical differences ($p < 0.05$) in sensitivity after the spacers were added to the reporters. For Cy5 signal-on, the sensitivity increased by more than a factor of three due to adding spacers to reporter. In the case of signal-off under 740 and 945 nm excitation, addition of the spacers showed a decrease in sensitivity for both Cy3 and Cy5. Upon comparison of Cy3 to Cy5 for signal-off, the Cy3 reporters with 0 spacers were the most sensitive (both about $-7.5 \times 10^{-3} \text{ nM}^{-1}$, $p < 0.05$) when excited at either wavelength. For Cy3, the addition of spacers had the least effect on sensitivity (reduced by $\sim 1.5 \times 10^{-3} \text{ nM}^{-1}$) when excited at 945 nm compared to excitation at 740 nm (reduced by $\sim 2.6 \times 10^{-3} \text{ nM}^{-1}$). These results show that reporters with 18 spacers excited at 945 nm will give optimal FOM to measure over- or under-expression of miRNA.

For signal-off there was no statistical difference in the 20 to 30 nM LODs when excited at 740 nm excitation and there was no statistical difference in ~ 13 nM LODs when excited at 935 nm. As before, to test for a difference in signal-off LOD based on excitation wavelength the

averaged LODs at each excitation wavelength were compared. From this comparison there was no statistical difference ($p < 0.05$) in signal-off LOD based on excitation wavelength.

There was no statistical difference ($p < 0.05$) in the signal-on LODs upon addition of spacers for the ATTO 633 because the error in the calculated LOD was very large for the reporter with 0 spacers. To test if there was statistical difference between the signal-on and signal-off, a similar analysis as described for Cy3|Cy5 was used. For the 6-FAM|ATTO 633 reporters there was no statistical difference ($p < 0.05$) between signal-on and -off over the 13 to 30 nM range. Much like the Cy3|Cy5 reporters, the general trend was that the 6-FAM|ATTO 633 reporters had LODs that were not influenced by addition of spacers, excitation wavelength, or direction of signal change.

The spacer's influence on the dyes' sensitivities (nM^{-1}) was determined following statistical comparisons previously outlined for LODs. For ATTO 633 signal-on when excited at 935 nm, addition of spacers showed a statistical ($p < 0.05$) increase in the sensitivity by almost a factor of 10. Signal-off sensitivity was only seen to decrease from addition of spacers to reporters for 6-FAM and ATTO 633 when excited at 740 nm. Spacer addition to the 6-FAM when excited at 935 nm did not show a statistical change ($p < 0.05$) in the signal-off sensitivity. Upon comparison of 6-FAM to ATTO 633 for signal-off, the 6-FAM reporters with 0 spacers were the most sensitive and similar at both excitation wavelengths ($p < 0.05$). For 6-FAM on the reporter with 18 spacers excited at 935 nm, the sensitivity was statistically similar ($p < 0.05$) to the reporter that had 0 spacers ($\sim 6 \times 10^{-3} \text{ nM}^{-1}$). These results establish that the reporter can be excited at just 935 nm to observe two colors without a major loss in the analytical FOM.

Compared to the other spectroscopic conditions and 6-FAM|ATTO 633 reporters with 0 spacers, the sensitivity and tens of nanomolar LODs for signal-off were maintained when the 6-FAM|ATTO 633 biosensor with 18 spacers was excited at 935 nm. The 6-FAM|ATTO 633-18 spacer reporters excited at 935 nm was able to leverage suitable sensitivities and LODs for both signal-on and signal-off. Thus a biosensor with the 6-FAM|ATTO 633-18 spacers will have the best chance to achieve good contrast to visualize the over and under expression of miRNA.

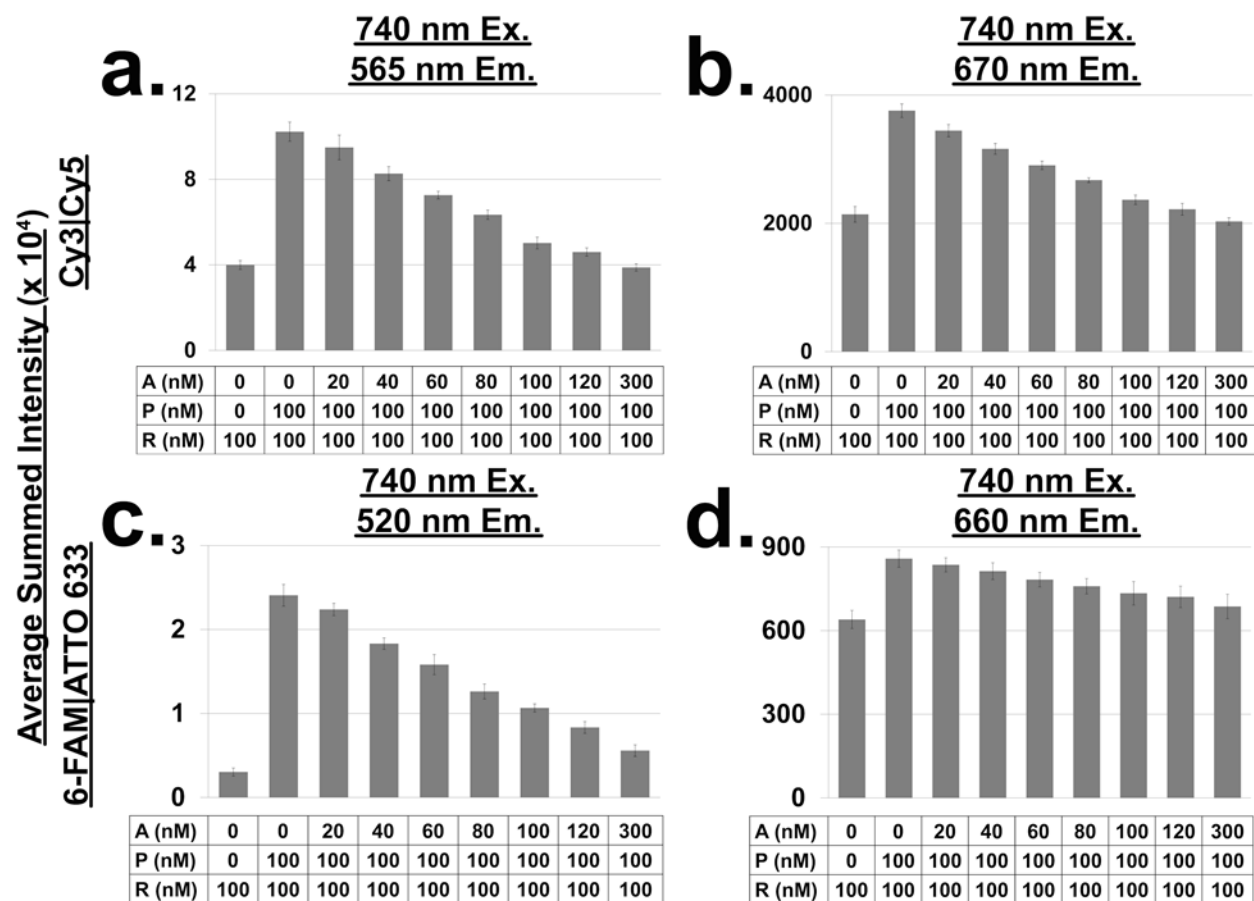


Figure A3.3 Calibration curves from miRNA analyte additions to 100 nM reporter+probe biosensors with Cy3|Cy5-18 spacers (a-b) and 6-FAM|ATTO 633-18 spacers (c-d). All sensors were excited at 740 nm. (a) Emission collected with the grating centered at 565 nm for the Cy3 dye. (b) Emission collected with the grating centered at 670 nm for the Cy5 dye. (c) Emission collected with the grating centered at 520 nm for the 6-FAM dye. (d) Emission collected with the grating centered at 660 nm for the ATTO 633 dye. N = 9 from three calibration experiments with three frames each collected and averaged.

Table A3.6 Biosensor figures of merit (FOM) from the ratio of ‘donor to acceptor’ emission centers for both Cy3|Cy5 and 6-FAM|ATTO 633 dye pairs with either 0 or 18 spacers. Cy3|Cy5 reporters excited at 740 and 945 nm, and 6-FAM|ATTO 633 reporters excited at 740 and 935 nm. Data obtained from normalized calibration curves using ‘donor to acceptor’ ratios over the 0-100 nM miR-26a range in 20 nM steps. N=3 for each FOM.

Reporter Type	740 nm Excitation		935/945 nm Excitation	
	Average Slope \pm RSD (Normalized counts nM ⁻¹)	LOD (nM Analyte) \pm STDEV LOQ (nM Analyte) \pm STDEV RSD	Average Slope \pm RSD (Normalized counts nM ⁻¹)	LOD (nM Analyte) \pm STDEV LOQ (nM Analyte) \pm STDEV RSD
Cy3 Cy5 Pair 0 Spacer	-4.24E-3 \pm 6.10 %	14.25 \pm 5.19 47.50 \pm 17.31 36.44%	-7.87E-3 \pm 1.62 %	10.53 \pm 0.53 35.10 \pm 1.76 5.01%
Cy3, Cy5 Pair 18 Spacer	-1.74E-3 \pm 27.54 %	19.2 \pm 9.99 64.03 \pm 33.32 52.04%	-7.32E-3 \pm 2.39 %	7.74 \pm 2.33 25.81 \pm 7.78 30.16%
6-FAM ATTO 633 Pair 0 Spacer	-2.78E-3 \pm 9.51 %	48.22 \pm 25.29 160.74 \pm 84.30 52.45%	-7.03E-3 \pm 1.55 %	23.34 \pm 5.81 77.79 \pm 19.37 24.90%
6-FAM ATTO 633 Pair 18 Spacer	-4.82E-3 \pm 8.91 %	37.33 \pm 9.21 124.43 \pm 30.70 24.67%	-9.01E-3 \pm 3.72 %	21.08 \pm 7.58 70.26 \pm 25.26 35.96%

For each FRET pair on each reporter excited at 740, 935, or 945 nm, the LODs from the D/A ratio did not show statistical differences ($p < 0.05$) based on number of spacers. In general, when excited at 740 nm the ~17 nM LODs from Cy3|Cy5 reporters were lower than the ~37 nM LODs from the 6-FAM|ATTO 633 analogs ($p < 0.05$). Reporters excited at 935 or 945 nm, showed a general trend of LODs near 8 nM for Cy3|Cy5 reporters and larger LODs near 23 nM from the 6-FAM|ATTO 633 reporters ($p < 0.05$). When 6-FAM|ATTO 633-18 spacers were excited at 935 nm instead of 740 nm, the LOD was lowered by ~20 nM ($p < 0.05$). All the other reporters did not show any difference in LOD based on the wavelength that excited the reporter.

The excitation wavelength did not influence how precise the LOD measurements were at a given spacer length except for the Cy3|Cy5-0 spacers that was more precise when excited at 945 nm than when excited at 740 nm. There was no difference in precision based on spacer lengths for either the Cy3|Cy5 or the 6-FAM|ATTO 633 reporters except for the Cy3|Cy5-0 spacers excited

at 945 nm. In the case of 945 nm excitation, the Cy3|Cy5-0 spacers were more precise than the Cy3|Cy5-18 spacers. At 935/945 nm excitation, only the Cy3|Cy5-0 spacers had precisions that were statistically smaller than each of the other reporters. The 6-FAM|ATTO 633-0 spacers excited at 740 nm were not very precise with a standard deviation of ~ 25 nM (50 % RSD). However, only the reporter with Cy3|Cy5-0 spacers was statistically more precise than the 6-FAM|ATTO 633-0 spacers. All other reporters were equally as precise with standard deviations in the 2 to 25 nM range when excited at 740, 935, and 945 nm. The small sample size was the expected reason why the 6-FAM|ATTO 633-0 spacers' 25 nM precision was not statistically different from the 2 to 10 nM precisions of the other reporters. Recall that much of the precision was dependent on the sample preparation rather than instrumental error. Since a majority of the precision was equal among the reporters, we suspect that the instances of improved precision were just instances of good sample preparation.

Regardless of the wavelength to excite the reporters the following trend in sensitivity was observed: Cy3|Cy5-0 spacers were more sensitive than 18 spacers and 6-FAM|ATTO 633-18 spacers were more sensitive than the 0 spacers. The reporters demonstrated the greatest sensitivity when excited at either 935 or 945 nm, depending on the donor dye excited. At 935 nm excitation, the 6-FAM|ATTO 633-18 spacers was the most sensitive of all the reporters ($\sim 9 \times 10^{-3}$ nM⁻¹, $p < 0.05$). The remainder of reporters decreased in sensitivity in the order: Cy3|Cy5-0 spacers, Cy3|Cy5-18 spacers, and 6-FAM|ATTO 633-0 spacers (excited at 935 or 945 nm). At 740 nm excitation, the sensitivity of the Cy3|Cy5-0 spacers and the 6-FAM|ATTO 633-18 spacers were statistically similar ($\sim 4 \times 10^{-3}$ nM⁻¹). The 6-FAM|ATTO 633-0 spacers were the next most sensitive followed by the Cy3|Cy5-18 spacers (740 nm excitation). Excitation at 935 and 945 nm was statistically more sensitive than the corresponding 740 nm excitation for each type of reporter. However, the precision was not statistically influenced by the excitation wavelength.

A3.4 MicroRNA-induced reporter+probe displacement efficiency

Table A3.7 Experimentally determined molar concentrations of reporter-hairpin and reporter+probe upon addition of either 100 or 300 nM miR-26a analyte. Calculations performed by comparison of 6-FAM|ATTO 633 dyes for 100 nM reporter-hairpin and reporter+probe. N =3.

	miRNA added (nM)	Reporter+Probe remaining (nM)	Reporter-hairpin formed (nM)	Reporter-hairpin + Reporter+Probe (nM)
Trial 1	100	35.20 ± 8.44	66.50 ± 2.80	101.69 ± 8.90
	300	11.25 ± 15.71	90.84 ± 4.86	102.10 ± 16.44
Trial 2	100	36.46 ± 10.71	67.14 ± 4.54	103.60 ± 11.63
	300	10.82 ± 15.38	94.16 ± 6.03	104.98 ± 16.52
Trial 3	100	33.21 ± 8.58	70.11 ± 2.62	103.32 ± 8.98
	300	9.71 ± 8.92	94.06 ± 2.95	103.77 ± 9.39

A3.5 Reporter+Probe formation analysis

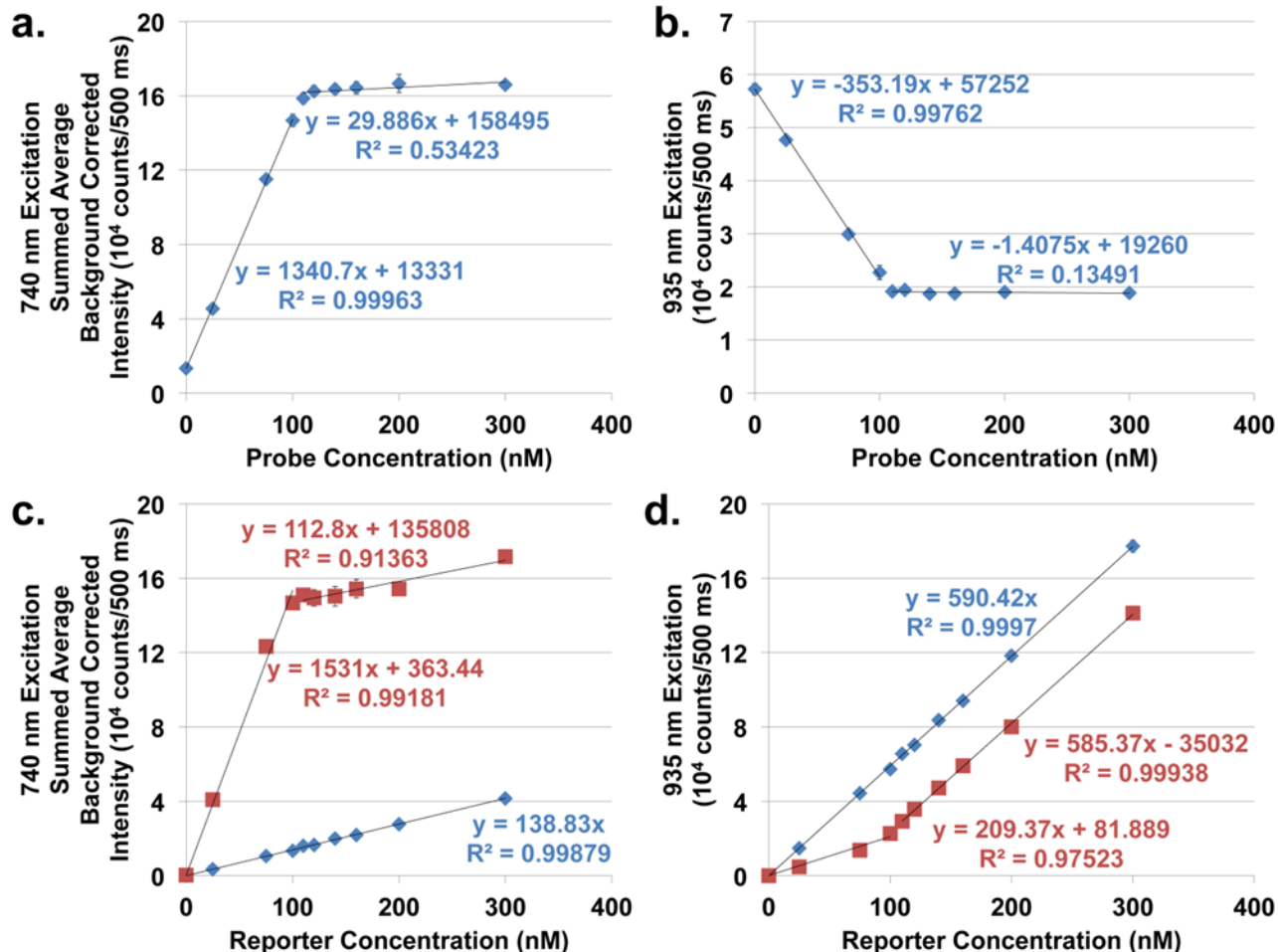


Figure A3.4 Extent of reporter+probe formation by analysis of changes in reporter 6-FAM|ATTO 633-18 spacers emission. Emission was taken from the ATTO 633 signal (660 nm emission center). Increasing concentration of probe to a constant 100 nM solution of reporter excited at 740 nm (a) and 935 nm (b). Increasing concentration of reporter to a constant 100 nM solution of probe excited at 740 nm (c) and 935 nm (d). Lines were fit from 0-100 nM and 110-300 nM. Additional controls for the reporter-hairpin in the absence of probe for (c) and (d) were fit from 0-300 nM reporter. Analysis of the changes in the signals slope aided in determination of the extent of reporter+probe formation.

In Figure A3.4a (740 nm excitation) and A3.4b (935 nm excitation), excess probe was added to saturate the reporter and cause the signal to plateau to a static-state. The line of fit for the dynamic and static signals were extrapolated to estimate the amount of reporter+probe formed. For 100 nM reporter the signal was expected to stabilize at 100 nM probe. The extrapolation analysis revealed the signal stopped changing at about 110 nM probe addition. This result suggested that the reporter concentration before probe addition was closer to 110 nM.

Next to further validate the extent of reporter+probe formed, the amount of reporter was increased with respect to a constant probe concentration (Figures A3.4c and A3.4d). After the

reporter and probe was fully complexed, addition of more reporter was expected to cause the ATTO 633 signal to increase but at a different slope. The reason for a different slope is due to the dependence of the ATTO 633 signal intensity on the FRET distance from the 6-FAM dye. The FRET distance between the dyes was controlled by the absence or presence of probe. To determine the slope of the ATTO 633 signal from uncomplexed reporter-hairpin, a control experiment was performed where the reporter concentration was increased in the absence of probe. The results in Figures A3.4c (740 nm excitation) and A3.4d (935 nm excitation) show how the ATTO 633 signal changed slope as the reporter concentration was increased.

The red data were for reporter additions to a constant probe concentration. The blue data were the control reporter-hairpin additions in the absence of probe.

The slope of the reporter-hairpin control was compared to the slope after all the probe was complexed. This approach helped guide which data points to fit in order to find the slopes before and after all the reporter and the probe was complexed. Finally, the data was interpreted by the intersection of the extrapolated slopes from reporter signal before and after all the probe was complexed. The amount of reporter that corresponded to where the two slopes intersected was taken as the amount of probe in solution.

Based on the slope extrapolation method there was about 100 nM probe in solution. The reporter- hairpin control slopes when excited at 740 and 935 nm were within 22 and 1 %, respectively, of the resultant slopes after all the reporter and probe was complexed. This confirmed that excess reporter- hairpin was in the solution with complexed reporter+probe. The discrepancy in slopes when excited at 740 nm was due to the weak signal from the quenched state of ATTO 633. The results from these titrations validated that the amount of reporter+probe formed was ~ 100 nM with an excess of about 10 nM reporter.

Appendix IV. Supplemental Information for Chapter 5 Sequence search results

See the [BLAST help pages](#) for detailed information about the meaning of the scores shown here.

Accession	ID	Query start	Query end	Subject start	Subject end	Strand	Score	Evalue	Alignment
MIMAT0000449	hsa-miR-146a-5p	1	22	1	22	+	110	6e-04	Align
MIMAT0002809	hsa-miR-146b-5p	1	22	1	22	+	92	0.020	Align
MIMAT0004608	hsa-miR-146a-3p	3	20	1	18	-	63	5.1	Align
MIMAT0004608	hsa-miR-146a-3p	7	16	4	13	+	32	1944	Align

Alignment of Query to mature miRNAs

```

Query: 1-22      hsa-miR-146a-5p: 1-22      score: 110      evalue: 6e-04
UserSeq          1  ugagaacugaauccauggguu 22
                |||
hsa-miR-146a-5p  1  ugagaacugaauccauggguu 22

Query: 1-22      hsa-miR-146b-5p: 1-22      score: 92        evalue: 0.020
UserSeq          1  ugagaacugaauccauggguu 22
                |||
hsa-miR-146b-5p  1  ugagaacugaauccauggguu 22

Query: 3-20      hsa-miR-146a-3p: 1-18      score: 63        evalue: 5.1
UserSeq          3  agaacugaauccauggg 20
                |||
hsa-miR-146a-3p  18  agaacugaauccauggg 1

Query: 7-16      hsa-miR-146a-3p: 4-13      score: 32        evalue: 1944
UserSeq          7  cugaaucca 16
                |||
hsa-miR-146a-3p  4  cugaaucca 13

```

Search parameters

```

Search algorithm:  BLASTN
Sequence database: mature
Evaluate cutoff:   2000
Max alignments:    100
Word size:         4
Match score:       +5
Mismatch penalty:  -4
Species filter:    hsa

```

Figure A4.1 miR search results from miRbase when searching for similar sequences to hsa-miR-146a-5p

One option (Query 3-20) was the direct reverse complement of miR-146a-3p (OA1) (Strand = '-'), which has a similar sequence similarity to miR-146a-5p (A) without the mismatches that naturally occur in the pre-miR. These mismatches can be seen in the pre-miR.

```

      c  -----u      u      uu      c  u      g  uc
5'  cgaug      guaucc cagcu  gagaacugaau ca ggguu ug  a
    |||||      ||||| |||||  |||
3'  gcuac      uauagg gucga  uucuugacuuaa gu uccag ac  u
    u      ugucuc      -      -c      a  c      -  ug

```

Figure A4.2 Binding of hsa-miR-146a pre-miR from miRbase. The sequence starts from the 5' end on the top left and moving right, then loops around to read from right-to-left on the bottom. Bound nucleotides are indicated by a vertical dash. Horizontal dashes are placeholders to indicate no nucleotide in that place.

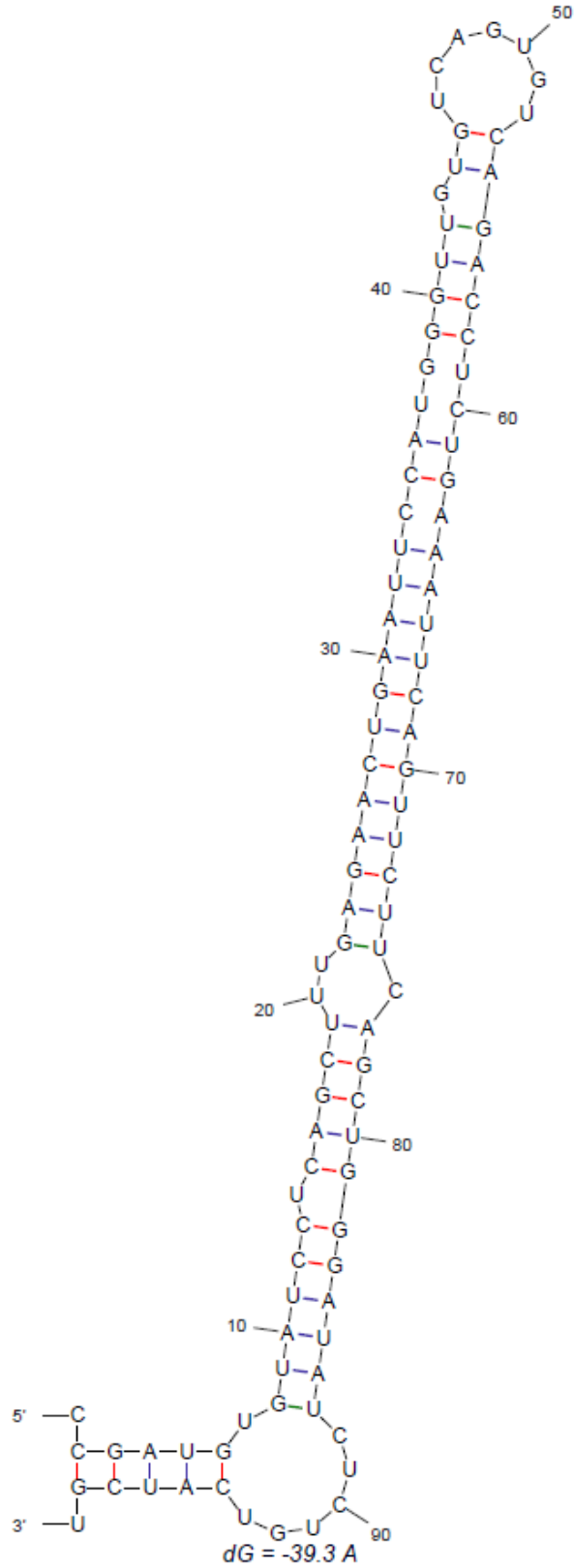


Figure A4.3 Pre-miR structure for hsa-miR-146a calculated by UNAFold. This calculated structure is similar to the structure presented by miRBase with the exception of the binding of nucleotides '38' (G) and '59' (U), which are predicted to bind in the miRBase model, but are not found to bind in the UNAFold model.

The following equation was used to calculate the FRET enhancement:

$$\text{FRET Enhancement} = \frac{R_{\text{acceptor}} - R + P_{\text{acceptor}}}{R + P_{\text{acceptor}}} \quad \text{Equation A4.1}$$

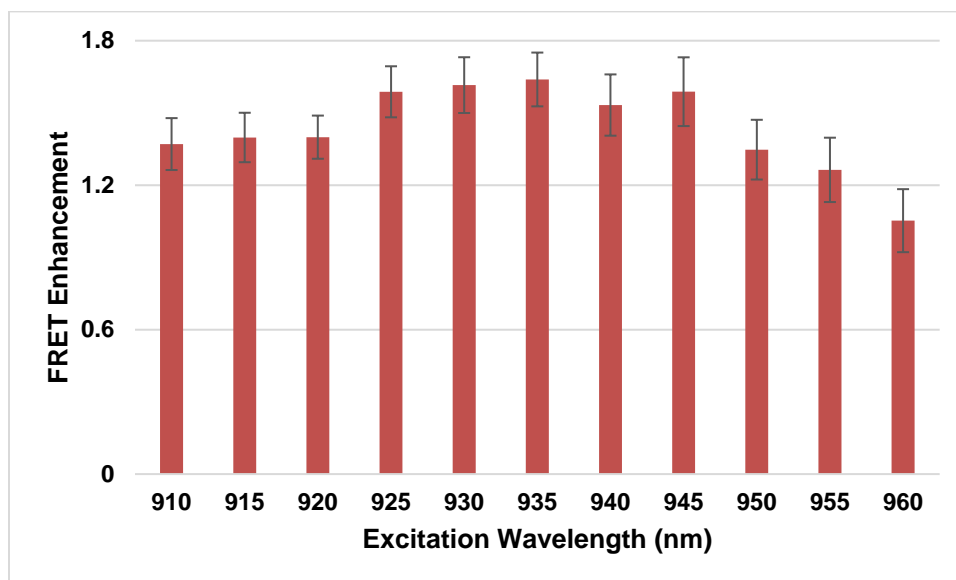


Figure A4.4 FRET Enhancement experiment for R1 to determine the optimal excitation wavelength

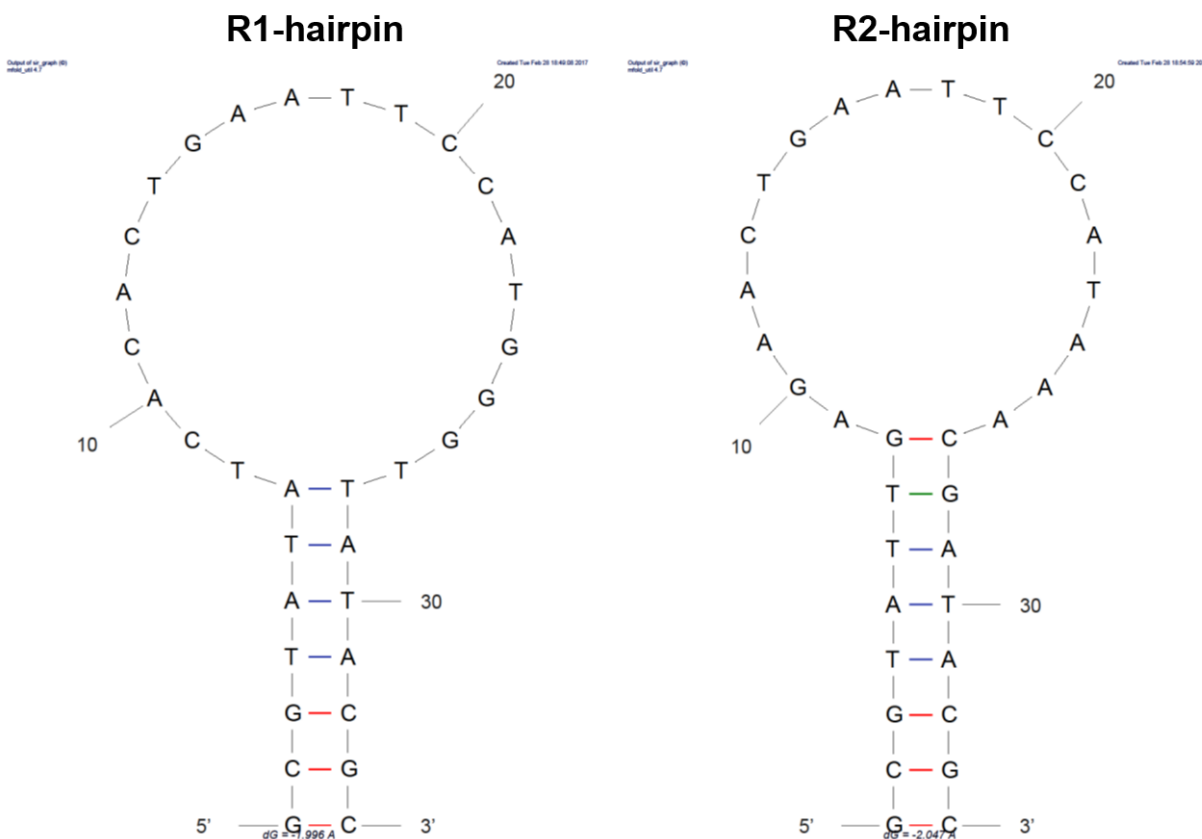


Figure A4.5 Predicted conformational binding structures for R1-hairpin and R2-hairpin. Structures were calculated from 'Quikfold' application in UNAFold, with parameters presented in materials and methods section 5.3.1.

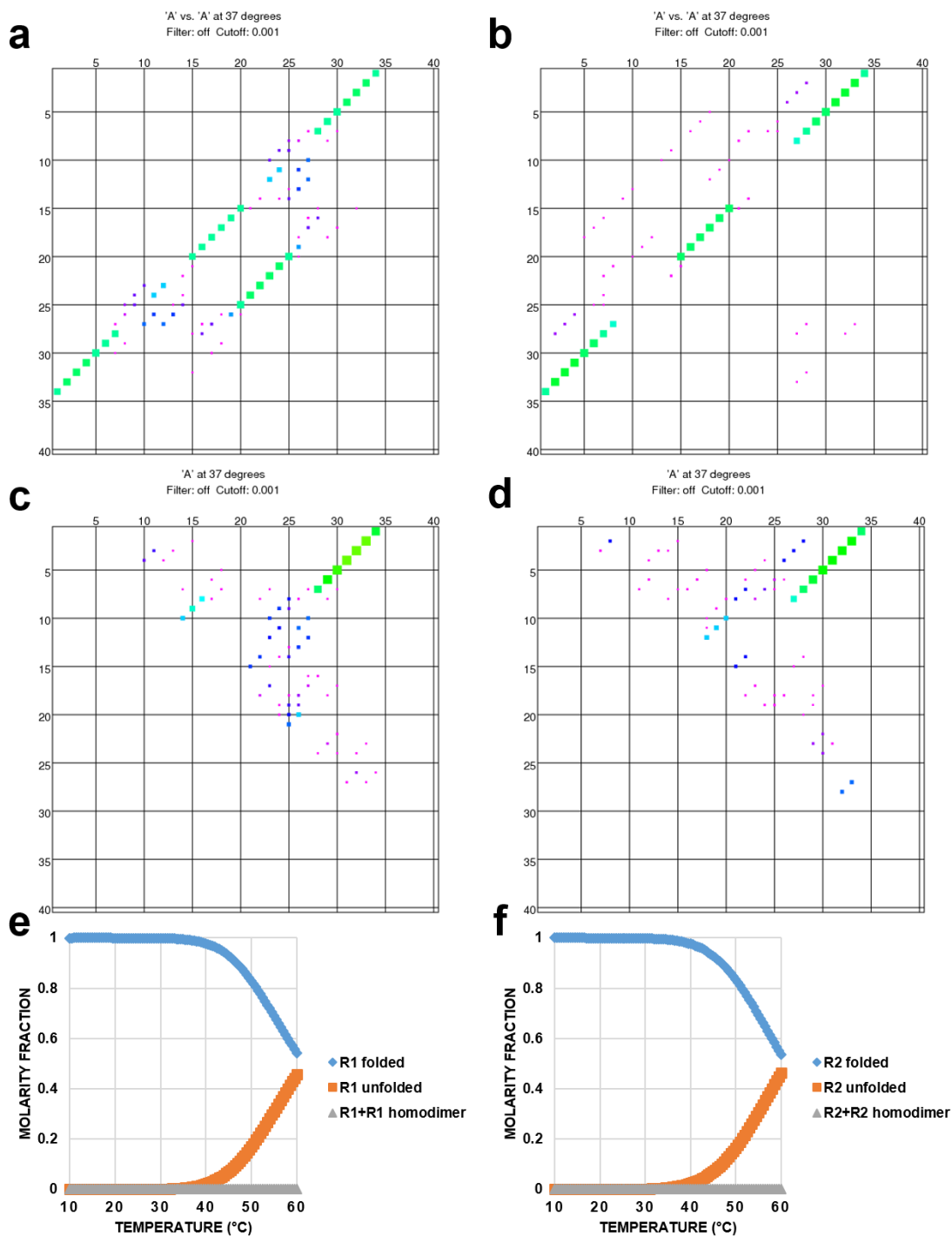


Figure A4.6 Probability dot plots and molarity fractions for R1 and R2 hairpins and homodimers. (a) is the probability dot plot for the R1 homodimer (b) is the probability dot plot for the R2 homodimer (c) is the probability dot plot for the R1 hairpin (d) is the probability dot plot for the R2 hairpin (e) is the molarity fraction for the R1 hairpin and homodimer (f) is the molar fraction for the R2 hairpin and homodimer. Probability dot plots obtained from UNAFold, and molarity fractions created from data obtained from UNAFold.

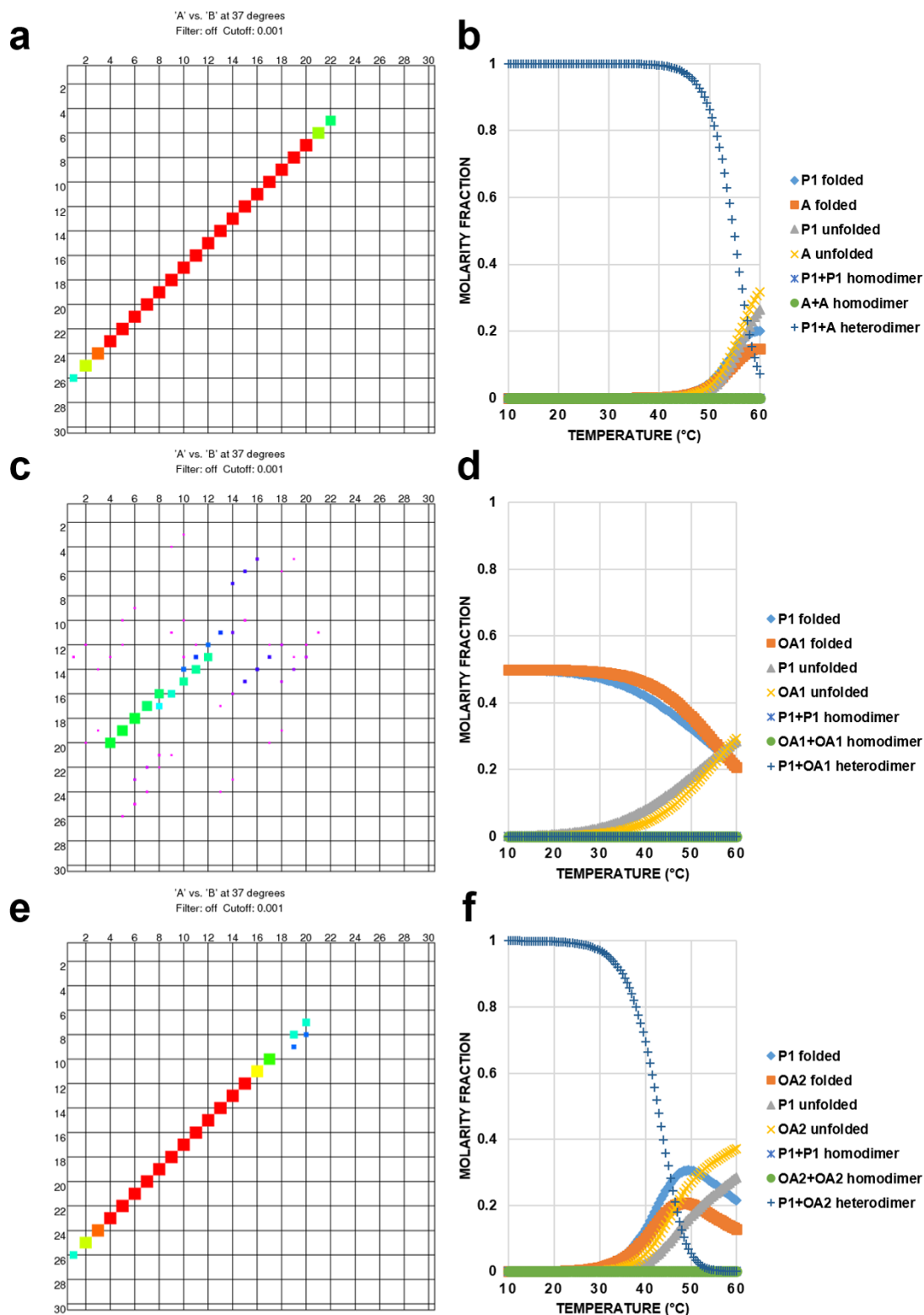


Figure A4.7 Probability dot plots and molarity fractions for P1 with analyte and off-analytes (a) is the probability dot plot for P1+A (b) is the molarity fraction for P1+A (c) is the probability dot plot for P1+OA1 (d) is the molarity fraction for P1+OA1 (e) is the probability dot plot for P1+OA2 (f) is the molarity fraction for P1+OA2. Probability dot plots obtained from UNAFold, and molarity fractions created from data obtained from UNAFold.

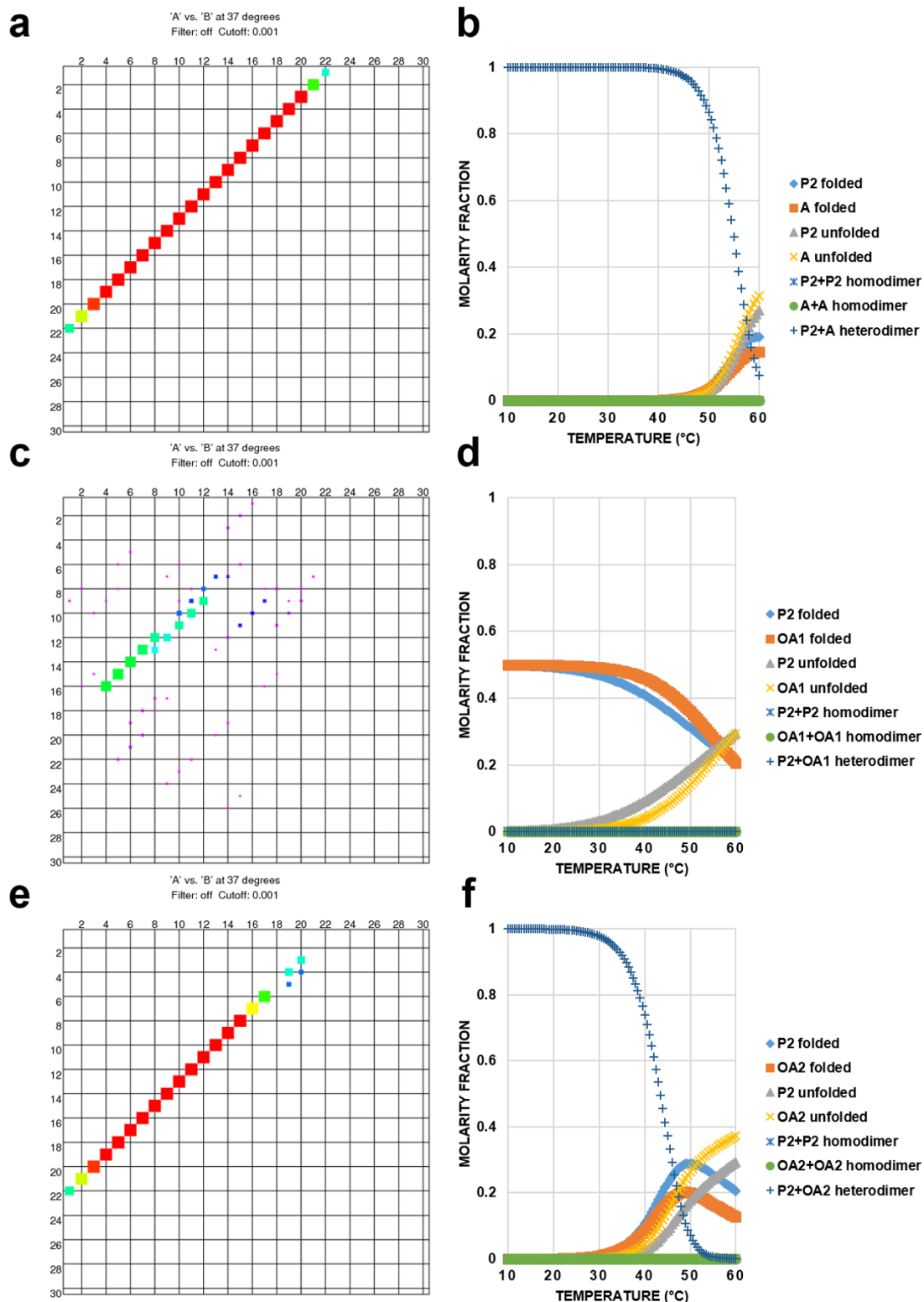


Figure A4.8 Probability dot plots and molarity fractions for P2 with analyte and off-analytes (a) is the probability dot plot for P2+A (b) is the molarity fraction for P2+A (c) is the probability dot plot for P2+OA1 (d) is the molarity fraction for P2+OA1 (e) is the probability dot plot for P2+OA2 (f) is the molarity fraction for P2+OA2. Probability dot plots obtained from UNAFold, and molarity fractions created from data obtained from UNAFold.

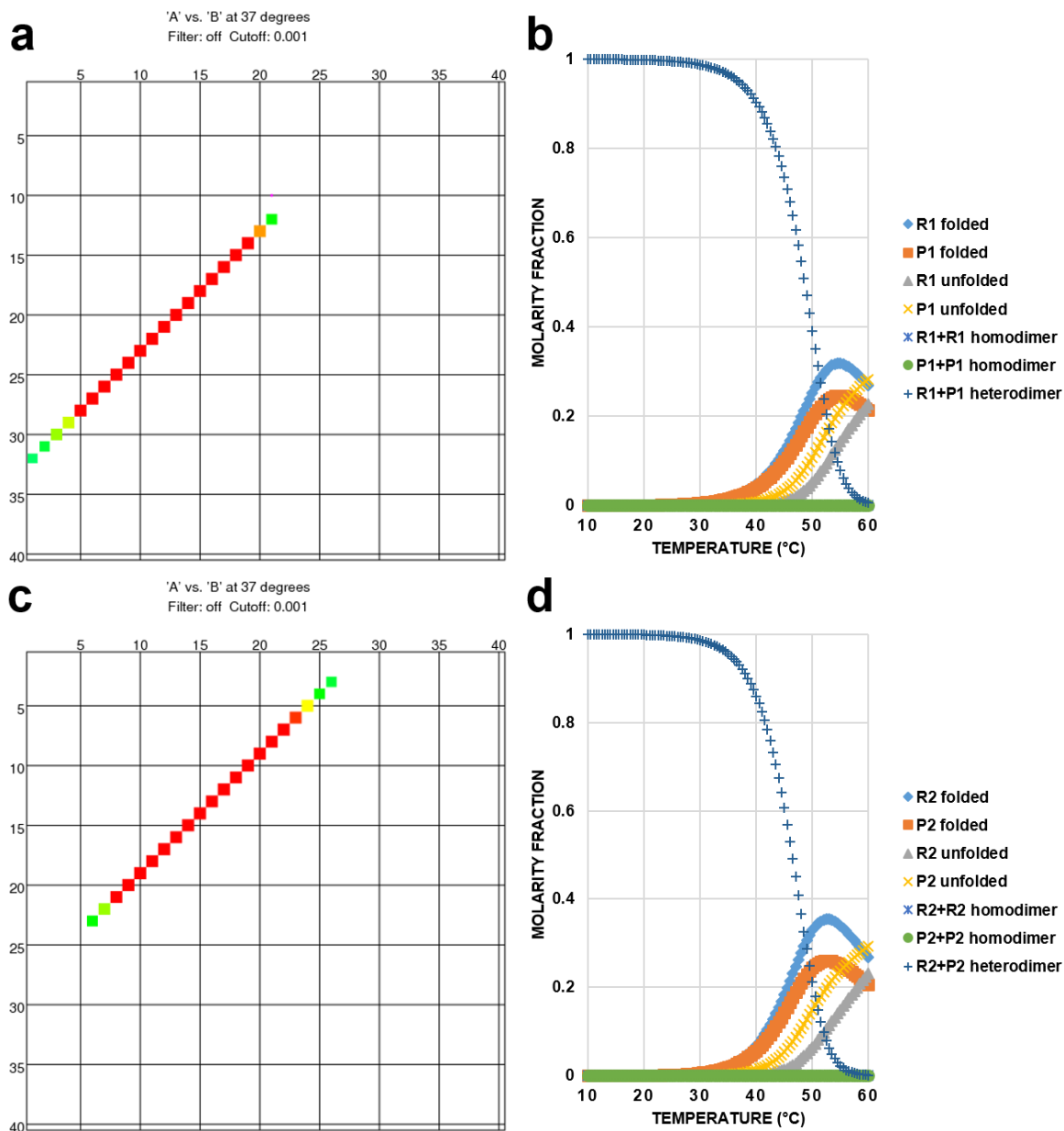


Figure A4.9 Probability dot plots and molarity fractions for reporter+probe biosensors (a) is the probability dot plot for R1+P1 (b) is the molarity fraction for R1+P1 (c) is the probability dot plot for R2+P2 (d) is the molarity fraction for R2+P2. Probability dot plots obtained from UNAFold, and molarity fractions created from data obtained from UNAFold.

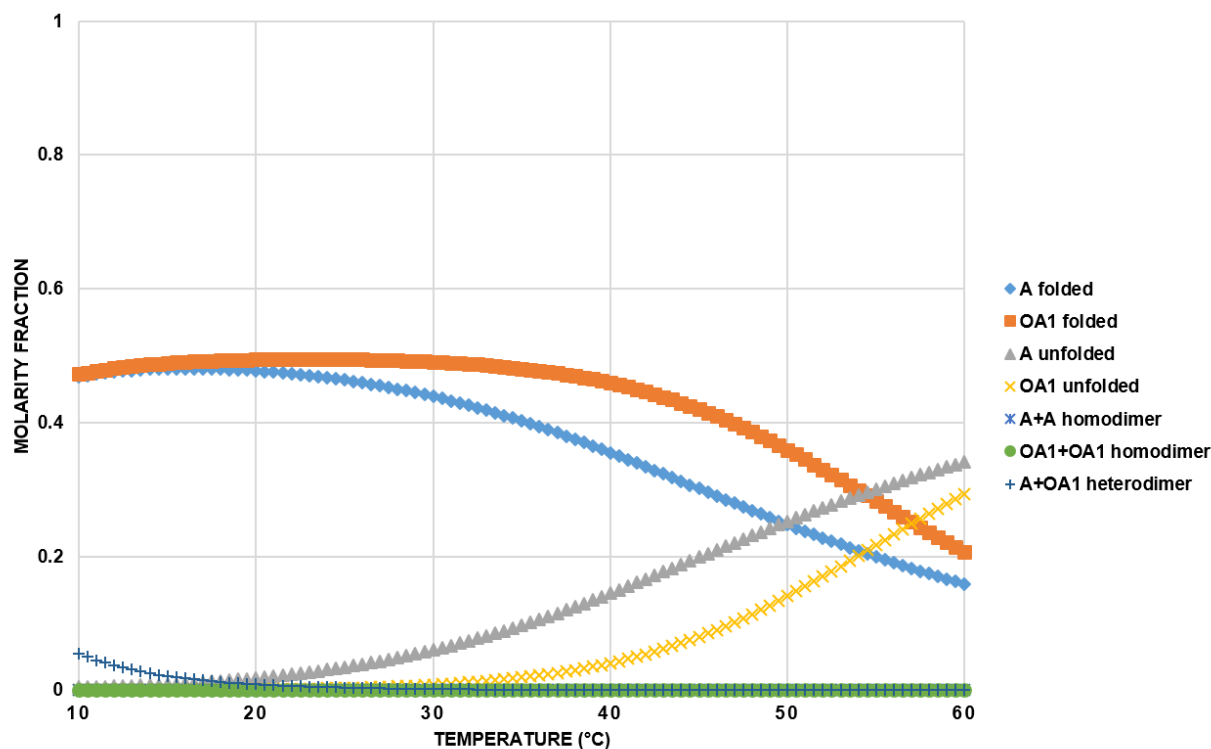


Figure A4.10 Molarity fraction for the A+OA1 heterodimer.

Table A4.1 Thermodynamic calculations for reporters binding to analytes/off-analytes. Calculations were performed using UNAFold applications described in materials and methods section 5.3.1

Name	ΔG (kcal/mol)	ΔH (kcal/mol)	ΔS (cal/mol*K)	T_m (°C)
R1+A	-6.1	-58.8	-160.1	4.7
R2+A	-4.0	-54.2	-160.0	-5.8
R1+OA1	-5.9	-43.2	-120.2	-4.8
R2+OA1	-9.1	-68.8	-192.5	21.8
R1+OA2	-4.0	-54.2	-162.0	-5.8
R2+OA2	-4.0	-54.2	-162.0	-5.8

Table A4.2 Percent complex formed for various equimolar (5 nM) interactions occurring at 37°C. Values were derived from molarity fraction calculations.

Name	Type of interaction	% formed at 37°C
R1+P1	heterodimer	94.79257
R2+P2	heterodimer	92.94164
P1+A	heterodimer	99.83871
P1+OA2	heterodimer	83.98497

P1+OA1	heterodimer	4.59E-06
P2+A	heterodimer	99.82686
P2+OA1	heterodimer	5.33E-06
P2+OA2	heterodimer	86.81492
A+OA1	heterodimer	0.053996
R1-folded	hairpin	99.05379
R2-folded	hairpin	98.8418
R1+R1	homodimer	9.32E-06
R2+R2	homodimer	3.82E-06
P1+P1	homodimer	0.000621
P2+P2	homodimer	0.000776

Table A4.3 Percent complex formed for various 10x (50 nM) analyte/off analyte interactions with either the reporter or probe at (5 nM) and 37°C. Values were derived from molarity fraction calculations.

Name	Type of interaction	% formed at 37°C
P1 + 10x OA1	heterodimer	8.35E-06
P1 + 10x OA2	heterodimer	9.989898
P2 + 10x OA1	heterodimer	9.7E-06
P2 + 10x OA2	heterodimer	9.993498
R2 + 10x OA1	heterodimer	0.005388
R2 + 10x OA2	heterodimer	4.27E-06
R2 + 10x A	heterodimer	4.53E-06
R1 + 10x A	heterodimer	0.000109
R1 + 10x OA1	heterodimer	2.43E-05
R1 + 10x OA2	heterodimer	4.91E-06

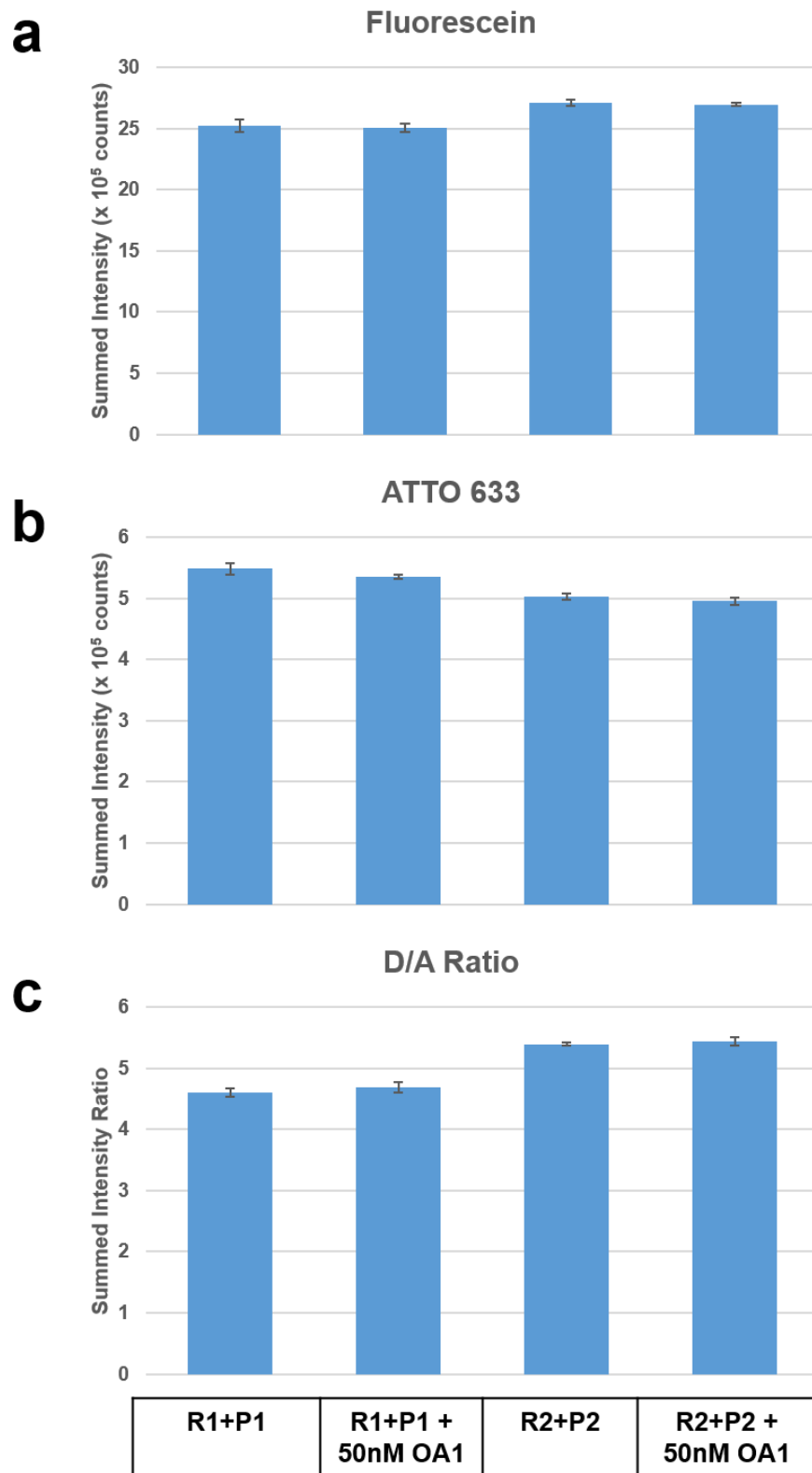


Figure A4.11 Control experiments with R+P OA1 (N=3), (a) Fluorescein signal of R1+P1 and R2+P2 with and without 50 nM (10x) OA1 (b) ATTO 633 signal of R1+P1 and R2+P2 with and without 50 nM (10x) OA1 (c) Donor/Acceptor ratio signal of R1+P1 and R2+P2 with and without 50 nM (10x) OA1.

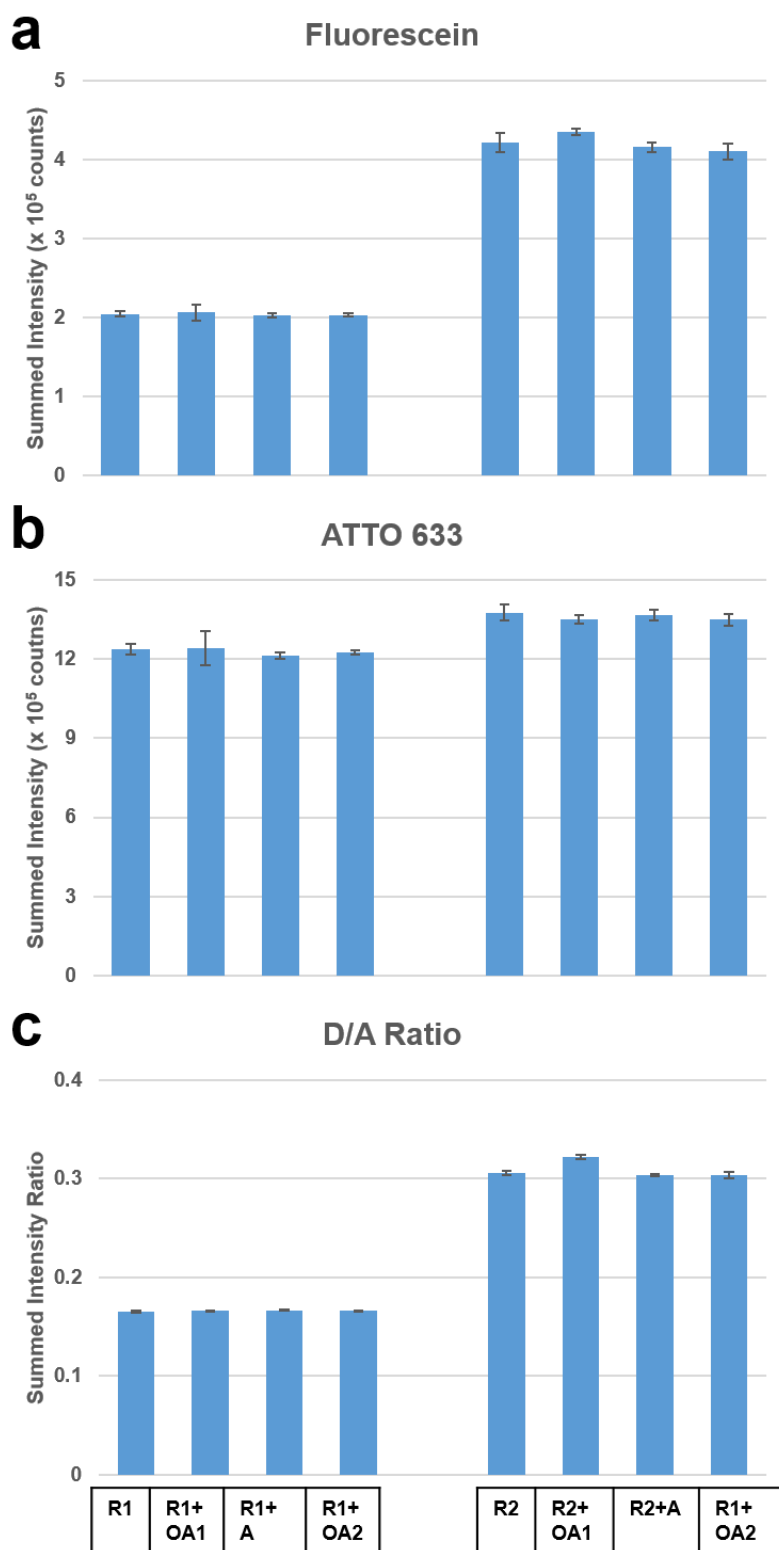


Figure A4.12 Reporters with analyte/off-analytes control experiments (N=3) (a) Fluorescein signal of R1 or R2 with or without 50 nM (10x) OA1, A, or OA2 (b) ATTO 633 signal of R1 or R2 with or without 50 nM (10x) OA1, A, or OA2 (c) Donor/Acceptor ratio signal of R1 or R2 with or without 50 nM (10x) OA1, A, or OA2.